STRUCTURAL HEALTH MONITORING USING ADAPTIVE WAVELET FUNCTIONS

SEYED HOSSEIN MAHDAVI

THESIS SUBMITTED IN FULFILLMENT
OF THE REQUIREMENTS
FOR THE DEGREE OF DOCTOR OF PHILOSOPHY

FACULTY OF ENGINEERING
UNIVERSITY OF MALAYA
KUALA LUMPUR

2016

University of Malaya

UNIVERSITY OF MALAYA

ORIGINAL LITERARY WORK DECLARATION

Name of Candidate: Seyed Hossein Mahdavi

Registration/Matric No: KHA120002

Name of Degree: PHD

Title of Project Paper/Research Report/Dissertation/Thesis ("this Work"):

STRUCTURAL HEALTH MONITORING USING ADAPTIVE WAVELET FUNCTIONS

Field of Study:

I do solemnly and sincerely declare that:

(1) I am the sole author/writer of this Work;
(2) This Work is original;
(3) Any use of any work in which copyright exists was done by way of fair dealing and for permitted purposes and any excerpt or extract from, or reference to or reproduction of any copyright work has been disclosed expressly and sufficiently and the title of the Work and its authorship have been acknowledged in this Work;
(4) I do not have any actual knowledge nor do I ought reasonably to know that the making of this work constitutes an infringement of any copyright work;
(5) I hereby assign all and every rights in the copyright to this Work to the University of Malaya ("UM"), who henceforth shall be owner of the copyright in this Work and that any reproduction or use in any form or by any means whatsoever is prohibited without the written consent of UM having been first had and obtained;
(6) I am fully aware that if in the course of making this Work I have infringed any copyright whether intentionally or otherwise, I may be subject to legal action or any other action as may be determined by UM.

Candidate's Signature Date:

Subscribed and solemnly declared before,

Witness's Signature Date:

Name:

Designation:

University of Malaya

ABSTRACT

In this study, two aspects of structural dynamic problems have been considered, involving direct structural dynamics as well as inverse problems. The first part of this research is directed towards improving an explicit and indirect time integration method for structural dynamic problems capable of using adaptive wavelets. The developed scheme is comprehensive enough for use with any wavelet basis function. To investigate the applicability of different wavelet functions for different problems, in particular, the simple family of Haar wavelets, the complex and free-scaled Chebyshev wavelets of the first (FCW) and second kind (SCW) and Legendre wavelets (LW) have been evaluated. A detailed assessment is carried out on the stability, accuracy and computational efficiency of responses calculated by Haar wavelet, FCW, SCW and LW. The proposed method lies on an unconditionally stable scheme, hence, there is no requirement on the selection of the time interval. This allowed the numerical procedure to be performed on long time increments.

Practically, an efficient structural health monitoring strategy is the resultant of the implementation of an enhanced structural simulation through inverse problem approach. As a consequence, the computational performance of structural health monitoring strategies will be directly influenced by the higher computational competency and convergence rate of the proposed wavelet-based method for structural simulation.

Accordingly, in the second part of this research, the procedure of structural identification and damage detection has been developed by employing the wavelet-based method through the modified genetic algorithms (GAs) to optimally solve inverse problems. For this purpose, a wavelet-based GAs strategy is improved by using free-scaled adaptive wavelets to optimally identify unknown structural parameters. The appropriateness and effectiveness of the proposed strategy have been evaluated both numerically and experimentally. The numerical assessment demonstrated the robustness of the proposed technique for identification and damage detection of large-scaled structures with the best performance. For the experimental validation, three test setups were conducted for identification and damage detection, including two different MDOF systems and a 2-dimentional truss structure. Consequently, it was shown that the computational efficiency of structural identification and relatively, damage detection strategies were significantly enhanced. This led the optimum results with the highest accuracies and provided the sufficiently reliable strategy in assessing the structural integrity, safety and reliability.

University of Malaya

ABSTRAK

Melalui kajian ini, pihak pengkaji telah menitikberatkan dua aspek masalah dinamik struktur, yakni yang melibatkan dinamik struktur secara terus dan masalah songsangan. Bahagian pertama kajian ini adalah menjurus ke arah meningkatkan kaedah integrasi masa yang nyata dan secara tidak langsung untuk masalah struktur dinamik yang mampu menggunakan penyesuaian gelombang kecil (wavelet). Skim yang disediakan cukup komprehensif untuk digunakan dengan sebarangan fungsi asas wavelet. Bagi Menyiasat penggunaan / keterterapan fungsi gelombang kecil (wavelet) yang berbeza untuk masalah yang berbeza, terutamanya, keluarga mudah (riak) wavelet Haar, wavelet Chebyshev pertama (FCW) yang kompleks dan berskala bebas dan jenis kedua (SCW) serta wavelet Legendre (LW) telah dinilai. Satu penilaian terperinci telah dijalankan terhadap kestabilan, ketepatan dan kecekapan dalam pengiraan tindak balas yang telah dikira dengan menggunakan wavelet Haar, FCW, SCW dan LW. Kaedah yang dicadangkan bergantung kepada skim yang stabil tanpa syarat, walhal, tidak ada keperluan terhadap pemilihan selang masa. Ini telah membolehkan prosedur berangka yang dilakukan ke atas pertambahan masa yang panjang.

Secara praktikalnya, struktur strategi pemantauan kesihatan yang cekap adalah paduan pelaksanaan simulasi struktur yang telah dipertingkatkan melalui pendekatan masalah songsang. Akibatnya, prestasi pengkomputeran strategi pemantauan kesihatan struktur akan terus dipengaruhi oleh kecekapan pengiraan dan penumpuan pada kadar yang lebih tinggi daripada kaedah berasaskan gelombang kecil (wavelet) yang dicadangkan untuk simulasi struktur.

Oleh itu, dalam bahagian kedua kajian ini, prosedur mengenalpasti struktur dan pengesanan kerosakan telah dibentuk dengan menggunakan kaedah berasaskan wavelet-melalui algoritma genetik yang telah diubahsuai (GA) bagi menyelesaikan masalah songsang

University of Malaya

secara optimum. Bagi tujuan ini, strategi GA berasaskan wavelet telah dipertingkatkan dengan menggunakan riak (wavelet) penyesuaian bebas untuk meningkatkan keupayaannya dalam mengenalpasti secara optimum parameter struktur yang tidak diketahui. Kesesuaian dan keberkesanan strategi yang dicadangkan telah dinilai secara berangka dan uji kaji. Penilaian berangka menunjukkan keteguhan teknik yang dicadangkan untuk pengenalan dan pengesanan kerosakan struktur berskala besar yang mempunyai prestasi terbaik. Untuk pengesahan eksperimen, persediaan tiga ujian telah dijalankan untuk mengenalpasti dan mengesan kerosakan, termasuklah dua sistem MDOF yang berbeza dan struktur kekuda 2-dimensi. Oleh yang demikian, ia menunjukkan bahawa kecekapan pengiraan dalam pengenalan struktur dan secara relatifnya, strategi pengesanan kerosakan telah dipertingkatkan dengan ketara. Ini telah menghasilkan keputusan yang optimum dengan ketepatan tertinggi dan menjamin strategi yang cukup dipercayai dalam menilai keutuhan, keselamatan dan kebolehpercayaan struktur tersebut.

University of Malaya

ACKNOWLEDGMENTS

Praise and thank Almighty God for giving me the wisdom, health and strength to complete this research.

I would like to express my deepest gratitude and appreciation to my supervisor, **Prof. Dr. Hashim Abdul Razak** for his kind supervision, valuable guidance, encouragement, and immense assistance throughout the preparation of this work.

I also would like to acknowledge the financial supports provided by the University of Malaya through the Bright Spark scholarship scheme (Scholarship no.: BSP/APP/1818/2013) and PPP research grant PG078-2013B.

Also, I express my deepest appreciation to the staff of Department of Civil Engineering, and the Faculty of Engineering, University of Malaya, for their kind help during my work, which has resulted in reaching my research objectives on schedule.

Finally, I wish to give my heartfelt and special thanks to my family; my parents, wife and son for their patience, encouragement and unwavering supports throughout the duration of my studies.

Seyed Hossein
February 2016

University of Malaya

TABLE OF CONTENTS

University of Malaya

University of Malaya

University of Malaya

University of Malaya

LIST OF FIGURES

University of Malaya

University of Malaya

University of Malaya

University of Malaya

University of Malaya

University of Malaya

University of Malaya

University of Malaya

University of Malaya

LIST OF TABLES

University of Malaya

University of Malaya

University of Malaya

LIST OF SYMBOLS AND ABBREVIATIONS

GA	:	Genetic algorithm
FCW	:	The first Chebyshev wavelet
I/O	:	Input-output
LL	:	Lower limit of search domain
LW	:	Legendre wavelet
MGA	:	Modified genetic algorithm
NN	:	Neural network
RMGA	:	Runge-Kutta based modified genetic algorithm
P	:	Product matrix of integration
SCW	:	The second kind of Chebyshev wavelet
SM	:	Segmentation method
SSRM	:	Search space reduction method
UL	:	Upper limit of search domain
WMGA	:	Wavelet-based genetic algorithm
k'	:	Transition parameter
$\psi_{a,b}$	:	Family of continuous wavelets
$\Psi(t)$	:	Operation vectors of wavelets
a	:	Transition of the mother wavelet
b	:	Scale of the mother wavelet
τ	:	Local time domain
t_i	:	Global time domain
$2M$	:	Scale of wavelets corresponding to number of adaptive collocation points
M	:	Order of scaled wavelets

University of Malaya

m	:	Order of orthogonal polynomials
h	:	Family of Haar wavelet functions
T_m	:	The mth order of first kind of Chebyshev polynomial
U_m	:	The mth order of second kind of Chebyshev polynomial
ω_n	:	Weight functions
ω	:	Natural frequencies
C^T	:	Wavelet coefficient vectors
[M]	:	Mass matrix
[K]	:	Stiffness matrix
[Cd]	:	Damping matrix
E	:	Modulus of elasticity

University of Malaya

CHAPTER 1: INTRODUCTION

1.1 General

In general, structural dynamics problems can be classified into direct (forward) problems and inverse problems. The main purpose for structural simulation (direct or forward analysis) of dynamical systems is to estimate the output (response) for a set of given input comprised of known structural parameters and lateral forces. In contrast, inverse analysis deals with identification of system parameters corresponding to a set of given input and output (I/O) information and relation between these data. Accordingly, structural health monitoring is emerging as a vital tool to help engineers improve the safety and maintainability of critical structures. This popular and of course fundamental paradigm involves structural identification and damage detection in order to analyze the current structural reliability, integrity and safety (Figure 1.1). Moreover, the advantages of structural identification procedures have been demonstrated in various disciplines of engineering. For instance, in the non-destructive evaluation of structures, prediction of parameters for active and passive control of structures, pattern predictions, image recognition and so forth.

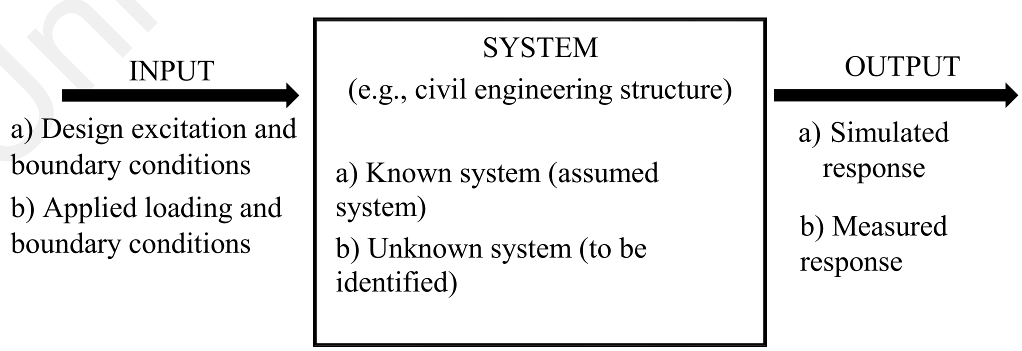

Figure 1.1: (a) Structural simulation (direct); (b) structural identification (inverse).

University of Malaya

Over the past two decades, wavelets have been effectively utilized for signal processing and solution of differential equations. There are many mathematical reports on characteristics of wavelet functions and wavelet transforms. For more than a decade, wavelet operators have been employed to solve and analyze problems associated with structural engineering and engineering mechanics. Subsequently, further to the previous discussion on direct and inverse analysis, implementation of wavelet functions and wavelet transforms in engineering can be viewed from two underlying perspectives. Firstly, in structural simulation (direct analysis), whereby, the solution of differential equations governing the structural systems is considered. Secondly, the practice of wavelets through an inverse problem (structural identification) to analyze the measured structural responses in order to extract the system properties, including time varying parameters, modal properties, damage measurement, sensitivity analysis, de-noising (filtering I/O data) and so forth.

Generally, the identification of structural parameters i.e., mass, damping and stiffness is commonly referred to as 'system identification'. System identification can be applied in order to update or calibrate the structural models so as to better estimate response and accomplish more cost-effective designs. Fundamentally, structural assessment, structural health monitoring and damage evaluation are concerned with recording and comparing identified properties over a period of time in a non-destructive way by tracking changes of the structural parameters. This is especially practical for firstly, identifying structural damages imposed by natural causes such as earthquakes, winds or tsunamis, and secondly for evaluation of the reliability and safety of aging structures.

Consequently, for any structural simulation and identification strategy, it is essential to achieve the most reliable and optimum results. In this regard, the computational efficiency, robustness and convergence rate of algorithms proposed for structural health monitoring approaches shall be evaluated in details. The research presented in this thesis develops an

University of Malaya

efficient and robust approach for solving structural dynamic problems (forward analysis) by using adaptive wavelet functions. Subsequently, the proposed wavelet-based scheme is implemented in conjunction with a heuristic optimization strategy based on modified genetic algorithms in order to optimally solve inverse problems, involving structural identification and damage detection problems.

1.2 Objectives and problem statement

Structural health monitoring using adaptive wavelet functions is the primary aim of this study. For this purpose, an indirect time integration method is developed to solve structural dynamic problems (structural simulation) using adaptive wavelet functions, initially. Later, the proposed procedure is implemented in order to solve inverse problems (structural identification). Detailed objectives and corresponding problem statements that contribute to this aim include:

- To develop an explicit and indirect time integration method capable of using various wavelet functions suitable for solving structural simulation problems.

  There are several reports available for the solution of dynamic problems using explicit methods. In fact, all of them lie on time domain analysis of either lateral excitation or inherent properties of structures. Consequently, the frequency components of outputs are not being considered through the numerical integration. Therefore, the size of data is significantly increased, and computational competency degrades. In addition, implementation of indirect approaches in structural dynamics problems using frequency domain analysis is sparsely addressed in literature. For instance, the practice of well-known Fourier transformation (FT) is reported as one of the frequency-domain procedures. However, the information about time cannot be captured by using FT scheme. So far no information is available regarding to a comprehensive procedure for numerical time integration concerning with frequency components as well as time information. For this reason, it seems inevitable to develop the solution of structural simulation problems in order to achieve a computationally efficient procedure that will result in an optimum implementation through the structural identification strategies.

- To investigate the efficiency of the proposed time integration approach for using various wavelet basis functions.

Mathematically, different wavelet basis functions have been implemented to solve ordinary differential equations (ODEs). The significant shortcomings observed in the literature are the limitations of proposed schemes for the solution of only unit time intervals, which, makes those numerical methods impractical for structural dynamics problems. In addition, there is no consideration on frequency components of equations. Consequently, the assessment of computational efficiency corresponding to different wavelet basis functions on various scales is not addressed, and therefore there is no considerable attempt on the practice of adaptive wavelet functions for different problems of structural dynamics.

- To evaluate the stability and accuracy of results calculated with the proposed time integration procedure using different wavelet functions.

No significant research has investigated the stability and accuracy of results obtained by adaptive wavelet functions. In structural health monitoring problems, either direct analysis or inverse analysis, the criterion on stability and accuracy of responses and thus, selection of the appropriate sampling rates (time intervals) play the underlying role to accomplish the most optimum strategies. There have been many researches conducted for this purpose on not only explicit but also implicit time integration methods. However,

University of Malaya

there is no study on the evaluation of wavelet-based procedures for structural dynamics problems.

- To improve a wavelet-based scheme in order to compute the third derivative of displacement with respect to time (namely, the jerk quantity) capable of using different wavelet basis functions.

One of the advantages of wavelet functions is undoubtedly the analysis of sensitivity of time varying parameters with respect to time. Particularly, for solving inverse problems through an online pattern, calculating and comparison of this quantity is very useful for identification and damage detection algorithms. Subsequently, there is little or no study in the literature addressing so-called jerk measurement.

- To modify and develop an efficient structural identification and damage detection (inverse analysis) strategy originating from the proposed method of time integration using adaptive wavelet functions.

The structural identification algorithms involve identification of unknown structural parameters such as mass, damping and stiffness for each existing degree of freedom or for each structural element. Accordingly, a structural identification strategy can be extended in order to improve a damage detection algorithm. Implementation of the proposed method using various wavelet functions through an inverse problem, significantly enhances the common non-classical algorithms of structural identification i.e., genetic algorithm (GA) and gains the most optimum and reliable results. Fundamentally, the proposed method lies on a time domain scheme, however its practice can be beneficial while it is not blind on the frequency contents of dynamic equilibrium. From the computational efficiency point of view, substantial discussions have demonstrated that an excessive computational cost is the main drawback of

University of Malaya

aforementioned non-classical procedures. Consequently, by using the proposed scheme the entire details of considered inverse problem is being optimally captured (especially, frequency contents), and resulting in the higher rate of convergence and accuracy of results.

- To develop an efficient wavelet-based procedure for identification of external forces (input data) suitable for output-only data inverse analysis that is referred in literature to 'operational inverse problems'.

  Basically, it is observed that methods utilized for force identification are mostly based on frequency domain analysis and thus, have fundamental drawbacks which will be discussed in subsequent chapters. Consequently, the capability and appropriateness of the proposed scheme as an explicit time integration method should also be evaluated for force identification problems. However, several limitations still remained for using the proposed method such as the bounded measurement of responses or restricted boundary conditions.

1.3 Scope of study

Basically, the overall scope of this study falls under two underlying prospects. Firstly, the numerical development of the proposed algorithms together with numerical validation and evaluations. Secondly, the experimental verifications. The former part of this study contains the mathematical development and improvement of a wavelet-based method for dynamic analysis of structures. For various structural systems a comprehensive program code is developed in MATLAB in order to formulate structural properties prior to implementation of the main scripts involving the operation of the proposed method using different wavelet functions. It is expected that, due to different ranges of frequency components of external excitations, the influence of various wavelet basis functions i.e., 2-dimensional (2D) wavelets will be totally different with 3D basis functions. As it is shown in Figure 1.2, for diverse structural problems i.e., single-degree-of-freedom (SDOF) and multi-degrees-of-freedom (MDOF), the adaptive analysis is achieved due to an iterative scheme using different wavelet basis functions. In addition, the proposed scheme is implemented for solving inverse problems and the robustness of using wavelet functions is demonstrated numerically and later is validated experimentally.

In order to accomplish the aforementioned objectives, the present research has been carried out in following steps:

- In order to investigate the influence of using various wavelets through the proposed method, four wavelet basis functions are considered i.e., 2D and simple Haar wavelets, family of 3D and complex Chebyshev wavelet functions of the first (FCW) and second kind (SCW) and finally, 3D and complex Legendre wavelet (LW) functions. An explicit and indirect time integration method is developed for structural dynamics problems capable of using foregoing wavelets. For this purpose, the dynamic equilibrium governing SDOF and MDOF structures is efficiently approximated by wavelet functions emphasizing on frequency-domain approximation. A simple step-by-step algorithm has been implemented and improved in order to calculate the response of finite element systems. A clear cut formulation is derived for transforming differential equations into the corresponding algebraic systems using wavelet operational matrices. A converter coefficient is developed in order to extend operations of wavelets from local times to global times. For the purpose of numerical evaluations, results are compared with simulated responses by common numerical time integration procedures such as the family of Newmark-β (linear and average acceleration method), Wilson-θ, central difference and Hilber-Hughes-Taylor (HHT-α) method. In all the procedures, the CPU computation time involved has also been considered for evaluating the computational efficiencies.

- In order to examine the efficiency of different wavelet basis functions, the operational matrices of integration corresponding to each basis function are compared in detail. For this purpose, various scales of 2D and 3D wavelet functions are employed in order to solve the first and second ordered differential equations. Accordingly, a comprehensive investigation on the computational efficiency of 2D and 3D wavelet functions is conducted prior to selecting the most compatible basis function with the lateral excitation.
- One of the preliminary aims of this study is to develop a robust technique for numerical time integration. The most important criterions on the use of numerical time integration procedures are the stability and accuracy of responses. For this reason, the stability and accuracy of results should be investigated in detail. The algorithm of stability analysis is different for 2D and 3D wavelet functions. For 2D and discrete wavelet functions such as Haar wavelet, an alternative scheme is proposed for analysis of stability. However, it is satisfied by utilizing a direct approach for 3D wavelet functions such as Chebyshev or Legendre wavelets.
- In order to optimally compute the derivative of time varying parameters with respect to time, an operator of derivative is proposed capable of using different wavelet basis functions. As long as the vector of accelerations is considered as one of the time varying parameters, then the quantity of jerk is optimally computed by using the proposed method. Accordingly, the effectiveness of jerk measurement is numerically investigated for different structures.

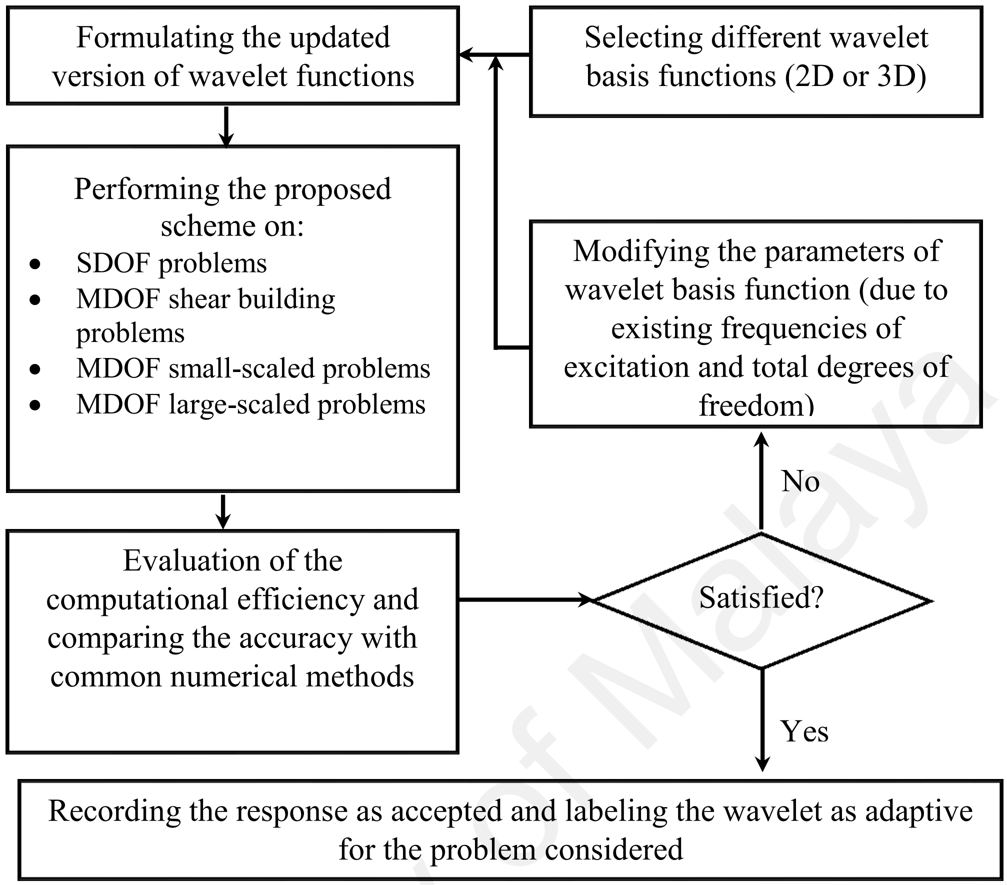

Figure 1.2: The proposed iterative algorithm for solving structural dynamics problems using adaptive wavelet functions.

- The proposed scheme for forward analysis is implemented for solving inverse problems. For this purpose, the non-classical genetic algorithms (GA) is first modified in order to dealing with complex problems. Then, a wavelet-based modified GA strategy is enhanced by using adaptive wavelet functions. In other words, by using 2D and 3D wavelet functions simultaneously, initial values of unknown parameters are predicted very fast, and therefore the computational efficiency is significantly increased compared to the simple and common GA strategies. The overall layout of the methodology utilized for solving inverse problems is illustrated in Figure 1.3. Accordingly, the algorithm of identification is extended for an optimum damage detection strategy. The capability of the proposed algorithms is numerically and experimentally evaluated on MDOF shear buildings (refers to only shear DOFs), 2D trusses and finally, for only numerical verifications on 3D truss structures (Figure 1.4). For this purpose, a comprehensive program code is developed in MATLAB for structural identification and damage detection algorithms.

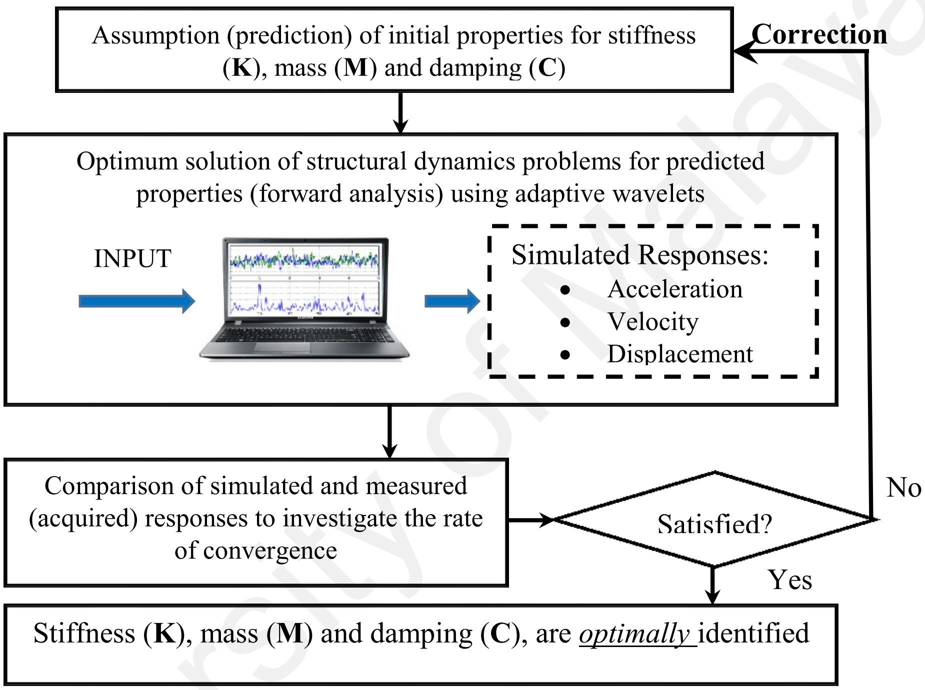

Figure 1.3: Overall schematic view of methodology utilized in this study for solving inverse problems.

- The essence of the proposed method lies on an explicit time integration method. Consequently, it allows to define an iterative procedure involving corrector and predictor iterations in order to optimally identify unknown forces. The measured accelerations corresponding to further time intervals constitute the current prediction on the magnitude of the unknown forces. Obviously, the accuracy of the former predictions is not desirable at all and it is supposed to be enhanced for further corrections, iteratively.

University of Malaya

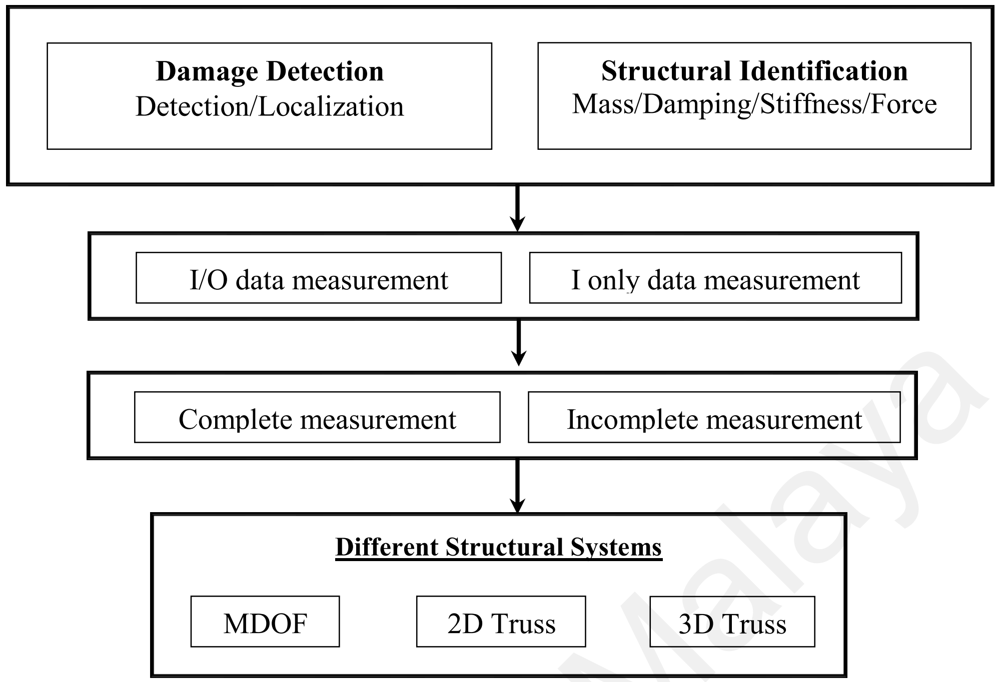

*where I: input, O: output

Figure 1.4: The scope of numerical and experimental work for inverse analysis.

1.4 Organization of thesis

Accordingly, this thesis has been divided into 6 chapters and the brief description on each chapter is provided as following.

The importance and the definition of the problem statement of this research have been highlighted in Chapter 1 along with the objectives and the scope of current study.

Chapter 2 is allocated to the literature review of time integration methods, application of wavelet functions in forward and inverse problems, the review of classical and non-classical approaches for structural identification and damage detection algorithms.

Chapter 3 is devoted to the numerical developments and applications of structural simulations (direct analysis) using adaptive wavelet functions. Operational matrices of integration and derivation are presented in this chapter. Furthermore, the stability and accuracy analysis are numerically evaluated in Chapter 3.

Accordingly, the proposed strategy in order to solve inverse problems is presented in Chapter 4. The numerical applications are given in order to investigate the robustness of the proposed procedure for both, direct (simulation) and inverse problems (structural identification).

Chapter 5 deals with the practical and experimental verifications of the proposed method, especially, for structural identification and damage detection algorithms.

Subsequently, Chapter 6 highlights the main results and conclusions drawn from the study carried out in the thesis together with the recommendations for further works.

University of Malaya

CHAPTER 2: LITERATURE REVIEW

2.1 Introduction

In general, dynamic problems in structural engineering are being categorized into two main categories. The first category involving low frequencies i.e., the order of few Hz to few hundred Hz (1e2), and is commonly called structural dynamics problems. The second category involves very high frequencies i.e., the order of kHz (1e3) to Tera Hz (1e12) namely wave propagation problems. The main objectives of this study contribute to the former classification relevant to the most common and practical problems in structural engineering.

This chapter presents the conceptual ideas of wavelet analysis and introduces some of the superior characteristics of this powerful tool compared with well-known Fourier analysis. In addition, a review of solution approaches for structural simulation and inverse problems is highlighted. For the purpose of consistency of the numerical developments, the available methods are classified into the appropriate classifications, accordingly. In addition, there are many attempts made for solution of inverse problems using wavelet transforms. However, the majority of them only contributed to damage detection problems; the main consideration in this chapter is taken for review of those applications in structural identification problems. Subsequently, some of the novel and earlier researches conducted on application of wavelet functions for both direct and inverse problems are presented.

2.2 Background of wavelet analysis

In general, the primary reference to the wavelet is referred to the early twentieth century Haar (1910), that is cited in Chui (2014). However, many researchers believe that

University of Malaya

fundamentals of the Fourier transforms (FT) have constituted the underlying definitions of wavelet functions. Over the past three decades, the practical applications of wavelet analysis have attracted much attentions among researchers in various disciplines of science and engineering. For the purpose of a brief review of the literature in this context, reference is made to the basic ideas of this powerful tool and relevant past works related to this study. Detailed mathematical definitions and surveys may be found in Refs. (Chui, 1992; Daubechies, 1992; Buades, Coll, and Morel, 2005; Chui, 2014). In addition, some of the underlying definitions and descriptions will be discussed in detail in Chapter 3 of this thesis.

2.2.1 Mathematical transforms

Structural analysis and design have undergone considerable development. In the recent decade, one of the general attempts to accurately modify design codes has been made by adding rigorous design restrictions. In other words, by considering these stringent restrictions, today's design is much more reliable and safer. This idea has led to a significant evolvement in structural engineering, especially in the area of structural simulation, structural health monitoring, structural identification, active and passive control of oscillators and damage detection problems. Moreover, numerical simulation and finite element analysis known as conventional analysis procedures cannot deal with these problems in initial design domains due to the complexity of modeling and then modelling restrictions resulting in excessive computational cost. Consequently, the only alternative option to handle such problems is to implement mathematical transforms (Strang, 1993; Jeffrey, 2001). As it is shown in Figure 2.1, the general idea of transforms is to take a problem from a complex setting domain (i.e., time domain), transform it to an alternative domain (i.e., frequency domain) where the problem can be more readily solved, then operating the inverse transform back to the original domain (Strang, 1993).

University of Malaya

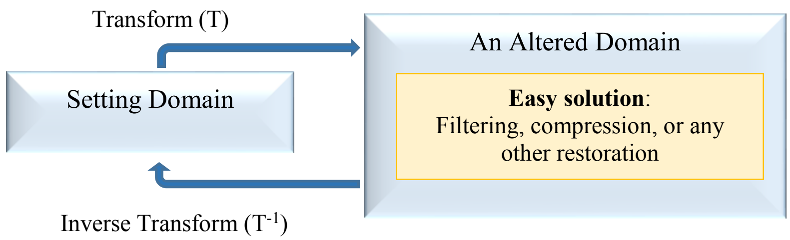

Figure 2.1: The schematic view of operation of transforms

The general idea of integral transform methods was established first by Laplace (1749-1827) and Fourier (1768-1830). Later, the theory of Laplace transform, family of Fourier transform (FT) and wavelet transform (WT) were expanded in order to solve variety of mathematical problems. However, in practical applications the most common transforms are referred to the use of FT and WT, especially for functional approximations and signal processing problems (Debnath and Bhatta, 2014).

2.2.2 Family of Fourier transforms

Basically, either simulated or measured outputs of a structure are represented on the basis of either simulated signals or signals measured by sensors, respectively. In addition, the general form of the foregoing signals is time-domain and thus they are indicated as time series signals (e.g., various forms of time-dependent signals for vibration problems, pressure, temperature, etc.). Fundamentally, an efficient and robust signal processing approach is needed in order to properly extract the dynamic features of aforementioned time-domain signals. Typically, in order to extract the dynamic characteristics of the time-domain signal, it is transferred into another domain of the analysis through a signal processing approach. In this regards, the signal processing aims to extract the dynamic characteristics' information contained within the time series that is otherwise not easily visible in its primary form (Strang, 1993).

Undoubtedly, the most practical integral transform to date is the Fourier transform (FT). It is well-known that a signal can be decomposed by the Fourier transform into its sinusoidal components (Debnath and Bhatta, 2014). One of the main benefits of using the Fourier transform for structural dynamics problems is that several basic features of the system can be directly obtained from the transformed frequency domain. Many studies have been done on application of the Fourier transform for solving differential equations and it is demonstrated that in differentiation problems, high precisions can be accomplished by using the Fourier transform (Haberman, 2013). Brigham (1988) stated that the family of Fourier transform comprised of continuous Fourier transform (CFT), Fourier series (FS), and discrete Fourier transform (DFT) and are being implemented analytically, semi-analytically and numerically, respectively. However, another perspective of the Fourier transform constitutes short-term Fourier transform (STFT) and windowed Fourier transform (WFT).

The CFT can only be applied to analytical functions i.e., signals which are given as continuous functions of time. Hence, it cannot be used for numerical analysis. Heil and Walnut (1989) highlighted that, this is the major drawback of CFT as the majority of the present problems are required to be solved numerically. For instance, in our case study, the signal is obtained as numerical data captured at certain time interval as it happens in most of real and practical engineering situations. Therefore, DFT was introduced in order to improve the numerical representation of FT. However, FS has been commonly used as an intermediate form of FT to solve real problems (Rader, 1968).

The widespread application of the DFT in its early stage was strictly limited due to the high computational cost of the analysis. In order to overcome aforesaid drawback, a more efficient approach, called the Cooley-Tukey algorithm, was introduced (Cooley and Tukey, 1965). This procedure is also referred to the fast Fourier transform (FFT), and what it does is to recursively break down a DFT of a large data sample (i.e., a large N) into a series of smaller DFTs of smaller samples by partitioning the transform with size N into two pieces of size N/2 at each interval.

Fundamentally, two major shortcomings have been reported for the numerical representation of FT, FS, CFT and also DFT. First, the necessity of a periodicity assumption. Second, time information during the time domain is lost and is referred to as the blind processing procedure. In other words, the considered signal should be stationary which impose many restrictions in actual cases (Rioul and Vetterli, 1991). In addition, the most probable phenomena can happen during the calculation of DFT lies on leakage and aliasing phenomena (Körner, 1989; Rioul and Vetterli, 1991). Basically, leakage is the resultant of the discontinuities involved when a signal is extended periodically for conducting the DFT. The only option to prevent leakage phenomena is to apply a window to the signal in order to force it to cover a full period of the signal. However, the window itself may contribute frequency information to the signal. On the other hand, when the Shannon's sampling hypothesis is violated, aliasing phenomena will be occurred (Bracewell, 1965) and causing the real frequency contents to be revealed at different places in the frequency spectrum. In order to solve this issue, it should be ensured that the sampling frequency to be at least twice as large as the maximum frequency content existed in the signal (Oppenheim, Schafer, and Buck, 1989). This requires several initial information which in practical cases is not defined at all.

To overcome the limitations of the Fourier transform, a straightforward solution is to implement an analysis window of certain length that glides through the signal along the time axis in order to perform a time-localized Fourier transform. Such a concept led to the short-time Fourier transform (STFT) introduced by Gabor (1946). Basically, the STFT employs a

University of Malaya

sliding window function that is centered at time interval. For each specific time interval, a time-localized Fourier transform is carried out on the signal within the window. Subsequently, the window is moved by time interval along the time domain, and another Fourier transform is performed. Through such consecutive operators, Fourier transform of the entire signal can be performed. The signal segmentation within the window function is assumed to be approximately stationary. As a consequence, the STFT decomposes a time-domain signal into a 2D time-frequency representation, and variations of the frequency content of that signal within the window function are revealed.

Diverse kinds of window functions have been improved and each of them is especially linked to a particular type of application (Oppenheim et al., 1989). For instance, for analyzing the transient signals the Gaussian window was constructed, and the Hann and Hamming windows are applicable to random signals and narrowband signals, respectively. Furthermore, the Kaiser-Bessel window is better suited for separating two signal components with frequencies very close to each other but with widely differing amplitudes. Cohen (1989) reported that the time and frequency resolutions of the analysis results are directly influenced by the choice of the window function. While higher resolution in general provides better separation of the underlying contents within a signal, the time and frequency resolutions of the STFT technique cannot be chosen arbitrarily at the same time, according to the uncertainty principle.

Experimentally measured signals are generally not known, and therefore the choice of an appropriate window size for effective signal decomposition by using the STFT approach is not guaranteed (Strang, 1993). The inherent shortcoming of the STFT motivates researchers to search for other applicable procedures that are better suited for processing and decomposition of non-stationary signals. One of the robust and popular techniques that has recently attracted much attentions is the wavelet transform.

2.2.3 Wavelet transforms

The conceptual and overall findings of wavelet transforms are reviewed in this subsection. Accordingly, one of the practical applications of wavelets will be elaborated in the next chapter of this thesis. As it was discussed earlier, mathematicians have been persuaded to employ wavelet transforms in order to overcome the shortcomings of family of the Fourier transforms. Haar (1910) developed the first family of wavelet functions comprised of positive and negative pulses (Chui, 2014). However, many researchers have reported that this wavelet function lies on discrete formulation; it is known as the simplest wavelet basis function till now. The basis function of Haar wavelet was used to illustrate a countable orthonormal system for the space of square-integrable functions on the time domain (Haar, 1910). It is also observed that Haar basis functions were used for compressing images (Devore, Jawerth, and Lucier, 1992). Lévy (1954) investigated the Brownian motion through a minor enhancement of Haar wavelets. He discovered that the scale-varying function, that is, the Haar basis function, was better suited than the Fourier basis functions for studying subtle details in the Brownian motion. Several studies have contributed to advancing the state of research in wavelets as it is called today (Littlewood and Paley, 1931; Ricker, 1953; Jaffard, Meyer, and Ryan, 2001). The main advancement was reported by Grossmann and Morlet (1984). They developed and implemented the technique of scaling and shifting of the analysis window functions in analyzing acoustic problems. They found that keeping the width of the window function fixed did not work (Mackenzie, 2001).

The resulting waveforms of varying widths were called by Mallat (1999) the “Wavelet”, and this marked the beginning of the era of wavelet research. Grossmann, Morlet, and Paul (1985) and Grossman, Morlet, and Paul (1986) introduced that a signal could be transformed into the form of a wavelet and then transformed back into its original form without any information loss (the main enhancement of FFT). Basically, the wavelet transform allows one to employ variable window sizes in order to analyze different frequency components within a signal, in contrast to the STFT procedure where the window length is remained constant. This is realized by comparing the signal with a set of template functions obtained from the scaling (i.e. dilation and contraction) and shift (i.e. translation along the time axis) of a base wavelet function and looking for their similarities with the original signal (Mallat, 1999).

Further developments of the theory of wavelet transform have been widely investigated by numerous researchers. Strömberg (2006) worked on discrete wavelets, while Grossmann and Morlet (1984) evaluated random signals in terms of scales and translations of a single base wavelet function, and Newland (1993) worked on harmonic wavelet transforms.

Mallat (1989b; 1989a), Meyer (1989; 1993) and Mallat (1999) invented the most important step that has led to the robustness of the wavelets and it is commonly referred to multi-resolution analysis. Multi-resolution analysis is to design the scaling function of the wavelet such that it allowed other researchers to construct their own basis wavelet functions in a mathematically grounded fashion. For instance, Daubechies (1988; 1992), created her own family of wavelet. She reported that this type of wavelet is orthogonal and can be utilized using simple digital filtering techniques. Significant attempt has been made in order to implement orthogonal functions (series) as the basis wavelet function. The property of orthogonality reduces the size of computations due to ignoring similar calculations in a sense of analysis. One of the popular orthogonal functions is the family of Chebyshev polynomials which lies on the first and second kind of Chebyshev polynomials. Mathematically, Runge phenomena will occur due to the end-point errors of interpolation and approximation. It has been demonstrated that the only option to reduce the effect of Runge phenomena for higher interpolations and approximations is to utilize Chebyshev polynomials (Wickerhauser and Chui, 1994; Razzaghi and Yousefi, 2000; Babolian and Fattahzadeh, 2007).

2.3 Structural dynamics simulation (direct or forward analysis)

Basically, the structural dynamic simulation lies on simulations of the response of the structure to externally applied excitation, the motion of boundary conditions (i.e. support motion) and so on. For a discrete system such as a multi-degrees-of-freedom (MDOF) structure, the governing equilibrium is a set of ordinary differential equations (ODEs) which in general are coupled. Bathe (2006) classified solution techniques for governing equations into mode superposition procedures and direct methods. Hughes (2012) presented that the first category involves decoupling these equations through the linear superposition by modal matrix and commonly called modal analysis.

The modal analysis may be interpreted as an eigenvalue analysis. Bathe and Wilson (1972a) and Bathe and Ramaswamy (1980) introduced matrix iteration method as one of the superior choices in order to solve aforementioned eigenvalue problems. Furthermore, they concluded that, the essence of a mode superposition solution of a dynamic response is that only a small fraction of total number of decoupled equations needs to be considered in order to obtain a good approximation solution to an exact solution. In general, the number of modes to be used for the accurate solution is dependent on the structure considered, the spatial distribution and frequency content of the lateral excitation. It is demonstrated that, assumption of linear behavior of structures is the major drawback for these methods (refers to the basic principle of superposition strategy) and they are impractical for non-linear analysis (Gavin, 2001; Hulbert, 2004).

The next category involves numerical time integration methods whereby the influence of all existing modes are included in the response. Step-by-step time integration methods are being widely considered for the solution of the second-ordered differential equation of motion. In this regards, it is observed that researchers are more interested to the practical and precise numerical integration schemes rather than only theoretical methods; particularly, for solving large-scaled MDOF systems (Chopra, 2001; Hulbert, 2004). Consequently, time integration approaches are the most capable schemes for either non-linear dynamic analysis or time-history evaluation of large-scaled systems (Wilson, Farhoomand, and Bathe, 1972). Moreover, numerical time integration approaches are the only options to solve the second ordered ODEs governing the dynamic equilibrium, because in most cases, the applied excitations are not explicit functions.

Mathematically, numerical time integration procedures have been classified into three aspects as follows:

- ***Direct vs. indirect*** time integration methods: Generally, there are two basic types of step-by-step time integration methods. First, direct integration schemes whereby the quantities of the dynamic system are being calculated through a direct space vector in the step-by-step solution of the equation of motion. Second, indirect integration schemes involving all corresponding equations being numerically transformed into a new space vector, e.g. from the time domain to the frequency domain. Afterwards, a step-by-step vibration analysis is accordingly performed and fulfilled on the current space vector. Background of aforesaid numerical approaches may be found in Dokainish and Subbaraj (1989), Chopra (2001) and Hughes (2012). Basically, Dokainish and Subbaraj (1989), Chung and Hulbert (1994), Chang (2002), Rio, Soive, and Grolleau (2005) and Chang (2010) reported that direct schemes are more effective for structural dynamics, where the response is calculated in set of short time intervals through the accurate approximation

University of Malaya

of complex loadings. As a result, it requires excessive long computational time to gain a desirable time history analysis of either large-scaled or nonlinear structures. Moreover, responses computed by direct algorithms are not sufficiently optimum over the wide range of natural frequencies, i.e., large-scaled space structures (Mahdavi and Razak, 2013). Rostami, Shojaee, and Moeinadini (2011) developed a new family of direct integration methods originated from spline functions. The smooth behavior of spline function for functional approximation led to computationally efficient method. However, the higher ordered functional approximations are not being satisfied.

- ***Explicit vs. implicit*** procedures: The explicit procedures do not require a factorization of the characteristics of the system in the step-by-step solution of the equation of vibration. On the other hand, the implicit schemes require a set of simultaneous linear equations for the time instant solution for vibration analysis (Chang, 2010). Accordingly, it has been inferred that implicit schemes are most effective for structural vibration analysis, in which the response is ascertained by a relatively small number of low frequency modes. In addition, it is reported that these procedures are more popular for the vibration analysis of fluids using longer time steps (Bathe, 2006). As a consequence, the shortcomings of numerical approaches have been revealed when encountering broad-frequency content excitations. In contrast, explicit schemes are very efficient for structural simulation of large systems. Consequently, in shaking or blast problems where a small-time step is needed to evaluate the response of large-scaled models, a practical and optimal algorithm has been implemented through the explicit procedure (Dokainish and Subbaraj, 1989).

  Chang (2002) proposed a pseudo-dynamic algorithm for time integration methods and have demonstrated that it lies on explicit time integration scheme. There have been many researches conducted to improve implicit and explicit time integration methods.

University of Malaya

However, it has been observed that the general classification of those schemes lies on direct time integration algorithms.

- ***Conditionally vs. unconditionally stable*** approaches: Hughes (2012) defined terms conditionally stable to methods that require a time step of analysis (along time domain) smaller than the critical time step and unconditionally stable approaches if the above condition is violated. Prior to this, Bathe and Wilson (1972b) deduced that this critical time step varies for different methods. However, the main criterion for selecting the smallest available time step is the minimum period of a structure. Consequently, the implementation of conditionally stable methods for the analysis of problems which consists high frequencies (for lowest periods are existing) is in fact impractical.

The review of the literature has shown that, a method of time integration may be direct and explicit while it is unconditional or some other combinations. The choice which numerical approach is to be utilized depends on engineering judgment about the physical phenomena being analyzed; external excitation, computational costs and so on. However, it is observed that for the same cases, similar combinations may be employed (Bathe, 2006).

2.4 Structural identification (inverse analysis)

Modelling and simulation of dynamic systems is generally concerned with determining the response of the unknown considered system to some given initial conditions and external excitation. In contrast, for inverse analysis or identification problems, the response of the system is measured and it is of course one of the main contributions to identify unknown systems properties. Over the last two decades, numerous procedures have been developed for efficiently solving inverse problems (Sirca and Adeli, 2012). Most classical identification techniques are being classified into two main categories. Firstly, frequency domain methods

University of Malaya

in which, identification scheme is carried out based on frequency information. Secondly, time domain methods whereby, the identification performed from direct measurement of time-history signal. The detailed comparison of time and frequency domain techniques can be found in Ljung and Glover (1981). They noted that frequency and time domain methods should be viewed as complementary rather than competing and discussed their ease of use under different experimental conditions.

As computer power has increased in recent time, the use of heuristic methods has become possible and thus non-classical methods have received considerable attention. The review of identification methods presented here is categorized into frequency domain methods, time domain methods and non-classical approaches.

2.4.1 Frequency domain methods

Basically, measured frequencies, mode shapes and modal damping ratios are the underlying data required in order to identify the dynamic properties of a structure and correspondingly detect damages in frequency domain. These system properties are commonly obtained by a fast Fourier transform (Cooley and Tukey, 1965; Ewins, 2000). However, Jinwen (2009) implemented the wavelet algorithm to convert dynamic responses from the time domain into frequency information.

2.4.1.1 Frequency based methods

In general, natural frequencies are the basic characteristics of a system and can be obtained using vibration analysis. In order to identify structural damage, one of the common procedures is investigating on shifts in natural frequencies. Cawley and Adams (1979) utilized variations in natural frequencies to identify damage in complex structures. To derive the ratio between frequency shifts for two modes, they proposed a grid between likely

University of Malaya

damage points and created an error term that related measured frequency shifts to those predicted by a modal based on a local stiffness reduction.

Farrar et al. (1994) used the shifts in natural frequencies to identify damage on the I-40 bridge. They observed that shifts in natural frequencies were not adequate for detecting damage of small faults. In order to improve the precision of the natural frequency approach, it was found to be more practical to conduct the experiment in controlled environments where the uncertainties of measurements were comparatively low. One example of such a controlled environment performed is in using resonance ultrasound spectroscopy to measure the natural frequencies and establishes the out-of-roundness of ball bearings (Migliori, 1991). Other satisfactory usages of natural frequencies were obtained by Williams, Messina, and Payne (1997) and Messina, Williams, and Contursi (1998) who successfully utilized the natural frequencies to locate single and multiple damages in a simulated 31-bar truss and tabular steel offshore platform. Damage was imposed to the two systems by reducing the stiffness of the individual bars by up to 30%. This procedure was experimentally evaluated on an aluminum test-rod structure, where damage was imposed by reducing the cross-sectional area of one of the members from 7.9 to 5.0 mm^2.

Further applications of natural frequencies include spot welding by Wang, Shang, Li, and Li (2008) and beam-like structures (Zhong and Oyadiji, 2008; Zhong, Oyadiji, and Ding, 2008). The use of natural frequencies in damage detection necessitates the development of models that can accurately predict natural frequencies. It has been inferred that the first few natural frequencies are easy to measure and represent a physical relationship between stiffness and mass of dynamic systems. Loss of stiffness, representing damage to the structure, is detected when measured natural frequencies are significantly lower than expected (Schulz, Pai, and Abdelnaser, 1996). A useful review on the use of frequencies in detecting structural damage is given in (Salawu, 1997). Foregoing research gives a good overview of frequency methods and also discusses some practical limitations.

There has been considerable discussion as to the change in frequency required to detect damage, and also if changes in frequencies due to environmental effects can be separated from those due to damage. Creed (1987) estimated that it would be necessary for a natural frequency to change by 5% for damage to be confidently detected. Case studies on an offshore jacket and a motorway bridge showed that changes of frequency in the order of 1% and 2.5% occurred due to day to day changes in deck mass and temperature, respectively. Simulations suggested that large damage, for example from the complete loss of a major member would be needed to achieve the desired 5% change in frequencies. Aktan, Lee, Chuntavan, and Aksel (1994) suggested that frequency changes alone do not automatically suggest damage. They reported frequency shifts for both steel and concrete bridges exceeding 5% due to changes in ambient conditions within a single day. They also reported that the maximum change in the first 20 frequencies of a RC slab bridge was less than 5% after it had yielded under an extreme static load.

Moreover, application of frequency-response function (FRF) which is the ratio of the response to excitation in the frequency domain have attracted much attentions among researchers to identify uncertain parameters. The direct use of the frequency-response functions without extracting the modal data to identify faults has become a subject of research by Faverjon and Sinou (2009). Sestieri and Damb (1988) directly applied the frequency-response functions to identify the presence of faults in a truss structure. Imregun, Visser, and Ewins (1995) observed that the direct use of the frequency-response functions to categorize faults in simulated structures, yields certain advantages over the use of modal properties.

The major drawbacks are reported for FRF analysis while they contain more information than is needed for structural identification (Ni, Zhou, and Ko, 2006; Liu, Lieven, and

Escamilla, 2009; Shone, Mace, and Waters, 2009). In addition, Todorovska and Trifunac (2008) and White et al. (2009) concluded that there is no procedure to choose the frequency bandwidth of interest. Eventually, they are generally noisy in the anti-resonance regions (Maia and Esilva, 1997).

2.4.1.2 Mode shape based methods

A mode shape depicts the estimated curvature of a plane vibrating at a given mode corresponding to a natural frequency. The mode shape depends on the nature of the surface and the boundary conditions of that surface. West (1982) used the modal assurance criterion (MAC), a criterion that was used to measure the degree of correlation between two mode shapes to locate damage on a space shuttle orbiter body flap. In applying the MAC, the mode shapes prior to damage were compared to those subsequent to damage. Damage was initiated using acoustic loading. The mode shapes were partitioned and changes in the mode shapes across a range of partitions were subsequently compared. Kim and Bartkowicz (1993) employed the partial MAC (PMAC) and the coordinate modal assurance criterion (COMAC). Salawu (1995) established a global damage integrity index, based on a weighted ratio of the natural frequencies of damaged to undamaged structures. The weights were used to specify the sensitivity of each mode to damage.

According to Steenackers and Guillaume (2006), the main shortcoming of the modal properties is that, they involve some optimization procedures, and therefore they are computationally expensive. Furthermore, mode shape based methods are merely appropriate for linear problems and lightly damped structures (Qiao, Lu, Lestari, and Wang, 2007). Finally, Sazonov and Klinkhachorn (2005), Qiao and Cao (2008) and Fang and Perera (2009) concluded that these approaches are vulnerable to additional noises.

2.4.2 Time domain methods

Fundamentally, because of the low signal to noise ratio, information for higher modes are not reliable and this constitutes the major shortcoming of frequency based methods. Furthermore, the frequency-based approaches generally involve modal superposition and limiting the applications to linear systems. Accordingly, frequencies are reasonably insensitive to local damage as they represent the global property of the structure. As a consequence, identifying and locating damage will be very difficult, particularly when only the first few modes of vibration can be measured. Time domain methods remove the need to extract frequencies and modes and instead make use of the dynamic time-history information directly. In this way, information from all modelled modes of vibration are directly included. Moreover, non-linear models can be identified as there is no requirement for the signal to be resolved into linear components (Perry, 2006). While, Ljung and Glover (1981) presented that frequency and time domain methods should be viewed as complementary rather than rivalling. In addition, its concluded that time domain methods should be adopted, if prior knowledge of the system is available and a model to simulate time-histories is to be obtained. A comprehensive review and comparison of time domain techniques is given in Ghanem and Shinozuka (1995). They categorized time domain methods into classical and non-classical procedures.

2.4.2.1 Classical methods

Maybeck (1982) and Welch and Bishop (2001) compared the performance of extended Kalman filter (Kalman, 1960), maximum likelihood (Ljung and Glover, 1981; Dipasquale and Cakmak, 1990), recursive least squares (Caravani, Watson, and Thomson, 1977; Ling and Haldar, 2004) and recursive instrumental variable methods (Söderström and Stoica, 2002). Aforementioned methods commonly known as classical methods. In addition, the classical methods were compared by Shinozuka and Ghanem (1995) according to the expertise required i.e., numerical convergence, on-line potential, sensitivity to initial guess and reliability of results. They found that while more sophisticated algorithms, such as the extended Kalman filter, gave more accurate results, they were more sensitive to initial guess and did not always converge.

Furthermore, a Bayesian approach is a procedure based on Bayes' Theorem (Beck and Katafygiotis, 1998) and functions for conducting statistical inference through using the evidence (observations) to update the probability that a hypothesis may be true (Marwala, 2002). Vanik, Beck, and Au (2000) applied Bayesian approaches for structural identification of a bridge model using sensor data, while Marwala and Sibisi (2005) applied this algorithm in beam structures. Zheng et al. (2009) applied a Bayesian approach for the identification of a long-span, steel sky-bridge. Hemez and Doebling (1999) successfully applied a Bayesian approach to solve inverse problems and applied this to linear dynamics, while Lindholm and West (1996) applied a Bayesian parameter approximation for the solution of inverse problem and applied this to model experimental dynamic response data.

Kitagawa (1996) proposed Monte Carlo filter (MCF) for structural identification problems. He presented that structural parameters are being derived by obtaining recursively the conditional distribution function of the state variable when observation values up to the present time step are given. A modified approach called the adaptive MCF method was developed by Sato and Chung (2005). In addition, Mares, Mottershead, and Friswell (2006) successfully applied Monte Carlo method for stochastic model updating.

There are substantial discussions been reported on application of gradient search methods under classical procedures. Bicanic and Chen (1998) proposed a Gauss-Newton least square method. Liu, Frangopol, and Kim (2009) derived an approach originated from Newton's method for structural identification problems. It is observed that these methods have the drawbacks such as the need of good initial guess and gradient information which in actual inverse problems cannot be obtained. More importantly, aforementioned classical methods tend to be ineffective in the presence of noise, because they lack global search capability and tend to converge prematurely to local optima (Liu and Chen, 2002).

2.4.2.2 Non-classical methods

It is observed that for an efficient structural identification using classical methods, a desirable initial guess for unknown parameters is essential. In addition, classical methods are very sensitive to signal-to-noise ratio and this limits the practical applications. Beside these drawbacks in the use of classical methods, it is very probable for the optimizer to converge to the local optima. Moreover, many classical methods work on transformed dynamic models, such as state-space models, where the identified parameters lack physical meaning. Koh, Hong, and Liaw (2003) stated that this may often make it difficult to extract and separate physical quantities such as mass and stiffness. Moreover, a recent trend of research is towards identification of large systems with many unknown parameters as possible. For large systems many classical methods suffer the ill-condition problem and the difficulty of convergence increases drastically due to numerous unknown parameters.

With the increase in computational speed available, non-classical methods have become increasingly popular. In particular, the use of heuristic-based non-classical schemes has become very attractive. For instance, artificial neural networks (NN), based on the networks present in the brain, and genetic algorithms (GAs), developed on Darwin's theory of survival of the fittest have received considerable attention in recent years. The identification strategy proposed in this thesis is based on enhancement of genetic algorithms using adaptive wavelet functions.

University of Malaya

In principal, genetic algorithms differs from traditional search strategies in several ways; first, they work with a coding of the parameter set rather than the parameters themselves. Second, they search from a population of points and not a single point. Third, they work based on probabilistic rules rather than deterministic ones. Fourth, they use an objective function rather than derivatives or other auxiliary information. Furthermore, GAs have a high level of concurrency and thus very suitable for distributed programming (Michalewicz, 1996).

More recently, the application of GA in civil engineering has attracted tremendous interest from researchers. The main strength of GA is the better capability to escape from local optima to find the global optima solution compared to many other available methods. Furuta et al. (2006) adopted an improved multi-objective GA to develop a bridge management system that can facilitate practical maintenance plan. The proposed cost-effective decision-support system was verified via the investigation on a group of bridge. Okasha and Frangopol (2009) incorporated redundancy in lifetime maintenance optimization based system reliability.

Marwala (2002) successfully applied a genetic algorithm to minimize the distance between the measured wavelet data and predicted parameter using wavelet data. The drawback of his approach for structural identification was the associated high computational expense of the GA simulation and the wavelet processing of the vibration data used.

Akula and Ganguli (2003) applied structural identification, based on genetic algorithms to helicopter rotor-blade design. Perera and Ruiz (2008) successfully applied a GA-based, structural identification for damage identification in large-scale structures, while Tu and Lu (2008) enhanced GA applications by considering artificial boundary conditions and Franulović, Basan, and Prebil (2009) implemented a GA for material model parameter identification for low-cycle fatigue.

University of Malaya

Other recent successful applications of GA include Balamurugan, Ramakrishnan, and Singh (2008) who evaluated the performance of a two-stage adaptive GA, enhanced with island and adaptive features in structural topology optimization, while Kwak and Kim (2009) successfully implemented a hybrid genetic algorithm, enhanced by a direct search for optimum design of reinforced concrete frames.

Perry (2007) developed a robust GA strategy for identifying parameters of dynamic systems. The identification strategy that he proposed, works at two levels. At the first level, a modified GA based on migration and artificial selection, using multiple species and operators to search the current search space for suitable parameter values. At the second level, a search space reduction method using the results of several runs in order to reduce the search space for those parameters that converged quickly. The search space reduction allowed further identification of the parameters to be conducted with greater accuracy and improved convergence of the less sensitive system parameters. However, the core of proposed GA for computation of fitness functions was adopted for average Newmark time integration method and from computational point of view, the proposed scheme was not satisfactory optimum.

Liu et al. (2009) applied fuzzy theory for structural identification. In their research, the model parameters and design variables were modeled as fuzzy variables and this technique was successfully implemented on an actual concrete bridge.

Jung and Kim (2009) implemented a hybrid genetic algorithm for system identification and tested this procedure on a numerical bridge model. A hybrid genetic algorithm was formed by combining a genetic algorithm with Nelder-Mead simplex method. The proposed technique was found to be effective on the identification of bridge structures.

Tan, Qu, and Wang (2009) applied support vector machines and wavelet data for inverse problems. The result obtained from the simulated data validated that this approach could successfully update the model.

Marano, Quaranta, and Monti (2011) modified a GA multi-species strategy to enhance the computational performance of simple genetic algorithms for structural identification. They implemented the modified GA procedure for identification of up to 50 story shear buildings. However, the convergence rate of results obtained by their method was outstanding. From the computational point of view, their identification procedure relies on a costly approach. This is due to the inner fitness evaluations for each particular species.

From the review of the literature, it has been concluded that the combination of coding, population points, blindness to auxiliary information and randomized operators give GAs the robustness required for implementation in wide range of problems such as identification of structures with many unknown parameters. However, observations on implementation of the simple GAs for simple problems (only one unknown) have demonstrated that, the computational time for more unknowns would be prohibitive and still many refinements are needed to make the GA strategy work efficiently.

On the other hand, neural networks (NN) work by combining layers of 'neurons' through weighted connections. At each neuron the weighted inputs are processed using some simple function to determine the output from the neuron. A fundamental NN usually comprises three layers, including an input layer, hidden layer and output layer. By correct weighting of the links and simple functions at the neurons, the inputs can be fed through the network to arrive at the outputs for both linear and non-linear systems. One of the strong points of NN lies in the fact that they can be trained. This means that through some process the network can adjust its weights to match given input/output sequences. This pattern recognition ability has allowed the application of NN to artificial intelligence applications. There have been several training methods developed for NN. One of the most popular training procedures is the back propagation algorithm. This involves feeding the errors at the output layer back through the net to adjust the weights on each link. Other methods such as the probabilistic NN have also

University of Malaya

been developed. An example of the application of NN to structural identification is given in Chen et al. (1990). They used multilayer NN for the identification of non-linear autoregressive moving average with exogenous inputs systems. Ko, Ni, and Chan (1999) and Ko and Ni (2005) inferred that the main drawback of NN for large scale systems identification is that huge amount of data are required to properly train the network prior to analysis. A lack of some patterns of data will cause the identification to return incorrect values.

Zapico, González, Gonzalez, and Alonso (2008) also applied non-classical method of NN for structural identification. The results showed that the updated finite element model could accurately predict the low modes that were identified from measurements.

2.5 Applications of wavelet functions

2.5.1 Structural simulation (direct or forward analysis)

One of the very popular basis functions to solve dynamical problems is the family of Haar wavelets. Haar basis function as a rectangular pulse pair was presented with Alfred Haar in 1910. Although in 1980s it was derived that the Haar function is the first order of Daubechies Wavelet; it is concluded that Haar basis is the simplest basis for wavelet analysis in numerical problems (Farge, 1992; Goedecker and Ivanov, 1998). Haar wavelet is not continuous and at the point of discontinuity, the derivatives do not exist. Hence, it is impossible to use this wavelet directly to solve high-ordered differential equations. Although, Lepik (2009) and Yuanlu (2010) used the practice of this discrete wavelet to solve several fractional differential equations. Moreover, the efficiency of Haar wavelet method was demonstrated by Lepik (2008b) in order to solve higher order differential equations.

In general, there are two possibilities to overcome the essential shortcoming of discrete Haar wavelet. Firstly, the piecewise constant Haar functions can be regularized with interpolation splines. This method that has been applied by Cattani (2004), greatly complicates the solution. Second convenient solution to utilize this wavelet is using the integral method, which the highest derivative objections in the differential equation are expanded into the Haar series. This approximation is integrated where the boundary conditions are incorporated by using integration constants. This approach has been considered for the Haar wavelet by Chen and Hsiao (1997) and an optimal control problem with the quadratic performance index was discussed by Cattani (2004).

In addition, Haar discrete wavelet transforms have been utilized by Cattani (2004) to achieve three main goals: first, in order to filter the data without removing localized effective changes which is capable in the case of structural engineering to shorten components of complicated loadings such as earthquake to achieve an optimum structural dynamic scheme. Second, to classify the detected jumps, and finally, in order to obtain a smooth trend to represent the time series evolution.

According to the technique of Chen and Hsiao (CHM), either linear differential equation or non-linear one are converted into an algebraic equation. Fundamentally, in time-history analysis of structures, durations of time intervals are very important to gain the stable responses. The main advantage of CHM method for solving structural dynamic problems is the possibility of using longer time increments, especially for problems where complicated loads such as base excitations are applied. In this regards, the use of longer time steps with many collocation points constitutes the accurate wavelet operational matrices in order to achieve desirable responses. Basically, in order to accomplish an adaptive analysis, time intervals are being divided into many collocation points for accurately capturing all dynamic

University of Malaya

properties (i.e., frequency contents). This procedure is referred to the “Segmentation Method” (SM) in the literature (Hubbard, 1998; Lepik, 2005).

Obviously, for smooth loadings (i.e. harmonic loadings) in order to reduce computational complexity and computation time involved, the time interval of integration requires to be divided into fewer points (Salajegheh and Heidari, 2005b), this method is called reduced Haar transform (Galli, Heydt, and Ribeiro, 1996). Meanwhile, in the reduced Haar transform technique the number of collocation points in each segment is smaller than that of in the CHM method. Consequently, for some specific and simple loadings, further simplification of the solution can be obtained as long as a segment is being divided into only one interval. It is assumed that the highest derivative is constant in each segment. This method is called Piecewise Constant Approximation (PCA) (Chen and Hsiao, 1997). Overall, review of the literature shows that for structural dynamic problems implementation of continues wavelet basis functions is inevitable to achieve the most adaptive and cost-effective analysis, while the Haar basis is discrete and mathematically cannot be used for higher derivatives.

More recently, orthogonal polynomials have received significant attention in dealing with dynamical systems of partial (Dahmen, Kurdila, and Oswald, 1997), ordinary (Babolian and Fattahzadeh, 2007; Lepik, 2008a; 2008b) or fractional differential equations (Benedetto, 1993; Heydari, Hooshmandasl, Maalek Ghaini, and Fereidouni, 2013). The main property of such series (i.e., family of Chebyshev and Legendre polynomials) is that, it converts these problems to solving a system of linear algebraic equations, whereby, the repeated and redundant calculations are neglected during the process of analysis and greatly simplifying the problem. In fact, one may conclude that, a family of wavelet functions are being constructed by developing diverse versions of orthogonal polynomials. Consequently, the effective characteristics of wavelets, such as localization properties and multi-resolution

University of Malaya

analysis, can be broadly extended in the use of such polynomials for solving dynamical problems.

The surveys on some of the earlier studies are reported in Dahmen et al. (1997), Fan and Qiao (2009) and Fang and Perera (2009). Theoretically, wavelet functions are categorized into two main categories. The first being the two-dimensional (2D) wavelets, whereby a definite basis function of wavelet is being shifted for all scaled functions. The second category comprises three-dimensional (3D) wavelets, which involves the use of a developed wavelet basis function for each new scale of the mother wavelet. Subsequently, a signal with broad-band frequency content is examined precisely by 3D wavelets rather than 2D ones (Mahdavi and Razak, 2013). In other words, the details of the signal (i.e., frequency contents) are accurately captured by a set of adaptive collocation points (Vasilyev and Paolucci, 1997). In this definition, scale, transition and time are expressed as individual dimensions, respectively. Moreover, the application of the family of Haar wavelets, known as a family of 2D wavelets, has attracted much attention for solving dynamic problems due to its simplicity. Due to the inherent properties of this wavelet, several shortcomings have been reported for this technique in order to solve dynamic problems. For instance, Mahdavi and Shojaee (2013) proposed an indirect algorithm because of the point of discontinuity existing at the middle point of Haar basis functions, thus major errors are recorded. However, because of the very simple basis function of this 2D wavelet, faster computations can be achieved.

On the other hand, 3D wavelets are employed for many linear or non-linear variation problems. However, no specific attention has been given to the capability of different 3D wavelet functions for structural dynamic problems (Mason and Handscomb, 2002; Babolian and Fattahzadeh, 2007). Three of those wavelets, such as Chebyshev wavelets of the first and second kind and Legendre wavelets have been effectively implemented for solving time varying problems. Essentially, two main gaps are observed from these contributions. Firstly,

University of Malaya

the considered time instant of the analysis is confined to the unity for only scalar variables, hence, the proposed schemes are not applicable in actual cases, involving long-time dynamic analysis of large-scaled problems. Secondly, the feasibility and capability of those wavelets (which in terms of inherent properties are very similar) have not been examined, comparatively.

There are several studies have been conducted on application of wavelet functions in order to de-noise the size of time-history data either the measured and simulated data or the lateral excitation. Proposed procedures lie on a pre-operating process prior to ordinary solution of dynamic equilibrium governing the structures (Salajegheh and Heidari, 2003; 2005a; 2005b). Consequently, an adaptive strategy has not been improved for time-history analysis simultaneous with reduction of the data size. It is predicted that, an optimum dynamic analysis will be achieved by using such adaptive algorithms especially for large scale structural systems.

Mahdavi and Razak (2015b) introduced an indirect time integration method for dynamic analysis of large-scaled space structures originated from adaptive wavelet functions. The proposed scheme lies on unconditionally stable method, hence, there is no requirement for selecting time interval lesser than a prescribed time step. They recognized that, adaptive wavelet functions states for the possibility of using different basis functions corresponding to different frequency contents in various scales (referring to multi-resolution analysis associated for diverse sets of collocation points). As a result, the computational costs are significantly reduced for dynamic analysis of large scale space structures.

2.5.2 Structural identification and damage detection

Since last two decades, due to the powerful characteristics of wavelet analysis, its applications for solving inverse problems have become the focus of interest in various

University of Malaya

disciplines of structural engineering. Different aspects of wavelet analysis have been established. Quek, Wang, Zhang, and Ang (2001) contributed to the sensitivity analysis using wavelet functions. They examined the sensitivity of wavelet technique in the detection of cracks in beam structures. The effects of different crack characteristics, boundary conditions, and wavelet functions employed, were investigated. Crack characteristics studied included the length, orientation and width of slit. The two different boundary conditions considered were simply supported and fixed-end support, and the two types of wavelets compared were the Haar and Gabor wavelets. It was demonstrated that, the wavelet transforms are more practical in damage detection problems. Moreover, they concluded that this powerful tool is one of the useful tools in detection of cracks in beam structures.

Several researchers proposed wavelet method in order to extract modal parameters. Zhong and Oyadiji (2011) presented an approach based on the difference of the continuous wavelet transforms (CWTs) of two sets of mode shape data which corresponded to the left half and the right half of the modal data of a cracked simply-supported beam. The simulated and experimental results showed that the proposed method has great potential in crack detection of beam-like structures as it does not require the modal parameter of an un-cracked beam as a baseline for crack detection.

Kougioumtzoglou and Spanos (2013) developed an identification approach for linear and non-linear time-variant systems subject to non-stationary excitations based on the localization properties of the harmonic wavelet transform. According to their method, first the system model is transformed into an equivalent multiple-input/single-output system in the wavelet domain. Next, time and frequency details generalized a set of harmonic wavelet-based frequency response functions.

Mahdavi and Razak (2015a) proposed a robust wavelet technique to improve iterative approaches for the solution of inverse problems. Subsequently, an efficient method is developed to compute operation of derivative, appropriate for computation of second ordered derivatives. They concluded that, their scheme is suitable for the solution of highly varying non-linear problems.

Ren and Sun (2008) combined the wavelet transform with Shannon entropy to detect structural damage from measured vibration signals. They defined damage features such as wavelet entropy, relative wavelet entropy and wavelet-time entropy. Subsequently, they investigated the proposed damage features for detecting and locating structural damages. It was demonstrated that, wavelet-time entropy is a sensitive damage feature in detecting the abnormality in measured successive vibration signals, while relative wavelet entropy was a good damage feature to detect damage occurrence and damage location through the vibration signals measured from the intact (reference) and damaged structures. In addition, they concluded that the relative wavelet entropy method is flexible in choosing the reference signal simultaneously measured from any undamaged location of the target structure.

Notwithstanding the bulk of reports on damage detection strategies using the superior features of wavelet functions (referring to the sensitivity property), there are less studies performed on structural identification problems. Zabel (2003) presented a method for structural identification based on wavelet packet transforms. His method was performing to compute the wavelet coefficients corresponding to the measured signals and it was originating solely from a fixed wavelet basis function. Accordingly, in order to solve the dynamic equilibrium through an inverse problem the simple genetic algorithm and least square were implemented. However, there are many questions should be answered on the use of his proposed strategy i.e., the problem of ill-conditioning of the algebraic system encountering with large values for identified stiffness compared to very small values of wavelet coefficients. Eventually, from the computational cost point of view, the use of his method seems to be not reasonably practical, as it should be performed at very large sampling rates (short time intervals).

2.6 Discussion

In general, from the review of the literature can be concluded that, the computational competency of available strategies for solving both structural simulation and inverse problems plays the underlying role in achieving a practical procedure. In other words, many of conducted studies are not reliable for especially large scale problems with many unknowns to be identified. On the other hand, it has been observed that wavelet solution technique can be very optimum one in structural dynamic problems as long as being adaptive with the problem considered. The emphasis is selecting the most adaptive wavelet basis function in order to solve different problems. The overall gaps inferred from the review of the literature are as following:

- There is no report on the application of wavelets in structural dynamics problems capable of using compatible collocation points for capturing entire details (i.e., frequency components) associated to the simple and complex problems.
- The implementation of different wavelet basis functions in structural dynamics problems has not been thoroughly investigated. In addition, the evaluation of their computational performance for solving structural simulation problems is sparsely addressed in the literature.
- So far, no report is available on the stability and accuracy analysis of wavelet-based methods in forward structural dynamics problems.
- The review of the literature indicated the lack of investigation on developing the wavelet-based techniques in structural identification problems, especially for complex cases

involving a comprehensive identification such as mass, stiffness, damping and force identification. It has been observed that wavelets are more practical in only damage detection problems in frequency domain. However, the employment of wavelets for both structural identification and damage detection problems in time domain has not been sufficiently addressed in the literature.

- So far, there is no report on the modification of non-classical procedures in time domain for structural identification and damage detection problems in order to achieve the most optimum strategy. It has been observed that, the main consideration is taken on improving the convergence of non-classical methods, however, improving the computational competency (referring to the cost of the analysis) has not been sufficiently addressed for time domain procedures. In addition, the majority of damage detection algorithms suffer from false detection, and therefore the location of damages will not be confidently detected as fast as it should be practical in real cases. For this reason, in most real cases the identification and damage detection are being performed several times to ensure precise and reliable results. Consequently, the use of a cost-effective approach for a reliable identification and damage detection is not only worthwhile but also inevitable.

It can be inferred that, the convergence and computational competency of results are interpreted as the sufficient and necessary conditions in order to investigate the robustness of any structural simulation and identification strategy. It is anticipated that, once the computational efficiency and convergence of the structural simulation (direct analysis) are significantly developed by using adaptive wavelet functions, the solution of inverse problems will be considerably improved.

University of Malaya

2.7 Chapter summary

Based on the literature review presented in this chapter, many numerical time integration methods have been introduced by researchers. It is observed that, the computational efficiency is the fundamental criterion for choosing a procedure for solving practical problems. However, the aforementioned feature of a time integration method is directly dependent to the dynamic problems considered. For this reason, there is a need to develop a robust time integration method compatible with the existing characteristics of structural systems i.e., the scale of structure and frequency components of external excitation.

The proposed method should be unconditional stable and explicit to achieve the optimum results for either direct problems or inverse problems. In this definition, optimum expresses the high computational performance of the proposed method. In addition, to simplify the solution of large scale systems, an indirect time integration is more effective than direct integration methods while most of the time the externally applied load lies on the complex one. As the major challenge is the frequency components of the both sides of the dynamic equilibrium i.e., frequency components of excitation (right side) as well as inherent properties of the structure (left side), the proposed method will be efficient as long as it is based on frequency transformations. On the other hand, as time domain methods for structural identification are more practical than frequency domain procedures, undoubtedly, the information along time domain should be recorded. Consequently, the application of Fourier transforms is impractical while the time information are lost during the analysis. There is no evidence on the improvement of such numerical method for solving either structural dynamics or inverse problems.

It can be concluded from the review of the literature that, by using multi-resolution feature of 2D and 3D wavelets, an adaptive time integration scheme can be developed with the most

University of Malaya

satisfactory results. In other words, an adaptive numerical approach will be improved capable of capturing details in the vicinity of highly varying structural responses. Accordingly, as an indirect integration method, all equations are being numerically transferred into the corresponding frequency domains, concurrent with the numerical integration scheme. Significantly, current transformation has made the prosperity of this procedure over the other numerical schemes, particularly, when a broad-frequency-content loading has been approximated in terms of its frequency contents in step-by-step piecewise approach.

Accordingly, in the context of inverse problems, the literature revealed that the major drawback of frequency based methods is that for real structures information for higher modes of vibration will be unreliable due to low signal to noise ratio. In addition, the methods usually involve modal superposition limiting the application to linear systems. Finally, frequencies are a global property and are reasonably insensitive to local damage. Identifying and locating damage is therefore very difficult, particularly when only the first few modes of vibration can be measured. In contrast, time domain methods remove the need to extract frequencies and modes and instead make use of the dynamic time-history information directly. In this regards, information from all modelled modes of vibration are directly included. Moreover, non-linear models can be identified as there is no requirement for the signal to be resolved into linear components. Consequently, a wavelet-based indirect time integration technique for solving inverse problems in time domain will be concerned in this research, however, the proposed procedure is not blind on frequency contents. This argument can be interpreted as the time-scale-frequency characteristic of the wavelet-based strategy.

Furthermore, structural identification problems will be considerably improved by using the aforesaid time integration method through an inverse problem. While the majority of studies till now, have contributed to the only damage detection strategies using the robust

University of Malaya

features of wavelets. In addition, there is a lack of investigation on practice of various wavelet functions in a sense of analysis to achieve an adaptive and cost-effective analysis.

From the review of the literature it can be inferred that, the heuristic and non-classical strategy of genetic algorithm can be considered as an effective method in order to solve inverse problems, provided that the computational competency of this algorithm is increased. The emphasis is on the capability of this strategy for identification of many unknown parameters i.e., mass, damping, stiffness and force. There is no report received in the literature for the enhancement of this strategy by using adaptive wavelet functions. The especial attention can be drawn on the employment of various wavelet functions for capturing entire details of measured data at longer time intervals concurrent with the running of the main algorithm for identification. It is observed that, the computational cost plays the underlying role to solve actual and real structural health monitoring problems. Consequently, developing a computationally efficient approach in this context is inevitable in order to overcome many issues encountered in structural health monitoring problems.

University of Malaya

CHAPTER 3: STRUCTURAL DYNAMICS

3.1 Introduction

Over the last two decades, application of wavelet technique has been the focus of interest in various domains of science and technologies. Particularly, engineers are interested in the wavelet solution method in time series analysis. This Chapter presents an explicit and indirect time integration method for structural dynamic problems capable of using 2-dimensional (2D) Haar wavelets, free-scaled Chebyshev wavelets of the first (FCW) and second kind (SCW) and Legendre wavelets (LW) known as 3D wavelet functions. For this purpose, the dynamic equilibrium governing single-degree-of-freedom (SDOF) and multi-degrees-of-freedom (MDOF) structures is efficiently approximated by wavelet functions. A clear cut formulation is derived for transforming differential equations into the corresponding algebraic systems using wavelet operational matrices. A converter coefficient is developed to extend operations of wavelets from local time to global time. A detailed assessment is carried out on the stability, accuracy and computational efficiency of responses calculated by FCW, SCW and LW. Furthermore, an optimal operator of derivative is developed using wavelet functions on adaptive collocation points.

Subsequently, the capability of the proposed approach is examined using several examples, and results are compared with those of the common numerical integration schemes, such as Hilbert-Hughes-Taylor (HHT-α), Wilson-θ, family of Newmark-β and central difference method. Accordingly, to investigate the cost of analysis as the indication of computational competency, CPU computation time involved is also considered in order to evaluate the computational efficiency corresponding to each numerical time integration method.

3.2 Solution of direct problems (forward analysis)

In this section, a wavelet-based approach is developed in order to solve structural dynamics problems (forward problems). For this purpose, the fundamentals of wavelet analysis utilized in this thesis are briefly discussed, initially. Later, the proposed procedures are consecutively presented. It should be noted here that, the proposed method is capable of using any wavelet basis function. However, in this study the free scales of 2D Haar wavelets, family of 3D Chebyshev wavelets and 3D Legendre wavelets are implemented.

3.2.1 Fundamentals of wavelet analysis

In this section, a brief background on wavelet functions is presented. Mathematically, the various versions of scaled and transformation of the mother wavelet $\psi(\tau)$ construct a family of wavelet functions. The main representation of the family of continuous wavelets is given as (Babolian and Fattahzadeh, 2007; Chui, 1995; S. Mallat, 1999):

$$\psi_{a,b}(\tau) = |a|^{-0.5}\psi\left(\frac{\tau - b}{a}\right) \quad , a, b \in \Re, a \neq 0 \tag{3.1}$$

where, a and b denote the scale and transition of the corresponding mother wavelet, respectively. Generally, wavelets those constituted by diverse transitioned scales of any basis function, i.e., different orders of Haar, Legendre or Chebyshev polynomials, have four arguments of $\psi_{a,b}= \psi(k', n, m, \tau)$. The indicator of transition k' can be any positive integer, n denotes the relevant scale, m is the order (degree) of the corresponding polynomials and τ indicates the local time of the wavelet.

In addition, Mahdavi and Shojaee (2013) presented that wavelet functions are theoretically characterized into two main categories. The first being the 2D wavelets whereby a definite basis function of wavelet is being shifted for all scaled functions. The other category is 3D

University of Malaya

wavelets involving used of an improved wavelet basis function being shifted on each new scale of the mother wavelet. Subsequently, a signal with wide-band frequency components is evaluated accurately by 3D wavelets rather than 2D ones, where scale, transition and time are expressed as dimensions, respectively. Consequently, for 2D wavelet functions such as family of Haar wavelets the order of polynomial is constant.

Basically, a function is decomposed by transition of the scaled wavelets on global time interval of t_i to t_{i+1} (i=0,1,2,….). This global time instant is divided into many subdivisions relevant to the degree of the corresponding wavelet. The idea of dividing the time domain into multiple partitions appropriate to the time-scaled-frequency analysis is known as Segmentation Method (SM) (Cohen, Dahmen, and DeVore, 2003; Gurley and Kareem, 1999). The main purpose of SM is to define several adaptive collocation points on the main setting domain (global points of t_i along the time domain), and therefore to relate components of those to the new alternative domain of the analysis (local points τ_i in frequency domain). In this study, $2^{k'-1}M$ is assumed as the number of partitions in each global time interval (in referring to the SM collocation points) and the corresponding wavelets are constructed by m= 0, 1, 2,… ,($2^{k'-1}M/2^{k'-1}$)-1 order of the considered polynomials. Accordingly, local times τ_i are defined through the concept of SM as follows:

$$\tau_i = \left({}^{1}\!/_{2^{k'-1}M}\right)(i - 0.5) \qquad , \quad i = 1, 2, 3, \dots, 2^{k'-1}M \tag{3.2}$$

M denotes the order of wavelet. Moreover, it is to be pointed out that in this study, $k' = 2$ is presumed for all derivations and calculations referring to the initial transition functions.

3.2.1.1 2D Haar wavelet functions

The simple family of Haar wavelet was presented by Alfred Haar in 1910 for $t \in [0,1]$ as follows (Lepik, 2005, 2008c, 2009a, 2009b):

$$h_{m-1}(t) = \begin{cases} 1 & t \in \left[\dfrac{a}{2^j} \quad , \quad \dfrac{a+0.5}{2^j}\right] \\ -1 & t \in \left[\dfrac{a+0.5}{2^j} , \dfrac{a+1}{2^j}\right] \\ 0 & \quad otherwise \end{cases} \tag{3.3}$$

where;

$$m = 2^j + a + 1\,, \quad j \geq 0\,, \quad 0 \leq a \leq 2^j - 1 \tag{3.4}$$

where, $M = 2^j(j = 0, 1, \dots, j)$ denotes the order of wavelet; $a = 0, 1, \dots, M - 1$ is the value of transition. In Equation (3.3), $m = 1$ and $m = 2$ indicate scale function and mother wavelet of Haar, respectively. As it was mentioned earlier, the signal is examined by scaled and delayed wavelet from t_i to t_{i+1} (known as global time; i = 0, 1, 2, …), and dividing this interval to many partitions corresponding to the order of wavelet. As a result, as long as a global time interval is partitioned to shorter subdivisions of time interval, a set of segments will collectively cover the whole signal. For the case of Haar wavelet $2M = 2^{j+1}$ denotes the 2^jth scale of Haar wavelet (Mahdavi and Shojaee, 2013).

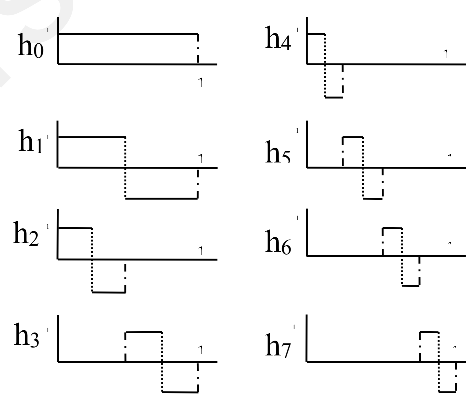

Figure 3.1: Different scales of Haar wavelets as scaled and transitioned pulse functions.

As it is apparent from Figure 3.1, the simple 2D Haar family is constituted from shifting the scale function of mother Haar wavelet corresponding to $m = 2$.

University of Malaya

3.2.1.2 First kind of 3D Chebyshev wavelets

The sequence of orthogonal Chebyshev polynomials are categorized into two main kinds. The first kind of Chebyshev polynomials $T_m(t)$ is defined by a recursive equation as follows (Mason and Handscomb, 2002):

$$T_0(t) = 1, \; T_1(t) = t, \qquad T_{m+1}(t) = 2t\, T_m(t) - T_{m-1}(t), \qquad m = 1, 2, \ldots \tag{3.5}$$

where, the orthogonality of polynomials $T_m(t)$ is satisfied with respect to the weight function $\omega(t) = 1/\sqrt{1-t^2}$ on $|t| < 1$.

Subsequently, Chebyshev wavelets of the first kind (FCW) are developed by substituting $T_m(t)$ in Equation (3.1) as follows (Babolian and Fattahzadeh, 2007):

$$\psi_{n,m}(t) = \begin{cases} (2^{k'/2}).\tilde{T}_m(2^{k'}t - 2n + 1), & \frac{n-1}{2^{k'-1}} \leq t < \frac{n}{2^{k'-1}} \\ 0 & Otherwise \end{cases} \tag{3.6}$$

where;

$$\tilde{T}_m(t) = \begin{cases} 1/\sqrt{\pi} & m = 0 \\ \sqrt{2/\pi}T_m(t) & m > 0 \end{cases} \tag{3.7}$$

where, in this study m= 0,1,2, …, $M-1$ and n= 1,2, …, $2^{k'-1}$imply the order of corresponding polynomials and the considered scale of the wavelet, respectively. $T_m(t)$ implies the recursive formula in Equation (3.5) corresponding to different orders of m. Accordingly, the aforementioned weight function of $\omega(t)$ is dilated and therefore transitioned as $\omega_n(t) = \omega(2^{k'}t - 2n + 1)$ in order to calculate orthogonal Chebyshev wavelets of the first kind (FCW).

3.2.1.3 Second kind of 3D Chebyshev wavelets

Chebyshev polynomials of the second kind $U_m(t)$ are defined by the recurrence relation of (Maleknejad, Sohrabi, and Rostami, 2007; Wang and Fan, 2012):

$$U_0(t) = 1,\ U_1(t) = 2t, \qquad U_{m+1}(t) = 2t\, U_m(t) - U_{m-1}(t), \quad m = 1, 2, \ldots \tag{3.8}$$

The weight functions of $\omega(t) = (2/\pi)\sqrt{1-t^2}$, ($|t| < 1$) satisfy the orthogonal relation between different orders of $U_m(t)$. Accordingly, the second kind of Chebyshev wavelets (SCW) are constructed as follows:

$$\psi_{n,m}(t) = \begin{cases} (2^{k'/2}).\, \widetilde{U}_m(2^{k'}t - 2n + 1), & \dfrac{n-1}{2^{k'-1}} \leq t < \dfrac{n}{2^{k'-1}} \\ 0 & Otherwise \end{cases} \tag{3.9}$$

where, $\widetilde{U}_m(t) = \sqrt{2/\pi}U_m(t)$ and arguments of k', n and m are the same as introduced before. Furthermore, for different degrees of m, $U_m(t)$ is defined from Equation (3.8).

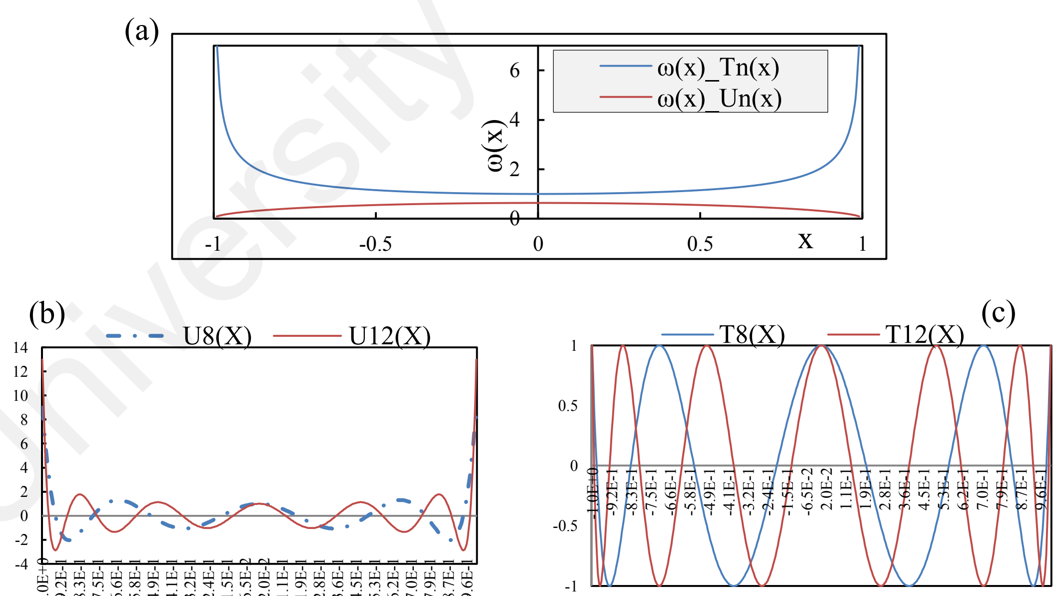

Figure 3.2: (a) Weight functions, (b) shape functions for the 8th and 12th order, (c) shape functions for the 8th and 12th order corresponding to the first ($\boldsymbol{T_n(x)}$) and second (($\boldsymbol{U_n(x)}$)) kind of Chebyshev polynomials.

University of Malaya

Similarly, delayed and transitioned weight functions of $\omega_n(t) = \omega(2^{k'}t - 2n + 1)$ are improved in order to calculate orthogonal SCWs.

Moreover, the shape functions for the 8th and 12th orders, corresponding to the first ($T_n(x)$) and second ($U_n(x)$) kind of Chebyshev polynomials as well as the weight functions are depicted in Figure 3.2.

3.2.1.4 3D Legendre wavelets

In mathematics, Legendre polynomials of m^{th} degree $L_m(t)$ are orthogonal with respect to the weight function of $\omega(t) = 1$ and are obtained by the following recursive formula (Razzaghi and Yousefi, 2000, 2001; Yousefi and Razzaghi, 2005):

$$L_0(t) = 1,\ L_1(t) = t,\ L_{m+1}(t) = \frac{(2m+1)}{(m+1)} t\, L_m(t) - \frac{m}{(m+1)} L_{m-1}(t), \quad m = 1, 2, \ldots \tag{3.10}$$

Subsequently, the family of Legendre wavelets are expressed as follows:

$$\psi_{n,m}(t) = \begin{cases} (m + 1/2)^{1/2}. L_m\left(2^{k'}t - 2n + 1\right), & \dfrac{n-1}{2^{k'-1}} \le t < \dfrac{n}{2^{k'-1}} \\ 0 & Otherwise \end{cases} \tag{3.11}$$

where, for diverse orders of m, $L_m(t)$ is obtained from Equation (3.10). It should be noted that, the nominations are similar for parameters of transition (k'), scale (n) and the order of corresponding polynomials and wavelets. The 2nd and 8th orders of Legendre polynomials and Chebyshev polynomials of the first and second kind are depicted in Figure 3.3.

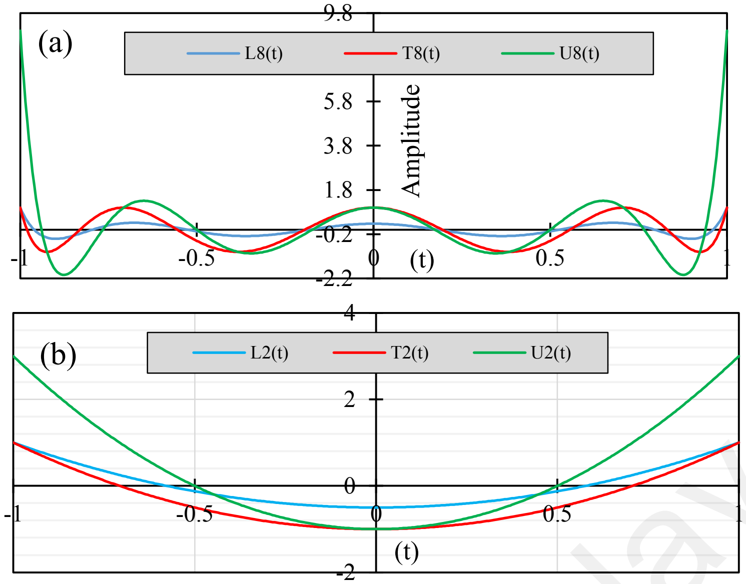

Figure 3.3: The mth degree of Chebyshev polynomials of the first ($T_m(t)$) and second kind ($U_m(t)$) and Legendre polynomials ($L_m(t)$). (a) m=8, (b) m=2.

As it is shown in Figure 3.3, the major amplitude of y-axis is covered by the second Chebyshev polynomials, however, the fluctuated patterns are converged at point zero of t-axis. As an initial inference, the widest band of frequencies can be captured by the family of wavelets, which are originated by this polynomials (in referring to SCW) rather than Legendre or the first Chebyshev wavelets (FCW).

3.2.1.5 Functional decomposition and operational matrix of integration

In subsequent sections, the derivation of wavelet coefficients and the operation matrix P of integration corresponding to 2D Haar wavelet and 3D FCW, SCW and LW are introduced.

3.2.1.5.1 2D Haar wavelet function

Basically, signal $f(t)$ can be decomposed in 2D Haar series as (Lepik, 2005):

$$f(t) \cong \sum_{i=0}^{2M} c_i h_i(t) \tag{3.12}$$

Accordingly, Haar coefficients c_i $(i = 0, 1, 2, \ldots)$ are defined by:

$$c_i = 2^j \int_0^1 f(t)\, h_i(t) dt \tag{3.13}$$

Hence, H_{2M} is a square matrix $(2M \times 2M)$, including the first $2M$ scales of Haar wavelet; Haar coefficients are directly given as:

$$c_i = f(t) H_{2M}^{-1}(t) \tag{3.14}$$

Equivalently, signal $f(t)$ may be rewritten as:

$$f(t) \cong c_{2M}^T H_{2M}(t) \tag{3.15}$$

Subsequently, integration of H_{2M} is obtained by Haar series with new square coefficient matrix of integration P_{2M} as (Lepik, 2005; Mahdavi and Shojaee, 2013):

$$\int_0^1 H_{2M}(t) dt \approx P\, H_{2M}(t) \tag{3.16}$$

It should be noted that, local times are calculated relatively to the scale of wavelet as:

$$\tau_l = \frac{l - 0.5}{2M}\ , \qquad l = 1, 2, \ldots, 2M \tag{3.17}$$

Finally, the local time divisions (τ_l), are adapted to the global domain. Assumption of d_t as global time interval one may obtain (Lepik, 2005):

$$t_{lt} = d_t(\tau_l) + t_t \Rightarrow \tau_l = \frac{t_t - t_{lt}}{d_t}\ , \qquad l = 1,2, \ldots, 2M \tag{3.18}$$

3.2.1.5.2 3D wavelet functions

Fundamentally, any quadratically-integrable function $f(t)$ may be expanded in terms of FCW, SCW or Legendre wavelets (LW) for $t \in [0,1)$ as (Babolian and Fattahzadeh, 2007; Razzaghi and Yousefi, 2001):

$$f(t) = \sum_{n=1}^{\infty} \sum_{m=0}^{\infty} c_{n,m} \psi_{n,m}(t) \tag{3.19}$$

Integrating both sides of Equation (3.19), and then multiplying by the components of wavelets, corresponding wavelet coefficients are being obtained as follows (the orthogonality is satisfied by employing the weight functions of $\omega_n(t)$):

$$c_{n,m} = \left(\psi_{n,m}(t), f(t), \omega_n(t)\right) = \int_0^1 \omega_n(t) \psi_{n,m}(t)\, f(t) dt \tag{3.20}$$

Subsequently, the function $f(t)$ can be decomposed by the truncated series of a wavelet's family as follows (Babolian and Fattahzadeh, 2007; Razzaghi and Yousefi, 2001):

$$f(t) \cong \sum_{n=1}^{2^{k'-1}} \sum_{m=0}^{M-1} c_{n,m} \psi_{n,m}(t) = C^T \Psi(t) \tag{3.21}$$

where, C denotes the coefficients vector of the relevant wavelets, i.e., FCW, SCW or Legendre wavelets, and the corresponding wavelet function vector is designated by $\Psi(t)$ as:

$$\begin{aligned} C = \left[c_1, c_2, c_3, \ldots, c_{2^{k-1}}\right]^T_{2^{k'-1}M\times 1} \quad &\Leftrightarrow \quad c_i \\ &= [c_{i0}, c_{i1}, c_{i2}, \ldots, c_{i,M-1}]^T, \qquad i = 1,2,\ldots, 2^{k'-1} \end{aligned} \tag{3.22}$$

$$\begin{aligned} \Psi(t) = \left[\psi_1, \psi_2, \psi_3, \ldots, \psi_{2^{k-1}}\right]^T_{2^{k'-1}M\times 1} \quad &\Leftrightarrow \quad \psi_i(t) \\ &= [\psi_{i0}(t), \psi_{i1}(t), \psi_{i2}(t), \ldots, \psi_{i,M-1}(t)]^T \end{aligned} \tag{3.23}$$

Eventually, a $2^{k'-1}M \times 2^{k'-1}M$-dimensional matrix of $\phi_{n,m}(t)$ is formed as:

University of Malaya

$$\phi_{n,m}(t) = [\Psi(t_1)\ \ \Psi(t_2)\ \ \dots\ \Psi(t_i)]_{2^{k'-1}M\times 2^{k'-1}M} \tag{3.24}$$

The square matrix $\phi_{n,m}(t)$ is populated with vectors of wavelet functions for a set of discrete SM local points $(t_i,\ \ i = 1, 2, 3, \dots, 2^{k'-1}M)$.

It is assumed that the integration of $\Psi(t)$ can be obtained as (assumption of $k' = 2$) :

$$\int_0^1 \Psi_{2M}(t)\,dt = P_{2M}\Psi(t) \tag{3.25}$$

In Equation (3.25), the subscripts of Ψ_{2M} and P_{2M}indicate the dimensions of matrices. Correspondingly, the $2^{k'-1}M \times 2^{k'-1}M$-dimension operational matrix *P* for FCW, SCW and LW, which plays the underlying role in dealing with solution of differential equations is derived as ($k' = 2$) (Babolian and Fattahzadeh, 2007; Razzaghi and Yousefi, 2000):

$$P_{2M} = \frac{1}{2^{k'}}\begin{bmatrix} [L]_{\frac{2M}{2}\times\frac{2M}{2}} & [F]_{\frac{2M}{2}\times\frac{2M}{2}} & F & \dots & F \\ [O]_{\frac{2M}{2}\times\frac{2M}{2}} & [L]_{\frac{2M}{2}\times\frac{2M}{2}} & F & \dots & F \\ O & O & \ddots & \ddots & \vdots \\ \vdots & \vdots & \dots & \ddots & F \\ O & O & \dots & O & L \end{bmatrix} \tag{3.26}$$

where, $\frac{2M}{2}\times\frac{2M}{2}$ square matrices *F* and *L* are given as follows ($[O]$ shows a zero matrix):

$$F = \begin{bmatrix} 2 & 0 & 0 & \dots & 0 & 0 \\ 0 & 0 & 0 & \dots & 0 & 0 \\ a_1 & 0 & 0 & \dots & 0 & 0 \\ 0 & 0 & 0 & \ddots & \vdots & \vdots \\ \vdots & \vdots & \vdots & \vdots & \ddots & \vdots \\ a_2 & 0 & \dots & \dots & 0 & 0 \end{bmatrix},$$

$$L = \begin{bmatrix} 1 & a_6 & a_9 & a_{12} & \dots & 0 & 0 & 0 \\ a_3 & 0 & a_{10} & a_{13} & \dots & 0 & 0 & 0 \\ a_4 & a_7 & 0 & a_{14} & \dots & 0 & 0 & 0 \\ a_5 & a_8 & a_{11} & 0 & \dots & \vdots & \vdots & \vdots \\ \vdots & \vdots & \vdots & \vdots & \ddots & \vdots & \vdots & \vdots \\ \vdots & \vdots & \vdots & \vdots & \vdots & \ddots & \vdots & \vdots \\ a_{15} & 0 & 0 & \dots & \dots & a_{17} & \ddots & a_{19} \\ a_{16} & 0 & 0 & \dots & \dots & 0 & a_{18} & 0 \end{bmatrix} \quad (3.27)$$

Generally, it is inferred from Equations (3.26) and (3.27) that, there is a similar population for components of *P* corresponding to considered wavelets. In details, particular coefficients of a_i are derived for FCW, SCW and LW, and tabulated in Table 3.1. It should be kept in mind that $\frac{2M}{2}$ implies $2^{k'-1}M/2^{k'-1}$. To calculate operation matrix of *P* for FCW, SCW and LW, a backward algorithm of program coding is recommended. In other words, only the first four rows and columns of *P* are being calculated, initially. At the second stage, the components of *P* are being calculated and replaced from the last row and column $\frac{2M}{2}$ th until computation of the 5th row and column. To clarify the expression of wavelets parameters of FCW, SCW and LW, matrices of $\phi_{4,4}$ and $P_{4,4}$ are computed and shown in Table 3.2 for $k' = 2, \frac{2M}{2} = 2$.

Table 3.1: Coefficients of a_i, defined in Equation (3.27) corresponding to FCW, SCW and Legendre wavelets ($2M/2 = M$).

$\boldsymbol{a_i}$	Legendre wavelet	FCW	SCW
a_1	0	$-2\sqrt{2}/3$	$2/3$
a_2	0	$\frac{\sqrt{2}}{2}(\frac{1-(-1)^M}{M} - \frac{1-(-1)^{M-2}}{M-2})$	$\left\|\sin(\frac{M\pi}{2})\right\| \frac{2}{M}$
a_3	$-\sqrt{3}/3$	$-\sqrt{2}/4$	$-3/4$
a_4	0	$-\sqrt{2}/3$	$1/3$
a_5	0	$\sqrt{2}/4$	$-1/4$
a_6	$1/\sqrt{3}$	$1/\sqrt{2}$	½
a_7	$-\sqrt{5}/(5\sqrt{3})$	$-1/2$	$-1/6$
a_8	0	0	0
a_9	0	0	0
a_{10}	$\sqrt{3}/(3\sqrt{5})$	¼	¼
a_{11}	$-\sqrt{7}/(7\sqrt{5})$	$-1/4$	$-1/8$
a_{12}	0	0	0
a_{13}	0	0	0
a_{14}	$\sqrt{5}/(5\sqrt{7})$	$1/6$	$1/6$
a_{15}	0	$\frac{\sqrt{2}}{2}(\frac{(-1)^{M-3}}{M-3} - \frac{(-1)^{M-1}}{M-1})$	$(-1)^{M-2}\frac{1}{M-1}$
a_{16}	0	$\frac{\sqrt{2}}{2}(\frac{(-1)^{M-2}}{M-2} - \frac{(-1)^{M}}{M})$	$(-1)^{M-1}\frac{1}{M}$
a_{17}	$-\frac{(2M-3)^{1/2})}{(2M-3)(2M-5)^{1/2}}$	$\frac{-1}{2(M-3)}$	$-\frac{1}{2(M-1)}$
a_{18}	$-\frac{(2M-1)^{1/2}}{(2M-1)(2M-3)^{1/2}}$	$\frac{-1}{2(M-2)}$	$-\frac{1}{2M}$
a_{19}	$\frac{(2M-3)^{1/2}}{(2M-3)(2M-1)^{1/2}}$	$\frac{1}{2(M-1)}$	$\frac{1}{2(M-1)}$

Note: FCW= first Chebyshev wavelet, SCW= second Chebyshev wavelet.

University of Malaya

Furthermore, from the computational time point of view, Equation (3.27) and Table 3.1 demonstrate that the cost of computation of F and therefore P for LW (because of its scaled weight functions) is less than either FCW or SCW, in which that, the whole arrays are zeros (except for the first one). Significantly, the foregoing point is highlighted when higher degrees of polynomials and scales of wavelets are employed. Basically, this is due to the simple weight function $\omega = 1$ of Legendre polynomials in contrast to the variable weight functions of FCW and SCW. Accordingly, it will be shown later that the total CPU time for solving especially large-scaled structures using free scales of LW is less than that of using FCW or SCW. However, from accuracy point of view, variable weight functions of FCW and SCW lead to less errors of end points of integration and resulting in more precise results compared to the results obtained with LW.

3.2.1.6 Comparison of 2D and 3D wavelet functions

In this subsection, the characteristic of 2D Haar wavelet has been compared with FCW known as a 3D wavelet function. It should be kept in mind that the characteristics of FCW, SCW and LW are very close, so only FCW is considered here in order to reasonably compare 2D and 3D wavelets.

3.2.1.6.1 Inherent characteristics

As it was mentioned before, each particular scale of corresponding wavelet is constituted by an improved wavelet function, related to the corresponding polynomial for 3D wavelets. In other words, provided that scales of functions are being increased, basis functions will be respectively developed.

University of Malaya

Table 3.2: Corresponding components of wavelets $\phi_{i,j}$ and P, calculated on four SM points for 2D Haar wavelet, 3D FCW, SCW and LW.

Column *i*		1		2		3		4	
Row ***i***		$\phi_{i,j}$	$P_{i,j}$	$\phi_{i,j}$	$P_{i,j}$	$\phi_{i,j}$	$P_{i,j}$	$\phi_{i,j}$	$P_{i,j}$
1	HA	1.0000	0.5000	1.0000	-0.2500	1.0000	-0.1250	1.0000	-0.1250
	FCW	1.1284	0.2500	1.1284	0.1768	0	0.5000	0	0
	SCW	1.5958	0.2500	1.5958	0.1250	0	0.5000	0	0
	LW	1.4142	0.2500	1.4142	0.1442	0	0.5000	0	0
2	HA	1.0000	0.2500	1.0000	0	-1.0000	-0.1250	-1.0000	
	FCW	-0.7979	-0.0884	0.7979	0	0	0	0	0
	SCW	-1.5958	-0.1875	1.5958	0	0	0	0	0
	LW	-1.2247	-0.1442	1.2247	0	0	0	0	0
3	HA	1.0000	0.0625	-1.0000	0.0625	0	0	0	0.1250
	FCW	0	0	0	0	1.1284	0.2500	1.1284	0.1768
	SCW	0	0	0	0	1.5958	0.2500	1.5958	0.1250
	LW	0	0	0	0	1.4142	0.2500	1.4142	0.1442
4	HA	0	0.0625	0	-0.0625	1.0000	0	-1.0000	0
	FCW	0	0	0	0	-0.7979	-0.0884	0.7979	0
	SCW	0	0	0	0	-1.5958	-0.1875	1.5958	0
	LW	0	0	0	0	-1.2247	-0.1442	1.2247	0

Note: HA=Haar wavelet, FCW= first Chebyshev wavelet, SCW= second Chebyshev wavelet, LW= Legendre wavelet.

University of Malaya

Figure 3.4 shows the first 8 scales of Haar and Chebyshev families. It can be seen from Figure 3.4(a) that, for the 8^{th} scale of Haar family, the simple basis function has been just compressed and afterward has been delayed from the first position. In contrast, Figure 3.4(b) shows the broad-band frequency function of the 8^{th} scale of Chebyshev that will be moved along the time axis.

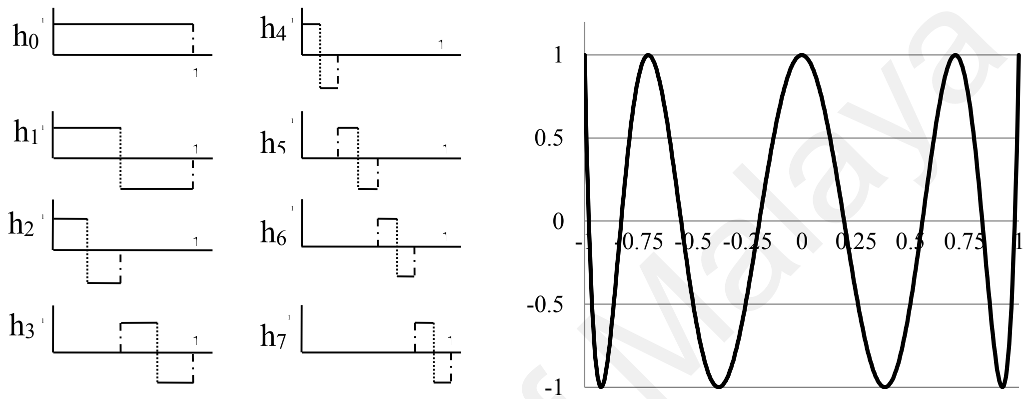

Figure 3.4: Comparison of the first 8^{th} scales of wavelet functions, (a) 2D Haar family, (b) 3D Chebyshev polynomial.

Additionally, the shortcoming of Haar wavelet is shown in Figure 3.4(a) at the point of 0.5, which the continuity is not satisfied at this point. According to a mathematical rule, the second derivation will not exist at the point of 0.5. As a result, it is just possible to implement an indirect formulation for solving the second-ordered differential equation of motion. Consequently, as will be shown in this chapter, large values of errors have been computed by using free-scaled Haar wavelet functions through the direct practice of the proposed scheme. However, with far lesser CPU time taken (analysis cost) that will be discussed later.

3.2.1.6.2 Functional approximation

Fundamentally, optimum structural dynamics can be achieved through a wavelet-based approach involving two parts of numerical analysis. Firstly, the external loading is accurately approximated according to its frequency contents simultaneously with numerical time

University of Malaya

integration procedure. Secondly, differential equations are accurately converted to an algebraic system by wavelet functions on a corresponding set of collocation points, even with a long time step. Consequently, it is inferred that accuracy of results are directly dependent on accurate approximation of equations.

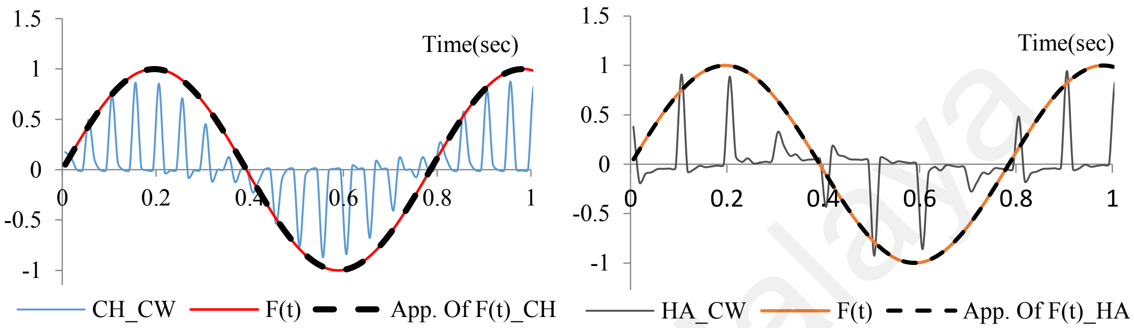

Figure 3.5: Approximation of F(t) and wavelet coefficients for the first 8th scale of (a) FCW, (b) Haar wavelet, at the first second of F(t) and $\boldsymbol{\omega}$=8 rad/sec (CH_CW= coefficients of FCW, HA_CW= coefficients of Haar wavelet, App. of F(t)_CH/HA= approximation of F(t) using Chebyshev/Haar wavelet).

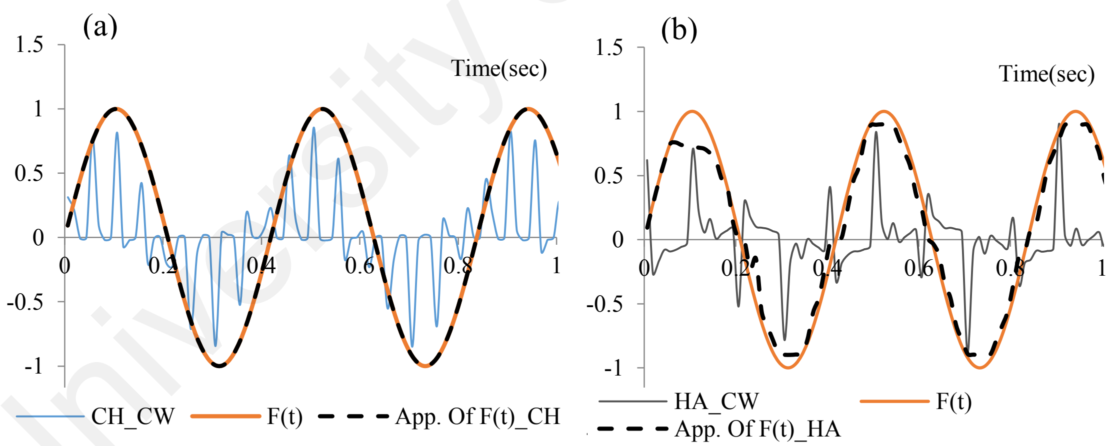

Figure 3.6: Approximation of F(t) and wavelet coefficients for the first 8th scale of (a) FCW, (b) Haar wavelet, for the first second of F(t) and $\boldsymbol{\omega}$=15 rad/sec (CH_CW= coefficients of FCW, HA_CW= coefficients of Haar wavelet, App. of F(t)_CH/HA= approximation of F(t) using Chebyshev/Haar wavelet).

In order to evaluate the accuracy of approximation by using wavelet functions, the first 8^{th} scale of Haar wavelet and FCW are exemplified for three different frequency-content

University of Malaya

signals, accordingly. For this purpose, a sinusoidal function of $F(t)= \sin(\omega t)$ is examined for ω equal to 8, 15 and 500 rad/sec, at the first second of excitation, respectively.

Figure 3.5 shows that the accuracy of approximation for ω=8 rad/sec through the calculated coefficients of FCW (designated by CH_CW) is more than Haar wavelet. The corresponding function is also examined to be almost accurate with Haar wavelet (coefficients of Haar wavelet are designated by HA_CW). Additionally, Figure 3.6 illustrates the capability of 8^{th} scale of 3D FCW which is a low scale of this wavelet, compared with acceptable decomposition by using the same-scaled 2D Haar wavelet. Despite the undesirable approximation of Haar wavelet for ω=15 rad/sec, from its optimization point of view the results could be interpreted as acceptable approximation. Finally, Figure 3.7(b) shows the rejected results through the 8^{th} scale of Haar wavelet, encountering with a high frequency-content signal with ω=500 rad/sec. It is clearly shown in the figure that the 128^{th} scale of Haar wavelet gave sufficient accuracy of approximation. However, with a very long computation time involved. Overall, figures demonstrate the efficiency of low-scaled FCW; although, for the case of $\boldsymbol{\omega}$=500 rad/sec higher scales shall be utilized in order to obtain accurate results.

University of Malaya

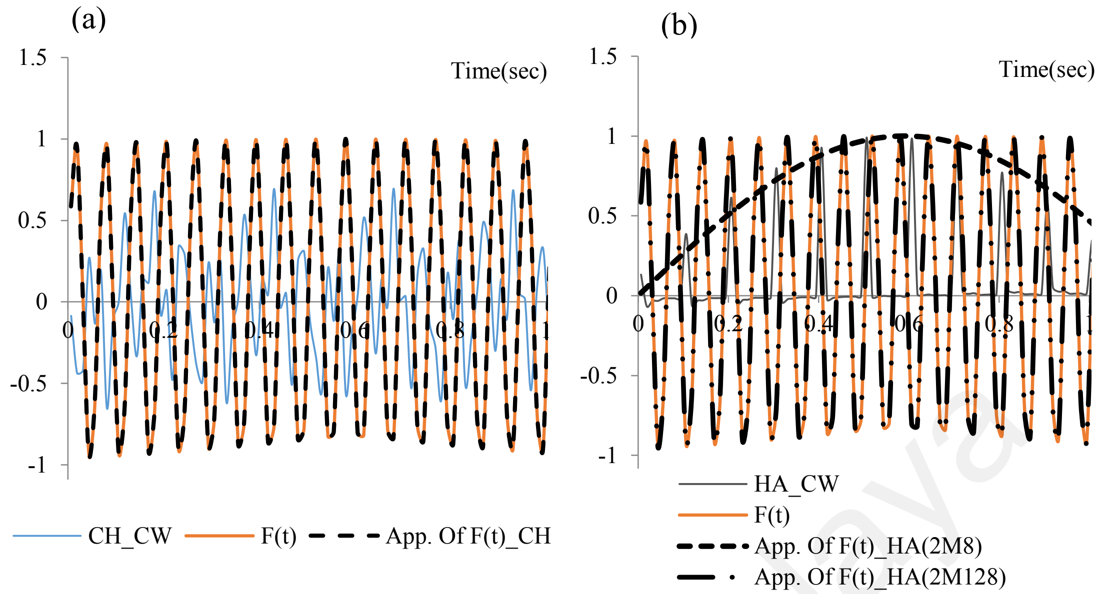

Figure 3.7: Approximation of F(t) and wavelet coefficients for the first 8th scale of (a) FCW, (b) Haar wavelet, for the first second of F(t) and $\boldsymbol{\omega}$=500 rad/sec (CH_CW= coefficients of FCW, HA_CW= coefficients of Haar wavelet, App. of F(t)_CH= approximation of F(t) using FCW, App. of F(t)_HA(2M8/128)= approximation of F(t) using the first 8/128th scale of Haar wavelet).

3.2.2 The proposed method for dynamic analysis of SDOF structures

Generally, the linear dynamic equilibrium (ordinary differential equation) governing the SDOF system of mass (m), damping (c) and stiffness (k) is expressed as follows (Hughes, 2012):

$$(m)\ddot{u}(t) + (c)\dot{u}(t) + (k)u(t) = F(t) \tag{3.28}$$

where, $\ddot{u}(t)$, $\dot{u}(t)$ and $u(t)$ denote acceleration, velocity and displacement vectors of response to the external dynamic load of $F(t)$, respectively. Using Equation (3.12) for 2D wavelets or Equation (3.19) for 3D wavelets, acceleration vectors can be decomposed on $2M$ adaptive (SM) points of analysis corresponding to Haar wavelet, FCW, SCW or LW as:

$$\ddot{u}(t) \cong \sum_{n=1}^{2^{k'-1}} \sum_{m=0}^{M-1} c_{n,m}\psi_{n,m}(t) = C^T\Psi(t) \tag{3.29}$$

In addition, $\Psi(t)$ represents the operation vector of FCW, SCW or LW, which can be replaced by $h(t)$ for Haar wavelet. Subsequently, using Equation (3.25) the first and second orders of integration vectors, namely, velocity and displacement vectors are approximated as (let $\dot{u}_n = v_n$initial velocities and u_n initial displacements):

$$\dot{u}(t) = C^T P\Psi(t) + v_n \tag{3.30}$$

$$u(t) = C^T P^2\Psi(t) + u_n \tag{3.31}$$

It is to be noted that, $u_n$and $v_n$are a constant initial value in global time interval of $d_t = t_{i+1} - t_i$. Furthermore, the numerical algebraic equation in Equations (3.30) or (3.31) is satisfied by decomposition of unity for $2M$ adaptive points of FCW, SCW and LW as follows:

$$1 \cong I^*\Psi(t) \cong D[1_{1,1}, 0,0, \dots, 1_{1,M+1}, 0,0, \dots]\Psi(t) \tag{3.32}$$

where, D=$\sqrt{\pi/4}$, $\sqrt{\pi/8}$ and $\sqrt{1/2}$ for FCW, SCW and LW, respectively.

It should be emphasized that, the size of vector in I^* is $1 \times 2M$. For FCW, SCW and LW, the first component and $(2M/2)$+1 are one. Similarly, for Haar wavelet it is also determined as:

$$1 \cong I^*h(t) \cong [1_{1,1}, 0,0, \dots, 0,0,0, \dots, 0_{1,2M}]h(t) \tag{3.33}$$

Therefore, the constant values of initial displacement and velocity (calculated from previous step) are approximated by corresponding wavelets as (designated by $S_2^T\Psi(t)$ and $S_1^T\Psi(t)$):

$$S_1^T \Psi(t) = v_n \times 1 \cong v_n I^* \Psi(t)$$
$$\cong v_n D\left[1_{1,1}, 0,0, \dots, 1_{1,M+1}, 0,0, \dots\right]\Psi(t) \tag{3.34}$$

$$S_2^T \Psi(t) = u_n \times 1 \cong u_n I^* \Psi(t) \tag{3.35}$$
$$\cong u_n D\left[1_{1,1}, 0,0, \dots, 1_{1,M+1}, 0,0, \dots\right]\Psi(t)$$

Quantities of velocity and displacement vectors are numerically developed on $2M$ points by substituting Equations (3.34) and (3.35) into Equations (3.30) and (3.31) as follows:

$$\dot{u}(t) = C^T P \Psi(t) + S_1^T \Psi(t) \tag{3.36}$$

$$u(t) = C^T P^2 \Psi(t) + S_1^T P \Psi(t) + S_2^T \Psi(t) \tag{3.37}$$

On the other hand, the external excitation $F(t)$, which most of the time (in actual cases) is a wide-band frequency content signal, can be decomposed with Haar wavelet, FCW, SCW or LW as follows:

$$F(t) = f^T \Psi(t) \tag{3.38}$$

The applied signal known as external loading of $F(t)$ may be constructed by several sets of discrete 1× $2^{k'-1}M$-dimensional vectors corresponding to $2M$ points of global time. Thus, coefficients vector of f^T is obtained for each separate vector as follows:

$$f^T_{1\times 2^{k'-1}M} = F_{1\times 2^{k'-1}M} / \phi_{(2^{k'-1}M)\times\left(2^{k'-1}M\right)} \tag{3.39}$$

Substituting Equations (3.36), (3.37) and (3.39) into Equation (3.28), the dynamic equilibrium is numerically developed as:

$$(m)[C^T \Psi(t)] + (c) d_t [C^T P \Psi(t) + S_1^T \Psi(t)]$$
$$+ \ (k) {d_t}^2 [C^T P^2 \Psi(t) + S_1^T P \Psi(t) + S_2^T \Psi(t)] \tag{3.40}$$
$$= \ {d_t}^2 f^T \Psi(t)$$

In addition, quantities of the dynamic system are transformed from the alternative domain of analysis ($2M$ local times of wavelets) into the setting domain ($2M$ global times) by multiplying d_t to each operation of derivative. This implementation makes the proposed scheme applicable for analysis of time domains larger than unity. Eventually, $\Psi(t)$ is omitted from the both sides of Equation (3.40), and the algebraic system is improved as follows:

$$(m)[C^T] + (c)d_t[C^T P + S_1^T] \;+\; (k){d_t}^2[C^T P^2 + S_1^T P + S_2^T] \\ = \; f^T {d_t}^2 \tag{3.41}$$

Calculating coefficient vectors of wavelets (C^T for Haar wavelet, FCW, SCW or LW) from Equation (3.41) and substituting into Equations (3.30) and (3.31), quantities of displacement and velocity vectors are computed corresponding to $2M$ global points for each wavelet function.

In theory, it is clearly distinguishable that vibration equations are being approximated undesirably with 2D Haar wavelets, because of its inherent simple shape function. However, in practice to gain the optimal time vibration analysis by taking into consideration the least computation time involved, this simple wavelet can be utilized for initial predictions.

3.2.3 The proposed method for dynamic analysis of MDOF structures

In structural dynamic problems, the constant values of mass (m), damping (c) and stiffness (k) relevant to a SDOF system are replaced by matrices of mass $[M]_{d\times d}$, damping $[Cd]_{d\times d}$ and stiffness $[K]_{d\times d}$ corresponding to the considered MDOF system with d degrees of freedom, subjected to the vector of applied forces of $\{F_t\}$. Hence, the dynamic equilibrium is developed as:

$$[M]_{d\times d}\ddot{U}^t_{d\times 2M} + [Cd]_{d\times d}\dot{U}^t_{d\times 2M} \;+\; [K]_{d\times d}U^t_{d\times 2M} = \{F_t\}_{d\times 2M} \tag{3.42}$$

The subscripts of $\ddot{U}_{d\times 2M}^{t}$, $\dot{U}_{d\times 2M}^{t}$ and $U_{d\times 2M}^{t}$ denote $d \times 2M$-dimensional acceleration, velocity and displacement vectors related to $2M$ adaptive collocation points of global time corresponding to each degree of freedom (DOF), respectively. Accordingly, the expansion of Equation (3.29) is employed for each DOF. Initial conditions corresponding to each DOF is also approximated with wavelet functions using Equations (3.34) and (3.35). Moreover, nodal forces are also decomposed by using Equation (3.39) on each DOF. Eventually, the convertor of local times to global times is executed by multiplying d_t, and therefore Equation (3.42) is numerically developed as:

$$[M]\begin{bmatrix} C_1^T\Psi(t) \\ \vdots \\ C_d^T\Psi(t) \end{bmatrix} + [Cd]d_t\begin{bmatrix} C_1^T P\Psi(t) + S_{1-1}^T\Psi(t) \\ \vdots \\ C_d^T P\Psi(t) + S_{1-d}^T\Psi(t) \end{bmatrix} + [K]d_t^2\begin{bmatrix} C_1^T P^2\Psi(t) + S_{1-1}^T P\Psi(t) + S_{2-1}^T\Psi(t) \\ \vdots \\ C_d^T P^2\Psi(t) + S_{1-d}^T P\Psi(t) + S_{2-d}^T\Psi(t) \end{bmatrix} = d_t^2\begin{bmatrix} f_1^T\Psi(t) \\ \vdots \\ f_d^T\Psi(t) \end{bmatrix} \tag{3.43}$$

Eliminating $\Psi(t)$ from the both sides, Equation (3.43) is represented as a vector for each row corresponding to each DOF (1-d) and $j = 1,2,\dots,d$ we have:

$$\sum_{i=1}^{d}[M]_{ji}C_i^T + d_t\sum_{i=1}^{d}[Cd]_{ji}(C_i^T P + S_{1-i}^T) + {d_t}^2\sum_{i=1}^{d}[K]_{ji}(C_i^T P^2 + S_{1-i}^T P + S_{2-i}^T) = {d_t}^2 f_j^T \tag{3.44}$$

Assumption of $I_{2M\times 2M}$ as an identity matrix, Equation (3.44) is simplified as follows:

$$C_i^T([M]_{ji}I + d_t[Cd]_{ji}P + {d_t}^2[K]_{ji}P^2) = {d_t}^2 f_j^T - \sum_{i=1}^{d}[d_t[Cd]_{ji}S_{1-i}^T + {d_t}^2[K]_{ji}(S_{1-i}^T P + S_{2-i}^T)] \tag{3.45}$$

University of Malaya

Calculating coefficients vectors of wavelet C_i^T $(i = 1,2, \dots, d)$ for each DOF in Equation (3.45), and therefore using Equations (3.31) and (3.30), velocity and displacement vectors are obtained corresponding to each DOF.

Note that in large-scaled linear systems, due to the sequence in the node numbering, the coefficient matrix on the left side of Equation (3.45) is nearly singular. Thus, it is recommended to solve the coefficients of wavelet in the above algebraic system using singular value decomposition (SVD) method. However, for many applications, simple decomposition techniques are applicable, i.e., the Choleski factorization method. The step-by-step algorithm of the proposed method is tabulated in Table 3.3.

To achieve an optimum analysis, it is recommended to determine $d_t = \Delta t \leq 2 \times T_{min}$ (T_{min}= minimum period of system), as long as the stability of results is satisfied. For this reason, the stability analysis is essential for the proposed method. The statement of optimum analysis refers to an accurate analysis with lesser computation time involved, and therefore lesser amounts of storage capacity (namely, the optimum cost of analysis). It is to be noted that, the sampling rate of external loading shall be considered as another important criteria to specify $2M$ and d_t.

University of Malaya

Table 3.3: Step-by-step algorithm to calculate the response of MDOF systems using the proposed method for Haar wavelet, FCW, SCW and LW.

A. Initial calculations:

(1) Form stiffness matrix [**K**], damping matrix [**Cd**] and mass matrix [**M**] of the system.
(2) Specify wavelet basis function, number of adaptive collocation points ***2M,*** the considered order of wavelet $\boldsymbol{m}$***=(2M/2)-1***.
(3) Select an appropriate time step $\boldsymbol{d_t}$.
(4) Specify vectors of applied forces on each DOF of system, in each $\boldsymbol{d_t}$ corresponding to collocation points.
(5) Form coefficients wavelet matrix corresponding to collocation points for free-scaled orders of wavelet function $\boldsymbol{\phi(t)}$.
(6) Form operation matrix of integration corresponding to collocation points for each particular wavelet function $\boldsymbol{P}$.
(7) Calculate square operational matrix $\boldsymbol{P^2}$.
(8) Approximate unity, with related coefficient of wavelets.
   - D=$\sqrt{\pi/4}$, $\sqrt{\pi/8}$ and $\sqrt{1/2}$ for FCW, SCW and LW, respectively.
(9) Initialize $\boldsymbol{u_0}$ and $\boldsymbol{v_0}$ as initial displacement and velocity vectors.
(10) Form $\boldsymbol{2M} \times \boldsymbol{2M}$ identity matrix of $\boldsymbol{I}$.

B. For each time step:

(1) Form initial vectors for velocity and displacement of $\boldsymbol{S_1^T}$ and $\boldsymbol{S_2^T}$.
(2) Calculate $\boldsymbol{u_{n0}}$ and $\boldsymbol{v_{n0}}$using:
$v_{n0} = S_1^T\Psi(t)$
$u_{n0} = S_2^T\Psi(t)$
(3) Calculate vectors of unknown coefficients of $\boldsymbol{C_i^T}$ for each DOF (i=1,2,…,d).
(4) For each DOF calculate displacement, velocity and acceleration vectors, simultaneously by:
$u(t) = C^T P^2\Psi(t) + u_{n0}$
$\dot{u}(t) = C^T P\Psi(t) + v_{n0}$
$\ddot{u}(t) = C^T\Psi(t)$

University of Malaya

3.3 Stability analysis of the wavelet-based method

As was shown in previous sections, the robustness of the proposed method is revealed while the quantities of the dynamic system (i.e., displacements, velocities and accelerations) have been transferred from t^{th} step to the $(t+d_t)^{\text{th}}$ step using a set of compatible collocation (SM) points. Subsequently, details (e.g., frequency contents) of either dynamic responses (left side of Equation (3.42)) or externally applied loadings (right side of Equation (3.42)) are precisely captured by adaptive collocation SM points. Consequently, it provides the possibility of using longer time intervals of d_t. However, different sets of collocation points may be utilized, relating to the diverse details of considered problem. For this reason, the stability analysis of calculated results using the proposed scheme is concerned in this section for the least number of $2M$=2 collocation points. The relationship between dynamic quantities of the current state ($\widehat{U}_{t+\Delta t}$) and the previous state ($\widehat{U}_t$) is presented as (Bathe, 2006; Bathe and Wilson, 1973):

$$\{\widehat{U}_{t+\Delta t}\} = [A]\{\widehat{U}_t\} + [L']\{\hat{f}_{t+\upsilon\Delta t}\} \tag{3.46}$$

where, L' and A denote the load operator and amplification matrix, respectively. $\hat{f}_{t+\upsilon}$ indicates external loads which are related to the current quantities (υ = 0,1,2,…). Note that, $\hat{f}_{t+\upsilon}$, L' and A can be obtained for any numerical integration method, i.e., explicit or implicit schemes. For the purpose of stability analysis, dynamic equilibrium of a SDOF structure in Equation (3.28) is considered when there is no external load ($\hat{f}_{t+\upsilon\Delta t}$) applied. Firstly, the representation of Equation (3.28) is changed from damping (c) and stiffness (k) to the damping ratio (ξ) and natural frequency (ω) as follows:

$$\ddot{u}_t(t) + 2\xi\omega\dot{u}_t(t) + \omega^2 u_t(t) = \frac{F(t)}{(m)} \tag{3.47}$$

The subscript $\ddot{u}_t(t)$ indicates the relevant quantities at the current state of t. To calculate amplification matrix of A, relatively with terms of accelerations, the third ordered derivative of displacement with respect to time $\dddot{u}(t)$ is approximated by using the expansion of Equation (3.29). Employing the operation matrix of integration P, quantities of acceleration, velocity and displacement are obtained as follows:

$$\begin{aligned} \dddot{u}_t(t) &= C^T\Psi(t) \\ \ddot{u}_t(t) &= d_t.C^T P\Psi(t) + \ddot{u}_{t-\Delta t} \\ \dot{u}_t(t) &= d_t^2.C^T P^2\Psi(t) + \dot{u}_{t-\Delta t} \\ u_t(t) &= d_t^3.C^T P^3\Psi(t) + u_{t-\Delta t} \end{aligned} \tag{3.48}$$

where, initial accelerations $\ddot{u}_{t-\Delta t}$ is also approximated as:

$$\begin{aligned} S_o^T\Psi(t) = \ddot{u}_{t-\Delta t} \times 1 &\cong \ddot{u}_{t-\Delta t}.I^*\Psi(t) \\ &\cong \ddot{u}_{t-\Delta t}.D\left[1_{1,1}, 0,0, \ldots, 1_{1,M+1}, 0,0, \ldots\right]\Psi(t) \end{aligned} \tag{3.49}$$

where, D is defined in Equations (3.33) and (3.34) for FCW, SCW and LW. The subscripts of $\ddot{u}_{t-\Delta t}, \dot{u}_{t-\Delta t}$ and $u_{t-\Delta t}$ denote acceleration, velocity and displacement which were calculated at the previous state, respectively. In addition, initial quantities in Equation (3.49) are numerically developed by Equations (3.33) and (3.34) corresponding to Haar wavelet, FCW, SCW and LW, substituting in Equation (3.47), after omitting $\Psi(t)$ yields:

$$\begin{aligned} C^T P + S_o^T + 2\xi\omega\Delta t[C^T P^2 + S_o^T P + S_1^T] \\ + \omega^2\Delta t^2[C^T P^3 + S_o^T P^2 + S_1^T P + S_2^T] = 0 \end{aligned} \tag{3.50}$$

University of Malaya

After a set of algebraic simplification, coefficients vector of C^T is derived from Equation (3.50). Substituting C^T in Equation (3.46), the amplification matrix of A which shows the relationship between quantities of the current state (i.e., $\ddot{u}_t(t)$) and the previous state (i.e., $\ddot{u}_{t-\Delta t}$) is derived for FCW, SCW or LW (for corresponding $\phi(t)$, D and I^*) as:

$$\begin{bmatrix} \dddot{u}_t \\ \ddot{u}_t \\ \dot{u}_t \\ u_t \end{bmatrix} = \begin{bmatrix} 0 & a\phi(t) & b\phi(t) & c\phi(t) \\ 0 & d\phi(t) & e\phi(t) & f\phi(t) \\ 0 & g\phi(t) & i\phi(t) & j\phi(t) \\ 0 & q\phi(t) & r\phi(t) & z\phi(t) \end{bmatrix} \begin{bmatrix} \dddot{u}_{t-\Delta t} \\ \ddot{u}_{t-\Delta t} \\ \dot{u}_{t-\Delta t} \\ u_{t-\Delta t} \end{bmatrix} \tag{3.51}$$

where;

$$\begin{gathered} a = \kappa\, \mu^{-1}\ , \qquad b = \eta\, \mu^{-1}\ , \qquad c = \Upsilon\, \mu^{-1} \\ d = I^* + \kappa\, \mu^{-1} P\ , \qquad e = \eta\, \mu^{-1} P\ , \qquad f = \Upsilon\, \mu^{-1} P \\ g = I^* P + \kappa\, \mu^{-1} P^2\ , \qquad i = I^* + \eta\, \mu^{-1} P^2\ , \qquad j = \Upsilon\, \mu^{-1} P^2 \\ q = I^* P^2 + \kappa\, \mu^{-1} P^3\ , \qquad r = I^* P + \eta\, \mu^{-1} P^3\ , \\ z = I^* + \Upsilon\, \mu^{-1} P^3 \end{gathered} \tag{3.52}$$

where;

$$\begin{gathered} \kappa = -\,I^* - 2\xi\omega(\Delta t)\, I^* P - \omega^2(\Delta t)^2 I^*\, P^2 \\ \eta = -2\xi\omega(\Delta t)\, I^* - \omega^2(\Delta t)^2\ \ I^* P \\ \Upsilon = -\omega^2(\Delta t)^2\ \ I^* \\ \mu = P + 2\xi\omega(\Delta t)\, P^2 + \omega^2(\Delta t)^2\, P^3 \end{gathered} \tag{3.53}$$

where, μ is a $2M \times 2M$-dimensional matrix; κ, η and Υ are $1 \times 2M$-dimensional vectors. Accordingly, the amplification matrix of A is decomposed into its eigen vectors $[\Phi]$ and diagonal eigenvalue matrix of $[\lambda]$ by $A = [\Phi][\lambda][\Phi]^{-1}$, and therefore stability of the proposed method is satisfied provided that the maximum norm of elements $[\lambda]$, namely, spectral radius being less than unity as follows (Bathe, 2006; Bathe and Wilson, 1973):

$$\rho(A) = \max(\|\lambda_1\|, \|\lambda_2\|, \|\lambda_3\|, \dots) \leq 1 \tag{3.54}$$

University of Malaya

In Equation (3.54), $\rho(A)$ is obtained as a function of Δt and denotes the spectral radius of the amplification matrix A. This value is calculated and plotted in Figure 3.8 for several time integration methods (damping ratio equal to zero), including, central difference, family of Newmark-β, Wilson-θ and the proposed scheme using the second scale of FCW, SCW and LW.

It should be noted that, for 2D Haar wavelet an alternative way is proposed for stability analysis and it is concluded that 2D Haar wavelet lies on unconditionally stable method (Mahdavi and Razak, 2015a).

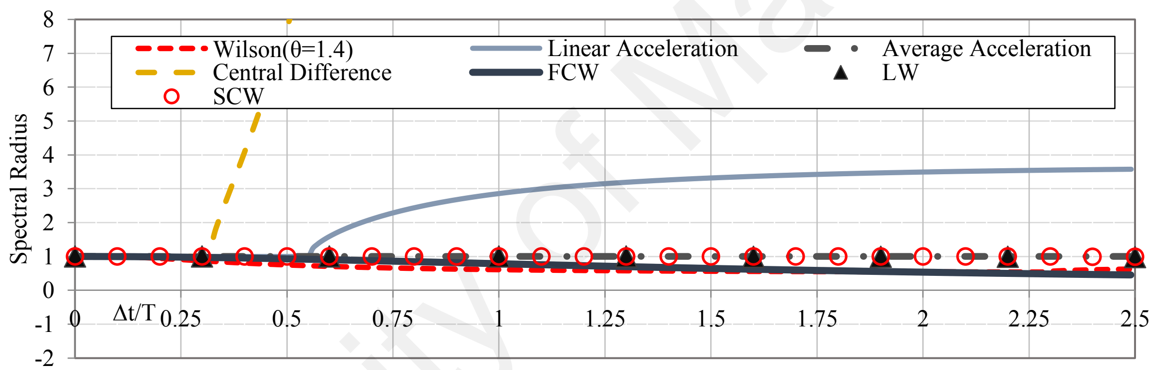

Figure 3.8: Comparison of spectral radius for the proposed method and another four integration schemes.

Figure 3.8 illustrates that, the proposed procedure as an explicit integration method and indirect scheme is unconditionally stable even at the first two scales of FCW, SCW and LW. Therefore, no requirements are made on the time step Δt used in the analysis. In addition, the explicit schemes of linear acceleration of Newmark- β family and central difference are conditionally stable. In contrast, the spectral radius of $\Delta t/T$ shows that Wilson-θ and average acceleration method of Newmark- β family, as two implicit schemes are also unconditionally stable with no restraints (such as Δt critical value) placed on time step Δt.

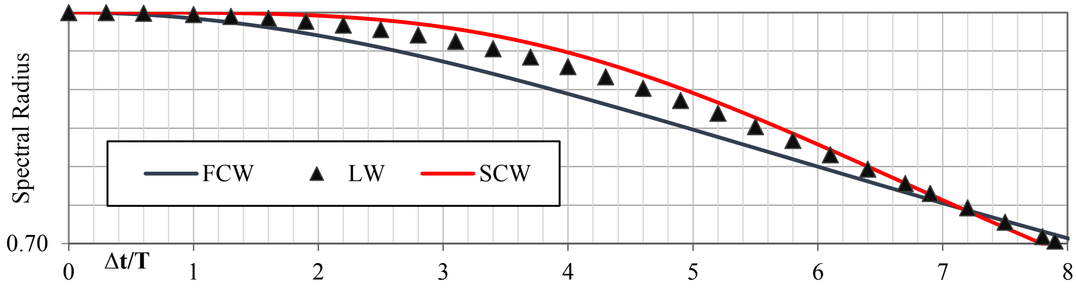

Figure 3.9: Comparison of spectral radius calculated for the second scale of FCW, SCW and LW.

3.4 Accuracy analysis of the wavelet-based scheme

In general, errors are inherent characteristic of numerical approaches (Bathe, 2006). Thus, in the following section, accuracy of the proposed method is investigated corresponding to free scales of Haar wavelet, FCW, SCW and LW. For this purpose, three operations are considered, i.e., implementation of the first and second operation of integration and accuracy analysis of functional approximation.

3.4.1 First ordered operation of integration

In order to investigate the accuracy of results calculated after the first ordered operation of integration, the first-ordered ordinary differential equation of $0.25\dot{u}(t) + u(t) = 1, u(0) = 1$ with the analytical solution of $u(t) = 1 - e^{(-4t)}$ is considered. For an accurate comparison, the measurement of percentile total average relative errors (PTARE) is compared, when free scales of FCW, SCW and LW are employed. Assumption of $\hat{\propto}$ for the measurement of exact results and $\hat{\beta}$ related to the responses calculated by each numerical integration scheme (relative errors corresponding to each $\hat{z}$ = time increments), PTARE is obtained as follows:

$$PTARE = (\sum_{i=0}^{\hat{z}} \frac{(\hat{\beta} - \hat{\propto}) \times 100}{\hat{\propto}})/\hat{z} \tag{3.55}$$

As mentioned earlier, from the optimization point of view, the CPU computation time involved is also considered for different operations. These values are computed and depicted in Figure 3.10 for FCW, SCW and LW using $2M$ =4, 6 and 64 of adaptive collocation points. It is to be emphasized that, this evaluation is carried out on the long time interval of $\Delta t = 1$ sec.

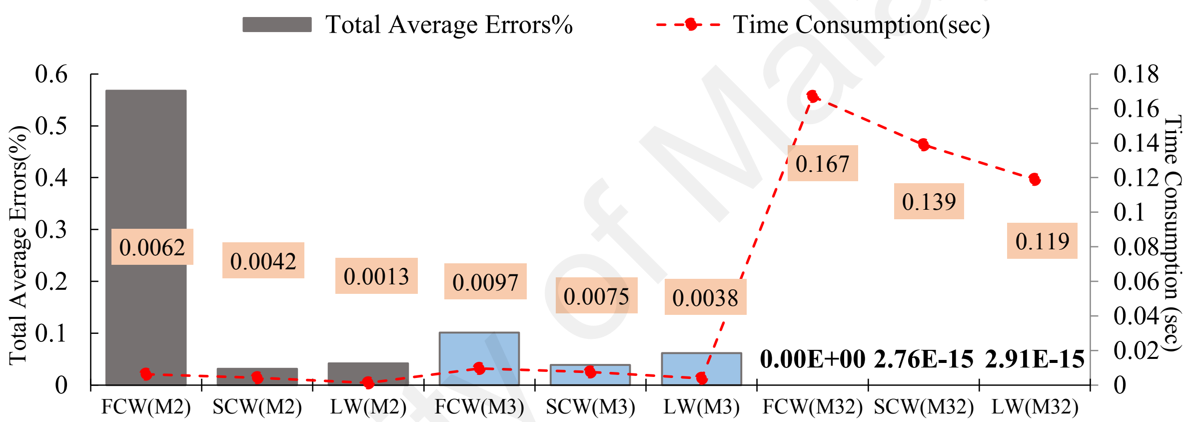

Figure 3.10: PTARE corresponding to the considered first-ordered differential equation and relative computational time of FCW, SCW and LW using the first 4^{th}, 6^{th} and 64^{th} SM collocation points related to the scales of wavelets (M=SM points/2).

As illustrated in Figure 3.10, the cost-effective results were computed by the various scales of LW. In referring to Equations. (3.26) and (3.27) and Table 3.1 (emphasizing the simple weight function of unity for Legendre polynomials), the calculation of corresponding matrices is faster than other wavelets, the emphasis is on using larger scales regarding to the more adaptive collocation points. In addition, it is shown that the SCW gave the least value of PTARE using the lower scales ($2M < 20$) of wavelets. However, for the higher scales ($2M > 20$) or shorter time intervals of $\Delta t \leq 0.01$sec, it is observed that, the accuracy of

FCW is better than SCW or LW. It should be noted that, at current assessment of accuracy there is no consideration on the frequency components.

3.4.2 Second ordered operation of integration

In order to evaluate the accuracy of results employing the second-ordered operation of integration, the linear and second-ordered ordinary differential equation governing a free vibrating and undamped SDOF system with constant circular frequency of ω is considered as:

$$\ddot{u}(t) + \omega^2 u(t) = 0 \tag{3.56}$$

Analytically, with the initial conditions of $\ddot{u}_0 = -\omega^2$, $\dot{u}_0 = 0$ and $u_0 = 1$, the closed-form solution of Equation (3.56) is $u(t) = \cos(\omega t)$. In addition, the natural undamped period is obtained by $T_0 = 2\pi/\omega$ sec. The considered SDOF system has a cyclic response with a constant maximum amplitude of $|u(t)|_{max} = (u_0^2 + (\dot{u}_0/\omega)^2)^{0.5}$. In general, the accuracy analysis can be achieved by presenting two kinds of error measurement; (a) period elongation PE and (b) amplitude decay AD. Accordingly, PE measures the extension in the time interval it takes to complete each cycle of harmonic response (Figure 3.11). While, AD is the absolute error of the calculated results for u (displacement) by each numerical scheme (shown in Figure 3.11). However, AD is also known as algorithmic damping which is obtained by $AD = 2\pi\xi$. Eventually, the explained SDOF system is solved using some of the common numerical integration procedures such as average acceleration (AA), linear acceleration (LA) from Newmark-β family, central difference and Wilson-θ. Accordingly, two kinds of error are measured, and therefore compared with the responses calculated using the proposed method of FCW, SCW and LW on $2M = 2$, SM points (in referring to the scale of the wavelets). The PE and AD measurements are plotted in Figure 3.11 for the variations of $\Delta t/T_0$.

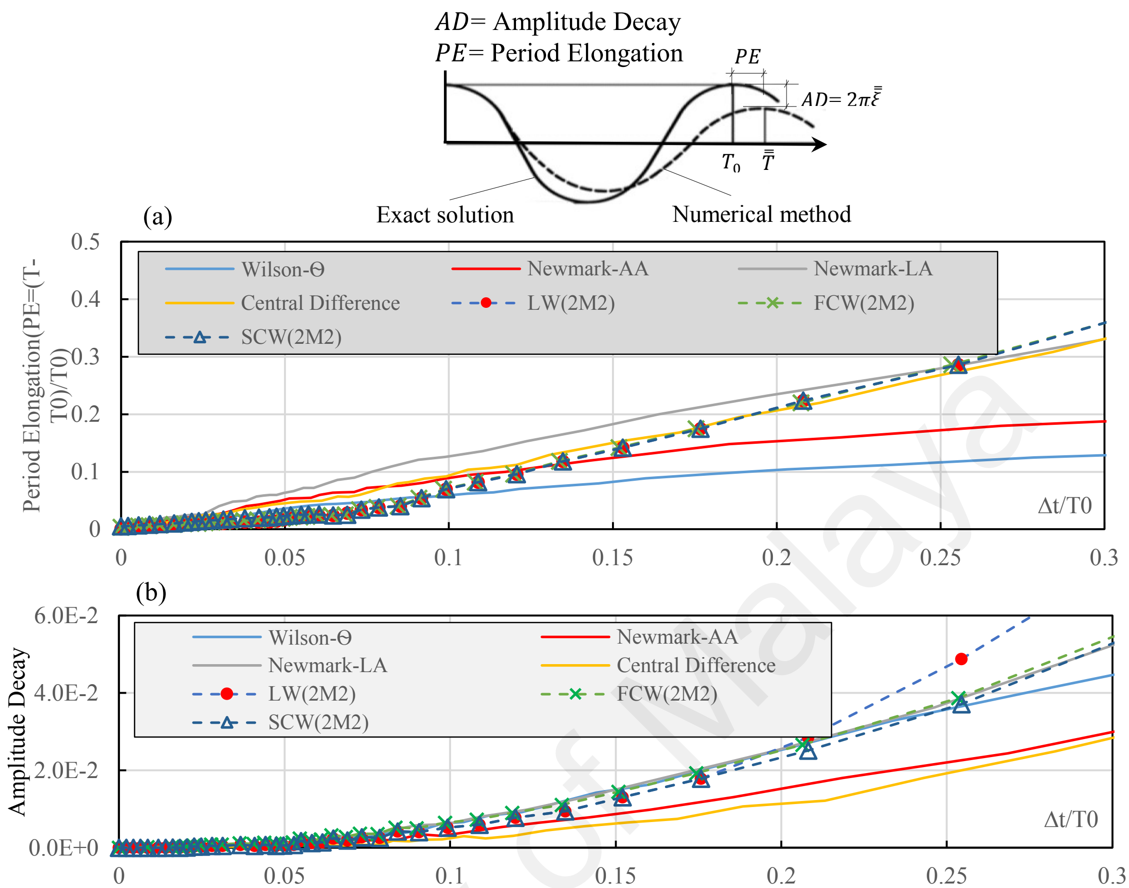

Figure 3.11: Error measurment. (a) Period elongation (PE=(T-T$_0$)/T$_0$). (b) Amplitude decay (AA= average acceleration, LA= linear acceleration of Newmark-β family).

As can be seen from Figure 3.11(a), the accuracy of the proposed method using only two points (the lowest scale of $2M = 2$ for FCW, SCW and LW) was constant for the error measurement of PE. However, the lowest accuracy is observed in Figure 3.11(b) for LW compared with FCW and SCW regarding to the error measurement of AD. This is because of the weight functions of the first and second Chebyshev polynomials, in which the end point errors are lesser than those of Legendre polynomials. Consequently, it is deduced that the most precise results are ascertained by the implementation of the second-ordered operation of SCW for solving the considered SDOF through the proposed method. It is to be pointed out that, frequency contents are considered at this evaluation in contrast to the

University of Malaya

previous assessment. It is to be noted that the same procedure is reported for Haar wavelet and the accuracy of results were compared with only FCW (Mahdavi et al., 2015).

3.4.3 Functional approximation

Basically, dynamic analysis is accomplished by approximation of several sets of second-ordered differential equations introduced in Equation (3.28) through the proposed method. This decomposition is simultaneously executed on both sides of aforementioned equations, i.e., approximation of differential equations as well as the external loadings. Furthermore, in actual engineering applications either the applied load or the response of structure (due to various natural frequencies), are mostly constructed with wide-band frequency content.

Accordingly, parts of high or low frequencies are approximated using adaptive SM collocation points of FCW, SCW and LW. Thus, in this section the accuracy of the proposed method for approximation of functions (is designated by App-F(t) in Figure 3.12) with different frequency components is evaluated. For this purpose, a sinusoidal function of $F(t) = 100\sin(\omega t)$ is examined by the first 8th and 32nd ($2M$=8 and 32) scales of FCW, SCW and LW for ω equal to 5 and 30 rad/sec. Moreover, the coefficients of FCW, SCW and LW are derived and comparatively plotted in Figure 3.12 (using bar charts). It is to be noted that, the comparison of 3D wavelets and 2D wavelets was presented before, and the only 3D wavelets are considered here. In addition, the previous evaluation of wavelet functions may be extended in the current form.

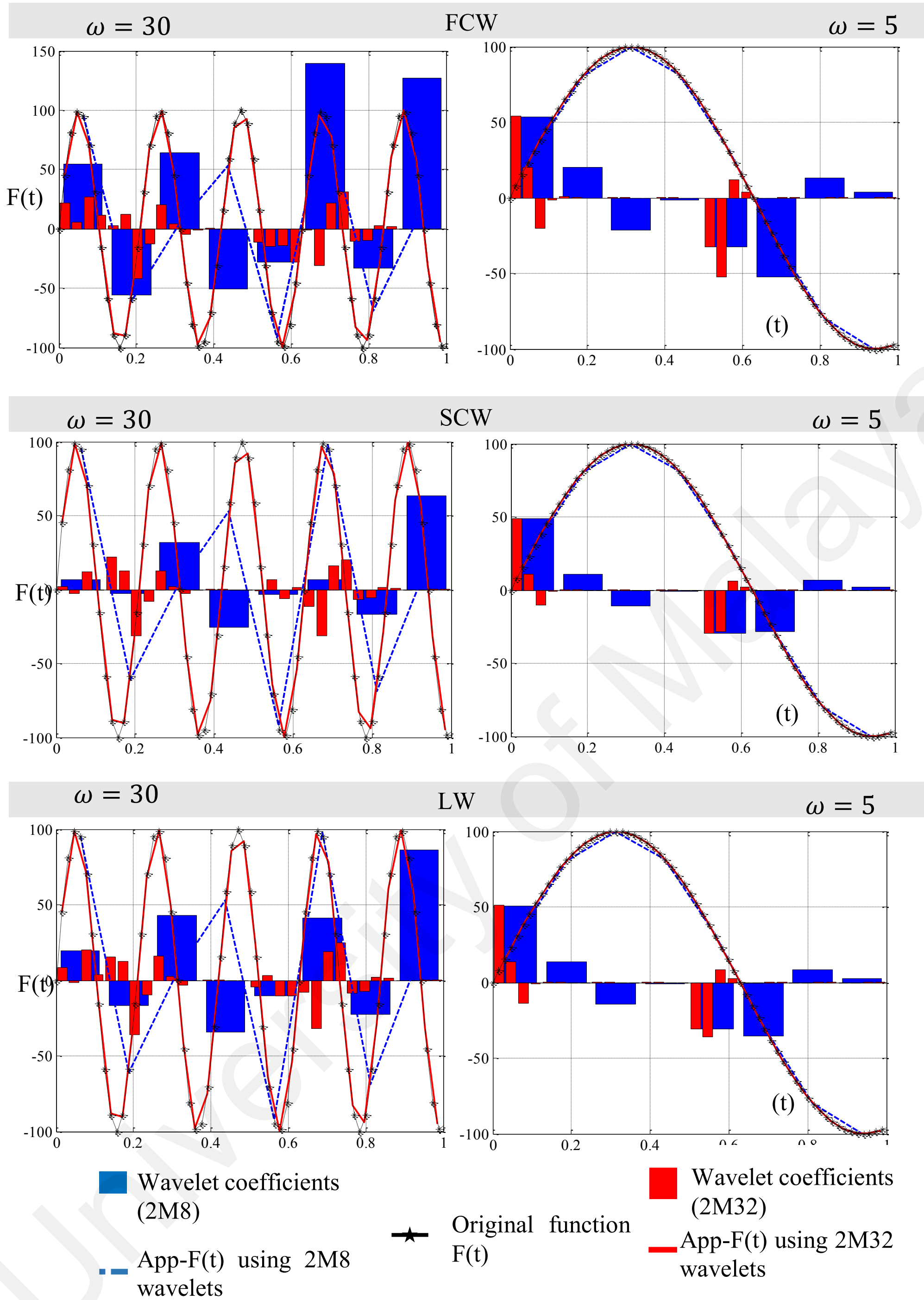

Figure 3.12: Comparison of the approximation of F(t)=100sin($\boldsymbol{\omega}$t) for $\boldsymbol{\omega}$=5 and 30rad/sec (App-F(t)), the original F(t) and the scaled wavelet coefficients corresponding to the first 8th and 32nd scales of FCW, SCW and LW.

University of Malaya

As shown in Figure 3.12, the similarity of the original F(t) to the decomposed version of F(t) is confirmed by the lowest scaled wavelet coefficients (shown with bar charts corresponding to the 8^{th} and 32^{nd} scales). Significantly, the rate of this similarity is more clear when 32^{nd} scales of FCW, SCW or LW is applied. However, for the low frequency of $\boldsymbol{\omega}$=5, there are minor differences observed on different SM points. In other words, high frequency contents of a function are accurately captured by using larger scales of corresponding wavelets. On the other hand, calculated coefficients of SCW (even using the 8^{th} scale for F(t) of $\boldsymbol{\omega}$=30, referring to the higher frequencies) demonstrate the appropriate accuracy of this wavelet function compared with LW and FCW. Although, it is observed that, for $\boldsymbol{\omega}$=5, SCW coefficients were more precise; for lowest frequencies the accuracy evaluation of SCW may be interpreted the same as FCW and LW. It is deduced that, despite the accurate results of FCW for error measurement of AD (Figure 3.11(b)), details of frequency components are precisely captured with LW (more accurate approximation of the both sides of Equation (3.42)). As shown later, errors measured at current step (functional approximation) diversely affect the accuracy of previous assessments. Overall, an engineering decision to use SCW, LW or FCW shall be made based on several factors, i.e., the existing frequencies from either inherent characteristic of the structure or applied loading, number of adaptive collocation points (given scale of wavelets) and computation time involved (an optimization point of view).

3.5 The proposed method for operation of derivative

In this section, an efficient approach is proposed for approximation of derivatives using free-scaled wavelet functions. The proposed method is applicable for various wavelet basis functions, since the product matrix of integration and wavelet coefficient vectors are available. For this purpose, integral functions are numerically developed from local coordinates to global system. For a differentiable function of $f(t)$: $x \in [t_n, t_{n+1}]$, indefinite formulation of Equation (3.57) is considered based on Newton theorem as follows:

$$f(t) = f(t_n) + \int_{t_n}^{t} f'(t)dt \tag{3.57}$$

Initializing $t_{n+1} = t_n - f(t_n)/f'(t_n)$ for definite form of Equation (3.57), let $d_n = t_{n+1} - t_n$. Using Equation (3.25) the derivative function is approximated on global coordinates as follows:

$$f'(t) = C^T.\Psi(t) \tag{3.58}$$

Substituting into Equation (3.57) we have:

$$f(t_{n+1}) = f(t_n) + \int_{t_n}^{t_{n+1}} C^T.\Psi(t)\ dt \tag{3.59}$$

Multiplying by operational matrix P of integration and adding initial constant of integration, gives:

$$f(t_{n+1}) = f(t_n) + d_n.C^T.P.\Psi(t) + f'(t_0) \tag{3.60}$$

where, d_n is operated for mapping local characteristics of wavelets to global ones. To simplify this equation, constant quantities are approximated by Haar, Legendre or Chebyshev wavelets in each step using the idea presented in Equation (3.32).

$$f'(t_0) = f'(t_0)I^*\Psi(t) \tag{3.61}$$

$$f(t_{n+1}) = f(t_{n+1})I^*\Psi(t) \tag{3.62}$$

$$f(t_n) = f(t_n)I^*\Psi(t) \tag{3.63}$$

Substituting Equations (3.61), (3.62) and (3.63) into Equation (3.57) yields:

$$f(t_{n+1})I^*\Psi(t) \;\; = f(t_n)I^*\Psi(t) + d_n.C^T.P.\Psi(t) + f'(t_0)I^*\Psi(t) \qquad (3.64)$$

Subsequently, eliminating $\Psi(t)$ from the both sides of Equation (3.64) and after algebraic calculations, C^T is being calculated. Using Equation (3.61), $f'(t)$ is approximated on $2M$ global points. The same approach is employed on $f'(t)$ to compute the second derivative of $f''(t)$. The proposed method is implemented on $f(x) = \sin(x^2)\,;\; x \in [0,2]$, in which that, its definite $f'(x) = 2x.\cos(x^2)$ and $f''(x) = 2[\cos(x^2) - 2x^2\sin(x^2)]$ existed. The first and second derivatives are calculated for $2M$=8 collocation points of FCW and SCW and have been compared with exact values (designated by original df/dx or d(df/dx)) in Figures 3.13 and 3.14, respectively. The approximated results for the first and second derivatives of $f(x)$ are designated in figures by App(df/dx) and App(d(df/dx)), respectively.

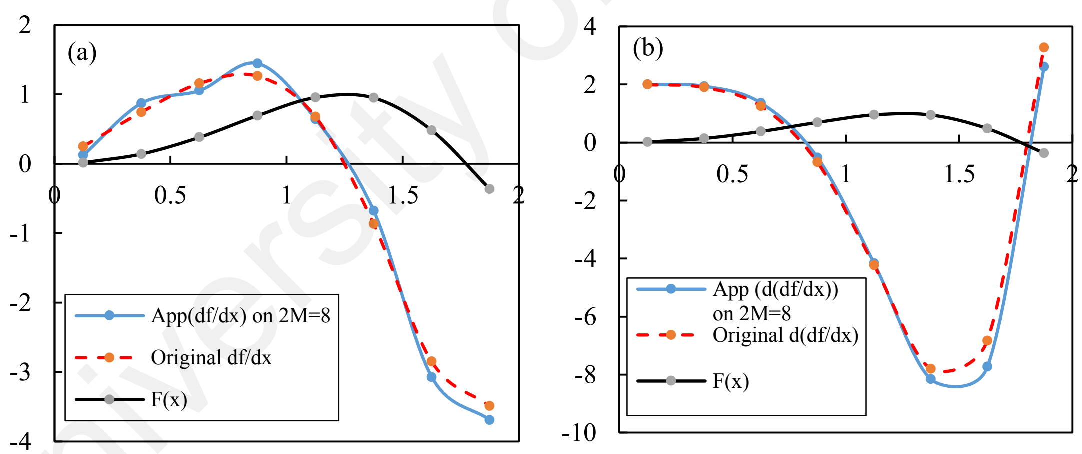

Figure 3.13: The approximated results using the proposed operation of derivative of FCW on $\mathbf{2M}$=8 collocation points for calculation of (a) the first, (b) the second derivative.

The schematic view of results in Figures 3.13 and 3.14 lies on better accuracy of SCW, when $2M$=8 is applied. For the purpose of detailed comparison, various $2M$ adaptive collocation points are employed through the proposed method corresponding to diverse scales of FCW and SCW to calculate the first and second derivative of considered $f(x)$. The comparison of results are depicted in Figures 3.15 and 3.16 with regards to the FCW and SCW, respectively. Accordingly, the percentile total average error (PTARE) measurement is presented for the purpose of comparison.

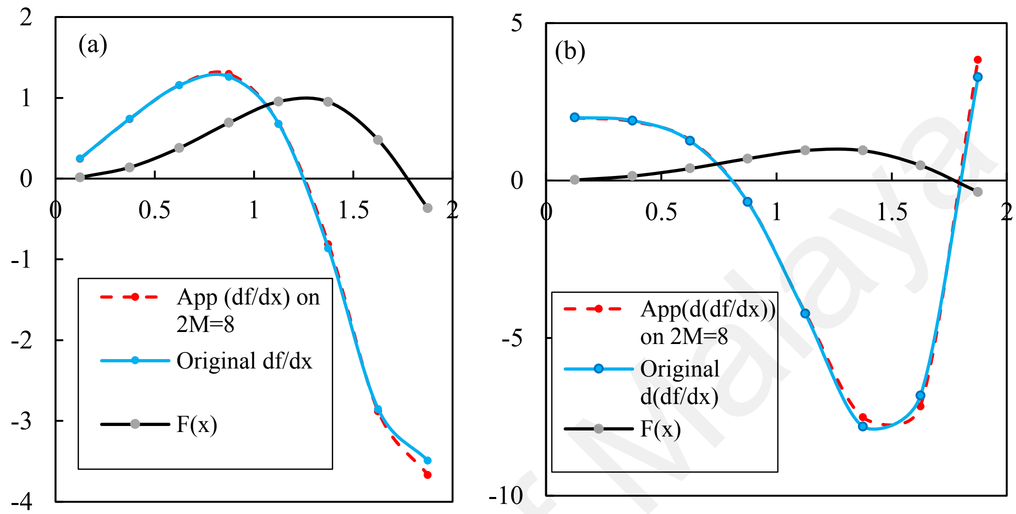

Figure 3.14: The approximated results using the proposed operation of derivative of SCW on $\boldsymbol{2M}$=8 collocation points for computation of (a) the first, (b) the second derivative.

The measured PTARE data shown in Figures 3.15 and 3.16 illustrate that free scales of SCW approximate the first and second derivatives more accurate than that of FCW. For instance, PTARE= 89.49% is measured for the second scale of FCW, while this value is considerably decreased to 9.32% for the same scale of SCW. As it is shown in Figure 3.16, the accuracy of the second derivative is more than the first one. This is most likely due to the fact that, the oscillatory shape of the results coincide with the exact result for the second derivative, in contrast to the calculated results by SCW for the first derivative. Significantly, the error measurement of the proposed method using higher scales of SCW demonstrate the superiority of this wavelet. Finally, it is apparent from the figures that, end point errors diversely affect on the accuracy of results for the higher order approximations shown for $2M$=64 collocation points.

It should be noted that, the third ordered derivative of displacement, namely, the quantity of jerk will be computed using the proposed procedure corresponding to adaptive collocation points. For this aim, initial $f(t)$ will be replaced by the displacement vector which may be acquired (measured) independent from structural materials and behaviors on discrete time points.

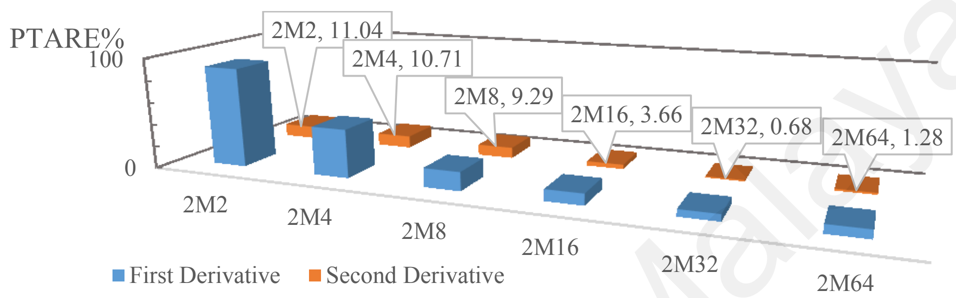

Figure 3.15: PTARE measurement corresponding to different scales ($\boldsymbol{2M}$ collocations) of FCW.

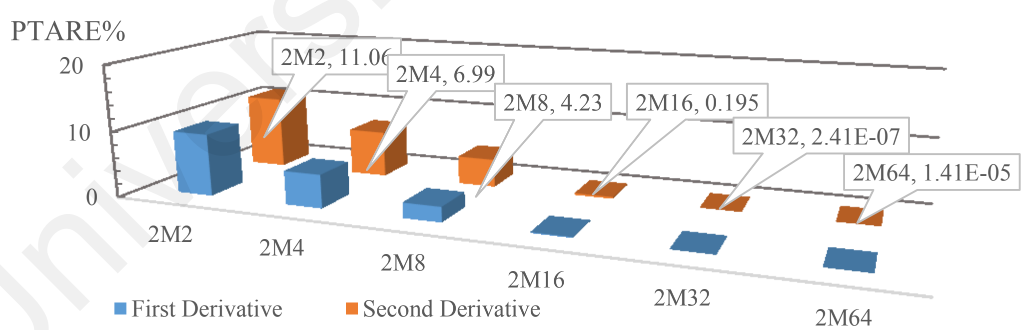

Figure 3.16: PTARE measurement corresponding to various scales ($\boldsymbol{2M}$ collocations) of SCW.

In addition, the proposed scheme is applicable in problems with several unknowns, where, the tangent line becomes a tangent (hyper) plane. For instance, Equation (3.59) is developed for a function of two variables $f(x, y)$ as follows:

University of Malaya

$$f(x, y = y_0) = f(x_n, y = y_0) + \int_{x_n}^{x} f_x'(x, y = y_0)dx \tag{3.65}$$

where, x and $y = y_0$ represent the first variable and the constant point for the second variable, respectively. $f_x'(x, y = y_0)$ indicates the derivative of $f(x, y)$ with respect to x while $y = y_0$ and the subscripts x and y are changed for the next variable as:

$$f(x = x_0, y) = f(x = x_0, y_n) + \int_{y_n}^{y} f_y'(x = x_0, y_n)dy \tag{3.66}$$

Consequently, f_x' and f_y' are calculated, and therefore the normal vector ($\vec{n}$) to the plane at x_0 and $y_0$is derived as:

$$\vec{n} =< f_x'(x_0, y_0)\, , f_y'(x_0, y_0)\, , -1 > \tag{3.67}$$

3.6 Numerical verifications

In the following subsections, the validity and effectiveness of the proposed method is examined by considering different structural systems. For this purpose, MDOF structural systems involving, a set of mass-spring system, a shear building under complex base excitation and two double-layer 3D space structures under impact loadings (very large scale as well as small scale structures) are considered. In addition, in order to compare the computational efficiencies, computation time involved is recorded for each example, which was computed using the same hardware for all the cases. Eventually, the percentile total average errors are also calculated in order to evaluate the accuracy of different numerical methods.

3.6.1 A set of mass-spring system

Figure 3.17 shows a 21 degree of freedom linear mass-spring system. A concentrated dynamic load is applied at all degrees of freedom. The characteristics of the considered

University of Malaya

system as well as time dependent loading are shown in the figure. In order to calculate time-history of responses, including horizontal displacements, the minimum period associated with the last degree of freedom by T_{min}= 0.177 sec and thus $\Delta t \leq 0.55 T_{min}$= 0.05 sec (Bathe and Wilson, 1973) shall be utilized as the time increment of analysis so as to satisfy the stability of conditionally stable methods. In addition, the friction between wheels and basic surface is neglected.

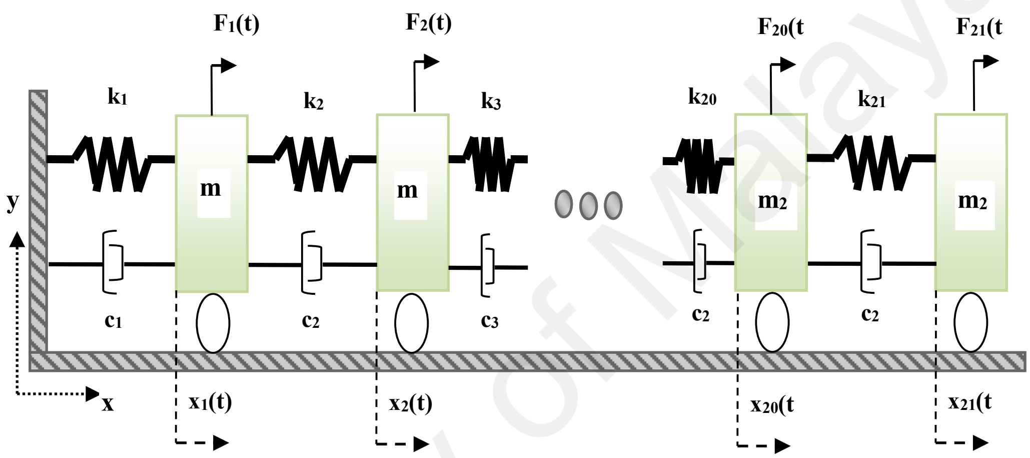

	1~3	4~10	11~18	19~21
Mass (kg)	2	3	4	5
Damping (N/sec)	98.1	147.15	98.1	196.2
Stiffness (N/cm)	5886	6867	7848	8829
$F_i(t)$-(kN)		*0.981.sin(8πt)*		

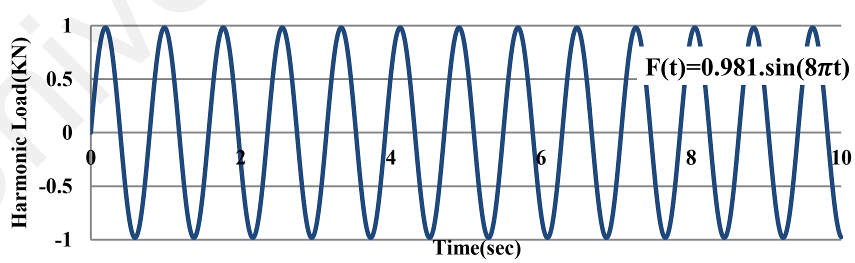

Figure 3.17: 21 DOF mass spring system vibrated by sinusoidal load (load frequency=8π Hz), Δt=0.05 sec.

This example is analyzed using five numerical methods, including linear acceleration (LA), central difference (CD), Wilson (θ=1.4), proposed method using 16th scale of Haar and

University of Malaya

the first kind of Chebyshev wavelet (designated by 2M16) and piecewise modal Duhamel integration. The responses obtained by Mode Superposition method using all modes are implied as Duhamel or modal exact solution. Eventually, the results, including time-history displacement of 7th degree of freedom and total amount of errors have been plotted in the figures below, respectively. Figure 3.18 shows the first 10 sec time-history displacements of the 7th mass, which are also calculated by the first 16 scale of Haar and FCW. It can be seen from the figure that the result of the proposed method (particularly, using a comprehensive wavelet function such as Chebyshev) is closer to the exact result than central difference and linear acceleration method. On the other hand, this figure shows that accuracy of results, which are calculated even by large scales of Haar is not acceptable, compared with other results.

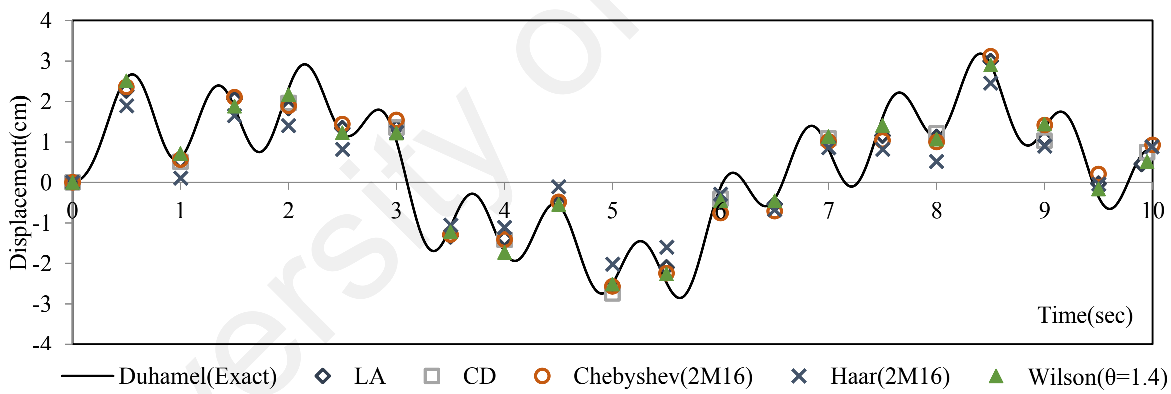

Figure 3.18: The first 10 sec horizontal displacement time-history of 7th mass, shown in Figure 3.17.

Table 3.4 compares the percentile error of time-history of displacements between 1 to 1.35 sec. It can also be seen that the result of the Haar wavelet solution gave the highest value of 76.08%, whereas for the first kind of Chebyshev wavelet at 1.05sec, the peak value was only 16.95%. Moreover, data on this table show some fluctuations on the results of other numerical methods with large amplitude, in comparison with the result of Chebyshev wavelet, which remained almost unchanged. Meanwhile, compared with solution errors after central difference, linear acceleration or Wilson-θ method only minor error was apparent for the first kind of Chebyshev wavelet and proves the capability of the proposed method using this wavelet. Finally, the total average error and computation time involved have been plotted in Figure 3.19. Subsequently, this figure comparatively illustrates errors and time consumption of relative numerical integration schemes. As mentioned earlier, the results calculated by Haar wavelet, significantly gave the highest value of 64% (total average). In contrast, the computation time involved gave the lowest value of 0.0083 sec compared with 0.0127 sec for the first kind of Chebyshev wavelet or 0.0336 sec for Wilson-θ method. For this reason, the responses calculated with Haar wavelet are being considered in this thesis as comparison for optimization. In the case of large-scaled continuum structures, time-history analysis is a time-consuming procedure. Thus this basis wavelet will be more applicable for rough and initial approximation of the dynamic responses in order to achieve an optimized scheme.

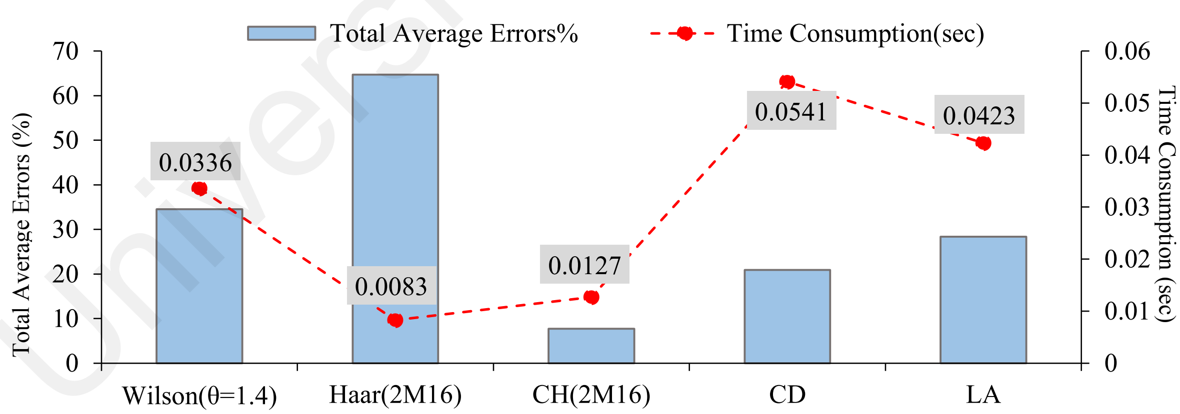

Figure 3.19: Total average errors in displacement of 7th mass, shown in Figure 3.17 and relative computation time involved (CH= First kind of Chebyshev wavelet, CD= central difference, LA=linear acceleration).

3.6.2 MDOF shear building

Figure 3.20 illustrates a thirty–story shear building under a complex base excitation. Shear building and complex excitation state the only one DOF existed for each story and wide-band frequency content loading, respectively. The structural characteristics as well as mass and stiffness of each story are shown in the figure. The damping is presumed proportional to 0.01 of stiffness. In addition, T_{min}=0.3167 sec (the minimum period), hence $\Delta t \leq 0.55 T_{min}$= 0.05 sec shall be utilized as time increment, so as to satisfy conditional stability of the numerical procedures, e.g., central difference method, whereas, large time step of Δt=0.1 sec is utilized for the proposed method. It should be pointed out that, the time-history of applied acceleration (El-Centro) is acquired on time increment of Δt=0.0001 sec.

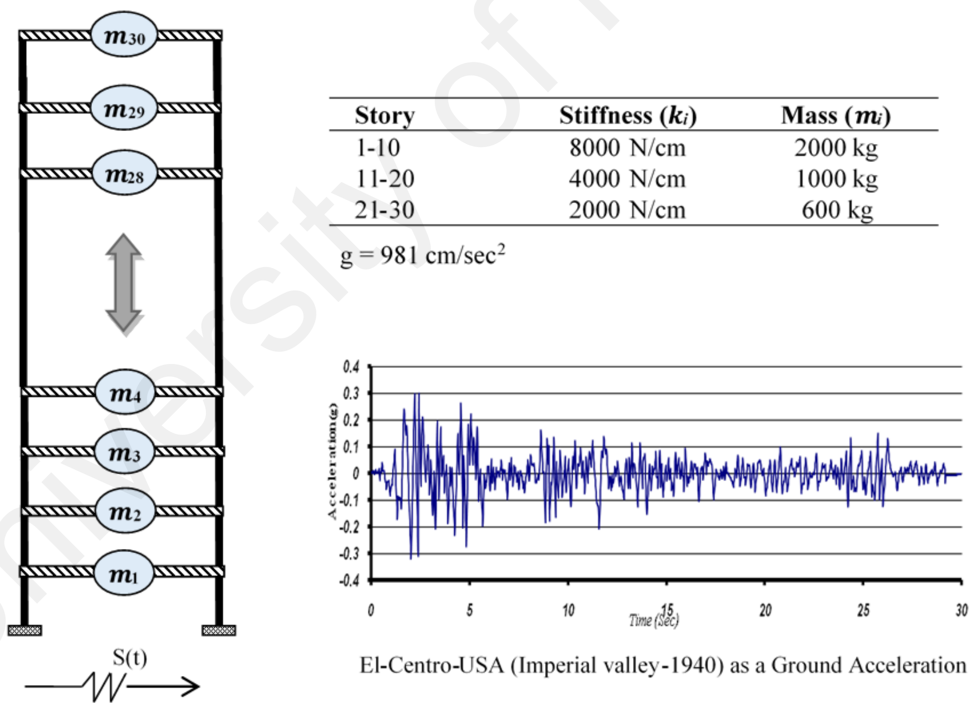

Story	Stiffness (k_i)	Mass (m_i)
1-10	8000 N/cm	2000 kg
11-20	4000 N/cm	1000 kg
21-30	2000 N/cm	600 kg

Figure 3.20: A thirty story shear building under El-Centro acceleration.

The first 10 sec time-history of displacements of the 5th story is plotted in Figure 3.21. Dynamic responses calculated with common integration methods of Wilson-θ, central

University of Malaya

difference (CD) and linear acceleration (LA) methods are compared with the proposed method using 16 scales of FCW, SCW and LW (designated by 2M16) and Duhamel integration method as analytical solution when all structural modes are included. It should be noted that, because of the complexity of the external load $2M$=16 is considered. The emphasis is on the precise decomposition (on adaptive collocation points) of the right side of Equation (3.42) at a long time step of the analysis, and therefore gaining very optimum solution.

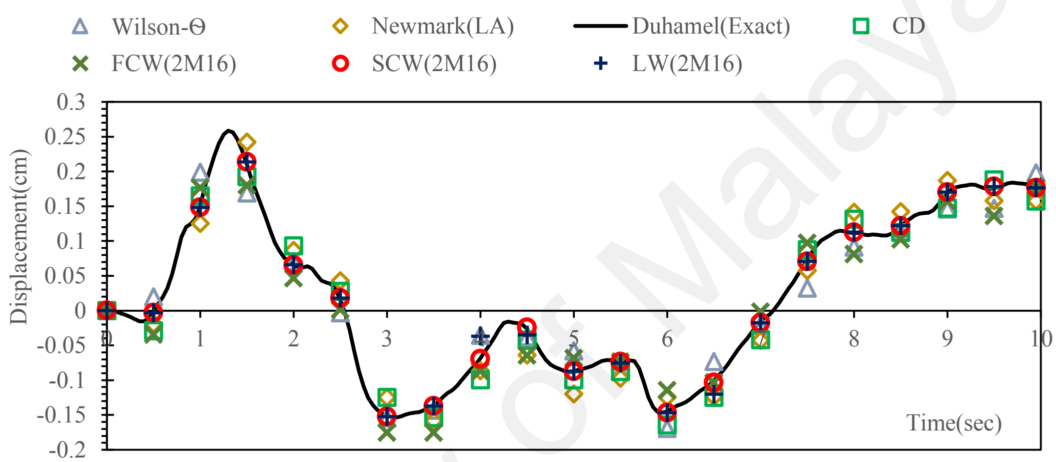

Figure 3.21: Displacement time-history of story 5, shown in Figure 3.20.

Figure 3.21 shows the results calculated by the proposed scheme of SCW are very close to the exact responses than those of LW, FCW or common numerical approaches. In addition, it is shown that, LW gave better accuracy of results than FCW (because of the accurate approximation of external load). In referring to Figure 3.12, in order to achieve the most accurate responses of FCW, the larger scales may be employed. However, the computed accuracy of $2M$=16 is still better than other numerical schemes. Furthermore, it is observed that calculated responses of Wilson-θ procedure (known as an implicit time integration approach), almost for the entire time of the analysis gave the least accurate results.

University of Malaya

For the purpose of a precise comparison, the value of PTARE is computed and compared in Figure 3.22 for different numerical methods. Furthermore, computation time involved which was recorded with the same hardware for all numerical integration schemes is also provided in this figure.

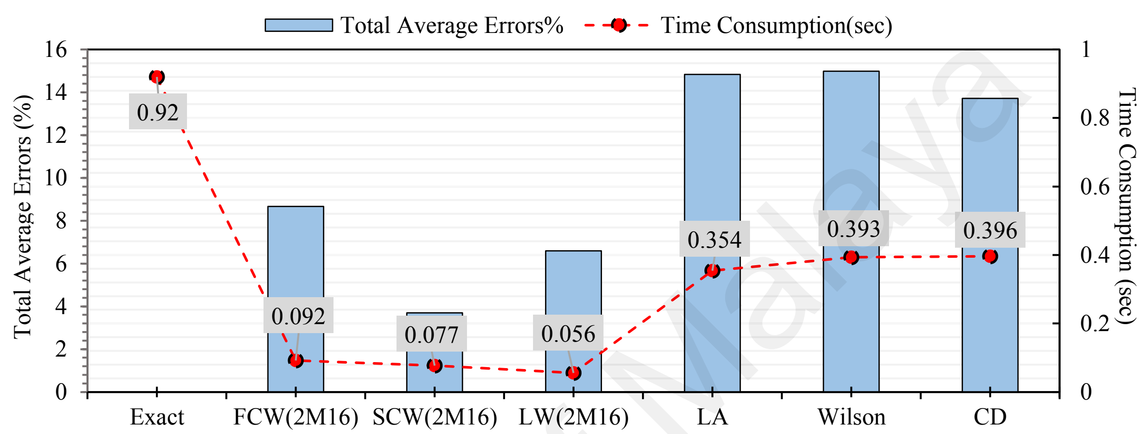

Figure 3.22: PTARE in time-history displacement of story 5, shown in Figure 3.20 and corresponding computational time (CD=central difference, LA=linear acceleration).

As can be seen from Figure 3.22, the minimum computational time recorded with a value of 0.056 sec was for LW compared with 0.077 sec for SCW or 0.092 sec for FCW. This is because of the fast computation of operational matrix of integration (P) of LW. Moreover, Figure 3.22 demonstrates the capability of SCW to handle the broad-band frequency content loading. It gave the minimum value of 3.74% PTARE, while it was 14.99% for the implicit numerical procedure of Wilson-θ, 14.83% for linear acceleration method (known as an explicit time integration scheme) or 13.71% for the explicit central difference method when conditional stability is satisfied. In agreement with Figure 3.3, the second Chebyshev polynomials of order 8 ($2M/2$), covers the major amplitude of y-axis (frequency) rather than the first Chebyshev or Legendre polynomials (Figure 3.3). It is concluded that, details of the external loading (i.e., wide-band frequencies) are accurately captured on adaptive collocation points using the proposed method even for the long time interval of Δt=0.1 sec.

Consequently, the optimum analysis is accomplished with lesser computational time, storage usage capacity and therefore minimum cost of the analysis. PTARE for time-history displacements of the 5th story is tabulated and compared in Table 3.5. The error measurement is between 1.2 and 1.5 second of loading corresponding to linear acceleration (LA), central difference (CD), FCW, SCW and LW numerical integration methods. It can also be seen that, errors reached the highest value of 26.35% for the linear acceleration method at 1.3 sec, whereas, the peak percentile error due to SCW at the same time, slightly reached the value of 6.44%. Table 3.5 shows that the lowest value of percentile error for the proposed method was obtained for SCW at 1.2 sec by 0.73%. However, it is 1.48% for LW or 3.88% for FCW.

3.6.3 A double layer Barrel truss structure

Figure 3.23 describes a complex and double layer space structure composed of 209 pinned connections, 768 truss elements and 579 degrees of freedom. Details of the structural members are shown in Figure 3.23, which include the geometry, cross-sectional area, mass per length and modulus of elasticity. In order to calculate modal damping ratios the Rayleigh damping is computed corresponding to different modes. The structure is restrained by fixed supports located all around the bottom joints shown in the figure. In addition, this system is subjected to two impact loadings of 40kN which strike two middle bottom nodes, highlighted in the figure. The complex geometry of this system is formulated in FORMIAN using Formex Algebra (Nooshin and Disney, 1991) and then nodal coordinates transferred to MATLAB to form the stiffness, damping and mass matrices prior to the implementation of the numerical approaches. Referring to the complexity of this large-scaled structure, high natural frequencies existed, i.e., the minimum period of T_{min}=0.0057 sec is computed. The shortest time increment of Δt=0.001 sec is utilized for the common integration methods, in contrast to the long interval of Δt=0.01 sec used for the proposed method of FCW, SCW and LW.

University of Malaya

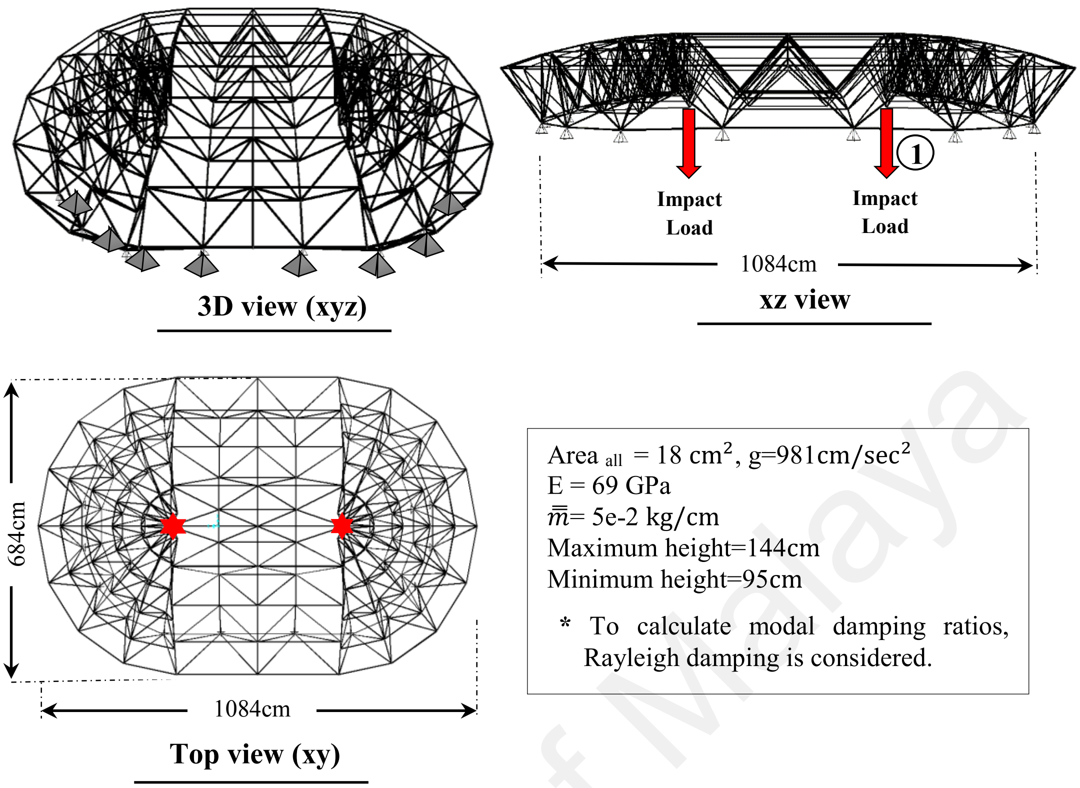

Figure 3.23: Double layer and pin-jointed Barrel space structure under two concentrated impacts.

This example is mostly concerned with the highly irregular dynamic responses of a complex system to impact loadings, which is to emphasize on the accuracy and optimum approximation of the left side of Equation (3.42) using a set of adaptive collocation points. Subsequently, the first 2 sec time-history vertical displacements of the node under impact 1 shown in the figure have been calculated and plotted in Figure 3.24. Results computed by the 8th scale of (designated by 2M8) SCW, FCW and LW are compared with those from Wilson-θ and central difference (CD) method.

University of Malaya

Table 3.4: Percentile errors in displacement of 7th mass in the mass spring system, shown in Figure 3.17.

Time	Modal(Ex) Displacement(cm)	LA	Error%	CD	Error%	HA(16)	Error%	CH(16)	Error%	WI	Error%
1	0.60157	0.5293	7.22	0.5131	8.83	0.10829	49.32	0.56822	3.33	0.79650	19.49
1.05	0.7826	0.6367	14.58	0.5729	20.96	0.17341	60.91	0.61304	16.95	1.03676	25.41
1.1	1.07495	0.7442	33.07	0.7786	29.63	0.37103	70.39	1.10716	3.22	1.28102	20.60
1.15	1.43050	1.0583	37.22	1.0954	33.51	0.67933	75.11	1.28895	14.15	1.7325	30.20
1.2	1.79217	1.3724	41.97	1.4720	32.01	1.03134	76.08	1.64067	15.15	1.16438	62.77
1.25	2.10285	1.6977	40.51	1.8484	25.44	1.3918	71.10	2.09593	0.69	1.41708	68.58
1.3	2.31447	2.0238	29.13	2.1654	14.90	1.6837	63.06	2.25856	5.59	2.15614	15.83
1.35	2.39503	2.1643	23.07	2.3737	2.12	1.87921	51.58	2.37134	2.36	2.05929	33.57

Note: CD=central difference, LA=linear acceleration, WI=Wilson (θ=1.4), CH(16)=Chebyshev wavelet (2M16), HA(16)=Haar wavelet (2M16).

Table 3.5: PTARE in displacement of the 5th story, shown in Figure 3.20.

Time	Modal(Ex) Displacement(cm)	LA	Error%	CD	Error%	FCW(16)	Error%	SCW(16)	Error%	LW	Error%
1.2	0.241	0.226	5.92	0.222	7.44	0.231	3.88	0.238	0.73	0.236	1.48
1.25	0.253	0.202	20.33	0.217	13.93	0.235	7.19	0.250	1.06	0.248	2.07
1.3	0.258	0.190	26.35	0.209	19.12	0.219	15.03	0.242	6.44	0.225	12.63
1.35	0.256	0.199	22.07	0.213	16.77	0.222	13.27	0.243	5.31	0.233	9.22
1.4	0.246	0.191	22.10	0.208	15.23	0.215	12.65	0.237	3.92	0.226	8.14
1.45	0.229	0.187	18.57	0.204	10.84	0.202	12.04	0.222	3.18	0.215	6.09
1.5	0.209	0.241	14.99	0.192	8.387	0.185	11.73	0.203	3.13	0.201	4.09

Note: LA=linear acceleration, CD=central difference, FCW (16)=first Chebyshev wavelet (2M16), SCW(16)=second Chebyshev wavelet (2M16) and LW(16)=Legendre wavelet (2M16).

University of Malaya

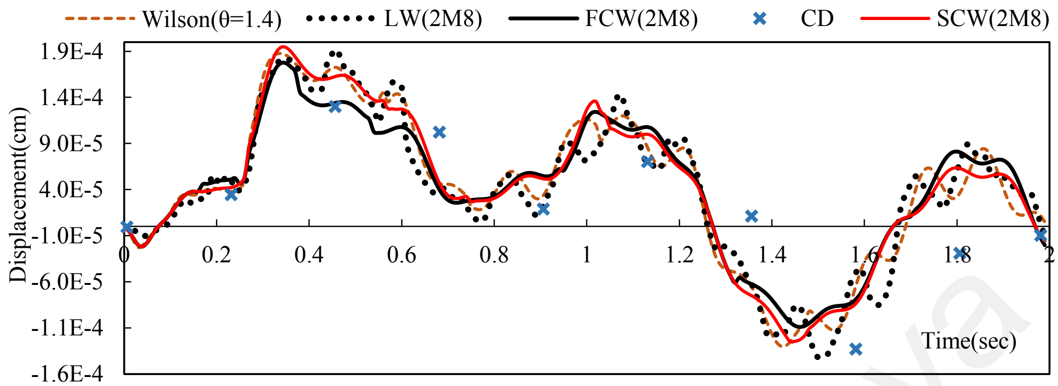

Figure 3.24: Vertical time-history of displacements of the node under impact 1, at the bottom layer shown in Figure 3.23.

As illustrated in Figure 3.24, central difference scheme computed the unacceptable results, in which conditional stability of this method is not satisfied for the selected time increment of Δt=0.001 sec. Finally, CPU time consumption for each numerical scheme is tabulated in Table 3.6. Data in this table show that from optimization point of view SCW and FCW recorded almost the same time consumption. The optimum value recorded was for the use of LW. The efficiency and capability of the SCW is confirmed in Figure 3.24 and Table 3.6, compared with LW, FCW and other numerical methods.

Table 3.6: Computation time involved (min) related to the example 3.

LW(2M8)	4.02
SCW(2M8)	5.58
FCW(2M8)	5.53
Wilson-θ	9.06
Linear acceleration	10.29
central difference	11.39

As demonstrated through this numerical application, the advantage of wavelet functions may be to develop an adaptive numerical approach for tracking details of highly varying structural responses. Aforementioned applicability of the proposed scheme is carried out by less computational time, and therefore the optimum cost of the analysis, particularly for large-scaled structures under complex and wide-band frequency content.

3.6.4 Large scaled 3D spherical truss structure subjected to impact

A complex and double layer space frame with 463 pinned connections, 1760 aluminum bar elements and 1353 degrees of freedom (Poisson's ratio=0.33) is shown in Figure 3.25. To generate the geometry of this system, as mentioned before, relevant program code has been codified in FORMIAN using Formex algebra. The overall dimensions of the structure are given in Figure 3.25 as well as the geometry, cross-sectional area, mass per length and modulus of elasticity which are constant for all members. It is restrained by fixed supports, located at the nodes of the base. Furthermore, this structure is subjected to a 50kN concentrated impact load, which strikes two internal nodes at the bottom layer highlighted in the figure. In addition, damping value is calculated proportional to 0.01 percent of stiffness. It should be noted that, in order to calculate time-history of responses, Δt=0.005 sec and a fairly long time step of Δt=0.01 sec have been selected as the computational time increment for common numerical schemes and the proposed method, respectively. However, the minimum period of the considered system is T_{min}=0.00731 sec.

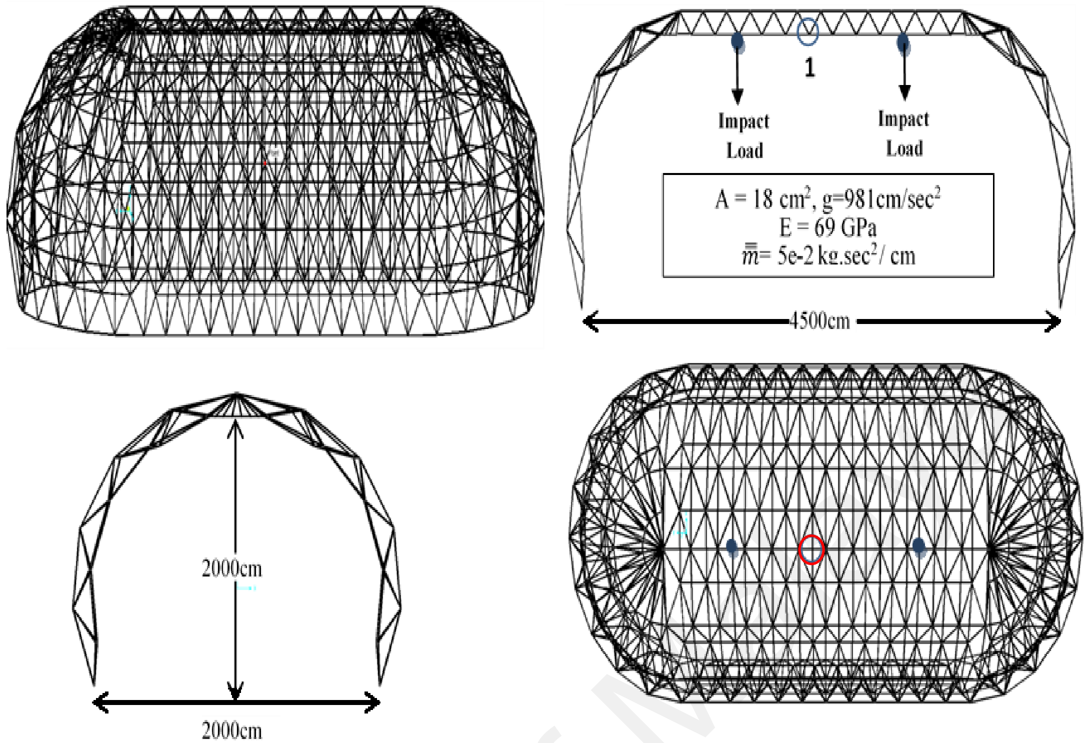

Figure 3.25: A double layer and spherical space structure (bar elements) subjected to two shock loadings.

Subsequently, the first 2 sec time-history vertical displacements of node 1 as shown in the figure have been calculated and plotted in Figure 3.26. In addition, results calculated by 4th scale of the second kind of Chebyshev wavelet (designated by SCW, 2M4) have been compared against 32nd scale of Haar wavelet (designated by 2M32) and common integration approaches, including linear acceleration family of Newmark-β (LA), Wilson-θ and Hilber-Hughes-Taylor (HHT-α). The HHT-α implicit scheme is an alternative approach for the Newmark-β that is more applicable for large-scaled and flexible structures.

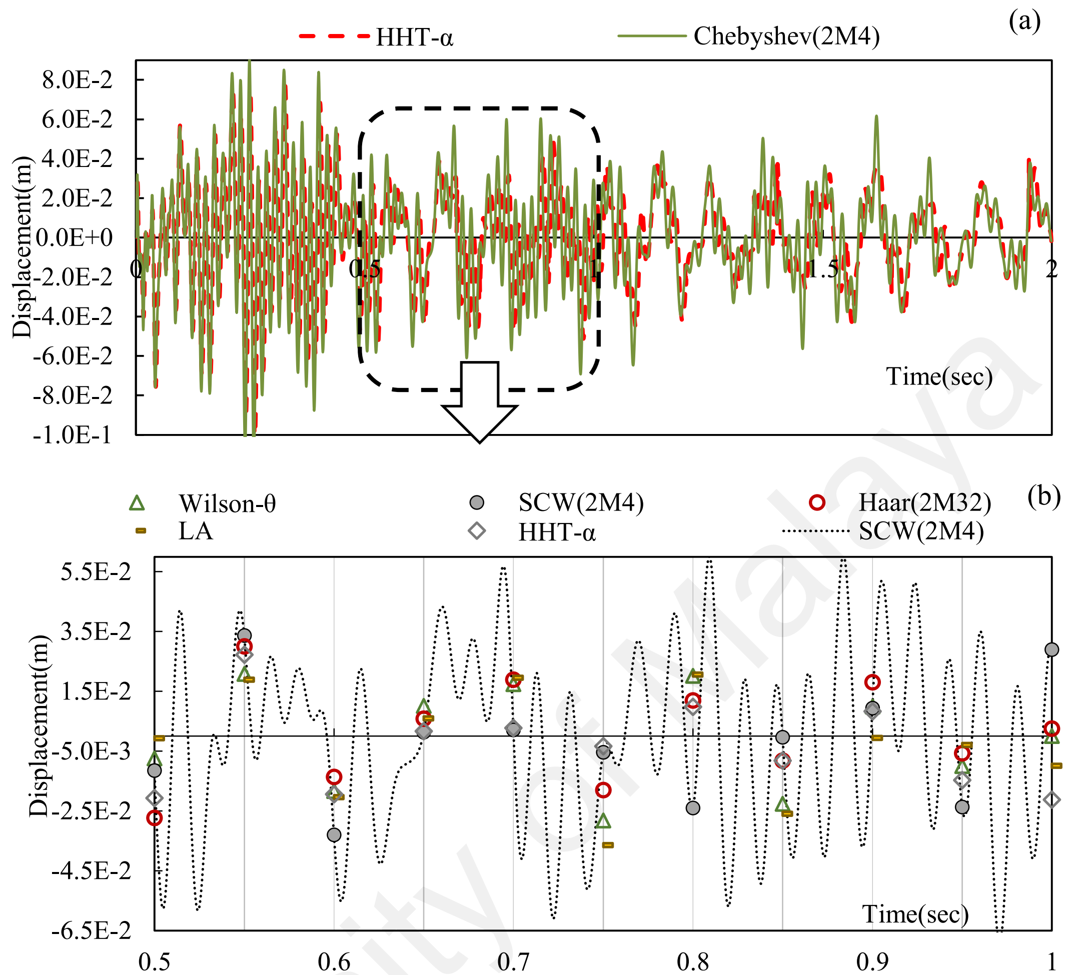

Figure 3.26: Vertical time-history displacement of node 1 shown in Figure 3.25, (a) the first 2 seconds after impact, (b) 0.5-1sec after impact (LA=linear acceleration, HHT- α =Hilber-Hughes-Taylor).

Figure 3.26 shows the closeness of the results computed by HHT (-0.33<α<0) and 4th order of SCW. Furthermore, results obtained using Wilson-θ and linear acceleration gave the second level of accuracy. It can also be seen from Figure 3.26(b) that, the stability and accuracy of responses calculated by the 32nd order of Haar wavelet are reasonably acceptable. The main reason for this is that, details of highly varying transient response of such a complex system is precisely and optimally captured by a high scale of the simple Haar wavelet. It is very important to keep in mind that, from computational time point of view, implementation of such high scales of Haar wavelet is impractical. Finally, it is concluded that, the 4th scale of 3D SCW wavelet is more appropriate for capturing the details than high scale of Haar wavelet.

For comparison purpose, computation time involved and percentile total average errors are given in Figure 3.27. Although it was anticipated that results calculated by the second order of Haar wavelet exhibited the least accuracy, it gave the minimum computational time.

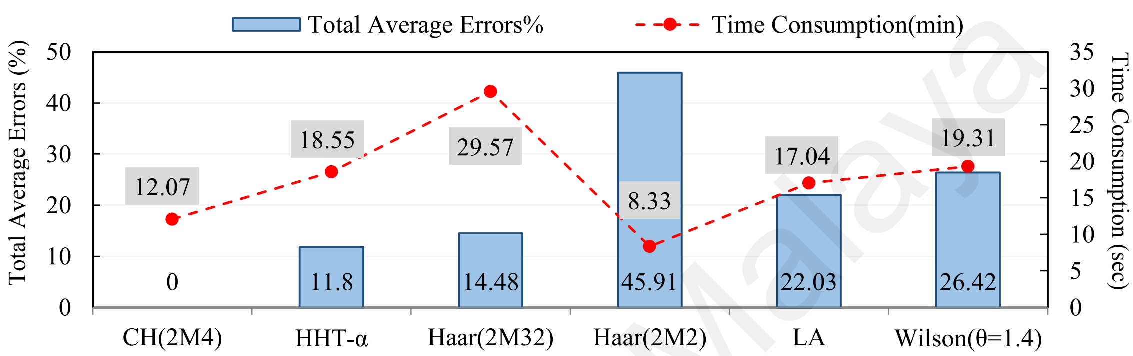

Figure 3.27: Percentile total average errors in vertical displacement of node 1, shown in Figure 3.25 and relative computation time involved. (CH(2Mμ)= μ scale of SCW, LA=linear acceleration, HHT- α =Hilber-Hughes-Taylor).

It is clearly shown in Figure 3.27 that, the proposed scheme computed the optimum responses. Particularly, for applications where impact loadings have been applied on complex structures, wherein the unique features of wavelet bases are used to track the highly varying transient response of systems, i.e. complex and 3D Chebyshev wavelet of the second kind or simple and 2D Haar wavelet. Consequently, it is demonstrated that, the proposed method is an adaptive numerical scheme capable of capturing details in the vicinity of highly varying structural responses.

3.7 Chapter Summary

In this chapter the numerical evaluation of structural dynamics problems (direct analysis) using free scales of Haar wavelet, Chebyshev of the first (FCW) and second kind (SCW), and Legendre wavelets (LW) has been presented. For this purpose, an explicit and indirect procedure has been proposed capable of using different wavelet basis functions. It was shown that, the second-ordered differential equation of motion in the setting domain of time is transferred into the alternative domain of frequency using adaptive collocation points. This transformation was also carried out through the proposed scheme for the broad-band frequency content external loading, simultaneously.

The solution of structural dynamics problems by using the proposed algorithm has advantages at two stages of analysis. Firstly, a compatible numerical approach was improved by being capable of capturing details in the vicinity of highly varying structural responses, and secondly, the external loading is accurately decomposed for its frequency components on compatible collocation points of wavelets.

The stability analysis of the proposed approach of using Haar wavelet, FCW, SCW and LW lies on an unconditionally stable method. The simple calculations for large scales LW generated the fastest operations of this basis functions compared with SCW and FCW. In addition, free scales of simple and 2D Haar wavelet gave the fastest results. However, the most accurate responses were computed by the free scales of SCW.

Consequently, from the optimization point of view, dynamic analysis is accomplished using the proposed scheme with less computation time involved and reliable cost of analysis (emphasizing on the best computational efficiency), particularly for the large-scaled problems subjected to complex loadings. This feasibility demonstrates the value of the proposed scheme for structural health monitoring, structural identification, structural damage detection or active control problems.

Finally, based on results obtained for structural dynamics problems in this chapter, it is anticipated that the application of the proposed method through an inverse problem can develop a very robust strategy to achieve a reliable structural identification and damage detection algorithm. For this purpose, the measured acceleration data can initially be

University of Malaya

decomposed with adaptive wavelet functions, and the velocity and displacement data will be optimally developed using free-scaled adaptive wavelet functions. The application of wavelet transforms for such problems not only provides pattern recognition, but also reduces input noise.

University of Malaya

CHAPTER 4: INVERSE PROBLEMS

4.1 Introduction

Over the past two decades, structural health monitoring has been the area of great technical and scientific interests. Structural health monitoring is a coincidence of the well-known structural identification concept approaching damage detection algorithms. In general, structural identification aims to create or update a model of structure based on experimental measurements or observations. This popular paradigm has been utilized for identification of various problems in civil and mechanical engineering. In fact, the structural identification targets to bridge the gap between the simulated model and the real structure by solving the corresponding inverse problems.

In this chapter, the proposed wavelet-based approach in Chapter 3 is extended to identify simple single-degree-of-freedom (SDOF) systems, initially. The proposed procedure is implemented directly as the identification of only one unknown parameter (stiffness) is considered. Later, for structural identification of multi-degrees-of-freedom (MDOF) systems where the number of unknown parameters to be identified are increased, the genetic algorithms are adopted capable of using the proposed wavelet-based strategy using adaptive wavelets. To be more practical, the identification of input force is developed by using adaptive wavelets applicable to output-only (O-only) measurements. Subsequently, the wavelet-based genetic algorithm is employed to develop an efficient damage detection strategy. Finally, the effectiveness of the proposed method is evaluated by three numerical applications, involving input-output (I/O) and O-only measurements. In order to solve the inverse problem governing to all numerical cases considered, the proposed scheme have been also operated on incomplete measurements as the real and practical measurements.

University of Malaya

4.2 Stiffness identification of SDOF systems

In order to illustrate the solution of inverse problem, structural identification of simple SDOF systems is firstly considered. In general, a linear dynamic equilibrium governing on SDOF mechanical systems of mass (m), damping (c) and stiffness (k) can be expressed as:

$$(m)\ddot{u}(t) + (c)\dot{u}(t) + (k)u(t) = F(t) \tag{4.1}$$

where, $\ddot{u}(t)$, $\dot{u}(t)$ and $u(t)$ represent measured acceleration, velocity and displacement response of the SDOF oscillator. Furthermore, $F(t)$ shows the measured input force. The mass (m) and the damping (c) are assumed as known parameters and the aim is to determine the unknown parameter of the stiffness (k). As there is only one unknown, the proposed wavelet-based method in Chapter 3 can be adopted to identify time-history of stiffness, directly.

4.2.1 Optimum measurement of displacement and velocity from acceleration

Practically, dynamic measurements are usually obtained using accelerometers and installation of extra tools for displacement or velocity measurements are most of the time either inaccessible or very expensive (i.e., laser sensors). In addition, numerical error is the inherent characteristic of numerical integration methods to measure displacement and velocity from acceleration. It is therefore essential to use an accurate and optimum integration scheme to achieve the computationally efficient identification strategies. In contrast to Chapter 3.2.2 where the forward dynamic analysis was carried out, the vector $\ddot{u}(t)$ is assumed as known accelerometer data (e.g., acquired by piezoelectric sensors embedded on SDOF system). Thus, the unit of input data coincides the unit of acceleration (m/sec^2). To numerically approximate the first-ordered (velocity) and the second-ordered integration (displacement), we first start to decompose the output data $\ddot{u}(t)$ on the $2M$ local collocation points of the wavelet basis, emphasizing on the scale of wavelet corresponding to the required accuracy of frequency decomposition of input data $F(t)$. In referring to Equation (3.29) and assumption of the first two transition (k' =2), known vector of measured accelerations is numerically decomposed using the family of Chebyshev wavelets (FCW and SCW), Legendre (LW) or Haar wavelets corresponding to the local fixed $2M$ collocation points as follows:

$$\ddot{u}(t) = C^T \Psi(t) \tag{4.2}$$

To be noted that, $\Psi(t)$ designates the corresponding wavelet coefficients matrix. Subsequently, the coefficient vector corresponding to the decomposed accelerations is calculated as:

$$C^T_{1\times 2^{k'-1}M} = \ddot{u}(t)_{1\times 2^{k'-1}M} / \phi_{(2^{k'-1}M)\times\left(2^{k'-1}M\right)} \tag{4.3}$$

Operating the product matrix of integration P (Equation (3.25)), quantities of relative velocity are then approximated on global time as follows ($d_t = t_{i+1} - t_i$):

$$\dot{u}(t) = d_t C^T P \Psi(t) + v_n \tag{4.4}$$

Eventually, relative displacements are numerically expanded as:

$$u(t) = d_t^2 C^T P^2 \Psi(t) + u_n \tag{4.5}$$

In Equations (4.4) and (4.5), v_n and u_n indicate initial conditions (velocity and displacement) calculated from previous interval for considered wavelet basis function as was clarified in Equations (3.33), (3.34) and (3.35), respectively. To transfer numerical calculations from $2M$ local fixed points of wavelet window to $2M$global points of considered time interval, $d_t$is operated as the coefficient of aforesaid transformation. In other words, quantities of dynamic system are modified corresponding to the local times as:

$$\dot{u}(t) = d_t . v \tag{4.6}$$

$$\ddot{u}(t) = d_t . F(t_n + d_t . \tau , u , v) \tag{4.7}$$

As was shown in Chapter 3, it is anticipated that numerical computations will be optimally satisfied on two steps of calculations. Firstly, the quantities of the first and second order of integration are independently approximated from mass, damping, stiffness and applied loadings. Secondly, details of the broad-frequency content accelerometer data are accurately captured using free scales of considered wavelets.

4.2.2 Optimum measurement of acceleration derivatives

In physics, the quantity of jerk $\dddot{u}(t)$ describes the derivative of acceleration with respect to time (namely, the sensitivity of accelerations). The efficient operator of derivative using adaptive wavelets was presented in Chapter 3.5. In this subsection, the proposed operator of derivative is extended to calculate the first derivative of measured acceleration with respect to time (namely, jerk). For the vector of measured accelerations $\ddot{u}(t)$, Equation (3.57) can be rewritten as follows:

$$\ddot{u}(t) = \ddot{u}(t_n) + \int_{t_n}^{t} \dddot{u}(t) dt \tag{4.7}$$

Using Equation (3.29) to expand the derivative function on global times yields:

$$\dddot{u}(t) = C^T \Psi(t) \tag{4.8}$$

Substituting into Equation (4.7):

$$\ddot{u}(t_{n+1}) = \ddot{u}(t_n) + \int_{t_n}^{t_{n+1}} C^T \Psi(t) \ dt \tag{4.9}$$

Accordingly, operational matrix of integration (P) is operated to numerically simplify (4.9) as:

$$\ddot{u}(t_{n+1}) = \ddot{u}(t_n) + d_t C^T P \Psi(t) + \ddot{u}(t_0) \tag{4.10}$$

University of Malaya

Calculating C^T (corresponding to the global times) and considering initial condition of $\ddot{u}(t_0)$ and substituting into Equation (4.8), the first-ordered derivative of acceleration with respect to time (namely, acceleration sensitivity) is numerically approximated. The quantity of jerk is one of the very sensitive dynamic quantities to the small changes in measured outputs (that mostly are accelerations). Thus, it will be shown later that our proposed method for structural damage detection also concerns with the evaluation of this quantity rather than acceleration itself. However, to enhance the computational efficiency of the proposed procedure in this research, the very optimum computation of jerk is developed by using adaptive wavelet functions on longer time intervals. To clarify the aforementioned concept, a simple example is given in Figure 4.1. Figures 4.1(a) and 4.1(b) show an arbitrary displacement and relative acceleration time-history, respectively. An impact is imposed to the system (i.e., due to the loss in stiffness) at the third second of evaluation. The effectiveness of the proposed idea for optimum analysis of jerk using various scales of wavelet functions (shown in right-hand column) is compared with the normal incremental computation of derivatives (illustrated in the left-hand column). For each case (each row of c to g in the figure), the same sampling rate (or time interval of Δt) is investigated. However, for a detailed comparison, the number of colocation points considered for wavelet functions varies with respect to the different time intervals. To be noted that, LW is considered as the wavelet basis function to evaluate this example.

It was anticipated that, for the purpose of an accurate evaluation of the quantity of jerk, the maximum sampling rate of 1000 sampling points should be considered e.g., Δt=0.001, shown in Figure 4.1 row (c). Although, using such sampling rates diversely affects the computational efficiency of the evaluation strategy. Significantly, this figure demonstrates the effectiveness of the proposed method to optimally compute the sensitivity with the considerable lesser sampling rates of only 2 points e.g., Δt=0.5 on the compatible collocation points of wavelet e.g., $2M$=4 or 8 shown in Figure 4.1 rows (f) or (g). It is apparent from the figure that, the proposed method magnificently detect the sudden changes in output signal through the very optimum computations. However, it will be shown later that the choice of sampling rate and number of adaptive collocation points should be accurately decided for integrating the broad frequency contents of the measured (output) signal. It should be pointed out that, the large-scaled structural systems and correspondingly measured data are the focus of interest in the most practical cases. In other words, the computational performance of identification strategy will be considerably enhanced by using an optimum operation for evaluation of very excessively large data.

4.2.3 Stiffness identification

The optimum measurements of responses were discussed for SDOF mechanical systems, emphasizing on only the measurement of one DOF. However, the proposed strategies are applicable for MDOF systems where the measurement of dynamic responses of each DOF may be considered. Accordingly, assumption of known mass and damping, the time-history of stiffness in Equation (4.1), is determined by solving Equation (3.40). For this purpose, quantities of measured acceleration, displacement and velocity are acquired from Equations (4.2), (4.4) and (4.5). To be noted that, the only one natural frequency of ($\omega = \sqrt{(k)/(m)}$) is obtained for the proposed SDOF oscillator in Equation (4.1). Consequently, the distinguishable influence of the proposed wavelet-based procedure of structural identification is efficiently capturing the broad-frequency contents of external loading $F(t)$. Eventually, fast and accurate computations constitute the main advantage of the proposed method for online health monitoring.

University of Malaya

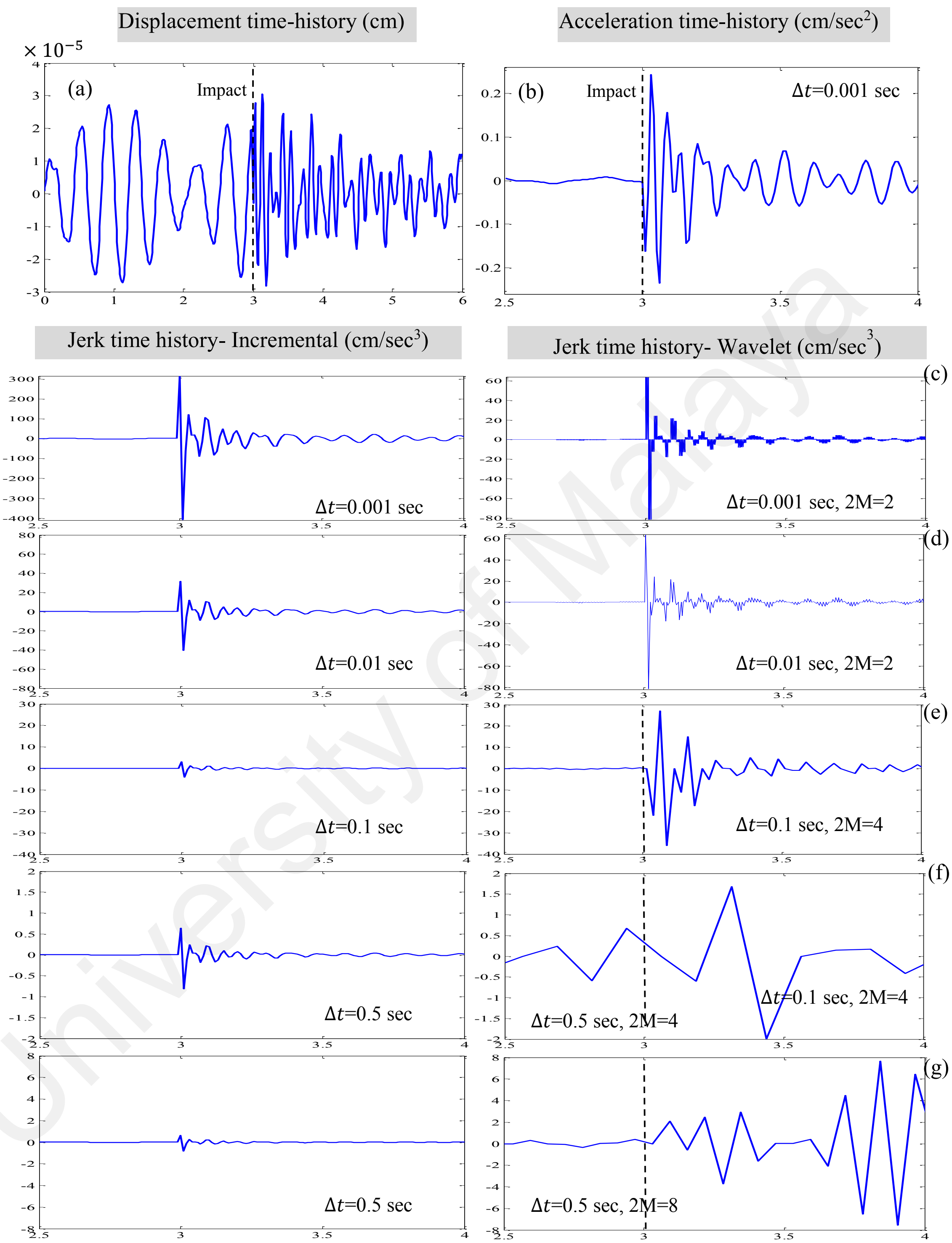

Figure. 4.1: The magnificent sensitivity of jerk using the wavelet operators on optimum collocations compared with the normal incremental procedure.

4.3 Structural identification of MDOF systems using genetic algorithms

Basically, structural identification of MDOF systems is a more controversial challenge rather than SDOF ones. In this regard, there are many unknown parameters should be identified corresponding to the number of structural DOFs (for shear structures) or structural elements (i.e. identification of structural mass, damping and stiffness). Moreover, it is very important to keep in mind that in many practical structural identifications, output-only (O-only) measurements are available and force identification should also be considered. Accordingly, solving the governing optimization problem on the MDOF system with measured inputs, is one of the popular options to identify unknown dynamic parameters.

Over the last two decades, solution of optimization problems has been undergone to the significant improvements. Two well-known strategies of genetic algorithms (GAs) and neural network (NN) have demonstrated their efficiency in various subjects of science and engineering. The basic neural network comprised of three layers, an input, hidden and output layer. The inputs may be fed by proper weighting of the connections and using simple functions at the neurons to reach at the outputs for linear or non-linear systems. The main advantage of NN is the possibility of training the network. However, this also constitutes the main drawback of NN where for identification of large-scaled systems, huge amount of data are required for the appropriate training. As a consequence, incorrect values will be identified if incomplete pattern data is measured.

The identification procedure utilized in this research for the solution of inverse problems lies on genetic algorithms which are inspired by Darwin's theory of natural selection and survival of the fittest. For this purpose, in subsequent sections the employment of simple GA is concerned for structural identification, and then the proposed improvement of GAs strategy

University of Malaya

will be introduced. The core of developed GAs is structured based on using adaptive wavelet functions which was discussed in previous chapter and sections.

Fundamentally, there are two possible aspects can be proposed for time-domain structural identification capable of utilizing wavelet analysis through GAs shown in Figure 4.2.

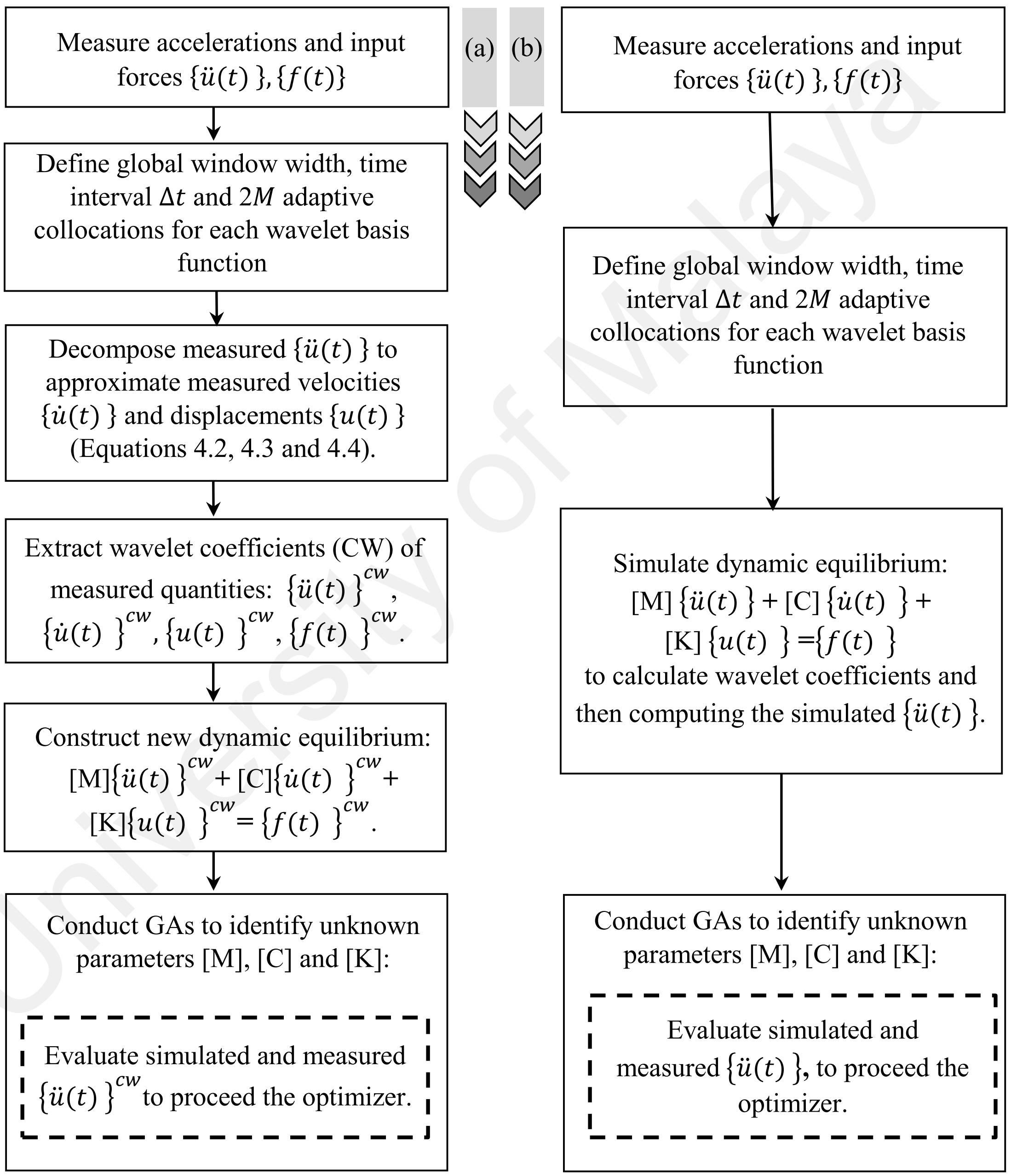

Figure 4.2: The proposed approaches capable of using adaptive wavelets through GAs, (a) for initial and rough identification, (b) for accurate and reliable identification.

University of Malaya

As illustrated in Figure 4.2, the first procedure (a) concerns with adopting GAs on the wavelet coefficients of responses and input forces which are mostly very small values. As a consequence, even by normalizing the unknown parameters to small values to overcome the computational difficulties, most of the time the solution of inverse problem lies on ill-condition problem and the accuracy of approximate solution degrades. In contrast, the second procedure (b) concerns with the comparison of simulated responses against measured responses to process the GAs strategy. From the preliminary investigation carried out on several applications, it is concluded that results of the first approach are not sufficiently accurate, and therefore the identification is less reliable. However, the computational process is faster than the second procedure especially by using longer time windows. For this reason, the first approach (a) may be preferred as initial predictions while for accurate corrections and therefore reliable identification the second strategy is strongly recommended.

4.3.1 Simple GAs

The major early work on adaption based on GAs was by John H. Holland (Goldberg and Holland, 1988). Adaption is regarded as a process of progressive variation of structures, leading to an improved performance. He recognized the similarities between natural and artificial systems. Recognizing that operators such as crossing over and mutation that act in natural systems were also presented in many artificial systems. GAs are search algorithms that combine a survival of the fittest mentality with a structured and random one and then exchange information in order to explore the search space. Mathematically, it is achieved by representing possible solutions as coded strings. Many such strings are created and each representing a different location on the given search space. These strings are then evaluated according to some criteria, and the fittest are given a higher probability of selection. Parts of the selected strings are combined to form new strings and occasionally part of the string is randomly assigned a new value. The method is similar to human search where good solutions receive more attention while bad solutions are less favored. The overall layout of a simple GA strategy is depicted in Figure 4.3.

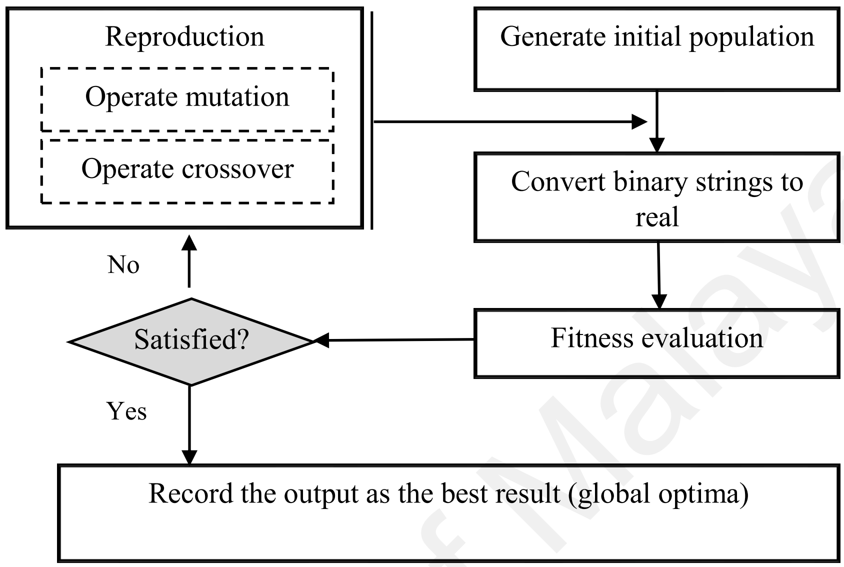

Figure 4.3: Overall layout of a simple GA.

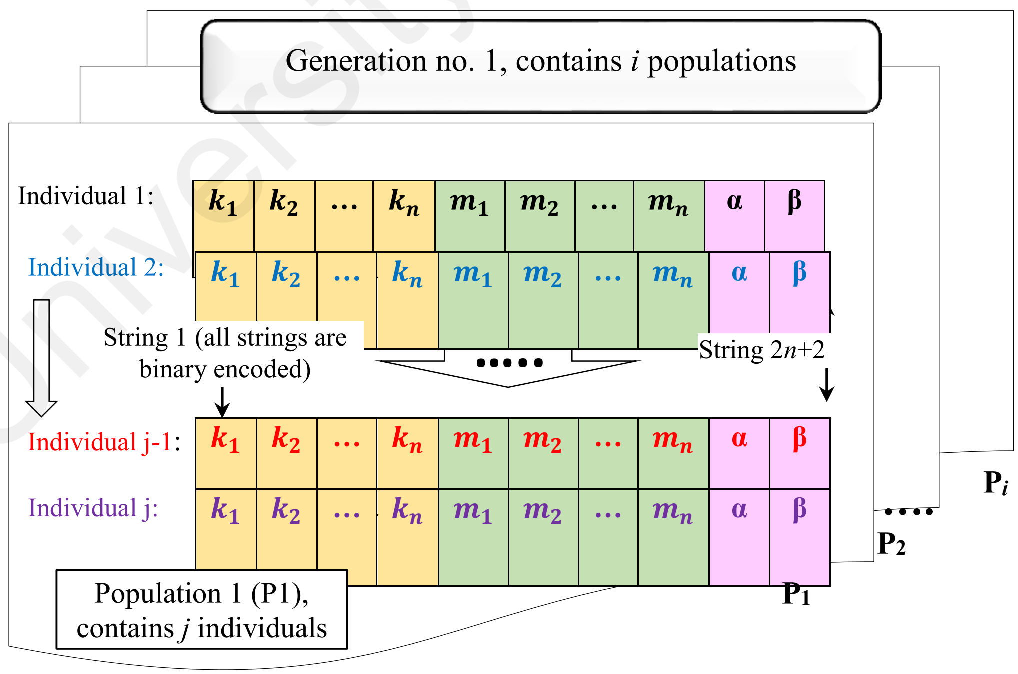

Figure 4.4: Representation and storage of a simple GAs for the identification problems comprised of n structural elements.

As shown in Figure 4.3, a simple GA is based on binary encoding. As a consequence, operations of mutation and crossover will be executed only uniformly, however, it will be discussed later that to enhance the performance of GAs strategies, implementation of non-uniform operators of mutation and crossover is essential. Some of the basic features of a simple GA is illustrated in Figure 4.4 for structural identification through an inverse problem. Figure 4.4 shows the capability of GA with different performances to find the global optima. In performing a GA strategy, the reliability and robustness of the solution is very important. The population size (number of individuals) involving j number of fixed $2n+2$ strings (referring to n structural elements) and number of populations in each generation are taken after an engineering judgment about the either prescribed convergence of results or computational efficiencies.

It is also possible to influence the search by selecting appropriate crossover and mutation rates, however in general, there is a trade-off between exploration (broad search) and exploitation (local search). For instance, small crossover and mutation rates help explore the domains around the current solutions, and thus are less likely to destroy good solutions. Although, it will make it more difficult to explore new possible solutions. On the other hand, large crossover and mutation rates help to cover wider domains, however at the expense that the desirable solutions are less likely to develop further and thus they find it harder to converge.

4.3.1.1 Fitness evaluation and selection

Two underlying features of any GAs strategy are the fitness evaluation of possible solutions and accordingly selection of good results. For the purpose of fitness evaluation, the response of structure i.e., acceleration is numerically simulated using the proposed wavelet-based approach for the predicted properties of structure (generated in different strings). On

University of Malaya

the other hand, the actual response of structure have been measured for each existing DOF of structure. Consequently, one may evaluate the fitness function as follows (Perry, Koh, and Choo, 2006):

$$Fitness = \frac{1}{0.001 + MS} \tag{4.11}$$

where, MS is the difference between measured and simulated responses. Thus, this value is obtained as follows:

$$MS = \frac{\sum(Measured - simulated)^2}{Measured\ DOFs} \tag{4.12}$$

As it is shown in Equation (4.12), the fitness is evaluated from the total sum of square error between the simulated and measured response of the structure at each time step. Finally, this value is divided by the total measured DOFs. This function bounds the maximum fitness at 1000 showing that, when errors approach zero (MS=0), results have converged. In addition, final selection will be carried out using roulette wheel procedure based on the maximum probability of selection for fitted individuals. The step-by-step algorithm of simple GA using adaptive wavelet functions is tabulated in Table (4.1).

It should be emphasized that according to the simple GA, the rate of crossover and mutation can be reduced from the initial populations to the later ones in a single generation. Therefore, the exploration (global search for promising solutions) and exploitation phases (local search around optima) of GA strategy will be proceeded much more properly.

University of Malaya

Table 4.1: Step-by-step algorithm of simple GA using adaptive wavelet functions.

C. Initial calculations:

(11) Define upper and lower limits for unknown variables (mass: **M*i***, damping ratio: **D*i***, stiffness: **K*i***). ***i*** refers to the ***i*** th DOF.
(12) Define the required precision for each variable.
(13) Define the crossover and mutation rate.
(14) Define the geometry of structure.
(15) Define the number of required populations in a single generation as well as the population's size.
(16) Specify the location of each variable on corresponding strings.
(17) Randomly generate the initial population (0 or 1 due to binary encoding).
(18) Specify wavelet basis function, number of collocation points, the considered order of wavelet based on the sampling rate of the measured responses.
(19) Select an appropriate time step $\boldsymbol{d_t}$ (concerning an efficient solution).
(20) Form coefficients wavelet matrix corresponding to collocation points for free-scaled orders of wavelet function $\boldsymbol{\phi(t)}$.
(21) Form operation matrix of integration corresponding to collocation points for each particular wavelet function $\boldsymbol{P}$.
(22) Calculate square operational matrix $\boldsymbol{P^2}$.
(23) Approximate unity, with related coefficient of wavelets.
(24) Form identity matrix of $\boldsymbol{I}$ on collocation points.

D. For each iteration:

(5) Convert binary strings to real value for each individual.
(6) For each individual form the properties matrices (predicted mass: **M**, damping ratio: **D**, stiffness: **K**) using the known geometry and structures behavior (i.e., MDOF shear building, 2D pin-jointed truss, 3D truss and so on).
(7) Use the proposed method of time integration (wavelet-based method) to solve simulated responses of dynamic equilibrium: $\mathbf{M}\,\ddot{u}(t) + \mathbf{C}\,\dot{u}(t) + \mathbf{K}\,u(t) = F(t)$
(8) For each DOF or member, corresponding to each individual, calculate displacement, velocity and acceleration vectors at each time interval, simultaneously by:
$u(t) = C^T P^2 \Psi(t) + u_{n0}$
$\dot{u}(t) = C^T P \Psi(t) + v_{n0}$
$\ddot{u}(t) = C^T \Psi(t)$
(9) Evaluate the fitness function using Equation (4.11).
(10) Investigate the rate of convergence of responses. If results are converged then ***exit*** iteration and record the identified values as the actual values; if not, continue to next step.
(11) Perform the roulette wheel selection method.
(12) Rearrange and sort the whole population's individuals from the best fit to the worst.
(13) Pair individuals.
(14) Operate crossover and mutation to paired individuals.
(15) ***Go*** to step B. (1).

University of Malaya

4.3.2 Modified multi-species GAs

Over the past two decades, there are diverse forms of GAs have been widely improved. A fundamental coding was using binary representation for simple GAs and set of operators i.e., crossover, mutation and reproduction. More recently, much efforts have also been made to alter the architecture of GA to be practical for solving complex problems. One of the popular modified GA (MGA) utilizes migration and artificial selection for real encoding variables. The underlying components that distinguish this strategy are not only inclusion of multi-species (sub-populations) but also a rank based selection and a new tagging procedure to ensure diversity in the best solutions (Michalewicz, 2013). In contrast to the simple GAs, the proposed multi-species strategy here is real encoded and as such adopts non-uniform operators. Floating point representation allows the focus of the search to vary, not just across species, but also over time. Therefore, the main advantage of performing multi-species is that various GA-based operators can be implemented to complement one another.

4.3.3 Wavelet-based MGAs

The proposed wavelet-based MGAs (WMGA) strategy in this research is benefitted by a computationally efficient scheme for fitness evaluation using adaptive wavelet functions. This enables using more sub-populations within a population and increasing the convergence of results and therefore improving computational competency and robustness of structural health monitoring strategies. The proposed procedure is developed in order to provide a reliable identification algorithm for large-scaled structures that simultaneously explores the search domain and focuses on promising individuals. The construction of the proposed WMGA strategy utilized in this research is depicted in Figure 4.5.

University of Malaya

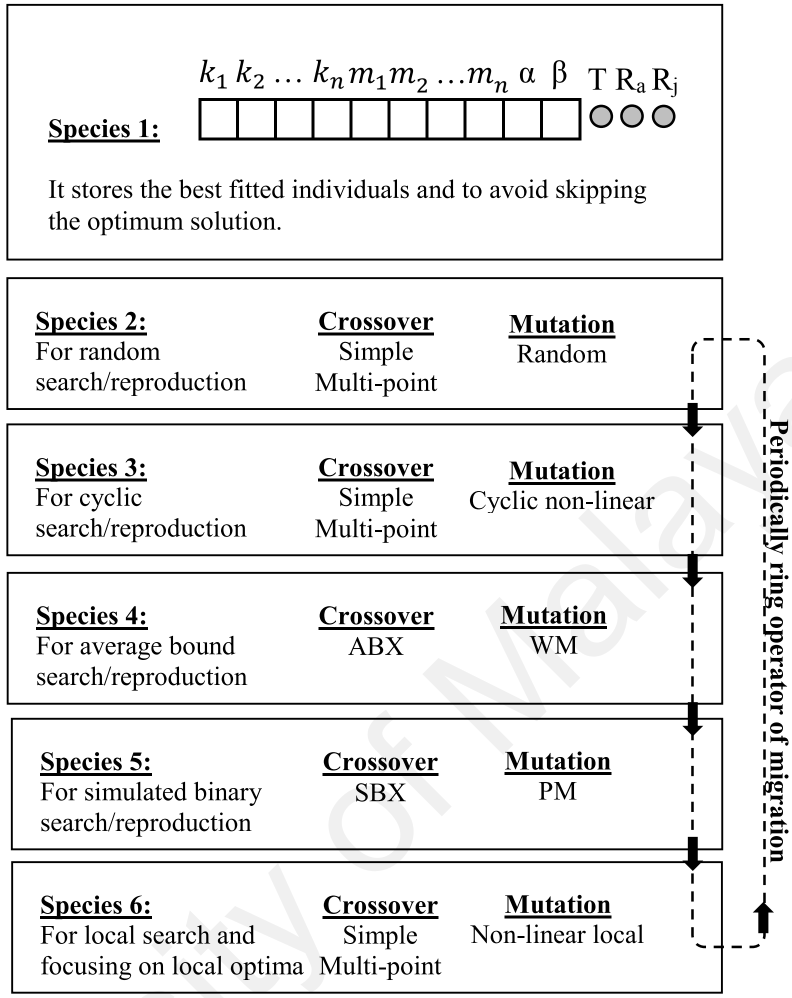

Figure 4.5: The construction of the proposed multi-species population capable of using WMGA.

Accordingly, the adopted WMGA strategy to identify unknown dynamic parameters is discussed in detail as following subsections.

4.3.3.1 Modification of multi-species populations

As shown in Figure 4.5, each population involves 6 species with different GA-based operators. In this section the corresponding features of each species 1 to 6 are elaborated.

University of Malaya

- ***The first species:***

Essentially, there is no GA-based operators are employed on this species so as this sub-population is solely designed to store the best results. The tagging procedure (designated by string T in Figure 4.5) prevents saturating this species by selecting a same individual many times. For this purpose, all individuals are initially assigned 0 as tag number and if an individual being selected for species 1 the tag is changed to 1. This tag follows individual wherever it goes until this individual being altered by any GA-based operator, in this case the tag will be changed back to 0, denoting a new individual and making it available to be selected as the best solutions for species 1.

- ***The second species***

The crossover operators utilized for species 2, 3 and 6 lies on the simple and multi-points operators of crossover. Assumption of P_{cs} and P_{cm} for the probability of simple and multi-point crossover operations, the total crossover rate P_{ct} which shows the effective probability rate of an individual being involved in at least one crossover is as follows (Perry et al., 2006):

$$P_{ct} = 1 - (1 - P_{cs})(1 - P_{cm}) \tag{4.13}$$

Furthermore, species 2 is designed for a wide and random search for possible optima within the search limits prescribed for unknowns. To randomly generate new possibilities, a random real number is generated as $r \in [0\ 1]$ and the random mutation is developed by:

$$x_i = LL_i + r \times (UL_i - LL_i) \tag{4.14}$$

In Equation (4.14), x_i, LL_i and UL_i indicate the ith altered unknown (parameter), the ith lower and upper limits of the search domain, respectively.

- ***The third species***

Mathematically, it is demonstrated that the accuracy and convergence rate of optimization problems are influenced by operating the so-called non-uniform mutation. This is because of the reduction of the average magnitude of mutations during the procedure of optimization (Michalewicz, 2013). The mutation operator designated for species 3 lies on the cyclic non-uniform mutation. The underlying principal is to slightly reduce the number of mutations as the optimizer proceeds. Logically, this operator will increase again after the regeneration, to allow a broad search for possible solutions. Assumption of a random real number $r_1 \in [0\ 1]$ and random integer $r_2 \in [0\ 1]$, the operator of cyclic non-uniform mutation is obtained as follows (Perry et al., 2006):

$$x_i = x_i + (UL_i - x_i) \times \left(1 - r_1^{\left(1 - \frac{0.9MOD(g,R)}{R}\right)}\right) \quad if\ r_2 = 0$$
$$x_i = x_i + (LL_i - x_i) \times \left(1 - r_1^{\left(1 - \frac{0.9MOD(g,R)}{R}\right)}\right) \quad if\ r_2 = 1 \tag{4.15}$$

In Equation (4.15), g and R denote the generation number and the number of generations between regenerations, respectively. In addition, MOD represents the operation of reminder.

- ***The forth species***

The Average and Bound crossover (ABX) is proposed as the crossover operator of this species. This operator was adopted by Ling and Leung (2007). However, they did not concern with the improvement of fitness evaluation (FE), as this operator requires inner FE and from the computational cost point of view is inherently a costly operator, especially for large-scaled structures with the numerous unknowns to be identified. Based on this method, four offspring ($o_1 - o_4$) are obtained from two parents ($p_1$and p_2) in new generation, including two of the average ($o_1$and o_2) and two of the bound ($o_3$and o_4) crossover as follows:

$$o_1 = \frac{x_i^{p_1} + x_i^{p_2}}{2}$$

$$o_2 = \frac{(UL_i + LL_i)(1 - \omega_a) + \left(x_i^{p_1} + x_i^{p_2}\right)\omega_a}{2} \tag{4.16}$$

$$o_3 = UL_i(1 - \omega_b) + \max\left(x_i^{p_1}, x_i^{p_2}\right)\omega_b$$

$$o_4 = LL_i(1 - \omega_b) + \min\left(x_i^{p_1}, x_i^{p_2}\right)\omega_b$$

Ling and Leung (2007) suggested that however the weight factor ω_a could be selected 1, the range of [0.5 1] is reasonable. In addition, they adopted $\omega_b \in [0\ 1]$ for several numerical investigations. The FE of $o_1 - o_4$ will be carried out and the fitted offspring will be selected. Subsequently, the mutation operator of species four is a wavelet-based mutation (WM) proposed by Ling et al. (2007). Assumption of ${UL_i}^{max}$ and ${LL_i}^{min}$ as the maximum and the minimum value for upper and lower limits of unknowns in an individual, the WM mutation is obtained as follows:

$$x_i = \begin{cases} x_i + \delta({UL_i}^{max} - x_i) & if\ \delta > 0 \\ x_i + \delta\left(x_i - {LL_i}^{min}\right) & if\ \delta \le 0 \end{cases}$$

$$\delta = \frac{1}{\sqrt{a}} e^{\frac{-(\varphi/a)^2}{2}} \cos(5\left(\frac{\varphi}{a}\right))\ ;\ \varphi \in [-2.5,2.5] \tag{4.17}$$

$$a = e^{-\log(\gamma)(1-g/G)^{\zeta} + \log(\gamma)}$$

In Equation (4.17), g, G and ζ represent the generation counter, the total number of generations and the shape parameter of the monotonic increase ($\zeta \in [0.2,5]$). γ is the upper limit of parameter *a* and could be assigned 10000. To be noted that, this operator behaves as a local search mutation, however it just designed to locally search around the promising random results in only species four and not for fine-tuning search on the best results of the

University of Malaya

whole population. To overcome this issue, the presented WMGA strategy in this research complemented with the sixth species, as well.

- ***The fifth species***

The crossover operator designed for this species is the Simulated Binary crossover (SBX) adopted by Deb and Agrawal (1994). Assumption of η_c=2 (Deb and Gulati, 2001) as a parameter to control the spread, SBX is derived as follows:

$$o_1 = 0.5[\left(x_i^{p_1} + x_i^{p_2}\right) - \beta|x_i^{p_2} - x_i^{p_1}|]$$

$$o_2 = 0.5[\left(x_i^{p_1} + x_i^{p_2}\right) + \beta|x_i^{p_2} - x_i^{p_1}|]$$

$$\beta = \begin{cases} (2r_1)^{\frac{1}{\eta_c+1}} & if\ r_1 \leq 0.5 \\ \dfrac{1}{2(1-r_1)^{\frac{1}{\eta_c+1}}} & otherwise \end{cases} \tag{4.18}$$

In Equation (4.18), r_1 is a real random number as introduced earlier. Accordingly, the Parametric-based mutation (PM) operator proposed by Deb and Gulati (2001) is considered for this species. Basically, it performs a polynomial probability distribution to generate a mutated individual in the neighborhood of the original one. Let r_1 a real random $\in$ [0 1] for problems concerning the upper and lower bounds it is obtained as follows:

$$\bar{\delta} = \begin{cases} [2r_1 + (1-2r_1)(1-\delta)^{\eta_m+1}]^{\frac{1}{\eta_m+1}} - 1 & if\ r_1 \leq 0.5 \\ 1 - [2(1-r_1) + 2(r_1 - 0.5)(1-\delta)^{\eta_m+1}]^{\frac{1}{\eta_m+1}} & otherwise \end{cases} \tag{4.19}$$

$$\delta = \min[(x_i - LL_i), (UL_i - x_i)]\,/(UL_i - LL_i)$$

In Equation (4.19), η_m is the distribution index for mutation and takes any non-negative value. This value regulates the achieved perturbation and may be selected around 100 to gain the mutation effect of 1%. To be emphasized that the total number of mutated individuals $N_m$for each species is defined and so the species size remains constant after reproductions.

University of Malaya

- ***The sixth species***

Species 6 is designed to focus on the local optima (i.e., the local search around the best results). For this purpose, small mutations are employed to refine the best solutions by operating a non-uniform mutation, whereby the mutation rate is slightly reduced as the optimization proceeds. The following mutation operator is considered to accomplish this goal (Perry et al., 2006):

$$x_i = x_i + 0.5 \times (UL_i - x_i) \times \left(1 - r_1^{\left(1-\frac{g}{G}\right)}\right) \quad if\ r_2 = 0$$
$$x_i = x_i + 0.5 \times (LL_i - x_i) \times \left(1 - r_1^{\left(1-\frac{g}{G}\right)}\right) \quad if\ r_2 = 1 \tag{4.20}$$

In Equation (4.20), G denotes the total number of generations to be run. Finally, a periodic operator of ring migration is designed to exchange the best results between species 2 to 6 as shown in Figure 4.5. This operator is regulated based on two parameters z_1 and z_2. The first parameter controls the number of generations between two migrations whereas the second one is the fraction of species size involved in the migration. In this study, z_1=5 and z_2=0.1-0.2 are utilized as the periodicity of the operator and the portion of sub-population to be involved in migration, respectively.

4.3.3.2 Modified search space reduction technique

Basically, the convergence rate and accuracy of the GA-based identification strategies are highly dependent to the width of the search space. As a consequence, by adaptively reducing the search limits, a more satisfactory identification is possible with the best computational efficiency (Perry et al., 2006). The SSRM strategy implemented in this study is illustrated in Figure 4.6.

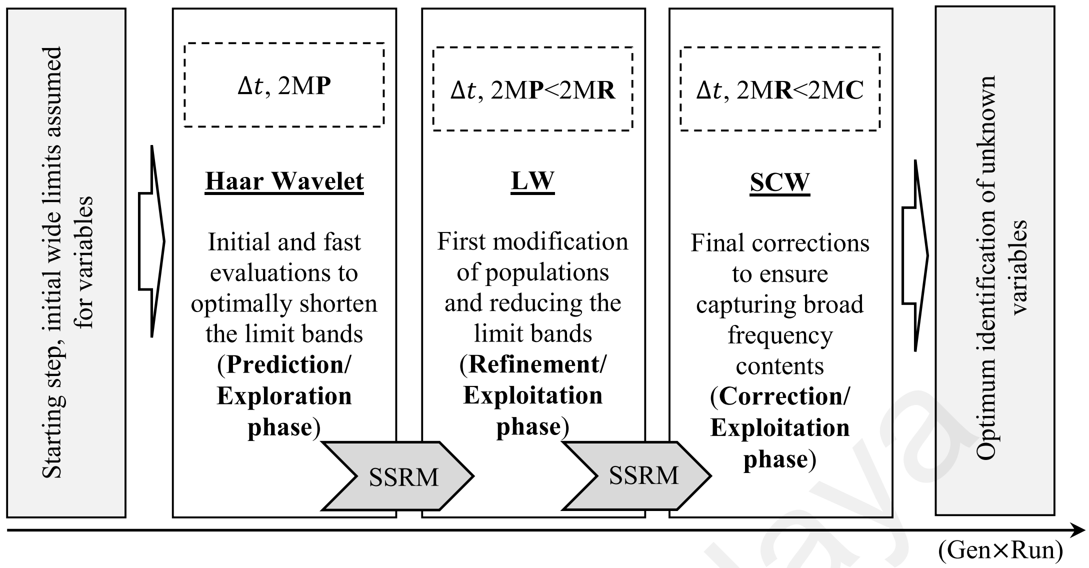

Figure 4.6: The proposed SSRM strategy capable of using adaptive wavelets for optimum identification through WMGA.

University of Malaya

As it is shown in Figure 4.6, the proposed SSRM involves a very fast prediction and therefore reduction of initial search limits by using simple and 2D Haar wavelets on optimum collocations ($2M$P). This phase may be interpreted as exploration phase and there is the most relevant variations around local optima. It should be emphasized that, initial search limits, in fact, lies on a wide limits for unknown parameters. At the second stage of the strategy, the search limits have been refined by using 3D LW for fitness evaluation of individuals as the same sampling rate as was considered for the first step. To ensure capturing all features of I/O signal more collocation points ($2M$R) are preferred at this stage. Accordingly, this stage is adopted for exploitation phase where the small variations around the global optima is existed. Finally, employing the accurate SCW for fitness evaluation guarantees the promising solutions being selected. In this regards, all details of I/O signals are collectively captured on adaptive collocation points ($2M$C), and therefore the last corrections of unknowns are optimally ascertained until the prescribed convergence rate is achieved (namely, the final exploitation phase). The motivation behind the proposed development arises from the fact that the overall computational efficiency of the identification strategy for large number of unknowns is rigorously dependent on optimally reducing the search limits with the emphasis on accuracy of results.

4.3.3.3 Fitness evaluation and artificial selection

Eventually, the fitness of each individual in all species proposed in this study are evaluated by adding the inverse of total sum of square errors between the measured and simulated time-history of accelerations for off-line applications and the quantities of jerk for online identification problems as follows:

$$Fitness = \frac{1}{\varepsilon + \frac{\sum(Acc_{meas.} - Acc_{simu.})^2}{DOF_{meas.}}} + \frac{1}{\varepsilon + \frac{\sum(jerk_{meas.} - jerk_{simu.})^2}{DOF_{meas.}}} \tag{4.21}$$

In Equation (4.21), DOF, meas. and simu. represent the total measured DOFs, measured and simulated data, respectively. ε may takes a small value of 0.001 to prevent computational difficulties. In this research, the first term in Equation (4.21) is proposed for the fitness evaluation due to the analysis of accelerations (designated by Fit_a) and the second term is the fitness due to the jerk analysis (designated by Fit_j). Later, the selection procedure is carried out by allocating the probability of selection to each individual due to its final fitness. To magnify the differences between different fitness values, a ranking procedure is employed to obtain the probabilities within each species. In other words, the fitted individual is ranked the total number of population size and the rest are descended due to the value of the fitness function for both Fit_a and Fit_j. The notable point on the proposed fitness evaluation (FE) lies on the sufficiently optimum evaluation of Fit_j by wavelet functions for the small sampling rates (in referring to Figure 4.1). This significantly improves the fitness values and rapidly yields the convergence rate. It will be shown later that in practical and large-scaled applications, whereby there is a loss in stiffness concurrent to the system identification (referring to the online damage imposed), by employing the second term of FE in Equation (4.21), not only the place of imposed impact on time axis but also the magnitude of the reduction in stiffness are confidently detected. In this research, LW(2M4) is performed with very small sampling rate of 20 S/s ($\Delta t = 0.05$ sec compared to the acquired $\Delta t = 0.001$ sec) for the effective jerk-based FE of all species. As it was mentioned before, the fast and precise computation of LW increases the computational competency of the proposed FE and leads the reasonably reliable online identification.

4.3.3.4 Practical algorithm of WMGA strategy

The optimum structural identification strategy is achieved by adopting the non-conventional wavelet-based GA operators (namely, WMGA). The procedure involves reintroduction, regeneration and artificial selection of ranked individuals. To guarantee that species 6 (designed for the local search around the best results) operates on a set of desirable solutions the reintroduction is necessary. This comprises copying individuals from species 1 (the best solutions) into species 6 at a prescribed period. The number of times that reintroduction should be done must consider that the best solutions require to be developed, and that species 6 requires some time to improve possible solutions, however, it is found that a large number of reintroductions commonly gains the better results. In addition, a common issue of GA-based strategy is that the optimization may be converged to the local optima. To overcome this issue a regeneration operator is designed for species 2 to 5 and the process will be effectively started to find global optima and new possibilities while species 6 focuses on refining the previously generated individuals. The schematic flowchart of the proposed WMGA is depicted in Figure 4.7.

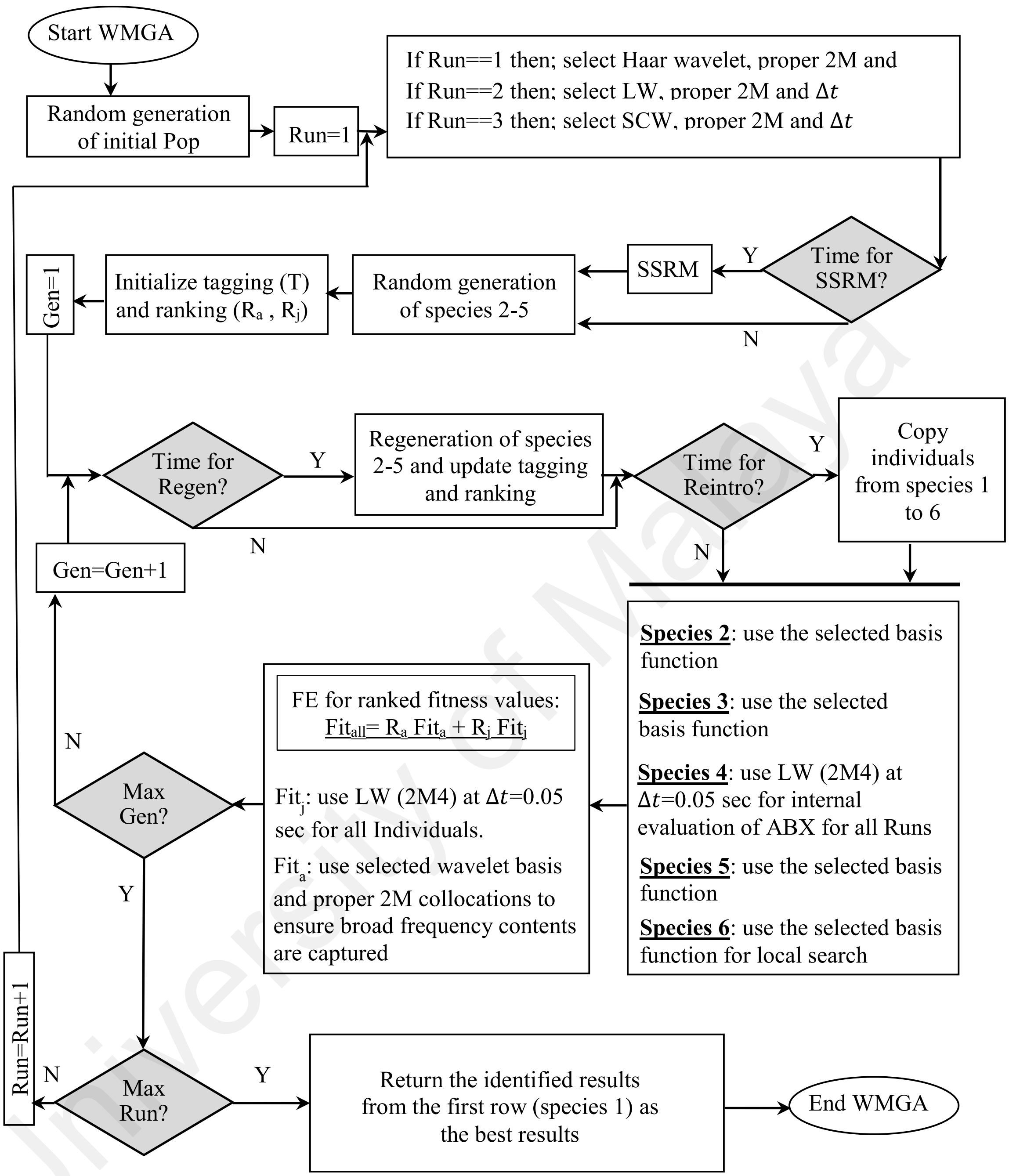

Figure 4.7: The proposed WMGA strategy by using adaptive wavelet functions.

To be noted that the fitness evaluation corresponding to online identification problems (referring to the presence of damage concurrent with measurement) contains the jerk evaluation (Fit*j*) by using LW (2M4) at 20 S/s sampling rates. With reference to Figure 4.6, three runs are carried out for 3 times of search space reductions corresponding to Haar, LW

University of Malaya

and SCW. To be emphasized that, LW(2M4) is optimally adopted for all runs for internal fitness evaluation (FE) of species 4. Subsequently, the schematic flowchart for structural simulation and relatively fitness evaluation is depicted in Figure 4.8.

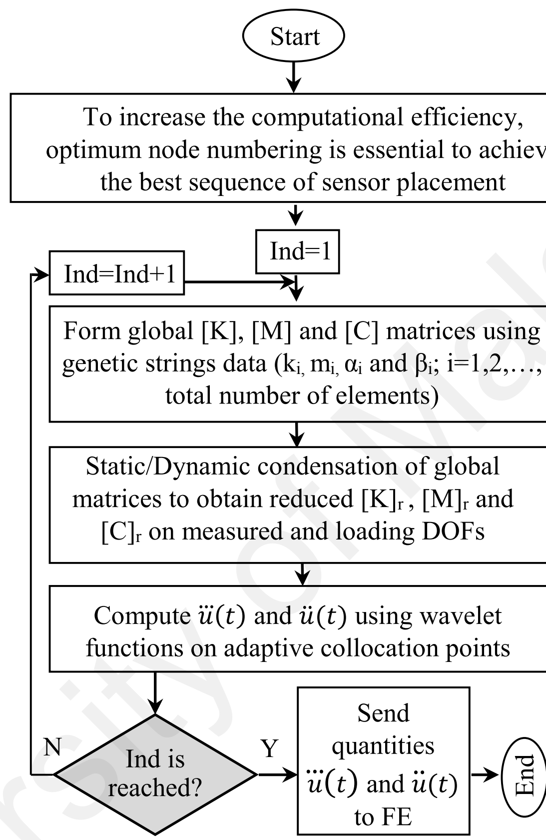

Figure 4.8: The practical flowchart to optimally simulate dynamic response using wavelet functions prior to fitness evaluation (FE) of genetic individuals (Ind).

As it is shown in the figure, the starting point for identification of large-scaled structural systems, undoubtedly is to optimizing the sequence of node numbering. The minimum upper (or lower) bandwidth of characteristics' matrices, and thus, the effective computations are the resultant of optimum sequence of node numbering (especially stiffness matrix, while mostly a lumped mass considered). To accomplish the most cost-effective identification

University of Malaya

strategy, whereby the FE is being carried out numerous times, this step is strongly recommended. We have utilized a GAs procedure based on decimal two-dimensional array coding for both optimal node numbering and sensor placement strategies (the brief discussion is provided in Appendices B and C). The next key point should be considered for any robust identification strategy is that in real cases the measurements of all DOFs are not always available. For this reason, the identification will be carried out on only measured DOFs and therefore the effect of unmeasured DOFs should be considered in relative characteristics' matrices (i.e., mass, damping or stiffness). Two popular methods are referred to static and dynamic condensation methods in order to condensate the characteristics' matrices from the entire DOFs existing in structure to the only measured DOFs (the brief discussion is provided in Appendices A).

4.4 Modification of WMGA strategy for output-only identification

In reality, measuring input forces in situations outside laboratory is not always feasible. In this section, the WMGA strategy proposed in previous sections for structural identification is adopted to cases where the input force(s) is not measured and it is so-called output-only (O-only) structural identification. Basically, there are many attempts have conducted for output-only identification using frequency domain methods. The strength and weakness of these methods were discussed in the second chapter. The most significant researches by Ling and Haldar (2004) used classical techniques to carry out the identification using an iterative approach. In addition, aforementioned iterative procedure, while reasonably efficient for a least squares identification, requires considerable computation time involved for a GA due to the larger time required for each iteration.

University of Malaya

In this section, a strategy involving simultaneous evolution of structural parameters and input force is introduced. The strategy utilizes WMGA to identify and update input force(s) as the search for structural unknown parameters proceeds. For the strategy proposed here, the mass of structure is assumed as known parameter since for many real applications this is a reasonable assumption as the mass may be predicted with sufficient precision. Furthermore, to modify the WMGA identification for output-only measurements, it is assumed that the structure is initially at rest and that the location of input force(s) is known. In addition, the damping is also assumed to be of Rayleigh damping, where the damping parameters are unknown. The major objective will be to identify time-history of input force(s) and stiffness parameters. It is to be pointed out that, because of the banded nature of property matrices (i.e., stiffness and mass), it is also assumed that the acceleration measurements are available at least at the DOF with unknown force and adjacent (coupled) DOFs.

Fundamentally, the time-history of input force(s) is treated as an unknown component of dynamic equilibrium in each iteration of WMGA rather than an unknown variable to be identified by WMGA strategy. In the modified procedure the computation of force is combined with the wavelet-based algorithm proposed in Chapter 3 for structural simulation. In this regards, input force is estimated while the strategy simultaneously is carrying out the simulation of response for evaluation with measured acceleration to calculate the fitness of the given solution. The proposed WMGA identification strategy lies on a predictor-corrector algorithm. An initial prediction of the displacements and velocities at measured DOFs at time step i+1 is first obtained from the measured accelerations at time step i+1. Accordingly, the corrected response at time step i is defined as predictor equations of:

$$\begin{aligned} \ddot{u}_{i+1}(t) &= Acc_{i+1}^{meas.} = C^T\Psi(t) \\ \dot{u}_{i+1}(t) &= d_t C^T P\psi(t) + v_i \\ u_{i+1}(t) &= d_t^2 C^T P^2\psi(t) + u_i \end{aligned} \tag{4.22}$$

University of Malaya

In Equation (4.22), d_t is the time step t_i to t_{i+1}. u_i and v_i represent initial displacement and velocity calculated from previous time step and taking into account that structure has been initially at rest ($u_0 = v_0 = 0$). The unknown force F^{Un} is therefore obtained from the known forces F^{Kn} (may be recorded by available force sensors attached to other DOFs) at time step i+1, measured accelerations, predicted displacements and velocities as follows:

$$F^{Un}{}_{i+1} = [M]\ddot{u}_{i+1}(t) + [C]\dot{u}_{i+1}(t) + [K]u_{i+1}(t) - F^{Kn}{}_{i+1} \tag{4.23}$$

The indirect wavelet-based method proposed in Chapter 3 is then performed to re-compute the responses at time step i+1, and thus it is resulting in corrected or revised estimates of accelerations, velocities and displacements. The fitness evaluation of WMGA is conducted on corrected accelerations compared with those of measured ones. The corrected response will then be implemented on the next time step and the procedure is repeated for the whole time-history resulting identification of input force(s). It should be emphasized that, the corrected responses are being utilized at time step i in Equation (4.22) rather than the measured or predicted responses. Consequently, there is no effect of accumulation of errors due to integration procedure as the corrected (simulated) response is used and the force is not computed from the response obtained by integration of measured accelerations. It should be kept in mind that, dynamic equilibrium governing to the structure is maintained at the end of each time interval as the corrected response have been employed.

4.5 WMGA strategy for structural damage detection

The WMGA developed in previous sections is applied to improve an optimum damage detection strategy. To be more practical, the proposed scenario of damage detection in this research utilizes the previous measurements of undamaged structure. However, the alternative for this is to identify unknown parameters and compare with those of theoretical

University of Malaya

values. Hence, the proposed strategy illustrated in Figure 4.9 deals with the scenario where the measurements of the system both before and after damage has taken place are available.

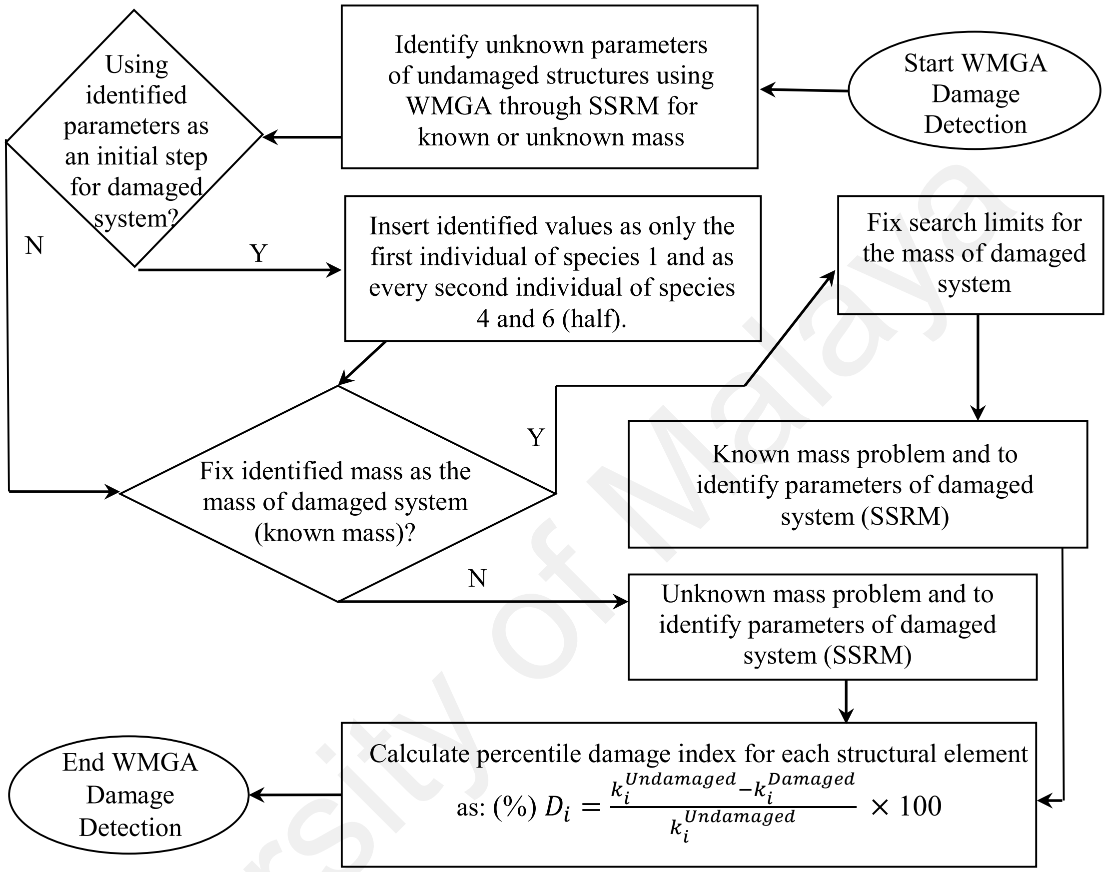

Figure 4.9: The proposed algorithm for damage detection strategy using WMGA.

As shown in Figure 4.9, the proposed strategy for damage detection is performed through two main steps. The first involving the calibration of unknown parameters of stiffness by providing the possibility of using identified parameters for the undamaged structure as a starting point for identification of damaged structure. This constitutes the distinguishable merit of the proposed strategy, in which that only changes require to be identified and providing the optimizer a desirable initial points, resulting in satisfactorily precise outcomes. For this purpose, the half of individuals in species 4 and 6 (were designed for local searches) and only the first individual of species 1 are initially set as the identified parameters. This ensure a good performance of the crossover operation at early stages. The second involves the possibility of fixing the mass to simplify the problem as in fact the mass is not altered from damaged to undamaged stage. Eventually, the damage index is computed for the reduction in stiffness of the element as a percentage of the original undamaged stiffness.

4.6 Numerical verification study

The capability and effectiveness of the proposed strategies for structural identification and damage detection are numerically evaluated in this section. For this purpose, three numerical applications are considered, involving a MDOF shear system composed of three connected MDOF structures for structural identification of known and unknown mass problems as well as force identification. Additionally, two truss structures are considered for identification and damage detection, including a 2D Parker truss structure subjected to El-Centro base excitation and a 3D and large-scaled hexagonal space structure under different concentrated loading scenarios. For both structures only transitional DOFs are existed so that they are modeled as pin-jointed truss structures. Initially, the configuration of each structure is modeled in Formex Algebra (FORMIAN) and later the nodal coordinates have been transferred to MATLAB. Prior to starting any conventional identification or damage detection strategy, the sequence of node numbering should be optimized in order to construct the most optimum mass and stiffness matrices (Appendix C).

For all cases considered, the mass of structures is lumped at each transitional DOF. Furthermore, damping is provided as Rayleigh damping by setting damping ratio of λ% for the first two modes and using the desirable values for α and β. For this purpose, λ=2 and λ=5 are selected for identification of example 1 and examples 2 and 3, respectively. In addition,

University of Malaya

the time-history of nodal accelerations is numerically simulated by the well-known average acceleration method of Newmark-β family, using the sampling rate of 200 S/s for the first example (it will be evaluated as the measured accelerations) and sampling rate of 1000 S/s corresponding to the truss structures.

Moreover, for truss systems where damage detection is conducted, two kinds of damage scenarios are considered as damage induced to the structural elements. The first involving the offline reduction of the stiffness of structural elements that denotes the measurement of damaged structure (designated by Off). The second being online reduction of stiffness that represents the damage has taken place on structural elements during the measurement of damaged structure (designated by On).

Fundamentally, the very important step prior to any identification strategy is selecting WMGA parameters to be utilized through the strategy. For this purpose, some preliminary studies were carried out for each numerical applications in order to determine the most reasonable WMGA parameter values. The underlying purpose of these studies was to identify balanced WMGA parameters that will give consistently desirable results rather than trying to find optimum WMGA parameters. It will be shown later that, for each numerical example, different combinations of WMGA parameters will have different effects due to the variations across structural systems and external loadings.

Eventually, the computational efficiencies and the robustness of the proposed WMGA strategy have been compared with some of the available methods. For the purpose of a comprehensive evaluation, the CPU computational time (as indication of the cost of analysis) is comparatively considered for different strategies, which was recorded with a same hardware environment (I-5 CPU @3.2GHz, Operation 64 bit).

University of Malaya

4.6.1 A MDOF shear building

The computational efficiency and robustness of the proposed WMGA strategy are evaluated through the first application regarding to the structural identification of I/O data, known and unknown mass problems, initially. Later, the strategy is conducted in order to verify the results of output-only identification of known mass problems. Figure 4.10 illustrates a MDOF shear system consists of three shear structures connected by two link bridges. Prior to identification, the simulation step is carried out using the structural properties given in the figure. Firstly, the 5 sec of measurement is considered for the only central building alone under two sinusoidal and concentrated loadings as illustrated in the figure $F_1^b(t)$ and $F_2^b(t)$. This problem is referred to Case (b) in Figure 4.10. The mass, stiffness and Rayleigh damping parameters (α and β) are treated as unknown values to be identified. The first 5 sec response of the central system is simulated using Newmark-β method at 200 sampling rates and the acceleration recorded for feeding into WMGA.

Second problem involves the output-only identification of the central building shown in Case (c) in the figure, when the entire coupled system is subjected to the base excitation. For this case, stiffness values of the central building, damping parameters and applied forces due to the link bridges ($F_1^c(t)$ and $F_2^c(t)$) are treated as unknown parameters to be identified. Link bridges are modelled as linear springs with the axial stiffness of 10e8 (N/m). For identification purposes damping parameters α and β are identified along with the unknown stiffness and forces. The mass of the system is presumed as known parameter and the seismic loading for each level is easily obtained from the ground acceleration multiplying by the mass of each level (applied in the inverse direction). Accordingly, the response of the entire system to the first 5 sec of north-south component of the El-Centro earthquake is simulated using Newmark-β method at 200 sampling rates (time step 0.005 sec). However, further to our preliminary studies on simple systems, it is observed that using a longer time-history analysis (longer than 5 sec) and more sampling rates (refers to small time steps) may be beneficial.

With any GA strategy it is essential to determine balanced parameters to be utilized. To identify the appropriate WMGA parameters, the considered problem was solved 10 times for known and unknown mass systems. The balanced WMGA parameters that were consistently producing good results without requiring excessive computational time are displayed in Table 4.2 corresponding to known mass and unknown mass problems considered in Case (b) and Case (c). Subsequently, a fairly wide search range, i.e., half to twice the actual values (for stiffness, mass) is adopted for identification of both cases. The search limits of damping parameters corresponding to the first two modes are set as 0 and 1. The identification is conducted 10 times for both cases and results presented for this example lies on the average of all results.

In addition, it is very important to keep in mind that real I/O measurements contain noise and the effectiveness of WMGA should be examined in the presence of I/O noise to signal. Accordingly, for identification of case (b) the input forces and the simulated accelerations (assumed as measured ones or outputs) are also contaminated with 5% and 10% noise levels. Applying noise to the both inputs and outputs is a much more real and also difficult case compared to the common case of only output noise. For this purpose, the noise level is defined as the ratio of standard deviation of the zero-mean white Gaussian noise to the root-mean-square value of the unpolluted time signals. It should be pointed out that, Case (c) is considered as the case of input noise as the noise on the measured ground motions is passed directly to the excitation.

For comparison purpose, implementation of the Newmark-β method is also considered for fitness evaluation of all 6 species and designated by MGA strategy. Subsequently, the identification of Case (b) is conducted using WMGA and MGA strategies, comparatively.

University of Malaya

To compare the results calculated by two strategies, there are two possible scenarios that may be proposed. The first is to compare the time taken in achieving a given accuracy, convergence rate or number of generations to be run. While, the second is to compare the accuracy, convergence rate or number of generations that can be achieved in a given time. In all examples presented in this research the former scenario is used by fixing the number of generations that are being conducted for WMGA and the algorithm of MGA will be stopped reaching the fixed value. Accordingly, the time taken after two strategies have been compared.

It should be emphasized here that complete measurements of output data corresponding to all DOFs in a structure are somewhat impractical for real applications, and therefore any proposed strategy for structural identification such as WMGA should operate on incomplete measurements. For this purpose, four different sensor placements (SP) are proposed for measurements of Case (b) and Case (c) as are tabulated in Table 4.3.

As displayed in Table 4.3, SP2 and SP4 correspond to Case (b) for identifying the stiffness values of known and unknown mass problems, where I/O data measurements are available. Whereas SP1 and SP3 correspond to the O-only identification of Case (c), where the mass is known and it is assumed that the measurements of only output data are available. The algorithm of incomplete measurement utilized in this research lies on dynamic condensation method. It is briefly discussed in Appendix A, and is compared against the static condensation scheme. This algorithm involves two steps. The first step is to set two tags to the all DOFs. The first tag refers to the master DOFs, those are being measured and are known as the available places (DOFs) for embedding sensors (referring to the sensor placement). The second tag consists of the omitted DOFs, where the measurements are not available on these DOFs.

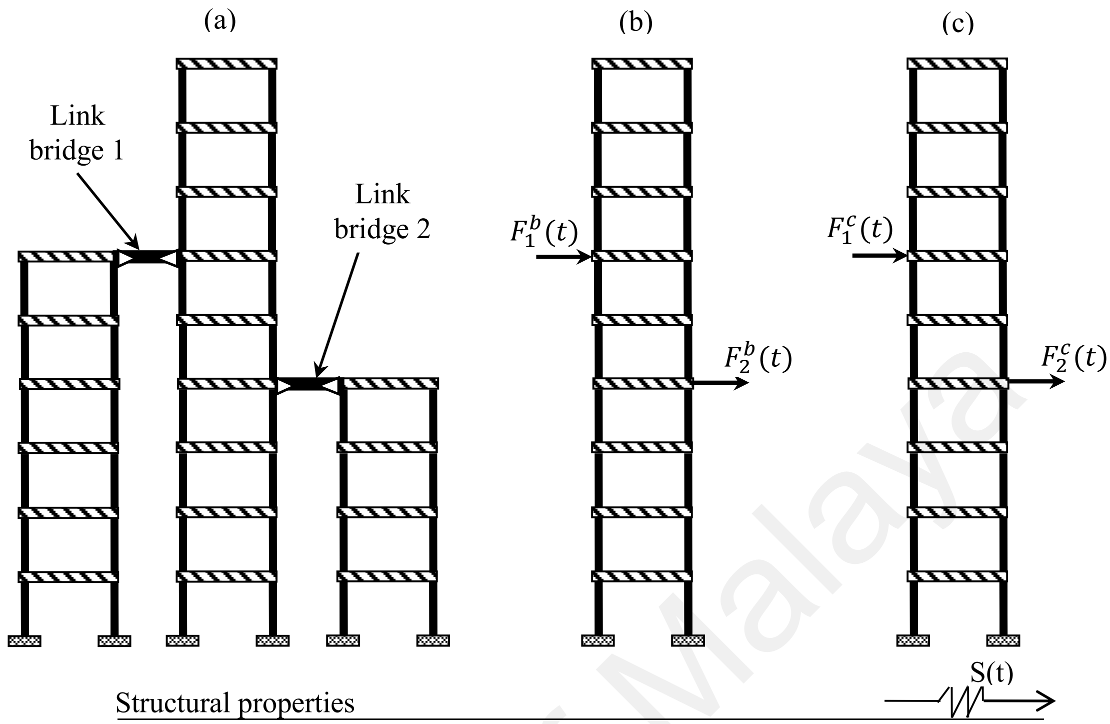

Structural properties

Stiffness (× 10^8 N/m)	Mass (× 10^5kg)	Story/link
5	6	1_4
4	4	5_7
3	2	8_9
10	-	Links (linear spring)

Case (b): I/O measurement and fixed base.
Case (c): O-only measurement and 3 MDOF shear systems are subjected to the base acceleration (stories are numbered from the bottom floor of MDOF).

Figure 4.10: MDOF shear building, (a) the entire three connected structures, (b) structural identification of the central structure under two known forces, (c) structure extracted for force identification.

Accordingly, the structural property matrices i.e., mass, stiffness and damping are being condensed into smaller matrices due to the order of master DOFs and omitted DOFs as the second step of the condensation algorithm. For instance, levels 2, 4, 6 and 8 shown in Table 4.3 for SP2, indicate the numbers of four measured DOFs among the all DOFs. It should be noted that, the DOFs corresponding to the external forces are also set as the master DOFs and will be considered through the matrix condensation approach. However, it is not essentially meaning that the measurements are available on forced DOFs, except for the force identification problems where the measurements of forced DOFs and adjacent DOFs must be available.

Table 4.2: WMGA parameters utilized for structural identification of the first numerical application.

	Known mass; Case (b) and (c)	Unknown mass; Case (b)
Pop-size	5×10	5×30
Runs	3	3
Generations	3×20	3×50
Conducted SSRM after;	20	50
Crossover rate	0.6	0.4
Mutation rate	0.2	0.2
Periodic migration (z_1,z_2)	5, 0.1-0.2	5, 0.1-0.2
Window width	4	4
Regeneration	3#	3
Reintroduction	40	90

Haar wavelet (2M=2), sampling rate 200 S/s.
Legendre wavelet (2M=4), sampling rate 50 S/s.
The second kind of Chebyshev wavelet (2M=8), sampling rate 50 S/s.

Number of times that regeneration or other GA operations are taking place.

Table 4.3: Sensor placement (SP) scenarios for data measurement.

Sensor placement (SP)	Known mass	Unknown mass	Level
SP1 (O-only data)	Yes	No	1, 3, 4, 5, 6, 7, 9
SP2 (I/O data)	Yes	Yes	2, 4, 6, 8
SP3 (O-only data)	Yes	No	Full measurement
SP4 (I/O data)	Yes	Yes	Full measurement

- ***Case (b) – I/O Structural identification***

As it was described earlier, Case (b) involves I/O data structural identification of the MDOF shear building subjected to the known and concentrated forces $F_1^b(t)$ and $F_2^b(t)$ as shown in Figure 4.10. The Eigen value problem governed to the central building is solved and the natural frequencies of 1.05, 3.07 and 14 Hz are computed corresponding to the first, second and the ninth modes. The first two modal periods are calculated as 0.95 sec and 0.33 sec, respectively. In addition, actual damping is provided as Rayleigh damping by setting

University of Malaya

damping ratio of 2% for the first two modes resulting α=0.4942 and β=0.0039. Furthermore, in order to simulate the responses of the structure and then to obtain the measured accelerations the sinusoidal forces are selected as two random and multi-sine forces to have an amplitude between [-2000, 2000] N. The random multi-sine forces are being generated containing the frequency components of 1-25 Hz to ensure that all modes are being vibrated. For the purpose of structural identification of Case (b), firstly the known mass problem is considered, namely 11 unknowns are treated as unknown values to be identified including $k_1 - k_9$, α and β. Secondly, the effectiveness of WMGA strategy is evaluated for operating on the unknown mass problems. Basically, the problem of identifying both mass and stiffness is much more complicated, where 20 unknowns are treated as unknown parameters to be identified including $k_1 - k_9$, $m_1 - m_9$, α and β. The reason for this is due to the facts that not only the number of unknowns is increased but also different combinations of mass and stiffness can produce the same natural frequencies and mode shapes. Consequently, similar response characteristics will be existed. To clarify this argument, two simple SDOF systems can be considered. The first system has the mass of 1 kg and stiffness of 900 N/m, and the second one has the mass of 5 kg and stiffness of 4.5 kN/m. It is easily noted that both structures have a frequency of 30 rad/s and would display the same vibration characteristics. Undoubtedly, only by conducting a reasonably comprehensive forced vibration test these contents can be separated and identified. As the unknown mass problems pose a greater challenge, it is found that the WMGA parameters utilized for unknown mass problems are increased (except for crossover rate). Increasing the WMGA parameters leads to better certainty in the mean and a robust solution. The exception for this is the reduction in crossover rate of unknown mass problems. It is logical to the crossover rate being decreased in unknown mass problems, where many crossovers occurring in the mass portion of an individual and will have little effect.

Before starting the identification strategy, the sensor placement has to be considered. Practically, sensor placement refers to finding the best places for embedding the limited number of available sensors, whereby these places provide the optimum and accurate capture of the structural responses (Appendix B). In this example the program of sensor placement is run for 4 and 7 number of available sensors and the best scenarios are obtained for SP1 and SP2, respectively.

The structural identification of Case (b) is carried out for known and unknown mass problems using WMGA and MGA using unpolluted signals (noise free). Accordingly, results are comparatively plotted in Figure 4.11 regarding to the different sensor placements SP2 and SP4.

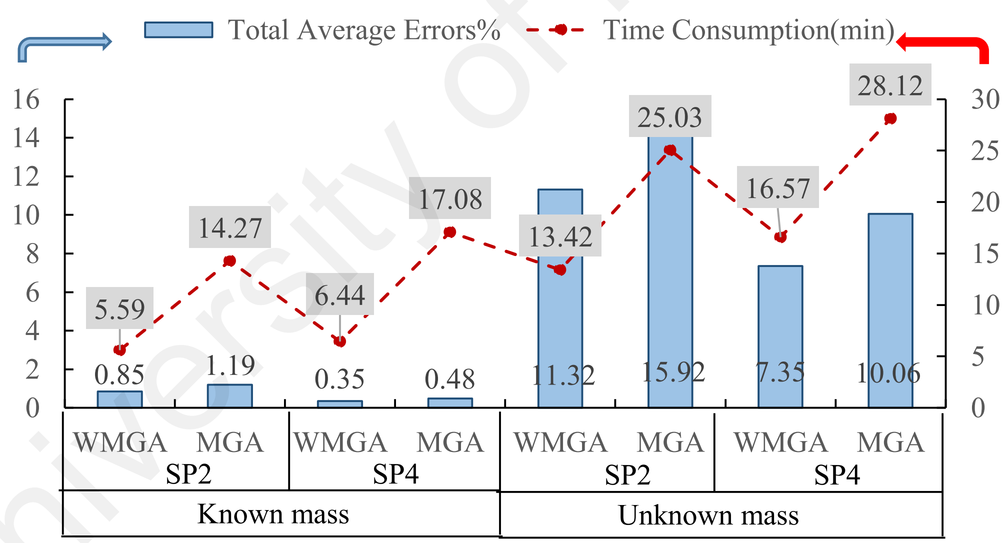

Figure 4.11: Total average error (%) in stiffness values and computation time involved for different sensor placements (known and unknown mass identification).

The first observation from Figure 4.11 lies on the outstanding results identified by WMGA strategy, when all DOFs are measured (SP4) for the known mass problem. In addition, it is shown that the CPU time consumption after WMGA is remarkably lesser than that of MGA. As was mentioned earlier, MGA strategy was adopted using time steps of 0.005

sec for the 5 sec of analysis. With reference to Chapter 3 of this study, the optimum fitness evaluations, and therefore the cost-effective identification were achieved using adaptive wavelets through the proposed WMGA strategy for different sampling rates. In contrast, MGA utilized common Newmark-β method at 200 sampling rates to perform fitness evaluations of 6 species and resulted in a costly identification approach. However, because of the robust construction of the proposed GA strategy (multi-species), the identified parameters by implementing WMGA and MGA were sufficiently accurate. On the other hand, despite the fact that the unknown mass problems are inherently difficult, this figure illustrates the acceptable results for WMGA strategy. Overall, Figure 4.11 demonstrates the computational efficiency and robustness of WMGA strategy for I/O identification where the most optimum and reliable results were computed with this method. Furthermore, the total average error in identified mass values and damping parameters compared with actual ones are displayed in Table 4.4 corresponding to known and unknown mass problems of Case (b).

Table 4.4: Total average error in mass and damping values for Case (b).

	Known mass	Unknown mass
Error in identified mass values	_	25.63%
Error in identified damping values	1.85%	1.99%

Results displayed in Table 4.4 are the average of results after ten times running the WMGA algorithm. It is seen that, the average error in mass values reached to about 26% for unknown mass problems. The identification of unknown mass structure is considered as very complicated and as such, the results displayed in the table can be interpreted as excellent results. The next step, of course is the quality of identification strategy using contaminated signals (noise-to-signal). This is investigated and the results are presented in Table 4.5 corresponding to the stiffness identification of Case (b) considering different noise levels to the I/O signals.

Table 4.5: Effect of noise in stiffness identification; Case (b) and SP4.

	Total average error in identified stiffness (%)			
	WMGA		MGA	
Noise level	Known mass	Unknown mass	Known mass	Unknown mass
0%	0.35	7.35	0.48	10.06
5%	2.79	10.16	8.47	19.73
10%	5.93	14.22	15.01	25.99

Generally, Table 4.5 shows that noise causes error in identified values to increase approximately in proportion to the applied noise level. Nevertheless, the identified stiffness values for both known and unknown mass systems are sufficiently accurate (in terms of error evaluation). Data in Table 4.5 demonstrate that as even under large 10% noise, stiffness values were identified with reasonable precision. This table also illustrates the efficiency of WMGA strategy compared with MGA, where the less effect of noise is recorded for the proposed wavelet-based method. The reason for this lies on the fact that WMGA strategy acts as a filter to de-noise data concurrent with the process of analysis. It is very important to keep in mind that, there is no filtering (de-noising) approach is conducted prior to analysis and the underlying key point of the proposed strategy is revealed here. In other words, using adaptive wavelet functions not only I/O data but also the extracted frequency contents from the inherent characteristics of the system are being de-noised due to different scales of considered wavelets. As a consequence, the minimum effect of the noise-to-signal is achieved.

- ***Case (c) – Output-only Structural identification***

This case involves output-only (O-only) identification of Case (c) shown in Figure 4.10, where the mass parameters are known as presented in this figure. The responses of the entire system are computed to the first 5 sec of El-Centro base excitation using time step of 0.005 sec. Accordingly, the accelerations corresponding to DOFs prescribed for SP1 and SP3 of

University of Malaya

the central shear system of Case (c) are extracted for use in identification. The first 5 sec time-histories of acceleration and displacement of the 9^{th}, 6^{th} and 4^{th} stories are obtained using average acceleration of Newmark-β family and results are depicted in Figure 4.12.

Practically, the link bridges shown in Figure 4.10 cause coupling between the shear buildings which, when considering the only single central building, they cannot be readily quantified. The rational for this example is to use the proposed WMGA strategy to identify the coupling forces without any information of the other two shear systems. In this regard, the stiffness values of the central building, damping parameters, $F_1^c(t)$ and $F_2^c(t)$ as the coupling forces from adjacent shear systems are treated as unknown parameters to be identified. WMGA parameters utilized for this case are as displayed in Table 4.2 for known mass problem. Subsequently, average errors in output-only system identification of Case (c) are obtained after 10 times running the program as displayed in Table 4.6.

Results shown in Table 4.6 demonstrates that the output-only results were outstanding. It can be seen that the accomplished mean error in stiffness value was only 1.13% and 0.28% for SP1 and SP3, respectively. This arises from the fact that, by identifying unknown forces, rather than trying to measure them, the strategy is able to avoid error that would otherwise be passed through the simulation. Furthermore, for the identification purpose the WMGA strategy obtains the time-history of unknown input data (forces). The time-history of identified forces $F_1^c(t)$ and $F_2^c(t)$ are plotted in Figure 4.13 compared to the actual forces.

Table 4.6: Mean errors in system identification for different sensor placements (SP); output-only data measurement of Case (c).

	Total average error (%)		
	Identified force		
SP	$F_1^c(t)$	$F_2^c(t)$	Identified stiffness values
SP1	8.67	11.93	1.13
SP3	1.54	3.09	0.28

University of Malaya

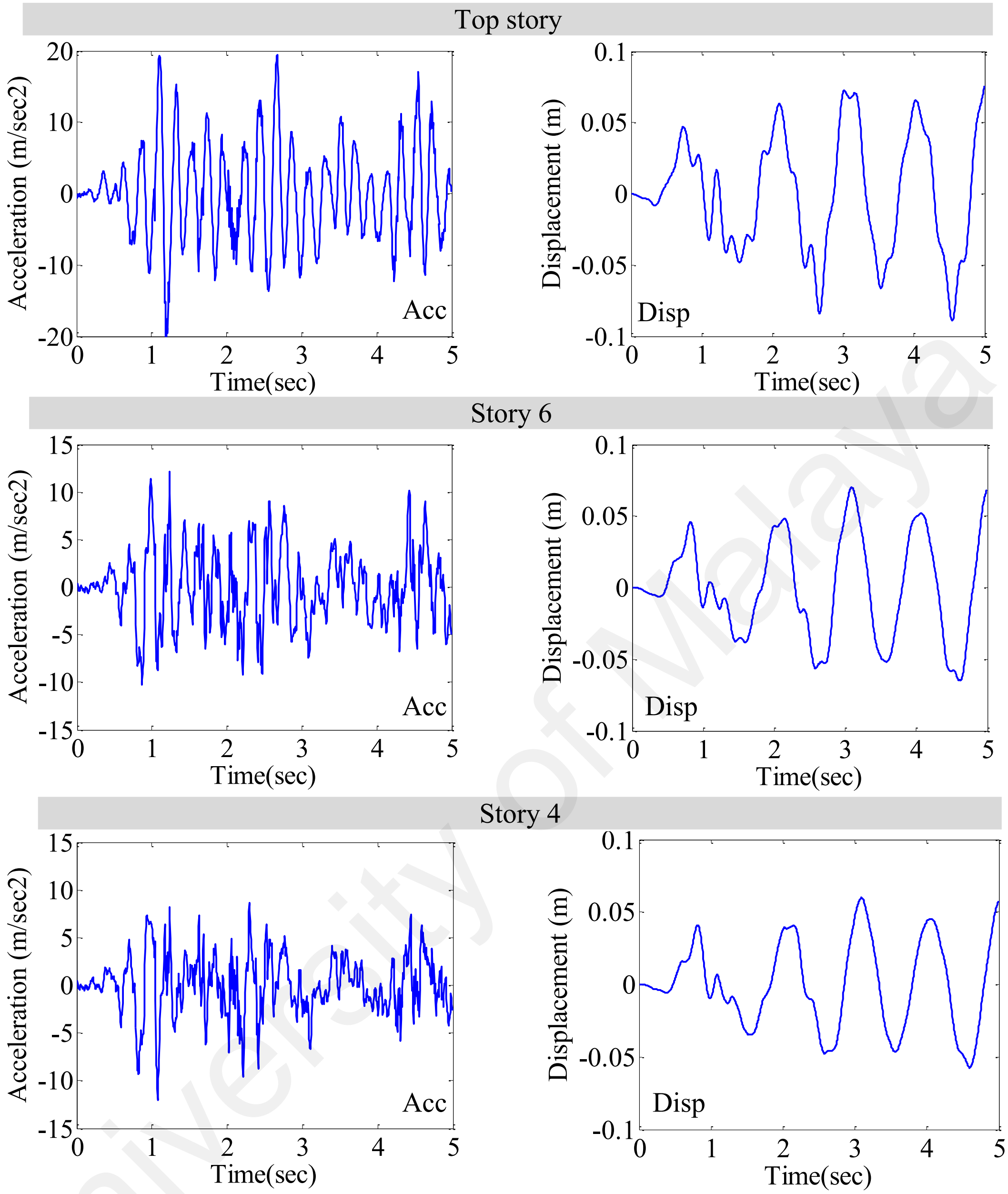

Figure 4.12: Simulated time-history of acceleration (Acc) and displacement (Disp) corresponding to the 9th, 6th and 4th levels; the full measurement of Case (c).

University of Malaya

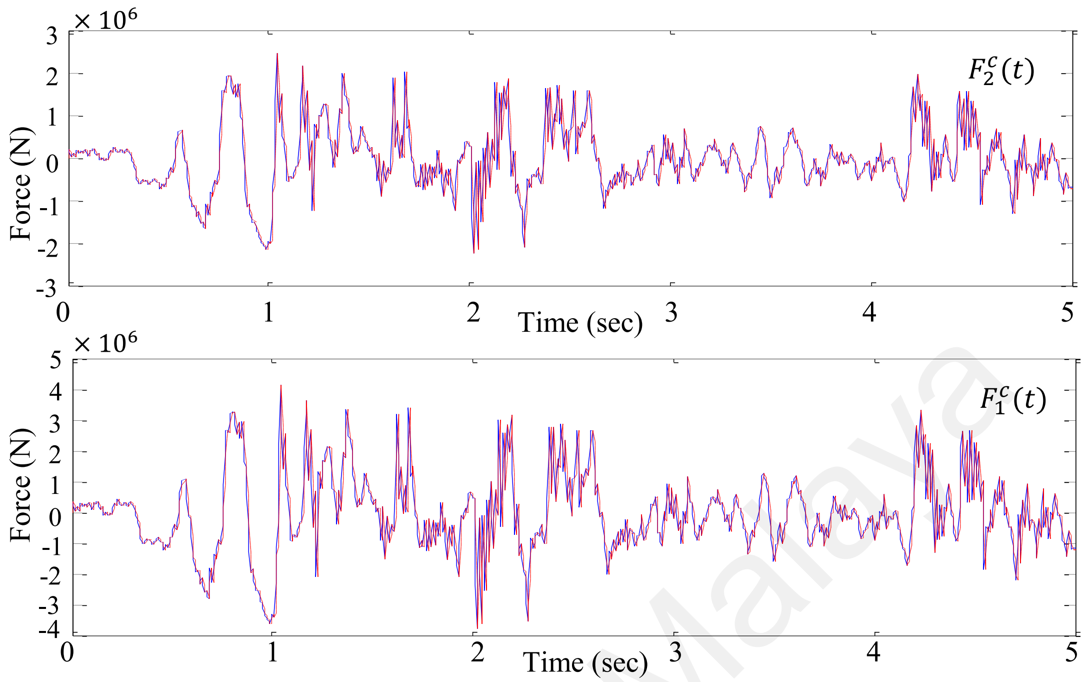

Figure 4.13: Force identification of Case (c) shown in Figure 4.10 (O-only and full measurement).

It is shown in Figure 4.13 that the identified forces matched the exact forces almost exactly. The figure demonstrates that, a reasonable estimate of the input forces is achieved. In addition, the wide-band frequency variation shown in the figure is due to the noise in measured accelerations that is transferred to the force data through the inertia term in the dynamic equilibrium. It should be kept in mind that, this effect can be reduced by filtering or re-computing forces using corrected accelerations. Finally, Figure 4.13 and Table 4.6 shows that identified $F_1^c(t)$ is more accurate than that of $F_2^c(t)$. This is most likely due to the fact that $F_1^c(t)$ is larger and excites the location that causes a larger influence than $F_2^c(t)$ on the measured response of the structure. Finally, stiffness identification results for story 1-9 corresponding to SP1 and SP3 are provided in Appendix E.4.

University of Malaya

4.6.2 A 2D truss structure

Figure 4.14 shows a 2D Parker truss structure composed of 12 pin joints, 21 I-shaped truss elements and 21 DOFs. All characteristics of this structure as well as cross-sectional area, mass density and the modulus of elasticity are kept constant for all members. To calculate the effective length of elements, 0.03 m is deducted from axis-to-axis of joints. The natural frequencies of 58 and 1039.6 Hz are initially calculated using the stiffness values for intact structure corresponding to the first and 21st modes, respectively. For comparison purpose, results of WMGA have been compared with those calculated from only the first 3 species considered by employing Newmark method for the fitness evaluation and referred to MGA in this example. It is anticipated that MGA strategy used here requires more generations to be conducted for gaining the prescribed convergence rate. It is to be emphasized that, the large sampling rate of 1000 S/s (Δt=0.001 sec) is utilized for accurate FE of MGA by using Newmark method. Additionally, the small sampling rates of 100 S/s (Δt=0.01 sec) and 20 S/s (Δt=0.05 sec) are utilized to simulate accelerations (Fit_a) and jerk (Fit_j) using the proposed wavelet-based scheme for structural simulation, respectively. For instance, considering the total time of 10 sec measurements of noise-free I/O responses, relatively 10000, 1000 and only 200 points have been evaluated for FE of each genetic individual. The WMGA parameters utilized in this example are tabulated in Table 4.7.

Table 4.7: WMGA parameters utilized in Example 4.6.2.

	Known mass	Unknown mass
Pop-size	5×20	5×30
Runs	3	3
Generations	3×20	3×50
Conducted SSRM after;	20	50
Crossover rate	0.6	0.4
Mutation rate	0.2	0.2
Periodic migration (z_1,z_2)	5, 0.1-0.2	5, 0.1-0.2
Window width	4	4
Regeneration	3	3
Reintroduction	40	90

Haar wavelet (2M=2), sampling rate 100 S/s.
Legendre wavelet (2M=4), sampling rate 100 S/s.
The second kind of Chebyshev wavelet (2M=8), sampling rate 100 S/s.

The theoretical stiffness of elements (*E*×Area/Length) varies from 12.75e-4 to 21.4e-4 kN/m, thus the lower and upper limits have been selected as 0.1 and 3 times the theoretical stiffness, respectively. It should be pointed out that, for each truss element the axial rigidity (*E*×Area) is treated as unknown stiffness. For the case of the unknown mass identification this ranges are also utilized for lower and upper search limits of the mass. In addition, the search limits of damping corresponding to the first two modes are set as 0 and 1. Subsequently, I/O noise-free signals have been considered for both structural identification as well as damage detection in this example. Two different sensor placement scenarios are proposed and tabulated in Table 4.8, to facilitate structural identification and damage detection strategies. Furthermore, for current test conducted in this example, identification is carried out 10 times using fresh input force and noise-free data and results presented here stand for the best result.

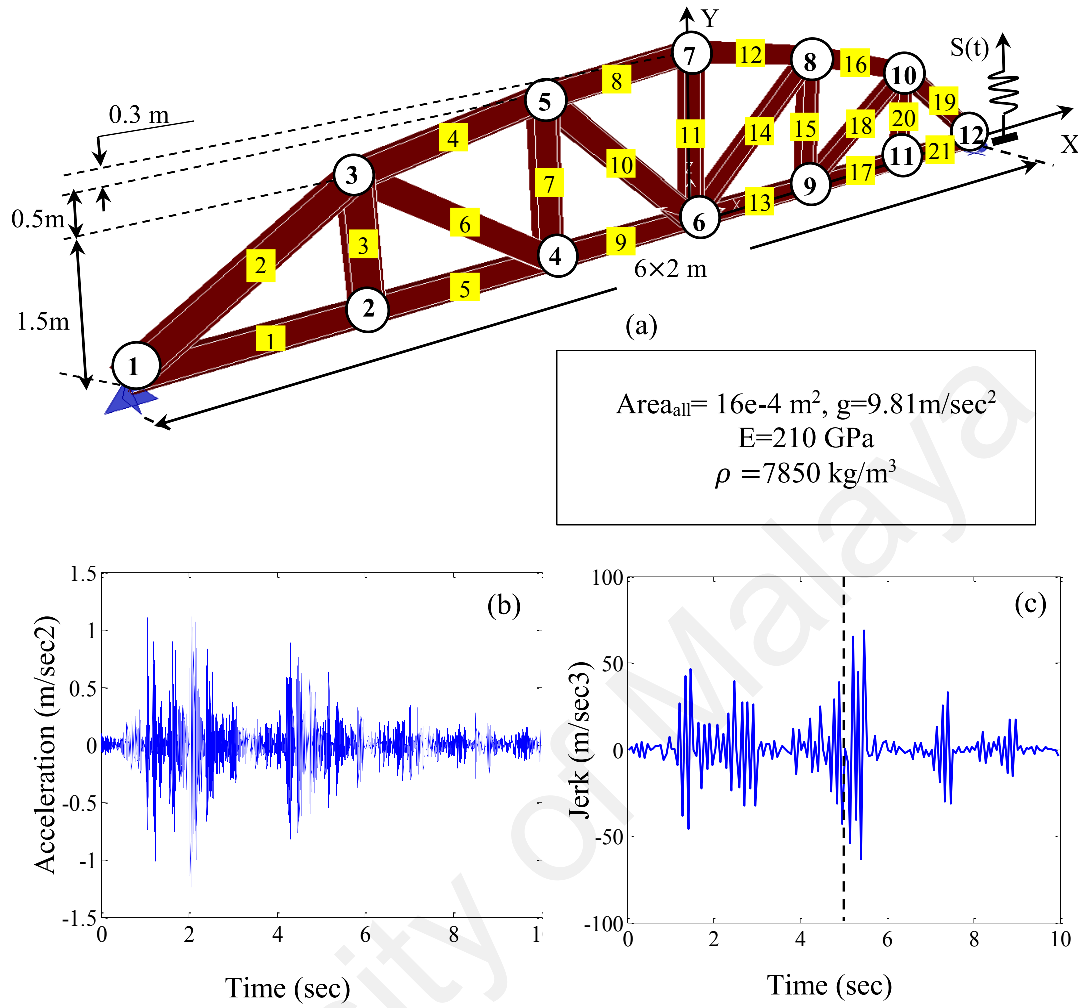

(a) Geometric configuration.
(b) Simulated time-history of acceleration of vertical DOF on node 6 (reference structure).
(c) Simulated time-history of jerk for vertical DOF on node 6 after 10 % reduction in stiffness of element 10 at the 5th second of loading (obtained by using LW, 2M4 and Δt=0.05 sec).

Figure 4.14: A 2D camel back pin-jointed truss structure considered for Example 4.6.2.

University of Malaya

Table 4.8: Sensor placement (SP) scenarios proposed for Example 4.6.2.

SP	Node number	X	Y
SP1	2, 3, 6, 7, 10, 11	Yes	Yes
SP2	Full measurement		

The identification of this structure is conducted using the proposed evolutionary process WMGA and MGA introduced earlier. The convergence history of the maximum error (%) in stiffness for all DOFs is computed for theoretical stiffness (K_{Th}) and the identified one (K_{Id}) as: 100×[(K_{Th}- K_{Id})/ K_{Th}]/DOFs. This value is plotted in Figure 4.15 for known mass and unknown mass identification corresponding to the different sensor placement scenarios. The total generations are assigned as in Table 4.7, thus the procedure is stopped achieving the total number of generations. Furthermore, for current test conducted in this example, identification is carried out 5 times using free signal-to-noise data and results presented here stand for the best result.

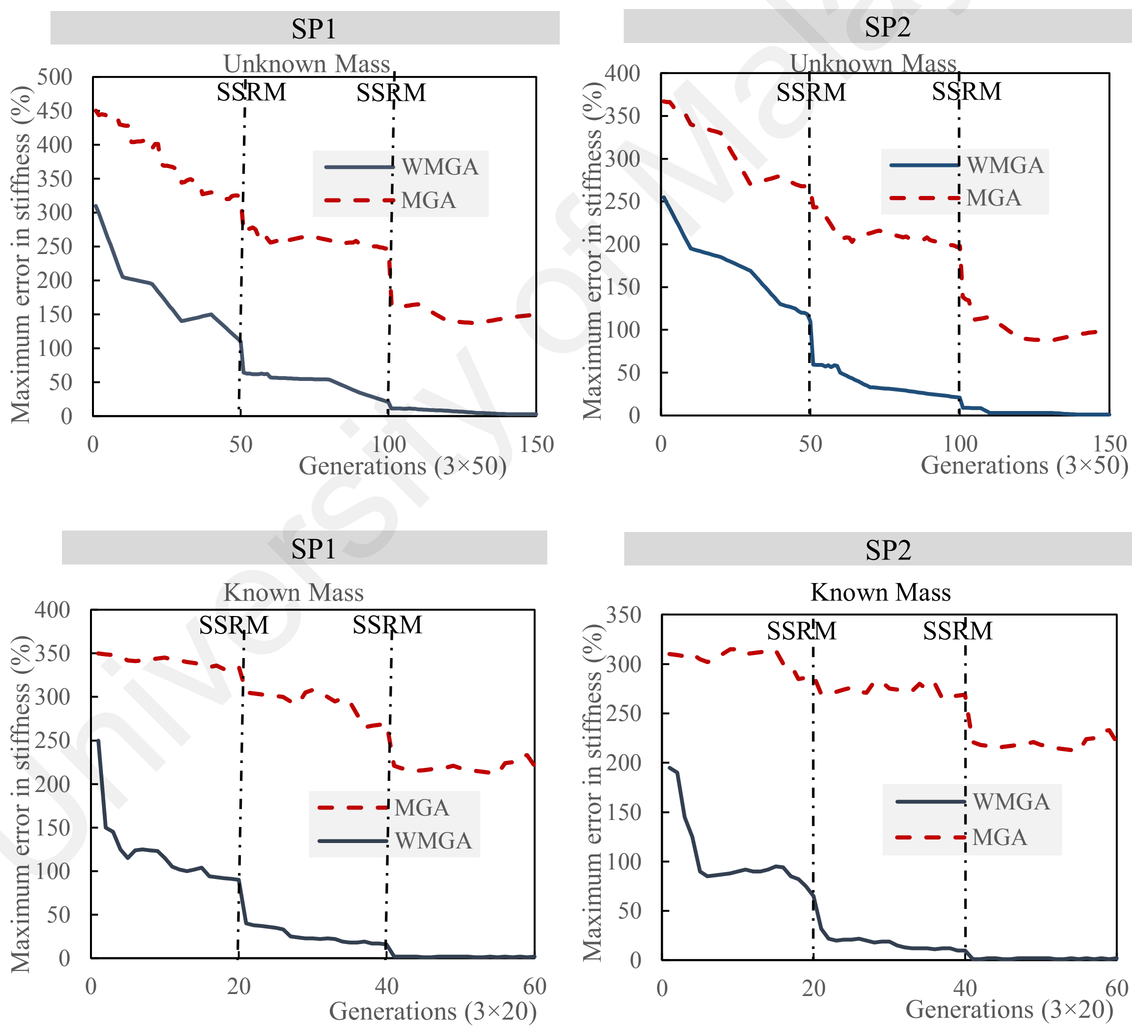

Figure 4.15: The convergence history of percentile maximum error in identification of stiffness for WMGA and MGA.

University of Malaya

The first notable consideration about the comparison of convergence history of MGA and WMGA deals with the highest speed of convergence due to WMGA. Basically, the prescribed accuracy of MGA is achieved after roughly 300 generations for this unknown mass problem, and for this reason there is a considerable difference between percentile maximum errors recorded for these two strategies. It is clear from the figure that for both known and unknown mass problems, the exploration phase (using Haar wavelet before the first SSRM) is optimally achieved by searching around local optimal solutions. Moreover, it is seen that the exploitation phase is widely focused on the second (using LW) and third SSRM (using SCW) where the small variations around global optima are existed. Significantly, Figure 4.15 illustrates sufficiently desirable convergence of SP1 scenario compared with SP2 (treated as the reference), however, only 29% DOFs were measured. Furthermore, one has to take into account that, however the evaluation of the convergence rate of an evolutionary strategy is necessary; it is not basically sufficient. The complementary evaluation should be carried out on the computational efficiency and relatively computational cost of the proposed strategy. One of the interesting observations for use of WMGA was recording the optimum cost of analysis compared to MGA (similarly, the procedure was stopped once it reached to the total generations of WMGA). Subsequently, computational time involved and the percentile total average of maximum errors are depicted in Figure 4.16.

University of Malaya

Figure 4.16: The percentile total average of maximum errors and computation time involved for SGA, WMGA and MGA.

For the purpose of a comprehensive investigation, an attempt has been made to evaluate the applicability of standard genetic algorithm (SGA) for identification of this example. Results shown in Figure 4.16 demonstrate the very bad performance of SGA compared to the WMGA proposed herein. Actually, it was predictable that because of undesirable exploration of large search space the convergence toward the local optima is more probable in used of SGA. This figure clearly shows the superiority of WMGA compared with MGA where the most optimum time consumptions were recorded with the highest accuracies. For instance,

University of Malaya

for the case of unknown mass problem (42 unknowns to be identified) the highest accuracies of (in term of errors) about 8.8% (for SP2) and 15.32% (for SP1) were measured by recording computational time of 42.51 and 36.38 min, respectively. In view of greater difficulty for unknown mass problems, computational cost of about 43 min is surprisingly improved compared with that of MGA about 60 min. This arises from the fact that by using accurate wavelet functions the wide-band frequency contents are optimally captured on adaptive collocation points especially using small sampling rates. Finally, in order to assess the performance of the damage detection strategy and to evaluate the effect of wavelet functions to detect the location and magnitude of damage, 9 scenarios are proposed for the presence of damage on structural elements as tabulated in Table 4.9.

Table 4.9: Damage scenarios (DS) imposed to structural elements highlighted in Figure 4.14.

	Scenario								
	1	2	3	4	5	6	7	8	9
Element	4	4	4	18,4	18,4	18,4	4,10,14,16	4,10,14,16	4,10,14,16
Stiffness reduction (%)	5	10	25	5	10	25	5	10	25
On/Off	off	off	on	off	on	off	on	off	off

Initially, the undamaged structure is treated as unknown mass problem and dynamic parameters are identified using WMGA. At the next stage, the identified mass is fixed for identification of known mass problem and the location and magnitude of damages are detected by the means of damage index in structural elements. The results of damage detection are presented in Table 4.10 after 10 times repeats.

University of Malaya

Table 4.10: Damage detection of 2D truss structure shown in Figure 4.14.

			Damage scenario								
			1	2	3	4	5	6	7	8	9
Detection success (%) after 10 repeats	SP1	Location	90	100	100	70	70	90	80	70	80
		Magnitude	75	93	100	71	90	97	68	73	98
	SP2	Location	100	100	100	80	100	100	90	80	90
		Magnitude	80	95	100	78	100	100	76	81	98
Median value of absolute error in damage	SP1		0.21	0.16	0.06	0.25	0.12	0.02	0.47	0.25	0.11
	SP2		0.17	0.14	0.03	0.23	0.09	0.01	0.37	0.24	0.09

In most of cases, it is observed that one bad result alters the mean value and the values of median may provide better indication of predicted efficiency. In addition, it is found that the false detection is very probable. In this regards, the damage detection strategy is conducted 10 times for this structure to be of the practical use, where in actual cases there is no information on exact values. The proficiency of WMGA for damage detection of single damages even 5% (both for location and magnitude detection) is well demonstrated in Table 4.10. Significantly, Table 4.10 shows that WMGR accurately detects the location and magnitude of up to four damaged elements for online scenarios with even 5% reduction of stiffness (damage scenario 7). The reason for this lies on the improved fitness evaluation using the optimum quantity of jerk. Our experiences consistently have confirmed that applying the same external load for identification of damaged and undamaged structure yields more satisfactory results for detection of the location and magnitude of damage.

University of Malaya

4.6.3 A large-scaled 3D truss structure

The identification and damage detection of a large-scaled and double-layered hexagonal space structure are considered for this application. The geometry of this structure is shown in Figure 4.17. This structure comprises 196 truss elements, 56 pinned joints, 15 fixed supports, and therefore 123 DOFs. The exact values of the cross-sectional area A= 0.000662 m^2, mass density of ρ=7850 kg/m^3 as well as the modulus of elasticity E=210 GPa are kept constant for all members. This structure is divided into 8 panel zones for the purpose of better indication of sub-structural elements. Panel T_L^N, represents the top layer, northen and left-hand panel. Similarly, the rest of the structure is assigned relevant to the location of panels and elements (shown in Figure 4.17). The natutural frequencies computed for exact values are 101.36 and 1310.55 Hz corresponding to the first and 123rd modes of this structure. It is to be noted that, the shortest period of this structure is 0.00076 sec, hence the most accurate simulation of responses of this structure may be achived by selecting at least 1428 sampling rates. This emphasizes the underlying keypoint of the proposed method (WMGA), whereby the small sampling rates of 100 S/s (Δt=0.01 sec) and 20 S/s (Δt=0.05 sec) are utilized to simulate acceleration (Fit_a) and jerk (Fit_j), respectively. In contrast, the sampling rate of 1000 S/s (Δt=0.001 sec) is utilized for the reasonable FE of Runge-Kutta algorithm to solve second ordered differential equation of motion (using ode45 MATLAB command and is referred to RMGA). In referring to the previous chapter, even by selecting long time intervals broad frequency components will be collectively captured (integrated) by adaptive collocations of wavelet, resulting in a cost-effective procedure for dynamic simulation of large-scaled structures. Subsequently, to accomplish reliable results as the resultant of a successful identification and damage detection, the total time of 15 sec is considered to either simulate responses or evaluate fitness functions. The WMGA parameters utilized in this example are displayed in Table 4.11. The axial rigidity is treated as unknown stiffness and the limits for the stiffness of truss elements (E×Area) are set as 0.5-2 times the theoretical stiffness. Fundamentally, the proposed strategy requires integration of accelerations, thus it is prefered to utilize a regular and smooth random force for this application rather than a very irregular and complex one. In this regard, a random multi-sinusoidal loading of 100-1000 cycle per second (Hz) with diferent magnitudes is applied as the concentrated nodal loading following the loading scenarios tabulated in Table 4.12. As it is shown in Table 4.12, the I/O signals are numerically contaminated with noise.

Structural identification is conducted using WMGA evolutionary strategy with respect to the various loading (Lo) and sensor placement (SP tabulated in Table 4.14) scenarios and the achieved computational efficiency and convergence rate have been compared with RMGA. The value of percentile maximum error and total computation time involved plotted in Figure 4.18 are considered as the indications of convergence rate and computational compatancy, respectively.

The notable observation on Figure 4.18 lies on the accurate identification strategy of this large-scaled structure by WMGA and RMGA, in case that the majority of DOFs are being excited. However, this loading scenario (Lo4) is in fact impractical in actual applications. It is overtly shown that, the accuracy of results are still desirable (about 20% of maximum error) considering SP1 (19.7% measured DOFs) in view of 10% noise imposed. Nonetheless, it is observed that according to Lo2 (5% noise) the maximum error returns the worst precision of results. This is because of the DOFs considered for this loading scenario.

University of Malaya

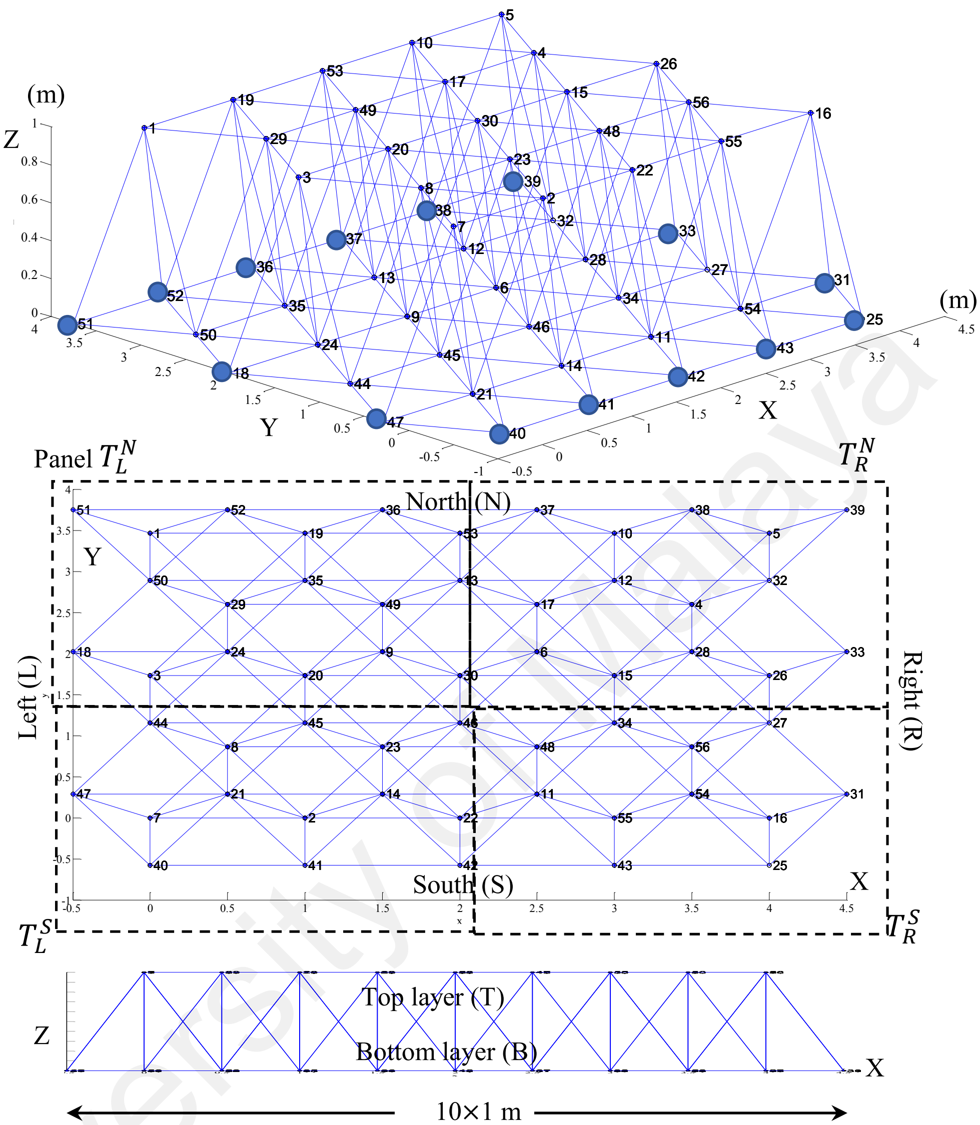

Figure 4.17: The large-scaled hexagonal space structure under concentrated loadings considered for Example 4.6.3.

University of Malaya

Table 4.11: WMGA parameters utilized in Example 4.6.3.

	Known mass
Pop-size	5×50
Runs	3
Generations	3×70
Conducted SSRM after;	70
Crossover rate	0.8
Mutation rate	0.1
Periodic migration (z_1,z_2)	5, 0.1-0.2
Window width	4
Regeneration	3
Reintroduction	120

Haar wavelet (2M=2), sampling rate 100 S/s.
Legendre wavelet (2M=4), sampling rate 100 S/s.
The second kind of Chebyshev wavelet (2M=8), sampling rate 100 S/s.

Table 4.12: Loading scenarios (Lo) applied to the 3D truss system.

Loading (Lo)	Node number	Noise ratio (%)	Magnitude (kN)	Direction
Lo1	6,9,11,14	10	2	Z
Lo2	35,12,54,21	5	2	Z
Lo3	6,9,11,14,19,53, 49,17,23,48,22,16	free	1	Z
Lo4	19,53,49,17,23,48, 22,16,35,13,12, 24,9,6,28,21,14, 11,45,46,34	free	0.5	X,Y,Z

University of Malaya

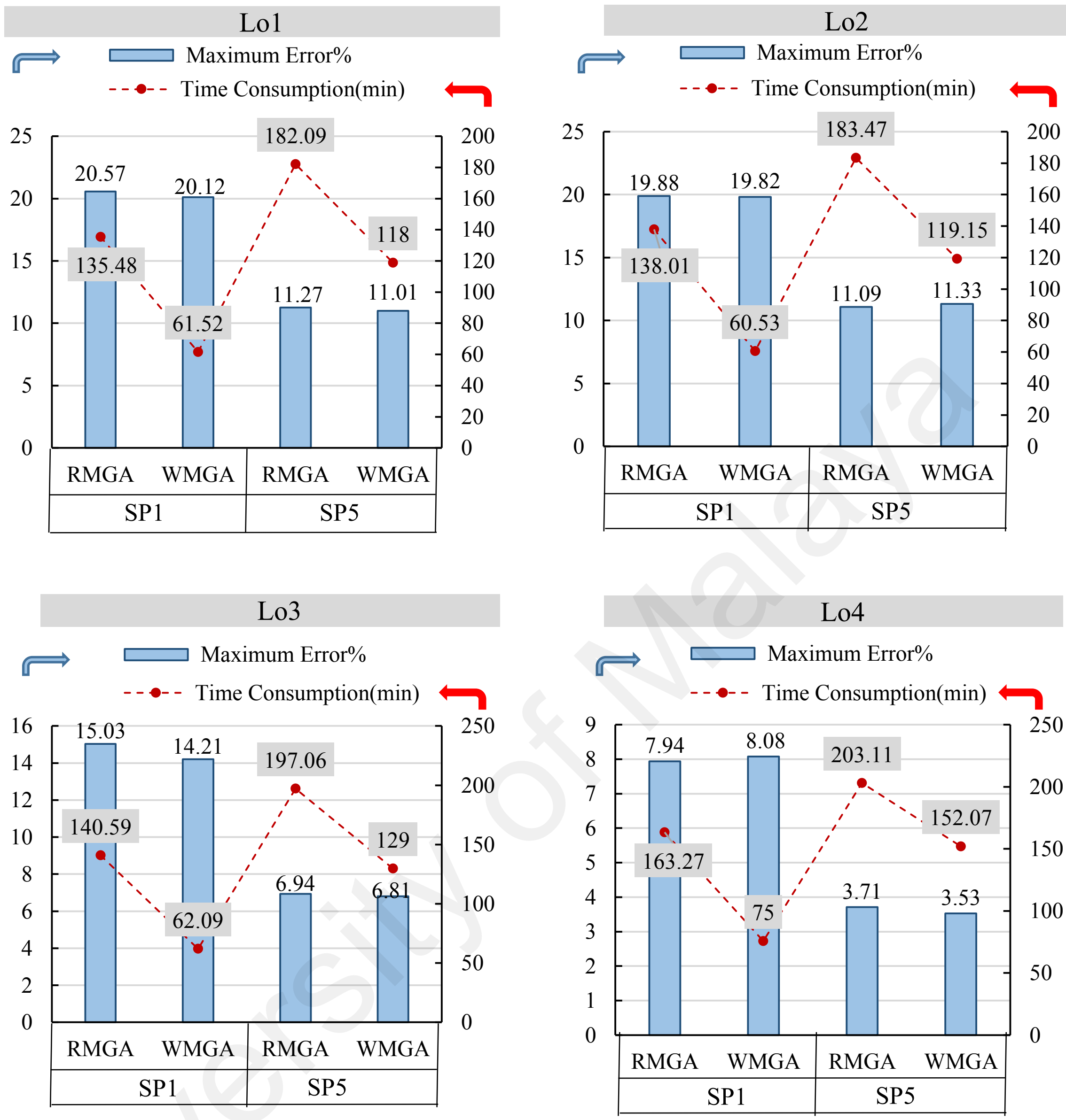

Figure 4.18: The percentile maximum errors and computation time involved recorded for RMGA and WMGA corresponding to different sensor placement (SP) and loading (Lo) scenarios.

From computational cost point of view this figure highlights the competency of WMGA, where, it generally records much better time consumption than RMGA. This can be interpreted as the better computational efficiency of this strategy. However, results depicted in this figure illustrate almost similar convergence rate for both strategies. Assumption of SP5 as the reference for comparison (100% DOFs are measured), it can be seen that the variations in maximum error measurement is not really noticeable. It can be concluded that, from the view of the convergence rate in only structural identification (and not damage detection) RMGA can compete with WMGA. Eventually, to assess the applicability and effectiveness of WMGA for damage detection of large-scaled structures, two damage scenarios (DS) have been proposed as tabulated in Table 4.13. It is observed that, damage is imposed on only 3 of 196 elements (about 1.5%) and 3% of all elements due to DS1 and DS2, respectively. Moreover, DS1 is proposed on elements placed at the northern and the left-hand panel zone, while, elements of DS2 are distributed in the whole structure.

Table 4.13: Damage scenarios (DS) imposed to the 3D truss shown in Figure 4.17.

DS	First node	Element	End node	Reduction (%)	Top/Bottom/Diag.	Off/On
DS1	36	68	52	30	Bottom (N,L)	Off
	20	33	49	25	Top (N,L)	Off
	13	29	53	20	Diag. (N,L)	On
DS2	35	46	50	25	Bottom (N,L)	On
	22	37	55	25	Top (S,R)	Off
	12	14	17	20	Diag. (N,R)	Off
	34	47	48	20	Diag. (S,R)	On
	5	8	10	30	Top (N,R)	On
	21	39	45	30	Bottom (S,L)	Off

Note: Reduction in stiffness (%) represents the magnitude of damage; north (N) and left (L) imply the position of panel zone in structure.

In addition, sensor placement scenarios (SP) that previously utilized for identification are tabulated in Table 4.14 corresponding to DS1 and DS2 for damage detection. Finally, damage detection is carried out for considered large-scaled structure by implementing WMGA (known mass). It should be pointed out that, there are several sub-structure techniques available to effectively analysis this system. In this study, reduction of the size of

University of Malaya

characteristic's matrices (i.e., stiffness, mass and damping) is governed by the sensor placement scenarios (measured and omitted DOFs), initially. Later, damage detection strategy proceeds, and by fixing identified parameters for undamaged members, the size of matrices is progressively reduced. To overcome the issue of false detection, a higher safety factor (threshold) is presumed to distinguish damaged and undamaged members. The identification and damage detection strategy are run 5 times and the percentile value of success in detecting location as well as the magnitude of damages are comparatively described in Figure 4.19 with respect to the various loading (Lo) and damage scenarios (DS).

Table 4.14: Sensor placement (SP) scenarios utilized for identification and damage detection of Example 4.6.3.

DS	SP	Panel zone							
		T_L^N	T_R^N	T_L^S	T_R^S	B_L^N	B_R^N	B_L^S	B_R^S
		Node number (X, Y and Z)							
DS1	SP1	1,20,53	10,17,26	7,8, 22	16,48, 56	13,24, 50	6,12, 32	14,44, 46	11,27, 54
	SP2	1,3,19, 20,29, 30,49,53	10,15,17	2,8	56	9,13, 24, 35,50	32,6, 28	21	27
DS2	SP3	1,49,53	10,15,17	7,8, 22	16,48, 56	13,24, 50	6,12, 32	14,44, 46	27,34, 54
	SP4	19,20,29	4,30,53	2,8, 23	22,48, 55	9,13, 35	12,28, 32	21,45, 46	11,34, 54
DS1, DS2	SP5	Full measurement							

Note: T_R^N represents the top (T) northern (N) and right-hand panel, B_L^S: the bottom (B) southern (S) and left (L) side panel, DS: damage scenario and SP: sensor placement scenario.

University of Malaya

In overall, it is observed that the detection of magnitude and especially location of damage for online scenarios are remarkably successful. For instance, in Figure 4.19 (a) and (b) in the cases where Lo1 (in view of 10% noise imposed) is applied on SP1-SP4 the satisfactorily high success is recorded for online damages. This arises from the fact that the optimum evaluation of the time-history of jerk considerably improves the proposed value of fitness for damages those were imposed online. In addition, Figure 4.19 shows much adequate success in detection of diagonal members rather than that of horizontal members on top or bottom layer. Consequently, the superiority of WMGA for damage detection is demonstrated in this figure, where 80% success in detecting the location and 60 % success in detecting the magnitude of damage for about 3% members are achieved by the measurement of only 20% DOFs of such large-scaled structures.

4.7 Chapter summary

In this Chapter, the wavelet-based strategy introduced in Chapter 3 for structural simulation was extended for structural identification and damage detection using enhanced genetic algorithms. An optimum operation was presented for sensitivity analysis of accelerations capable of using different basis functions (namely, jerk analysis), initially. It was shown that, the proposed operation of derivative is very sensitive to small changes of accelerations even selecting considerably small sampling rates (long time intervals). It was confirmed that, because of the property of unconditional stability, from the computational efficiency point of view the fitness evaluation is significantly improved by using the longer time intervals. The emphasis was on the precisely capturing broad frequency contents with adaptive collocation points of wavelets.

University of Malaya

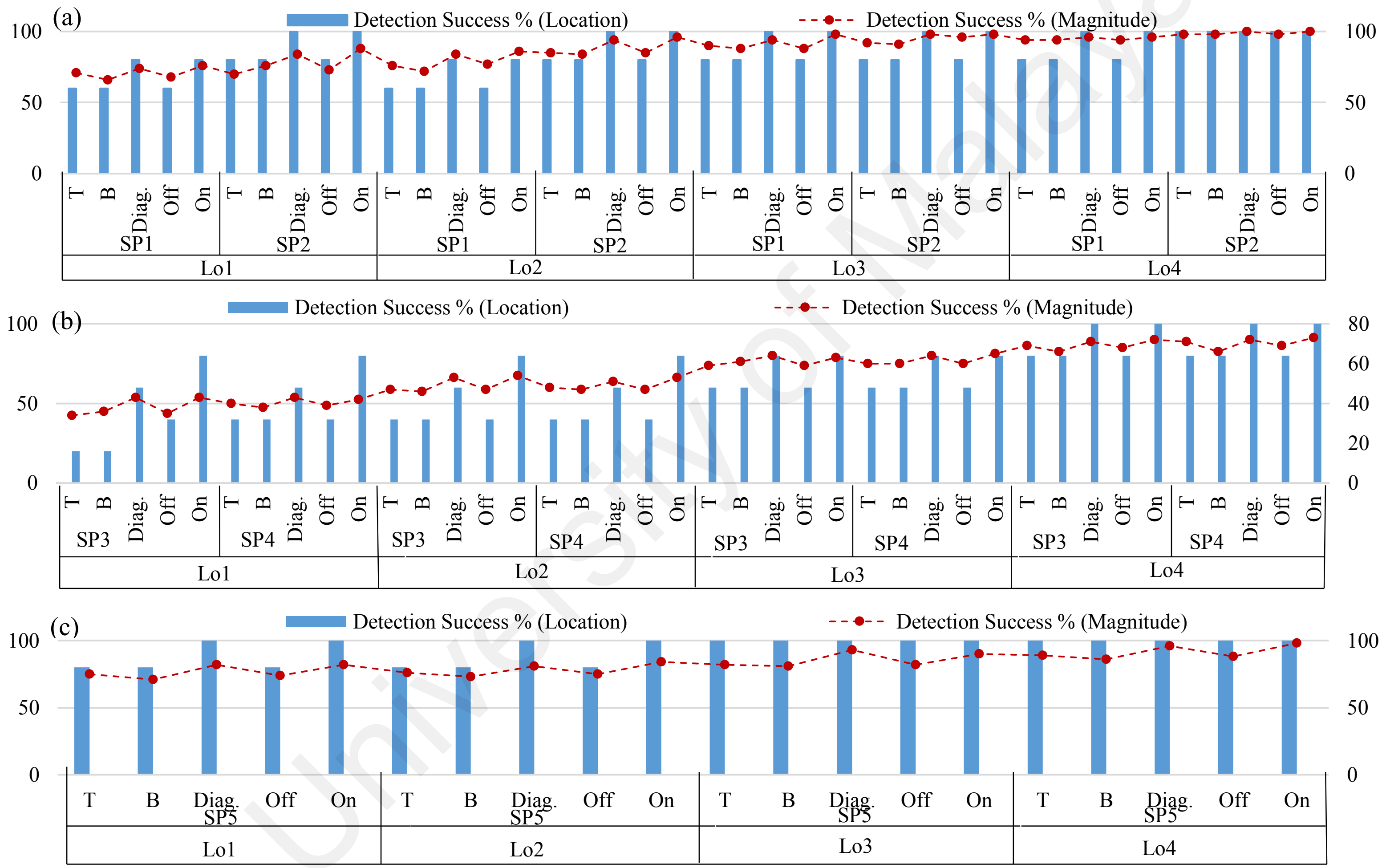

Figure 4.19: Damage detection success % (location and magnitude) using WMGA for different sensor placements (SP), loadings (Lo) and damage scenarios (DS); (a) DS1, (b) DS2, (c) DS2 (presented in Tables 4.13 and 4.14).

University of Malaya

Later, the wavelet-based scheme was implemented through a modified GA-strategy for structural identification and damage detection. In this regard, the fitness evaluation (known as the core of GA) was developed toward the most optimum strategy. As a consequence, a combined multi-species GA was adopted through a compatible search space reduction algorithm (SSRM) suitable for large-scaled structural identification to identify unknown stiffness, mass and damping ratios. In addition, a predictor/corrector approach was proposed for output-only identification using WMGA strategy in time domain. The strategy works by simultaneously calculating the input forces as the structural parameters (stiffness and damping) were identified.

Eventually, the proposed evolutionary process was extended to the structural damage detection through a progressive calibrating algorithm. The analysis of convergence and computational efficiency were introduced as the necessary and sufficient criterions to evaluate evolutionary procedures. Accordingly, the convergence rate of the proposed strategy was examined on three numerical applications. It was inferred that, the GA-based exploration and exploitation phases are optimally satisfied by the used of improved SSRM, and therefore a great convergence rate is accomplished. In addition, the lesser effect of I/O noise to the signal were recorded for the proposed WMGA.

On the other hand, computational cost (time taken to solve the problems) was investigated in the view of computational competency. It was concluded that, especially for large-scaled structures the identification of numerous unknowns is optimally achieved by the remarkably lesser computation time involved and resulting the very cost-effective strategy compared with existing algorithms. Damage detection was conducted and results demonstrated the superiority of the proposed method especially for online scenarios. It was also shown that, the proposed method gave the minimum false detection for online imposed damages, where the jerk evaluation gained the much better indication of damage rather than acceleration

University of Malaya

itself. Consequently, the proposed algorithm can be considered as a sufficiently reliable strategy especially for long time identification and online assessment of large-scaled structures.

University of Malaya

CHAPTER 5: EXPERIMENTAL VERIFICATION

5.1 Introduction

In order to investigate the effectiveness and capability of the proposed structural identification and damage detection strategies in Chapter 4 on more realistic data, three structural models have been constructed and tested in the laboratory for different scenarios of loading and damages. The first experiment involves the output-only identification of a four story MDOF system. The aforesaid system is designed with rigid beams (provided by rigid Plexiglas) and relatively flexible aluminum columns (thin aluminum columns) in order to invoke shear building behavior. The structure is subjected to base excitation and the force identification is also considered along with identification of stiffness values and damping parameters. The second structure is also a four story shear building constructed with thick aluminum columns and rigid beams. This MDOF system is subjected to different nodal excitations, and structural identification of known and unknown mass systems is considered on intact structure first. Later, the damage detection strategy proposed in Chapter 4 is conducted to detect the location and the magnitude of damages imposed to the structure. Eventually, the third experiment involves a 2D steel and pin-jointed truss designed with rectangle hollow sections as horizontal and vertical elements and double strips used for diagonal members. The structural identification and damage detection of this system are considered for different scenarios. Accordingly, for the last two experiments I/O data measurements are available. As there is no online damage induced to the structures, the only first term of Equation (4.21) is considered for fitness evaluations and the effect of jerk evaluation is ignored. Finally, the results obtained from the experiments are presented and discussed in subsequent sub-sections.

University of Malaya

5.2 Experiment 1 - A MDOF shear structure subjected to the base acceleration

Figure 5.1 illustrates the schematic view of a four story MDOF shear building considered in the first experiment. As it is shown in the figure, this structure is constructed with 8 aluminum columns which are fixed to the 4 rigid beams (provided with Plexiglas). The width of columns are taken 50 times the thickness in order to invoke ideal behavior of shear building. The dimensions of structural elements are given in the figure in centimeter. This structure is fixed at the base for impact test. Moreover, the mass of each floor is estimated by lumping the distributed mass of the relevant floor (i.e., the mass of beam, column and connecter screws) added with the external mass provided by two different weights at the 2nd and 4th levels. Measured values of mass are rounded off to the nearest 10 grams. Accordingly, the diagonal mass matrix of the MDOF system is shown in the figure. The beams and beam-column connections are assumed 100% rigid so that the theoretical stiffness for each story may be calculated for the column height (H=centre-to-centre height) as; $k = 24EI/H^3$. In addition, the stiffness matrix of the considered MDOF shear building is obtained as follows:

$$[K] = \begin{bmatrix} k_1 + k_2 & -k_2 & 0 & 0 \\ -k_2 & k_2 + k_3 & -k_3 & 0 \\ 0 & -k_3 & k_3 + k_4 & -k_4 \\ 0 & 0 & -k_4 & k_4 \end{bmatrix} \tag{5.1}$$

The response of the considered MDOF system was measured using four ICP accelerometers (KISTLER magnetic piezoelectric sensors) attached to each floor. The sensors utilized for the first and second experiments are described in Table 5.4. In addition, the mass of sensors (4.01-4.19 grams) were ignored. However, as the structure was very flexible, hence it was sensitive to the asymmetric mass values, and therefore another four sensors were attached to the structure to only balance the actual mass at both sides of structure as shown in Figure 5.1(b).

University of Malaya

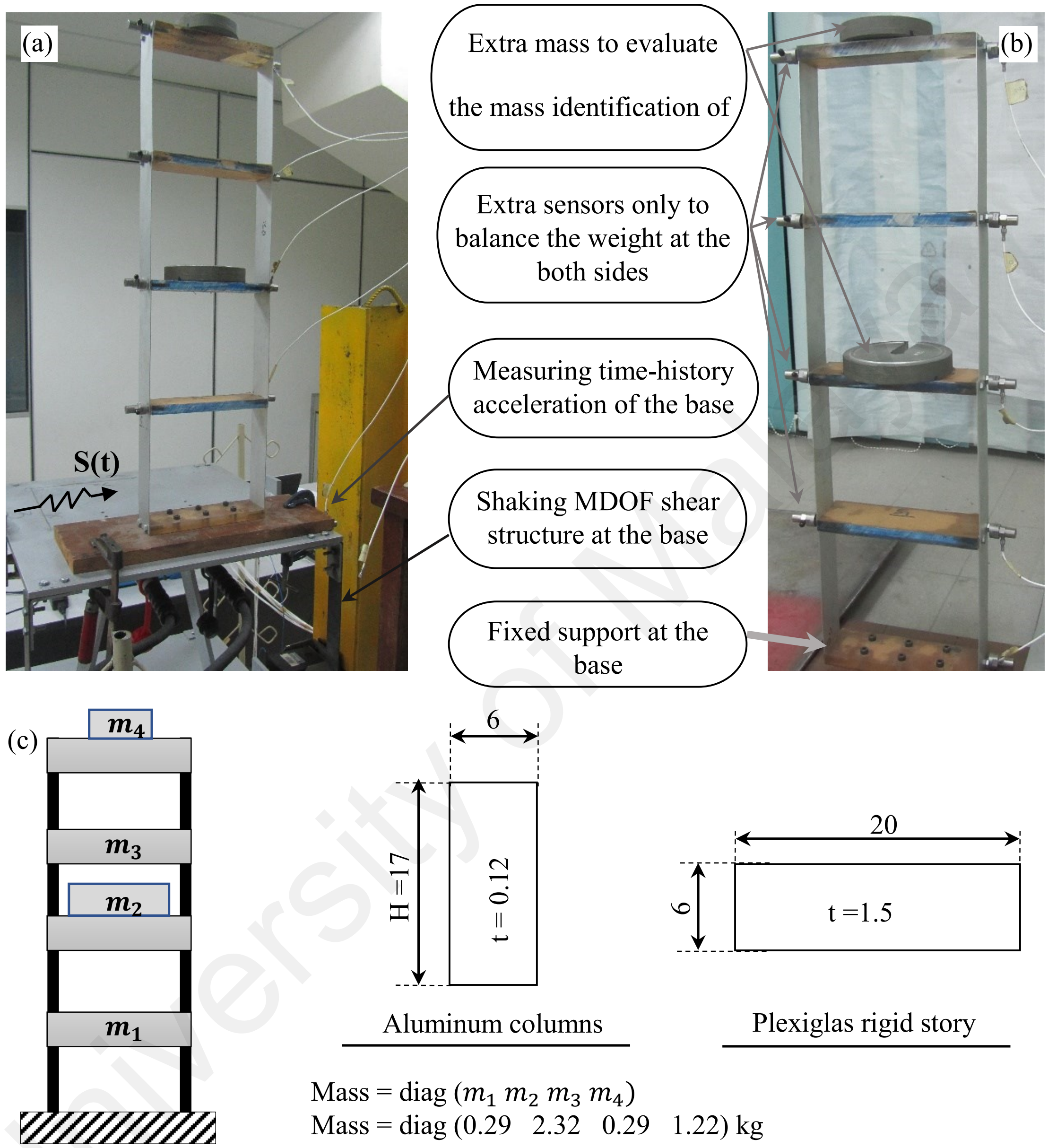

Figure 5.1: The schematic view of test setup in lab for output-only identification of the flexible MDOF shear system, (a) large shaking MDOF shear system at the base (S(t): base acceleration), (b) fixed support at the base for impact test, (c) dimensions (cm).

For the purpose of output-only identification, this structure was fixed on a flexible MDOF shear building shown in Figure 5.1(a). Subsequently, the time-history of acceleration S(t) was measured at the top surface of the base structure and was assumed to be the records of base excitation for the main experiment.

5.2.1 Preliminary measurements and calculations

As a reference for comparison of the calculated results, and in order to properly perform the identification and therefore structural health monitoring tests, a set of preliminary tests were first conducted. This sub-section contains static tests to predict the as-built stiffness of the structure (static), as well as several impact tests to extract the as-built natural frequencies.

Taking E as 69 GPa for the modulus of elasticity of the aluminum columns, the theoretical stiffness value of k =3455.09 N/m will be calculated for each story. As there was no information available on the actual material and also the as-built stiffness of the considered structure, static tests were conducted. The schematic view of static tests performed in the lab is shown in Figure 5.2. As apparent in the figure, the first story of the considered system was mounted horizontally to a fixed vertical support. Different weights were hung from the first story while displacement transducer recorded the displacement. For this purpose, non-contact laser sensor (KEYENCE; precision 0.01mm) was utilized to record the displacements due to the different weights added.

University of Malaya

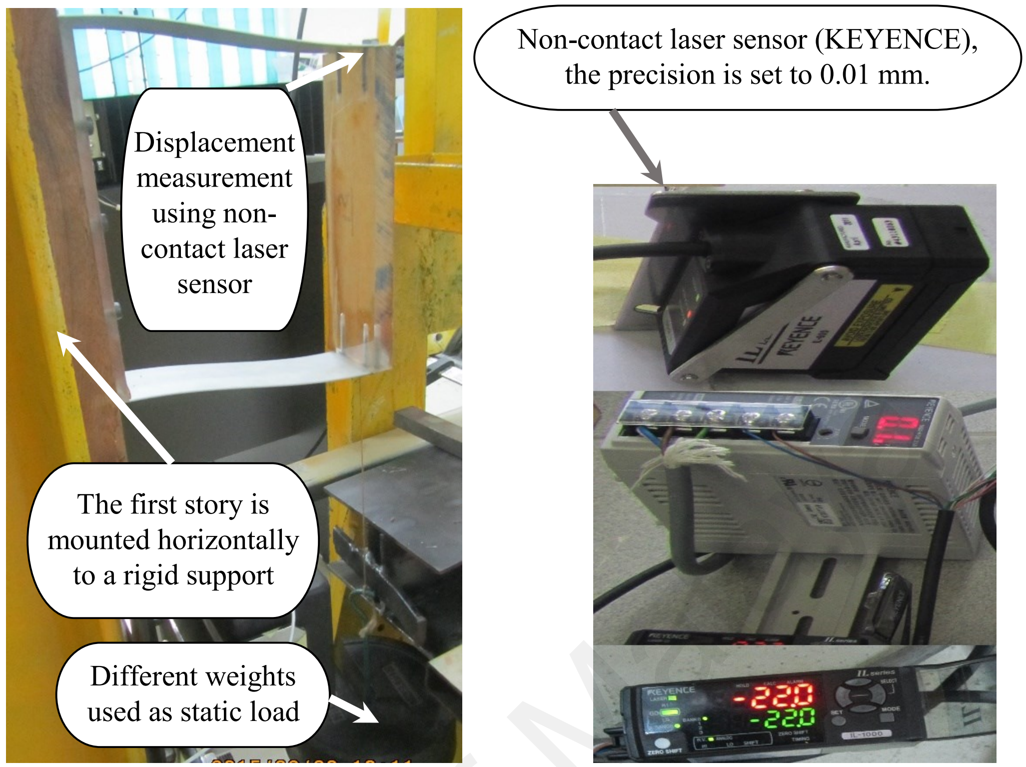

Figure 5.2: The schematic view of static test performed in lab for the first MDOF system (O-only identification).

Accordingly, the as-built stiffness of one story was determined from the slope of the regression line obtained from different load-displacement points measured for several different weights applied. In this regard, the stiffness value of k =2421.18 N/m was measured per story from the static tests. It was recognized that the difference between the static and theoretical stiffness was noticeable. This could be due to the fact that the actual material properties of considered structure were not available in lab. However, the stiffness value obtained from the static tests was logically more accurate than that of the theoretical values.

The impact tests were performed in order to compare stiffness values. Initially, the structure was fixed to a rigid base as shown in Figure 5.1(b). Later, the considered MDOF shear structure was excited by a hammer and the response recorded with sensors (accelerometers) at each story using a 16 channel digital data analyzer (OROS36) at a sampling rate of 2.048 kS/s. In addition, the structural frequencies were extracted by implementing the fast Fourier transform (FFT) to convert the response signal from time domain into the frequency domain (power spectrum of the signal). The natural frequencies obtained from the solution of eigenvalue problems adopted for theoretical and static stiffness values and those determined from the power spectrum of response are tabulated in Table 5.1 corresponding to the four modes of the MDOF system. It was observed that the response at other levels and for other impacts, identified almost the same frequencies. However, data in Table 5.1 correspond to the response at the 4th story due to impact at the same story.

Table 5.1: Calculated and measured natural frequencies of MDOF shear structure.

	Theoretical stiffness = 3455.09 (N/m) per story		Static stiffness = 2421.18 (N/m) per story		Measured frequencies from power spectrum of response	
	f (Hz)	Period (s)	f (Hz)	Period (s)	f (Hz)	Period (s)
Mode 1	3.12	0.32	2.61	0.38	2.59	0.38
Mode 2	7.85	0.13	6.57	0.15	6.55	0.15
Mode 3	24.81	0.04	20.77	0.05	20.72	0.05
Mode 4	25.83	0.039	21.63	0.046	21.08	0.047

Note: The mass is lumped at each story as shown in Figure 5.1 for all 3 cases considered.

Table 5.1 shows that, the natural frequencies extracted from the impact test and those obtained from the static measurements were reasonably close. Consequently, the stiffness value determined from static tests will be considered as the actual stiffness of the structural elements and this should form the reference value of stiffness for further comparisons.

University of Malaya

5.2.2 Main identification test

The main objective of this experiment is to evaluate the applicability and efficiency of WMGA strategy proposed in previous chapter for structural identification problems when output-only measurements are available. In other words, the stiffness and damping parameters of each story are treated as unknown values to be identified while the measurement of input forces is not available. The base structure was excited manually for 5 sec in the same direction with the attached MDOF shear building (Figure 5.1). As both systems are supposed to be shear building structures, it is reasonable to transfer the acceleration at the base structure (shaking MDOF system) to the dynamic equilibrium governing the top structure in order to determine the actual forces. The response of the top MDOF structure as well as the base acceleration were measured using five ICP accelerometers (KISTLER magnetic piezoelectric sensors) attached to the base and each story, respectively. The measured data of accelerometers are then recorded using a 16 channel digital data analyzer (OROS36) at a sampling rate of 5.128 kS/s. Despite the fact that, the highest frequency of the structure is only 21.08 Hz (for the 4^{th} mode), selecting such high sampling frequency allows for a better capture of excitation and resulting in a more precise simulation of the response during identification. Finally, WMGA parameters utilized for structural identification of this experiment are given in Table 5.2. It should be emphasized here that the fairly broad range of 2.2 and 0.4 times actual values is selected as the search limits of unknown stiffness. In addition, the search limits of damping parameters corresponding to the first two modes are set as 0 to 3 for α and 0 to 0.0002 for β.

Table 5.2: WMGA parameters utilized for force identification (Experiment 1).

	Known mass
Pop-size	5×30
Runs	3
Generations	3×100
Conducted SSRM after	100
Crossover rate	0.6
Mutation rate	0.2
Periodic migration (z_1,z_2)	5, 0.1-0.2
Window width	4
Regeneration	3
Reintroduction	80

Haar wavelet (2M=2), sampling rate 500 S/s.
Legendre wavelet (2M=4), sampling rate 200 S/s.
The second kind of Chebyshev wavelet (2M=8), sampling rate 200 S/s.

5.2.3 Results and discussion

Figure 5.3 illustrates the first 4000 points of acceleration time-histories recorded for corresponding nodes at a sampling rate of 5.128 kS/s. It should be pointed out that, complete data measurement is considered for this experiment. In addition, as this experiment involves force identification, a known mass problem is considered. As shown in Figure 5.3(e), the maximum effect of noise was observed for the recorded accelerations at the base (designated by S(t)). However, the noise effect was gradually reduced for the higher levels of the considered MDOF shear system. The reason for this comes from the fact that the main excitation was applied to the base manually as an ambient excitation with the highest signal-to-noise ratio.

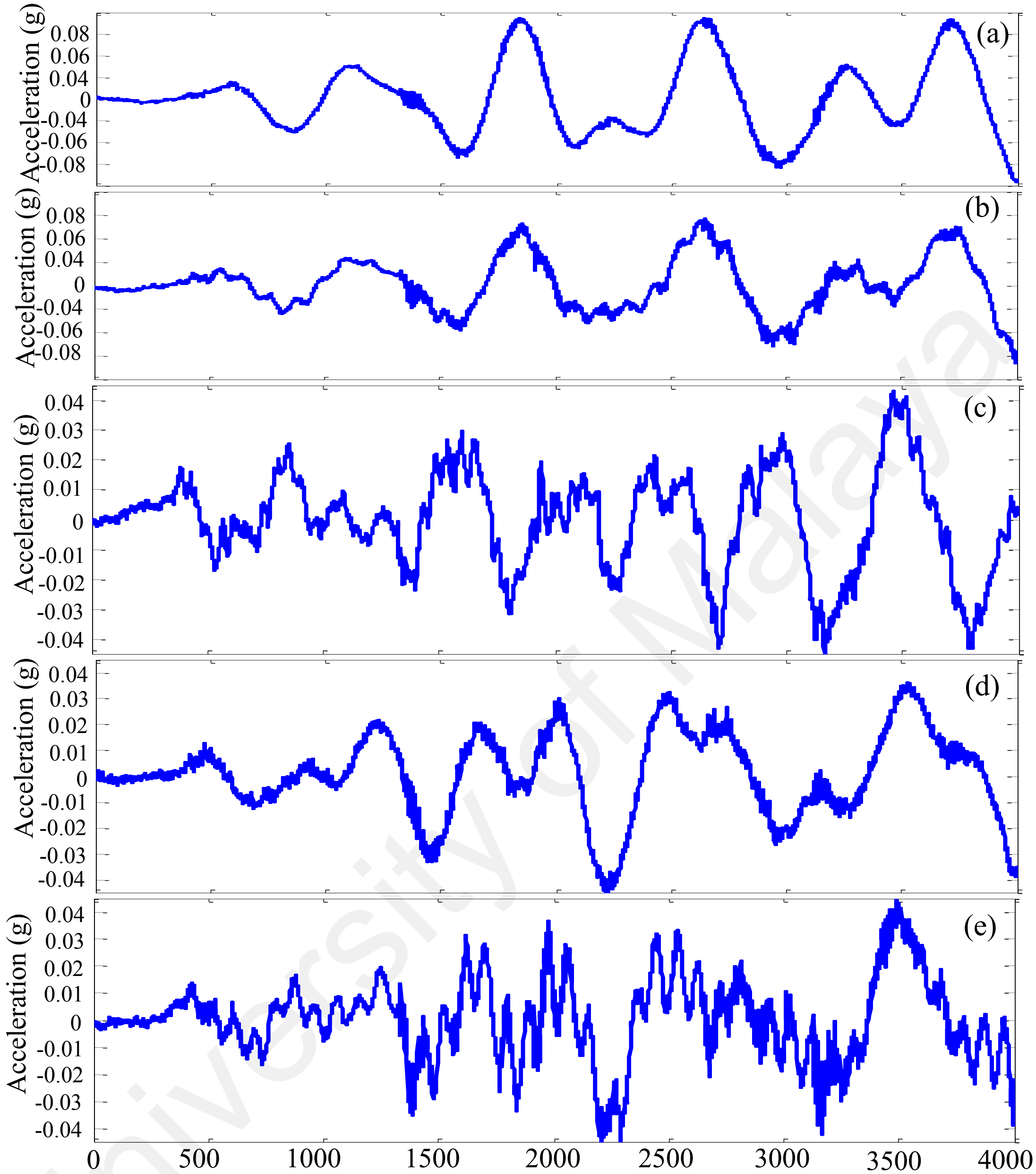

Figure 5.3: Time-history of acceleration (the first 4000 points) corresponding to, (a) story 4, (b) story 3, (c) story 2, (d) story 1, (e) S(t): the base acceleration (g = 9.81 m/sec^2).

Therefore, the uncontrolled excitation to the unknown base structure causes the larger effects of the signal-to-noise. The structural identification is conducted using WMGA parameters presented in Table 5.2. The time-history of identified force for 250 measured data

University of Malaya

(between 500-750 acquired points) corresponding to the second and third levels is plotted in Figure 5.4.

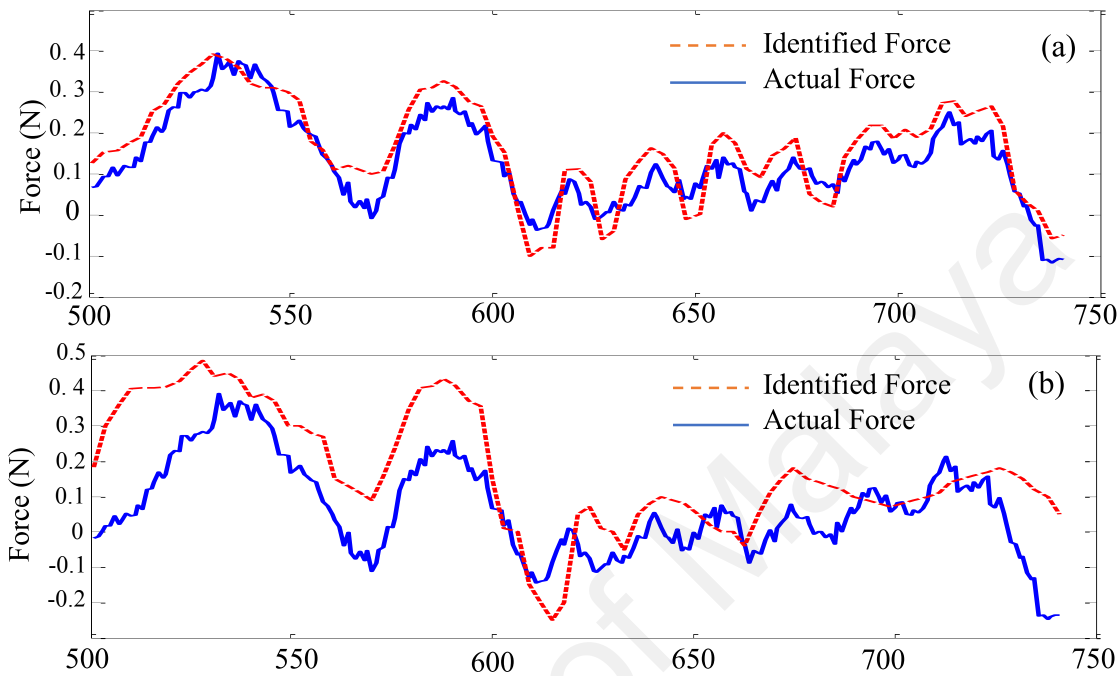

Figure 5.4: Time-history of identified force (500 to 750 acquired points) corresponding to, (a) story 2, (b) story 3.

The actual forces for each level were obtained by multiplying the base acceleration S(t) to the actual mass at each level in inverse direction. As shown in Figure 5.4, the proposed WMGA force identification strategy acts as a filtering procedure in order to reduce the effect of noise. This is most likely due to the various scales of adaptive wavelet functions and relatively compatible collocation points utilized for capturing the response of structure. It is demonstrated that even with high signal-to-noise ratio data, the force identification is reasonably reliable for ambient excitation done manually. It should be emphasized here that, in order to implement the proposed procedure of force identification the first underlying presumption is that the structure should be at rest condition. Providing such ideal condition for this test was either impossible or very difficult. Undoubtedly, the aforementioned difficulty causes errors in identification procedure. Furthermore, this figure shows more noticeable errors recorded for identified force at the third level rather than the second one. This probably is because of the very light mass at this level in the vicinity of two heavy masses corresponding to the second and fourth levels.

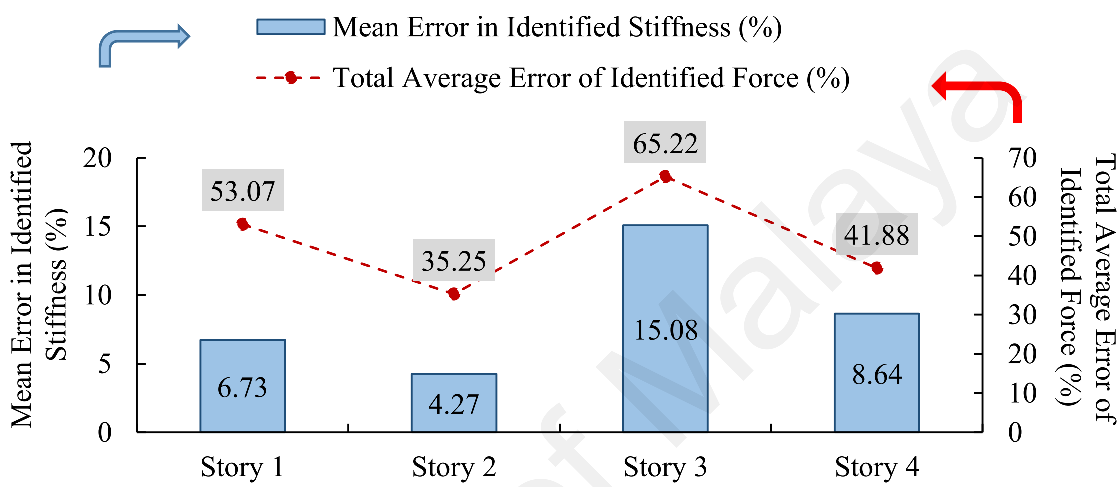

Figure 5.5: The percentile total average error of identified force and the mean error (%) in identified stiffness of each story for output-only measurement.

Subsequently, by considering the initial stiffness values obtained from the static test, the percentile total average error computed for identified force (at 5 sec of excitation) and the percentile mean error in identified values of stiffness corresponding to each level of MDOF system are comparatively plotted in Figure 5.5. This figure demonstrates acceptable identified values for stiffness. For instance, about 6.7%, 4.3% and 8.6% of mean error were recorded for identified stiffness values of level 1, 2 and 4, respectively. In contrast, the highest error of 15.8% was measured for the identified value of stiffness corresponding to level 3. This results are in the agreement with the results shown in Figure 5.4, where the maximum differences are observed for the identified force at level three compared with the second or other levels. Moreover, the percentile total average errors obtained for four identified forces demonstrate the average error of about 48.8% for all levels. This value seems undesirable compared to the very accurate numerical results achieved in Chapter 4 for force identification. This probably arises from two factors. Firstly, the ambient excitation applied to the base is an unrealistically irregular one, while it could be applied with an actual instrument in order to be controlled in particular ranges of frequencies or amplitudes. Secondly, the effect of high signal-to-noise ratio was not considered in Chapter 4 for force identification (especially for irregular distribution of mass at different levels) to accomplish the precise results. Furthermore, the effect of rest condition may be another source of error measurements. Overall, the structural identification results demonstrate that the proposed strategy for output-only data is a very good strategy, especially for real cases of irregular ambient data. However, it could be perfected by proper planning in identification. It is very important to keep in mind that, one of the main source of errors observed in Figure 5.5 is the assumption of lumped mass matrix for structural modeling in this real case. Undoubtedly, aforesaid assumption diversely affects the identified stiffness values, especially for ambient vibration data.

5.3 Experiment 2 - A MDOF shear structure under nodal excitation

The schematic view of the test setup performed in lab for the second experiment is illustrated in Figure 5.6. The MDOF shear system considered for this experiment was constructed with 8 thick columns (provided with aluminum) and 4 rigid beams (provided with Plexiglas). The width of columns are taken 12 times the thickness and allows for the assumption of the shear behavior of the MDOF system (existing for only one DOF per story). This structure is fixed at the bottom for impact and the main structural health monitoring tests. Moreover, the mass of each floor is estimated by lumping the distributed mass of the

University of Malaya

corresponding story (i.e., the measured mass of beam, column and connecter screws) added with the external mass provided by two different weights at the 2nd and 4th levels. Measured values of the mass are rounded off to the nearest 10 grams and the diagonal mass matrix of this system is shown in the figure. In addition, in this experiment the mass of four accelerometers attached to structure is ignored. The beams and beam-column connections are assumed 100% rigid. Therefore, stiffness matrix of the system is obtained from Equation (5.1).

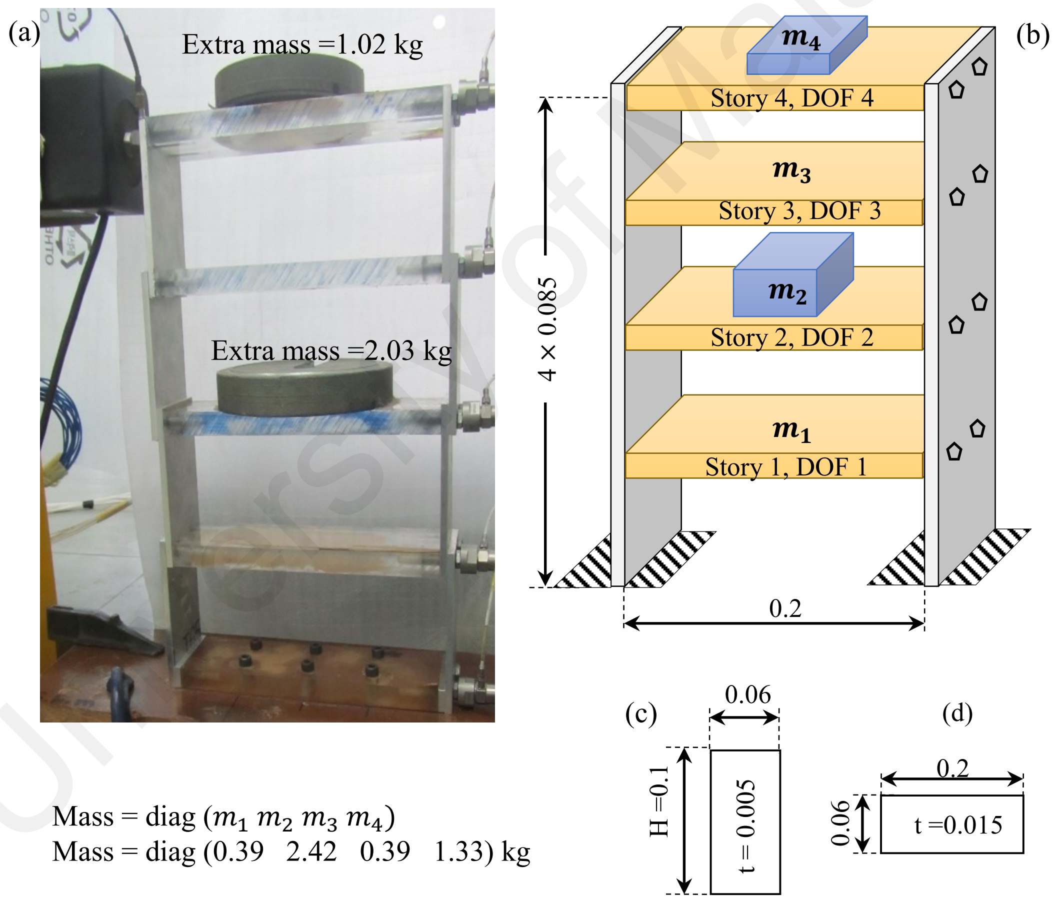

Figure 5.6: The schematic view of the test setup: (a) the laboratory aluminum MDOF shear building, (b) dimensions of the frame (m), (c) dimensions of the columns (m), (d) dimensions of the rigid beam (m).

University of Malaya

Accordingly, structural health monitoring of this structure is considered using the proposed WMGA strategy in the previous chapter. To examine the performance of the strategy, WMGA is conducted for structural identification of intact structure, initially. Later, two different magnitudes of damage and locations are utilized in order to evaluate the efficiency and capability of the proposed strategy for damage detection.

5.3.1 Preliminary measurements and calculations

- ***Stiffness estimation***

As a basis for comparison of the obtained results, and to properly perform the identification and therefore structural health monitoring tests, a set of preliminary tests were first conducted. This sub-section contains static tests in order to predict the as-built stiffness of the MDOF shear structure, as well as several impact tests to extract the as-built natural frequencies.

Taking $E = 69$ GPa for the modulus of elasticity of the aluminum columns, the theoretical stiffness value of $k =$1820.15 kN/m will be calculated for each story. As there was no information available on the actual material and also the as-built stiffness of the considered structure, static tests were conducted. The schematic view of static tests conducted in the lab is illustrated in Figure 5.7. The first story of the considered system was mounted horizontally to a fixed vertical support. Different weights were hung from the first story while displacements were measured by displacement micrometer (precision 0.01 mm).

Subsequently, the as-built stiffness of one story was obtained from the slope of the regression line determined from the different load-displacement points measured for several different weights applied. The stiffness value of $k =$1203.46 kN/m was measured per story from the static tests. It was seen that the difference between the static and theoretical stiffness was about 617 kN/m. Subsequently, the impact tests were performed to compare stiffness values and select the reference value of stiffness.

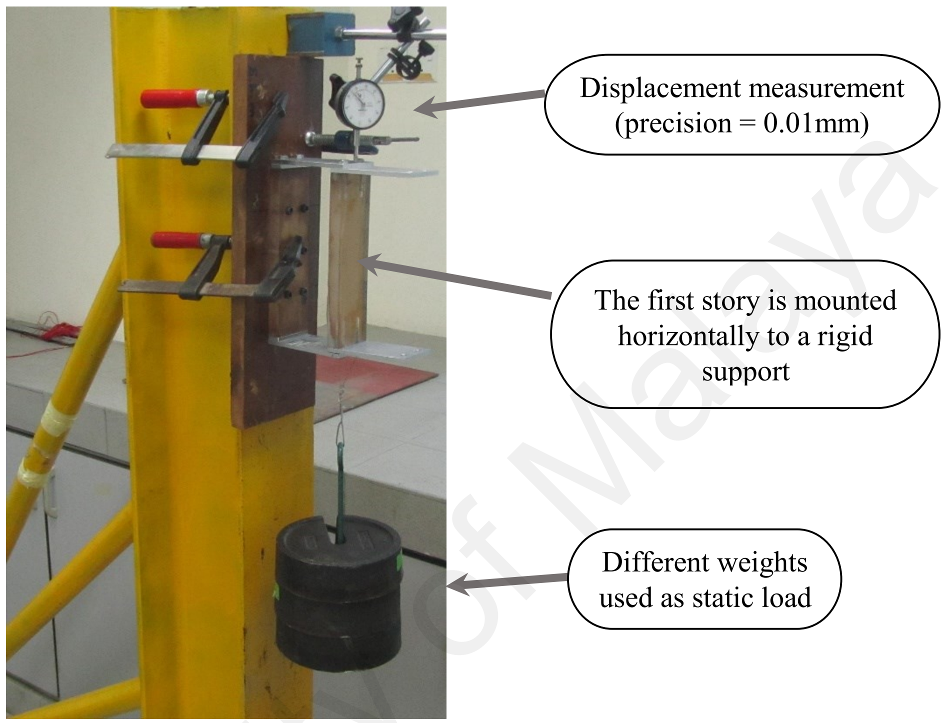

Figure 5.7: The schematic view of static test conducted in lab.

As in the previous experiment, the MDOF shear structure was fixed to a rigid base and it was excited by a hammer and the response recorded with sensors (accelerometers) at each story using a 16 channel digital data analyzer (OROS36) at a sampling rate of 2.048 kS/s. Accordingly, the FFT algorithm was then utilized to convert the response signal from time domain to the frequency domain and the natural frequencies were determined from the plot of power spectrum as illustrated in Figure 5.8 for one of the examples. It should be noted that, a frequency band width of 1024, and therefore 2048 data points were utilized for the FFT. Thus, the accuracy of measured frequencies was approximately $\pm$0.5 Hz. Figure 5.8

University of Malaya

shows the power spectrum of the response at fourth story due to the impact at that story. It was observed that the response at other stories and for other impacts, identified the same frequencies.

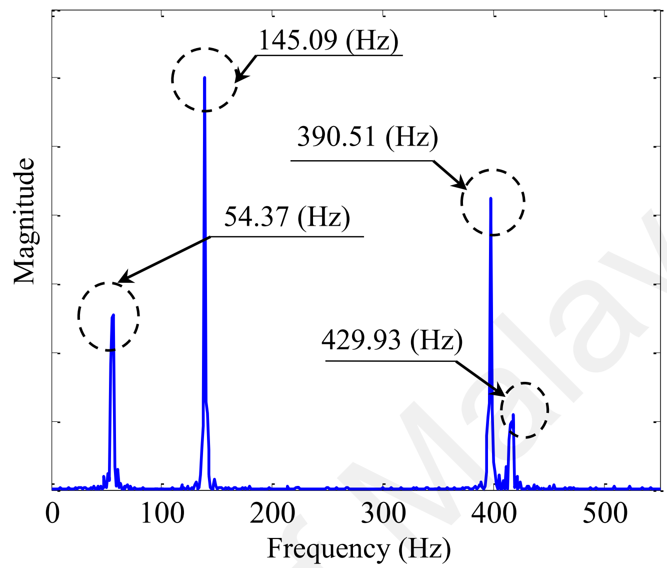

Figure 5.8: Power spectrum of response at fourth story due to impact at that story.

The natural frequencies obtained from the solution of eigenvalue problems adopted for theoretical and static stiffness values and those determined from the power spectrum of response are tabulated in Table 5.3 corresponding to the four modes of the MDOF system.

Table 5.3: Calculated and measured natural frequencies of undamaged MDOF shear structure.

	Theoretical stiffness = 1820.15 (kN/m) per story		Static stiffness = 1203.46 (kN/m) per story		Measured frequencies from power spectrum of response	
	f (Hz)	Period (s)	f (Hz)	Period (s)	f (Hz)	Period (s)
Mode 1	69.39	0.0144	55.63	0.0179	54.37	0.018
Mode 2	175.25	0.0057	141.42	0.0070	145.09	0.0069
Mode 3	538.26	0.0019	398.95	0.0025	390.51	0.0025
Mode 4	561.85	0.0018	419.68	0.0023	429.93	0.0023

Note: The mass is lumped at each story as shown in Figure 5.6 for all 3 cases considered.

Data displayed in Table 5.3 shows the closeness of obtained frequencies from the impact test with those calculated based on the stiffness determined from the static test. This table shows that especially for the first two modes of the structure results are very close. As a consequence, the stiffness value obtained from static tests will be considered as the actual stiffness of the structure and this should form the base value of stiffness for further comparison.

- ***Damage scenarios***

Two different magnitudes of damage and correspondingly two different locations are utilized in order to evaluate the capability and performance of the strategy. As it is shown in Figure 5.9, damage magnitudes are categorized as small and large while the locations differ corresponding to different damage scenarios one to three (DS1-DS3) imposed to the different stories.

Accordingly, DS1, DS2 and DS3 indicate damage scenarios when only small damage is induced in story 4, only large damage induced in the first story and the combination of this two scenarios, respectively. Controlled damage is created by cutting the columns at the proposed locations. As shown in Figure 5.9, small damage is created as partial cuts near to the beams (in order to be in an area of high bending), whereas large damage is formed by a longer cut at the center of columns. It should be pointed out that, the small and large damages are induced on both sides of the structure. In order to predict the reduction in stiffness due to the small and large damages, three columns are numerically simulated in a finite element (FEM) software (ABAQUS 1998). The FEM models of the intact columns as well as damaged columns with one end fixed and the other one free are shown in Figure 5.9. Shell elements are used to model all three cases. An arbitrary distributed force of 25 N/cm is applied to the top free nodes in the perpendicular direction. For all three cases the resulting displacements are compared with the result of intact column and the reduction in column

University of Malaya

stiffness is presented as the damaged index in Figure 5.9. It is to be noted here that, the reduction in story stiffness is the same as the expected reduction in column stiffness e.g., 42.69% for small damage, as damages are symmetrically applied to the both columns in a story.

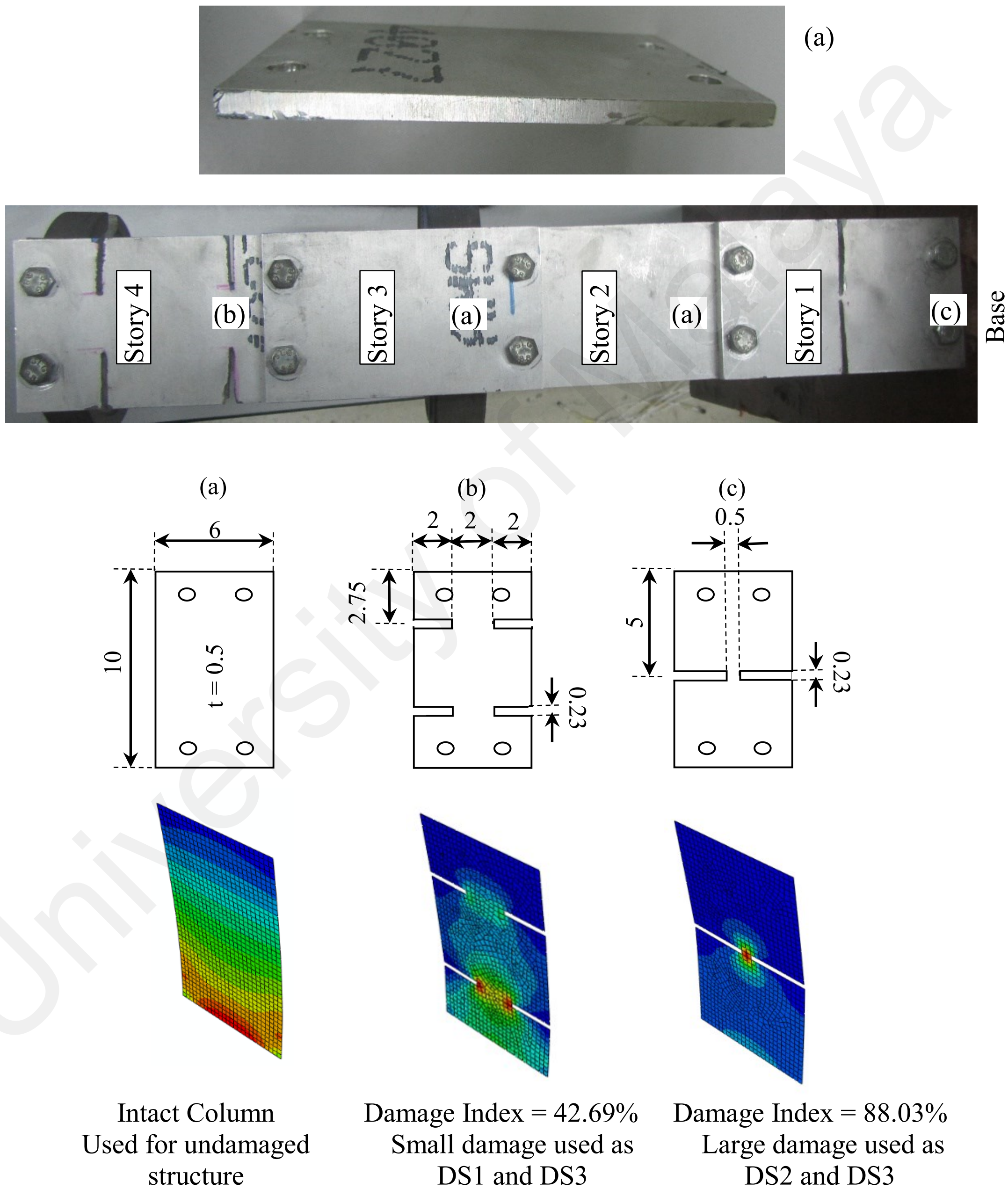

Figure 5.9: Damage scenarios and relative finite element models to estimate damage index (%), (a) undamaged column, (b) small damage, (c) large damage (dimensions are given in cm).

University of Malaya

5.3.2 Main identification and damage detection test

- ***Excitation force***

Basically, the proposed WMGA strategy requires integration of accelerations. Thus it is prefered to utilize a regular and smooth random force for this test rather than a very irrigular and complex one. In this regard, a random multi-sinusoidal loading of 50-500 cycle per second (Hz) with random magnitude of [-20, 20] N is utilized at a sampling rate of 5.128 kS/s. Accordingly, the force described above is applied through a shaker by roving it at different levels of the structure.

- ***Test setup***

Figures 5.10 and 5.11 illustrate the test setup utilized in lab and a schematic view of the dynamic testing and data acquisition system, respectively. The excitation force was input to a 16 channel digital data analyzer (OROS36) and the signal was then passed through a power amplifier in order to produce sufficient power for the electromagnetic shaker. The force generated by the shaker was transferred to the structure and an ICP force sensor measured the applied force (the specification of force sensor is presented in Table 5.4). The force transducer (shaker) placement as well as the shaker-sensor-structure connection are shown in Figures 5.10(a) and 5.10(b), respectively. The response of MDOF system to 10 sec of excitation was measured by 4 ICP accelerometers (KISTLER magnetic piezoelectric sensors) attached to each level of the MDOF structure. The classifications of sensors (accelerometers) utilized are tabulated in Table 5.4. The signals measured by force sensor and accelerometers are recorded by a 16 channel digital data analyzer (OROS36) at a sampling rate of 5.128 kS/s. In addition, only the first 5 sec of response starting from just before the application of the force are selected and copied to the input file for the damage detection program.

University of Malaya

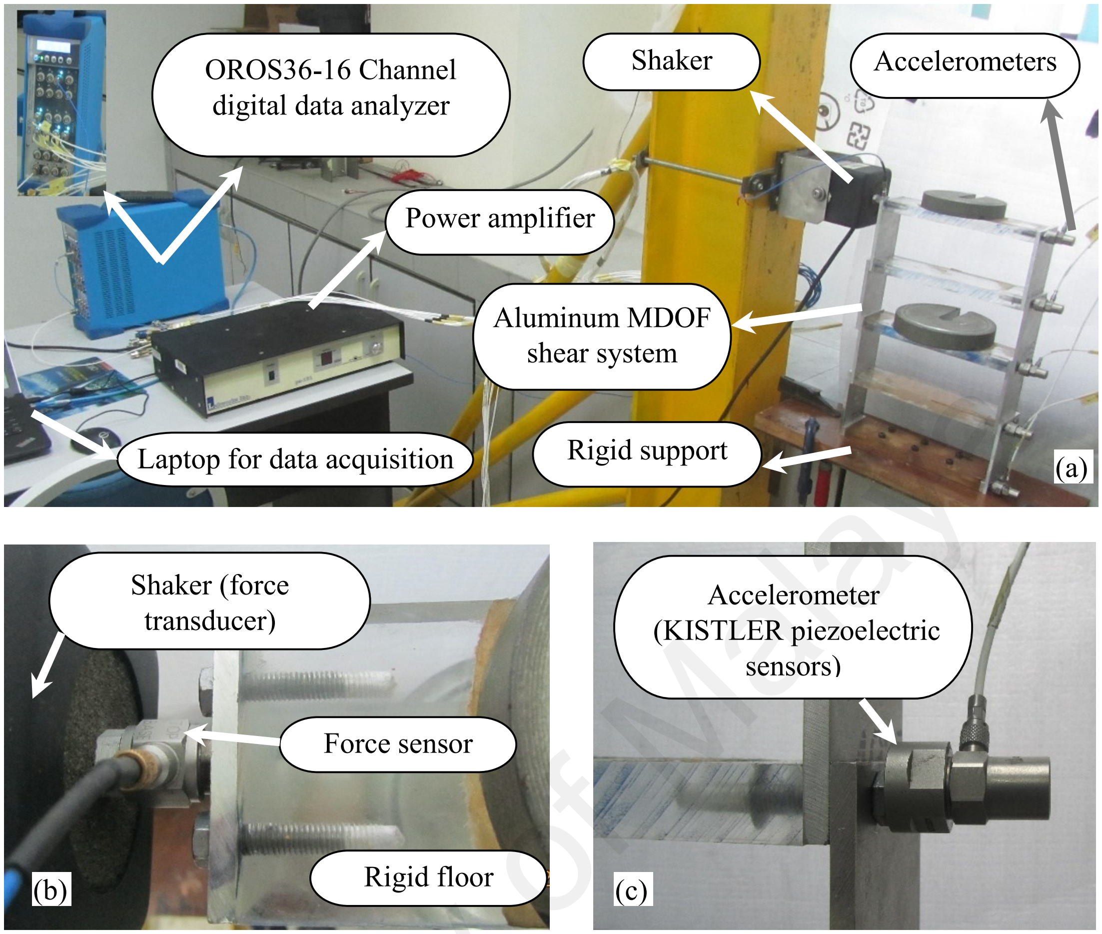

Figure 5.10: Test setup and instruments used in lab, (a) main test setup, (b) shaker installation, top view, (c) accelerometer installation, side view.

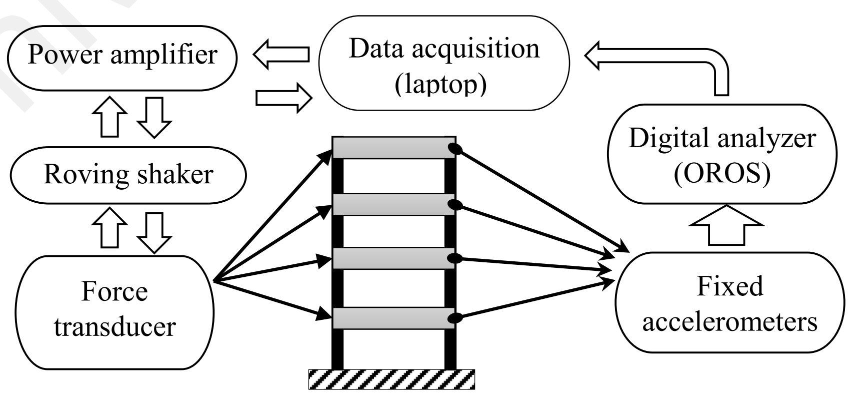

Figure 5.11: The schematic diagram of data acquisition and test setup.

University of Malaya

Table 5.4: The specification of accelerometers and force transducer.

Story	Transducer	Sensitivity	Range peak (acceleration or force)
1	Acceleration	103.9 m(V)/(g)	96 g
2	Acceleration	106 m(V)/(g)	94.3 g
3	Acceleration	99.2 m(V)/(g)	101 g
4	Acceleration	99.4 m(V)/(g)	101 g
1_4	Force	11.241 m(V)/(N)	890 N

Note: The gravity acceleration (g) = 9.81 m/sec^2.

Accordingly, WMGA parameters utilized for the identification of intact structure and damage detection are displayed in Table 5.5. In addition, half and twice the measured static stiffness and mass values are used as the initial search limits of stiffness and mass, respectively. The search limits of damping parameters corresponding to the first two modes are set as 0 to 3 for α and 0 to 0.0002 for β.

Table 5.5: WMGA parameters utilized for Experiment 2.

	Undamaged Structure (unknown mass)	Damaged Structure (known mass)
Pop-size	5×50	5×30
Runs	3	3
Generations	3×180	3×100
Conducted SSRM after	180	100
Crossover rate	0.4	0.6
Mutation rate	0.2	0.2
Periodic migration (z_1,z_2)	5, 0.1-0.2	5, 0.1-0.2
Window width	4	4
Regeneration	3	3
Reintroduction	140	80

Haar wavelet (2M=2), sampling rate 500 S/s.
Legendre wavelet (2M=4), sampling rate 200 S/s.
The second kind of Chebyshev wavelet (2M=8), sampling rate 200 S/s.

University of Malaya

5.3.3 Results and discussion

Accordingly, for structural damage detection, the unknown mass problem is first considered for initial structural identification. Later the identified mass from the initial step is fixed as the known mass at each level corresponding to each DOF of structure. As it was proposed before, the identified mass values are set as fixed values for all individuals (for known mass problems) while the identified stiffness values are set as the initial predictions of the first individual of species one and as the half of species 4 and 6 for local searches. This resulted in a desirable calibration of the dynamic model using precise initial values. Furthermore, the initial (reference) mass values were measured while the initial (reference) stiffness values were obtained from the static tests.

Subsequently, identification of intact MDOF system is first performed in order to perceive the changes in the identified values from those estimated from static tests or measurements. The search limits are set as the half and twice the actual values. For instance, the search limits of mass are set as [0.2-0.78], [1.21-4.84], [0.2-0.78] and [0.67-2.66] kg for the 1st, 2nd, 3rd and 4th levels, respectively.

From our preliminary tests, it was concluded that the dynamic model does not perfectly present the structural system, and that the first step of identification in the damage detection serves to calibrate the model so damage can be precisely detected. In addition, it was included that, for tests applying a same force input (in referring to the same frequency content and the same amplitude bandwidth) at a same location, the strategy were consistently achieving better detection results rather than applying different forces at different locations for identification step and damage detection stage. For this reason, the same force as presented in previous chapter is applied for both structural identification and damage detection at the last level of MDOF system.

University of Malaya

For comparison purpose, the modified genetic algorithm composed of 6 species proposed in Chapter 4 (designated by MGA) is also adopted for structural identification of current experiment. Accordingly, the well-known average acceleration of Newmark-β method is performed for fitness evaluations of MGA at a sampling rate of 2000 S/s (time step of 0.0005 sec) for 10 sec of measured response at a sampling rate of 5.128 kS/s. The percentile total average errors and corresponding CPU time consumption for stiffness identification of undamaged structure regarding to the known and unknown mass problems are comparatively depicted in Figure 5.12 (complete measurement).

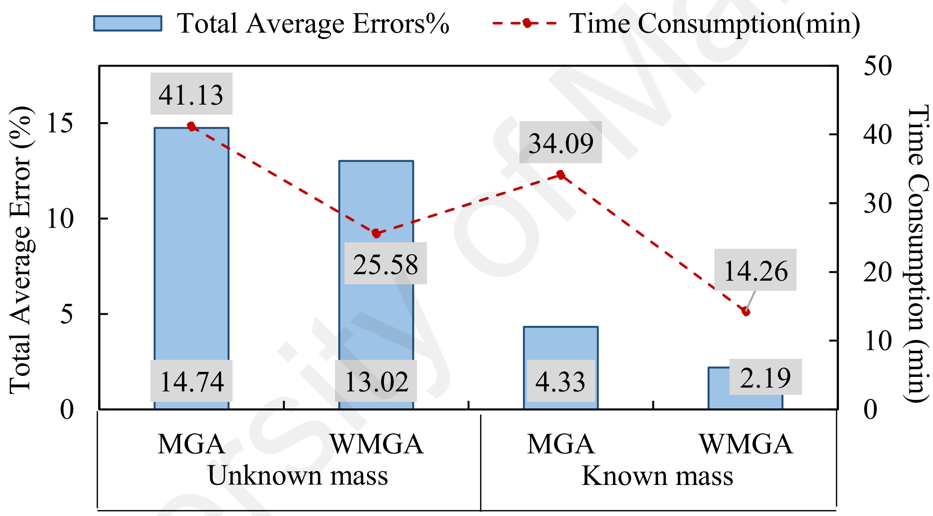

Figure 5.12: Total average error and computation time involved for stiffness identification of undamaged MDOF system shown in Figure 5.6 (known/unknown mass problems and full measurement).

The first observation from Figure 5.12 lies on the computational efficiency of the proposed WMGA method where the accurate identification results (in terms of error evaluation) were obtained for known mass and unknown mass with less CPU time consumption. It can be seen from the figure that the percentile average error reached about 4.33% for known mass identification using MGA whereas for the same case it was about only 2.2% for WMGA.

However, the convergence rate of results (in terms of accuracy evaluation) after two approaches is almost the same; the remarkable finding lies on the worst performance of MGA by higher computation time involved. In addition, Figure 5.12 demonstrates the higher error measurements for stiffness identification of unknown mass problems where ten unknown parameters are considered to be identified and making the problem much more complicated. It should be emphasized that one of the main source of errors in both cases may be the assumption of lumped mass for real mass matrix of this structure and this resulted in modelling errors.

Subsequently, the next stage is the damage detection of the considered MDOF system due to the damage scenarios imposed to the structure as outlined in Tables 5.6 and 5.7. For this purpose, the first 5 sec of measured response due to the same force applied at the last level was utilized at the same sampling rate by using the given WMGA parameters in Table 5.5. To assess the performance of strategy for incomplete measurements the damage detection is then carried out for a limited numbers of measured responses of damaged structure (presented as sensor placements). It should be pointed out that, the results of identification of undamaged structure for complete measurements are set as starting values for damage detection program. Two aspects of known mass and unknown mass problems are evaluated through the WMGA strategy and represent known or unknown mass identification whereas damage detection is only performed by fixing identified mass values as the actual mass. Moreover, success in detection of damage magnitudes is plotted in Figure 5.13 corresponding to different damage scenarios (presented in Table 5.6) and different sensor placement (measured DOFs).

University of Malaya

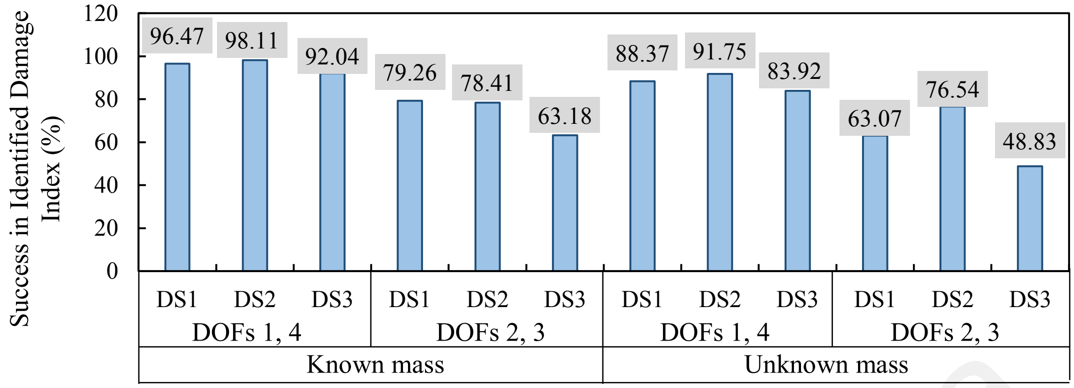

Figure 5.13: Success in identified damage index for different damage scenarios, known/unknown mass problems and incomplete measurement (DOFs represents measured DOFs).

One of the observations indicates that, the false detection is inevitable for the use of such probability based procedures as in the proposed WMGA strategy. In this regard, the program of damage detection is repeated 5 times and the success in identified damage index due to the different damage scenarios (DS) presented in Figure 5.13 refers to the best identified value of damage index. Despite the fact that a special attempt is made to establish the best WMGA parameters which are consistently producing the best results for each particular case, it can be seen that the false detection is still probable. As shown in the figure, the most promising result of about 98 % was obtained for damage scenario 2 (large damage at the first level) where the measurements of DOFs 1 and 4 were considered for a known mass problem. In contrast, only about 49% success was gained for the third damage scenario (both large and small damages induced) regarding to the measurements of only DOFs 2 and 3.

In addition, the CPU time was 25.58 min for structural identification of undamaged structure corresponding to an unknown mass problem using the presented WMGA parameters at 10 sec of excitation. It should be kept in mind that the identification of intact structure is in fact a calibration step and requires to be performed on undamaged structure once. As the recorded response due to the only 5 sec of excitation is considered for damaged structure, CPU time reached the optimum and fast record of 5.33 min for damage detection strategy (known mass problem) on an I-5 CPU, 3.2GHz personal computer. As a consequence, damage detection strategy can be conducted on site several times if it is essential to check for the damage.

Moreover, as it was mentioned earlier the planning in identification of undamaged structure and then damage detection of damaged structure plays the underlying role in order to achieve the best success in damage magnitudes and locations. It is recognized that, for damage detection of damaged structures, applying the same input force at the same location as was applied for identification of undamaged structures is really beneficial. In this argument, the same input force refers to the same frequency content and amplitude domain while the same location refers to the same DOFs. Accordingly, to evaluate the effects of different excitation scenarios, damage detection of current MDOF shear structure is carried out for two different procedures. In this regard, the identification of undamaged system is first conducted using the considered multi-sinusoidal force at level four. Later, damage detection strategy is performed for the cases that the force is applied at level four and that at level 2.

Results are Tabulated in Tables 5.6 and 5.7 corresponding to applying input force at different location of MDOF system for damage detection. As was mentioned before results are obtained after 5 repeats of test. The noticeable observation lies on more false detections of location of damages for the case that the input force was applied at different DOF (level 4 for identification and level 2 for damage detection). For instance, Table 5.7 illustrates that the success in detection of location was only 3 times of 5 repeats for the third damage scenario (DS) when the initial identification was performed for unknown mass problem. In contrast, the detection of location was successful 4 times due to the same case in Table 5.6.

Table 5.6: Results of damage detection due to the same input force applied at the same location as for undamaged MDOF system and full measurement (after 5 repeats).

Damage scenarios (DS)	Known mass			Unknown mass		
	Ave. for small	Ave. for large	Success (%)	Ave. for small	Ave. for large	Success (%)
DS1: Small at story 4	43.91	_	100 (5/5)	44.78	_	80 (4/5)
DS2: Large at story 1	_	88.37	100 (5/5)	_	85.04	80 (4/5)
DS3: Small at story 4 and large at story 1	40.02	87.49	80 (4/5)	38.11	92.37	80 (4/5)

Note: Ave = average damage index (%) identified except false detections.

Table 5.7: Results of damage detection due to the same input force applied at the different location as for undamaged MDOF system and full measurement (after 5 repeats).

Damage scenarios (DS)	Known mass			Unknown mass		
	Ave. for small	Ave. for large	Success (%)	Ave. for small	Ave. for large	Success (%)
DS1: Small at story 4	49.06	_	80 (4/5)	36.09	_	60 (3/5)
DS2: Large at story 1	_	83.77	80 (4/5)	_	93.15	80 (4/5)
DS3: Small at story 4 and large at story 1	51.91	80.47	80 (4/5)	31.68	74.32	60 (3/5)

Note: Ave = average damage index (%) identified except false detections.

University of Malaya

In addition, it can be clearly seen in Table 5.6 that the location detections were satisfactorily successful, especially for the single damage imposed to the structure. Comparing the results of location detection with that of the magnitude detection demonstrates sufficiently reliable results for the proposed strategy. With reference to the damage indices obtained from FEM modelling (about 42.7% for small damage and about 88% for large damage), the data displayed in Table 5.6 shows the promising results of the proposed damage detection strategy. Consequently, accuracy of results in Tables 5.6 and 5.7 suggests that for damage detection employing the same input force gains considerably reliable results than cases where different input forces are implemented.

5.4 Experiment 3 - A 2D truss structure under nodal excitation

Figure 5.14 shows the schematic view of test setup for Experiment 3. A 2D pin-jointed truss structure is considered for this experiment. As illustrated in the figure, this structure is constructed with nine horizontal and vertical bar elements (provided with steel hollow sections) and four diagonal bar elements (provided with double steel strips). It is to be noted that six stiffeners are utilized in order to stiffen the diagonal elements and preventing buckling phenomena in these slim members. All truss elements are connected with 8 pin connections so that they are free to rotate. The structure is fixed to a moment free support at the left and to a roller support (moment free) placed at the right side. In addition, to limit the nodal responses of the structure only in horizontal and vertical directions (namely, x and y directions), 4 larger hollow sections (shown by lighter colour frame in the figure) are used to fix the perpendicular degree of freedom (z direction). As shown in Figure 5.14, all pin joints are supported in z direction so that it is reasonable to assume 2D behavior. The intact structure comprise of 13 DOFs indicated by red arrows in the figure.

University of Malaya

The mass of each structural element is measured and compared with theoretical mass value calculated with the mass density of steel 7850 kg/m^3 for member sizes shown in Figure 5.14. It is observed that the measured mass matches the theoretical mass to approximately $\pm$ 20 grams. Eventually, in order to calculate the effective length of the structural members, 2.4 cm (1.2 cm from each side) is deducted from actual axis-to-axis length of the horizontal and vertical members due to the connector plate in the joint. The effective length of diagonal members is the actual axis-to-axis of diagonals as they are directly connected to the pin joints. It should be emphasized that, the width of hollow sections (in principle direction) is selected to about two times of the height in order to ensure 2D behavior.

5.4.1 Preliminary measurements and calculations

- ***Stiffness estimation and structural natural frequencies***

In order to estimate the stiffness of truss members and extract structural natural frequencies to employ in the identification strategy, a finite element model of the considered structure is modelled in ABAQUS. The FEM is constructed using 13 bar elements and 2 different cross sectional areas corresponding to horizontal, vertical and diagonal members. The mass density of steel 7850 kg/m^3 and modulus of elasticity of steel $E = 207$ GPa are used for the modeling. Furthermore, at this stage the diagonal members are modelled as only couple strip and the effect of internal stiffeners is not considered.

University of Malaya

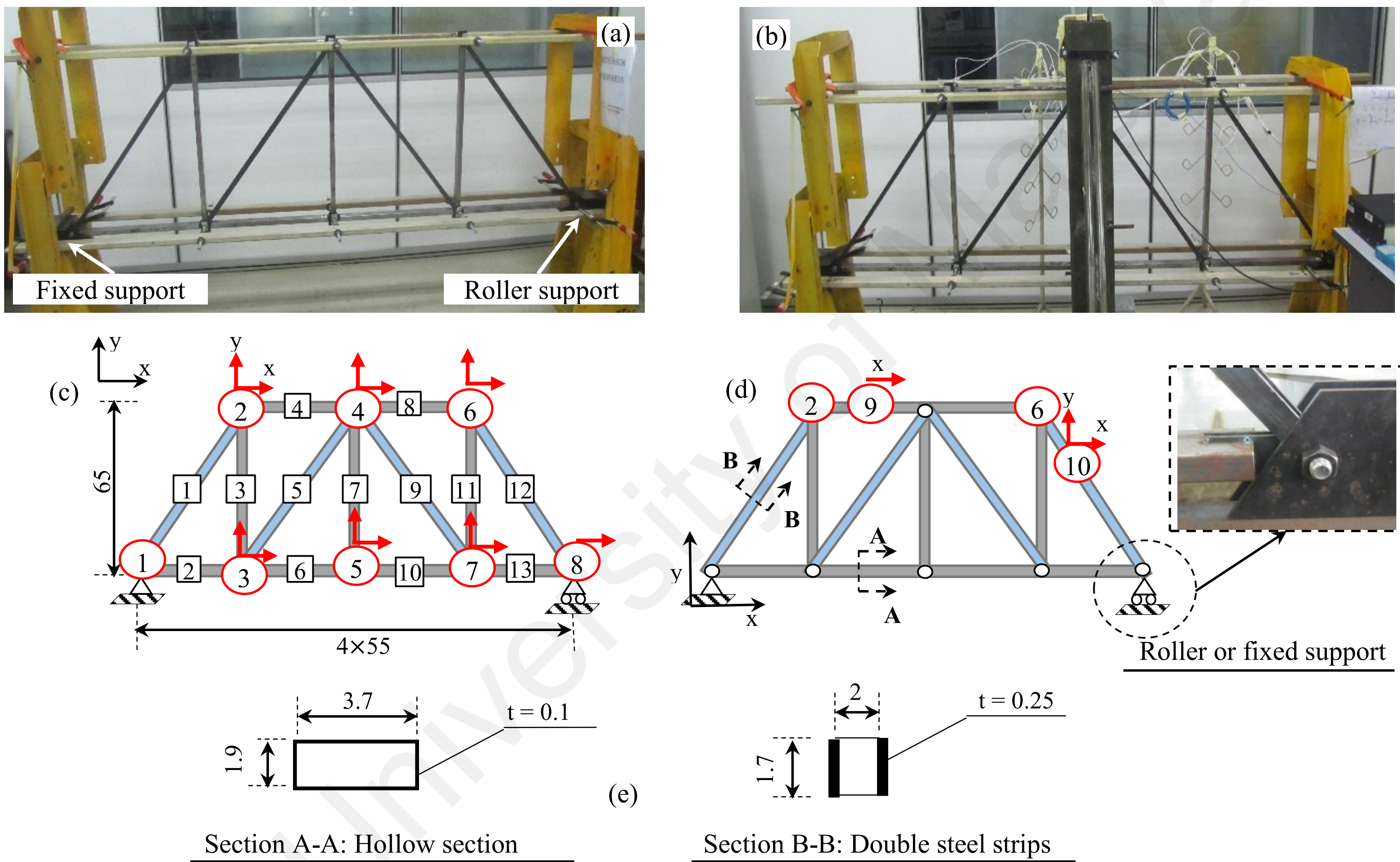

Figure 5.14: The schematic view of the test setup for Experiment 3: (a) the laboratory 2D truss, (b) sensor placement, (c) dimensions of the truss (cm), node and element numbering, (d) new nodes and elements for the progressive damage detection strategy, (e) section details (cm).

University of Malaya

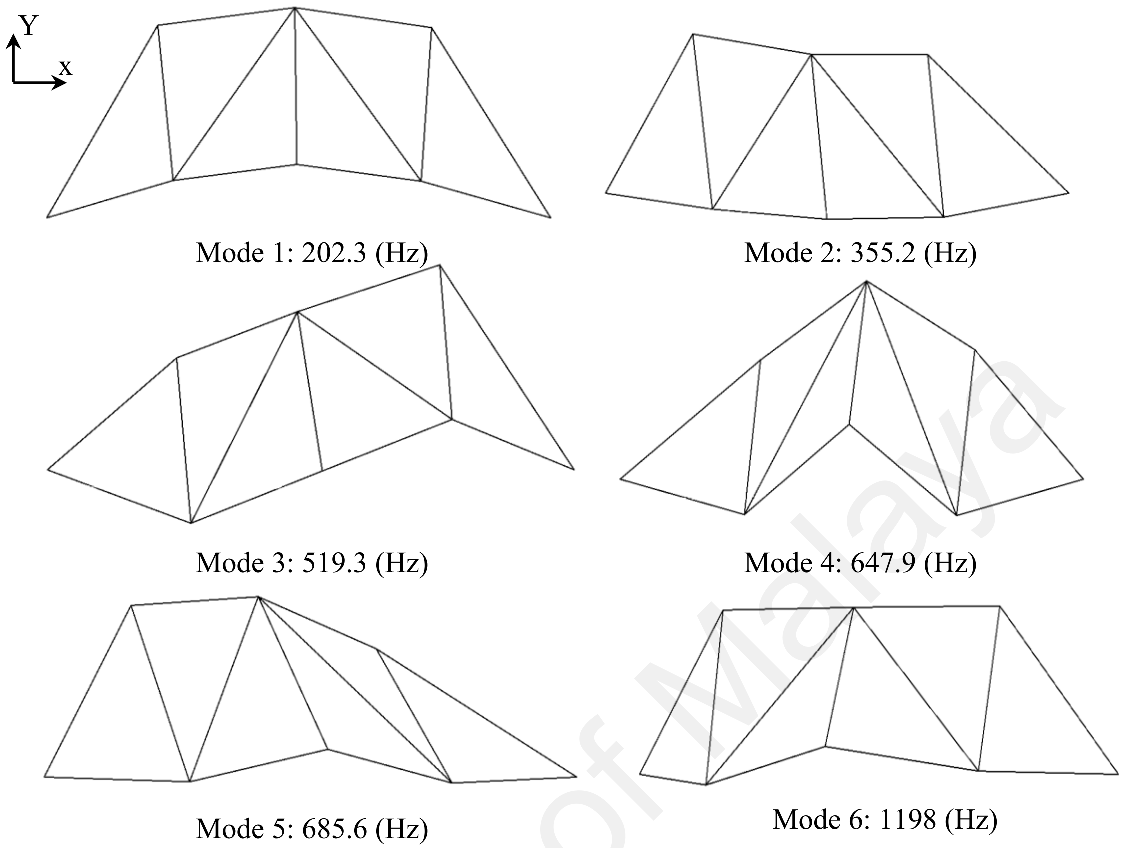

Figure 5.15: The first six mode shapes and natural frequencies obtained from FE model of 2D truss structure.

The natural frequencies obtained from the software corresponding to the first 6 and 13 modes of the structure are displayed in Figure 5.15 and Table 5.8, respectively. As it is displayed in Table 5.8 and Figure 5.15, the natural frequencies obtained from the FE model of 2D truss varies from about 202 to 2120 Hz corresponding to the first and thirteen modes of the structure. Moreover, impact tests were carried out to extract natural frequencies and compare with those from the FE model. One of the clear results was obtained when a hammer excited node 4 in y direction and the power spectrum of response at 4-y was taken using FFT algorithm. The power spectrum of response is plotted in Figure 5.16.

University of Malaya

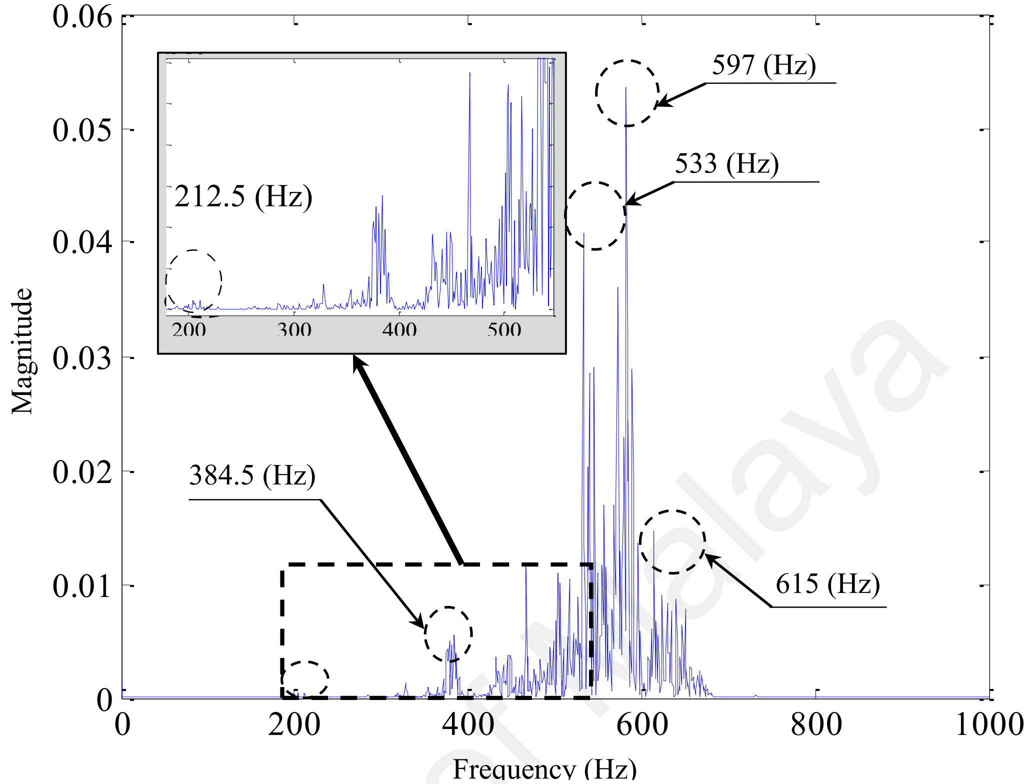

Figure 5.16: Power spectrum of response at DOF 4-y due to impact at 4-y (shown in Figure 5.14).

University of Malaya

Table 5.8: Natural frequencies (Hz) obtained from FE model of 2D truss.

	Mode												
	1	2	3	4	5	6	7	8	9	10	11	12	13
(Hz)	202	355	519	647	685	1198	1234	1397	1518	1588	1771	1823	2120

Due to the complexity of the structure, it was anticipated that the extracted natural frequencies from the impact test are not obviously distinguishable. Especially, it is observed that the natural frequencies corresponding to the higher modes cannot be detected. This is most probably due to the local vibrations of structural elements, whereby they produced significant energy in 1800-3000 Hz range and diminish at the higher structural frequencies. It is very important to keep in mind that, in planning the identification experiments these frequencies and relatively these modes are not excited. Accordingly, the peak points shown in Figure 5.16 may be considered as the first five natural frequencies. However, the extracted values of only the first two modes from the impact test are almost close to the obtained ones from the FE model. In addition, it can be deduced from Figure 5.16, the major shortcoming of the frequency domain procedures for structural identification, where the structural frequencies corresponding to the higher modes cannot be detected in practical and real structures. Consequently, the theoretical stiffness values are taken as the predicted ones and assumed as the reference values for further comparison. The theoretical stiffness of elements is calculated by $E\times$Area/Length. It should be pointed out that, for each truss element the axial rigidity ($E\times$Area) is treated as unknown stiffness.

- ***Damage scenarios***

To evaluate the performance of the proposed damage detection strategy on a complex and a larger scale structure, there are two damage magnitudes used at different locations of the considered 2D truss experiment. The large damage magnitude is shown in Figure 5.17(a), while Figure 5.17(b) shows the small one.

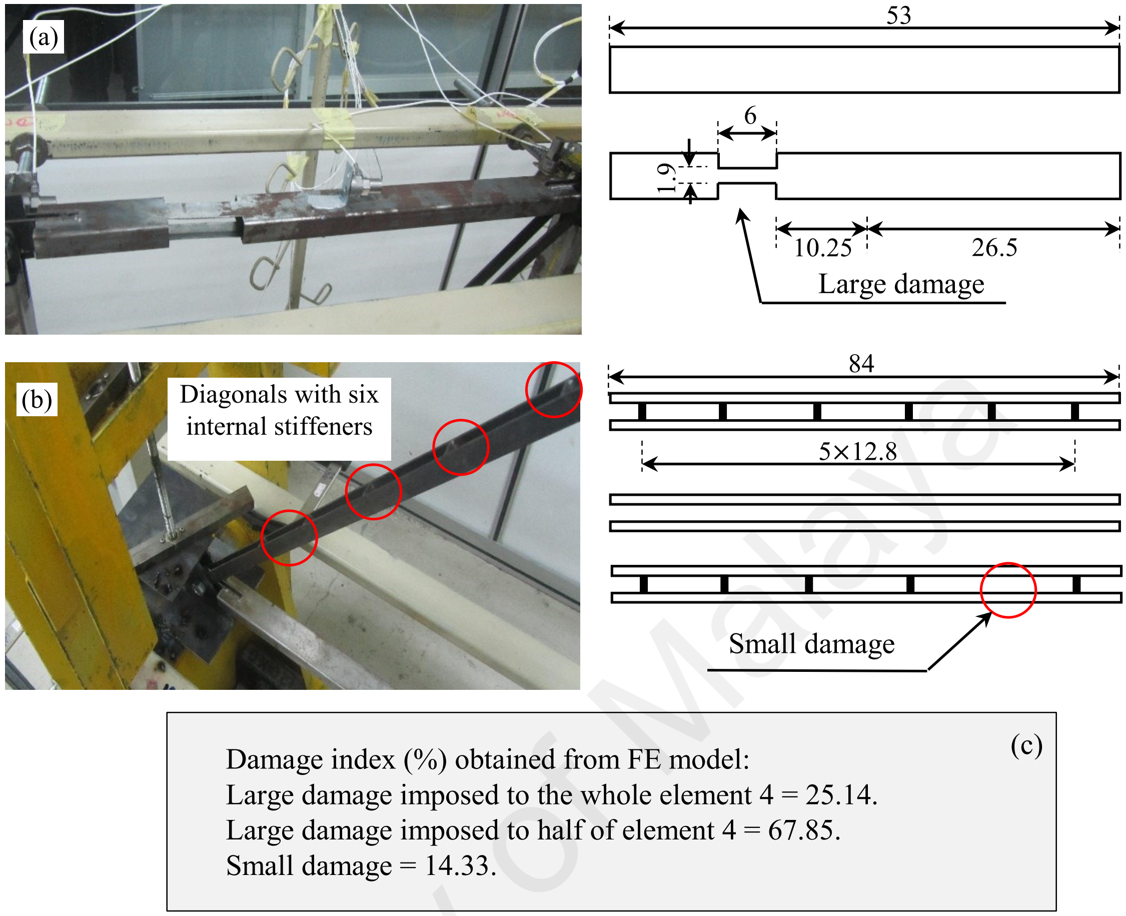

Figure 5.17: Damage scenarios imposed to the 2D truss, (a) large damage on element 4 shown in Figure 5.14, (b) small damage on element 12, (c) damage index obtained from FE model (dimensions are given in cm).

Figure 5.17(a) illustrates the location and dimensions of the large damage. Different damage scenarios (DS) are displayed in Table 5.10. It is seen that the large damage magnitude is induced only for element 4. However, the small damage magnitudes are induced for diagonal members. As shown in Figure 5.17, the small damage magnitude is formed by removing one of the six internal stiffeners from the actual diagonal members. In order to estimate the expected reduction in stiffness due to the large damage magnitude on element 4 and small damage magnitude on diagonal members the finite element analysis is conducted using ABAQUS. For this purpose, firstly the whole element 4 (intact element) is modelled

University of Malaya

in the software as one bar element (node 2 to node 4 shown in Figure 5.14) under +800 N arbitrary axial force applied to node 4 (shown in Figure 5.14). The first model is considered as the basis for further comparison. Secondly, element 4 is modelled using 3 bar elements, involving a 10.25 cm bar from node 2 with the intact cross-sectional area, followed by the next element (6 cm) as the damaged one with the reduced cross-sectional area and the last being 36.75 cm intact bar element. The same axial force is then applied in order to compute displacements. The resulting damage index is the expected reduction in stiffness of member 4 due to the large damage. The same procedure is performed to estimate the reduction in stiffness of the new bar element (node 2 to node 9) due to the large damage in this element. It is concluded that, when large damage is used for the whole element 4, the damage index is estimated as 25.14%, while it is 67.85% when only half of element four is considered. Accordingly, the FEM modeling is used to estimate the reduction in stiffness of diagonal members due to the small damage (formed by cutting one of the stiffeners as shown in the figure). Bar elements are utilized to model couple steel strips subjected to +500 N axial force. A damage index of 14.33% was calculated for estimation of reduction in stiffness of diagonals when one of the stiffeners is removed. As a consequence, the values obtained for damage index corresponding to different damage scenarios are utilized to compare with the identified values.

5.4.2 Main identification and damage detection test

Generally, there are many scenarios available in order to perform the main identification and damage detection in this experiment. As this structure contains 8 nodes with 13 perpendicular DOFs, therefore planning for identification is the underlying step. The test scenario described here refers to the one of the best scenarios, which was consistently producing desirable results. In order to proceed for this experiment and recording the response of the structure, complete measurement is considered. However, some of the results for incomplete measurements are provided in Appendix E.

- ***Excitation force***

As mentioned earlier, the proposed WMGA strategy requires integration of accelerations. Thus it is prefered to utilize a regular and smooth random force for this test rather than a very irregular and complicated one. For this purpose, a random multi-sinusoidal loading of 150-1800 cycle per second (Hz) with random magnitude of [-25,25] N is utilized for 15 sec at a sampling rate of 5.128 kS/s. Accordingly, the force described above is applied by two shakers in the vertical direction at node 4 placed at the center and horizontal direction at node 8 (free DOF of the roller support) placed at the right side of the structure. In addition, a weight of 400 N is gradually hung to the node 5-y in 2 steps during 15 sec and is assumed as externally constant load (shown in Figure 5.18). The constant load acts as a complementary force for larger influence in response measurements. In other words, using such load helps to remove the local vibrations of individual members and correspondingly higher frequencies which most of the time appeared in terms of signal-to-noise. From our preliminary experiments, the use of this load is worthwhile as the errors in measurements are significantly reduced. However, it should be taken into account that, the use of a flexible basis i.e., very soft plastic block is essential for applying the above mentioned incremental loads (constant load) in order to damp the local vibration of the link member when applying the constant force.

- ***Test setup***

The excitation forces explained in previous section were input to a 16 channel digital data analyzer (OROS36) and the signal was then passed through a power amplifier in order to produce sufficient power for the electromagnetic shaker. The forces generated by the two shakers were applied to the structure at node 4 in vertical direction as well as the horizontal DOF of node 8 while two ICP force sensors measured the applied forces. The response of

University of Malaya

2D truss structure to 15 sec of excitation was measured by 13 ICP accelerometers (KISTLER magnetic piezoelectric sensors) attached to each DOF of the 2D truss structure i.e., 2-x, 2-y, 3-x,…8-x. The signals measured by force sensor and accelerometers are recorded by a 16 channel digital data analyzer (OROS36) at a sampling rate of 5.128 kS/s. In addition, only the first 10 sec of response starting from just before the application of the force (constant load equal to zero) are selected and copied to the input file for the damage detection program.

Actually, from the preliminary tests, the initial stiffness of diagonals was assumed as the calculated axial rigidity due only to the double strips and the effect of stiffeners was not considered. The identification was consistently giving a larger stiffness value for diagonals which was constant for all intact diagonals. The results were predictable in presence of the internal stiffeners. It should be kept in mind that, theoretically it is not possible to measure or calculate the actual stiffness of diagonals due to the internal stiffeners. For this reason, the identified stiffness value of intact diagonals including the internal stiffeners is set as the basis for presenting the so-called damage index value. The procedure of damage detection is carried out through four steps. The first step involving the structural identification of undamaged structure. The second stage is identification of damaged structure and detecting damaged members. In order to detect damaged members a threshold value of 5% is considered. In this regard, the damage indices more than 5% indicated the presence of damage in the member. It should be noted here that even for undamaged members, damage index of 1 to 5% could be identified. Then the identified stiffness for undamaged members is fixed for these members and the damage detection proceeds to the next step, progressively. In addition, assumption of identified stiffness values as known parameters for progressive steps allows the damage detection strategy to be applied to a broad range of complex and real problems (such as this experiment). In fact, the aforementioned assumption resulted in desirable calibration of the structural system. Calibrating the structural model simultaneously

University of Malaya

with identification and damage detection provides a reasonably fair judgment for identified stiffness values of members when there is no information on their actual values. Accordingly, at the third step of analysis, based on the location of damage identified from the previous step i.e., damages detected in elements 4 and 12 shown in Figure 5.14, adding extra nodes and therefore extra accelerometers are required for the structure i.e., nodes 9 and 10. It is very important to keep in mind that, even though the extra data are supposed to be acquired, the current step is much simpler than previous ones as many unknown values have been already identified and the number of unknowns is considerably reduced. It is seen that the program automatically navigates user towards the location of damages. Subsequently, the last step is conducted to finalize the locations and magnitude of damages. For this purpose, new unknown stiffness values can be appended to the WMGA strategy due to the identified results requiring reconsideration. However, for most of the cases the structural identification and damage detection results obtained from the second step were sufficiently accurate and reliable. It should be noted that, for the identification and damage detection in this experiment it is assumed that the mass is known, since the mass of structure is not altered due to the damages. Eventually, WMGA parameters utilized for this experiment are presented in Table 5.9 corresponding to the different steps of damage detection strategy.

Finally, half and twice the theoretical axial rigidity (E×Area) for each truss element is used as the initial search limits of stiffness. The search limits of damping parameters corresponding to the first two modes are set as 0 to 4 for α and 0 to 0.00001 for β.

University of Malaya

Table 5.9: WMGA parameters utilized in Experiment 3.

	Undamaged Structure (known mass)	Damaged Structure (known mass)		
		Step 1	Step 2	Step 3
Pop-size	5×40	5×40	5×30	5×20
Runs	3	3	3	3
Generations	3×120	3×120	3×90	3×50
Conducted SSRM after	120	120	90	50
Crossover rate	0.6	0.6	0.6	0.6
Mutation rate	0.2	0.2	0.2	0.2
Periodic migration (z_1,z_2)	5, 0.1-0.2	5, 0.1-0.2	5, 0.1-0.2	5, 0.1-0.2
Window width	4	4	4	4
Regeneration	3	3	3	3
Reintroduction	90	90	70	40

Haar wavelet (2M=2), sampling rate 500 S/s.
Legendre wavelet (2M=4), sampling rate 200 S/s.
The second kind of Chebyshev wavelet (2M=8), sampling rate 200 S/s.

Table 5.10: Damage scenarios imposed to 2D truss shown in Figure 5.14.

	Damage scenarios (DS)			
Element No.	DS1	DS2	DS3	DS4
4	Large	_	Large	Large
12	_	Small	Small	Small
1,5,9	_	_	_	Small

5.4.3 Results and discussion

There are several possible scenarios in planning the structural identification and damage detection of this system. The identification of this structure was first evaluated numerically in order to accomplish the best strategy for identification. For this purpose, the considered 2D truss structure was simulated numerically for its actual geometry as well as boundary conditions. One of the very important steps of the structural identification is to select the characteristics of externally applied excitation(s) and its relative location to be applied in

University of Malaya

order to achieve the maximum influence in the dynamic response of the structure. However, care must be taken in considering the limitations of as-built structure for initial evaluations. In other words, for initial assessments the available locations in real structure are considered for applying input forces or sensor placements. From several available scenarios the best results were consistently obtained for the case of two multi-sinusoidal input forces applied at 4-y and 8-x shown in Figure 5.18(a). Additionally, an incremental constant load is applied at node 5-y. The detailed characteristics of input forces are discussed in previous section. The locations of input forces (shaker placement) are shown in Figure 5.18(b). Accordingly, the response of the considered system is numerically simulated using average acceleration of Newmark-β approach for three input forces at a sampling rate of 5000 for 15 sec of excitation. Complete measurements and the known mass problem are considered in order to process both the numerical and experimental evaluations.

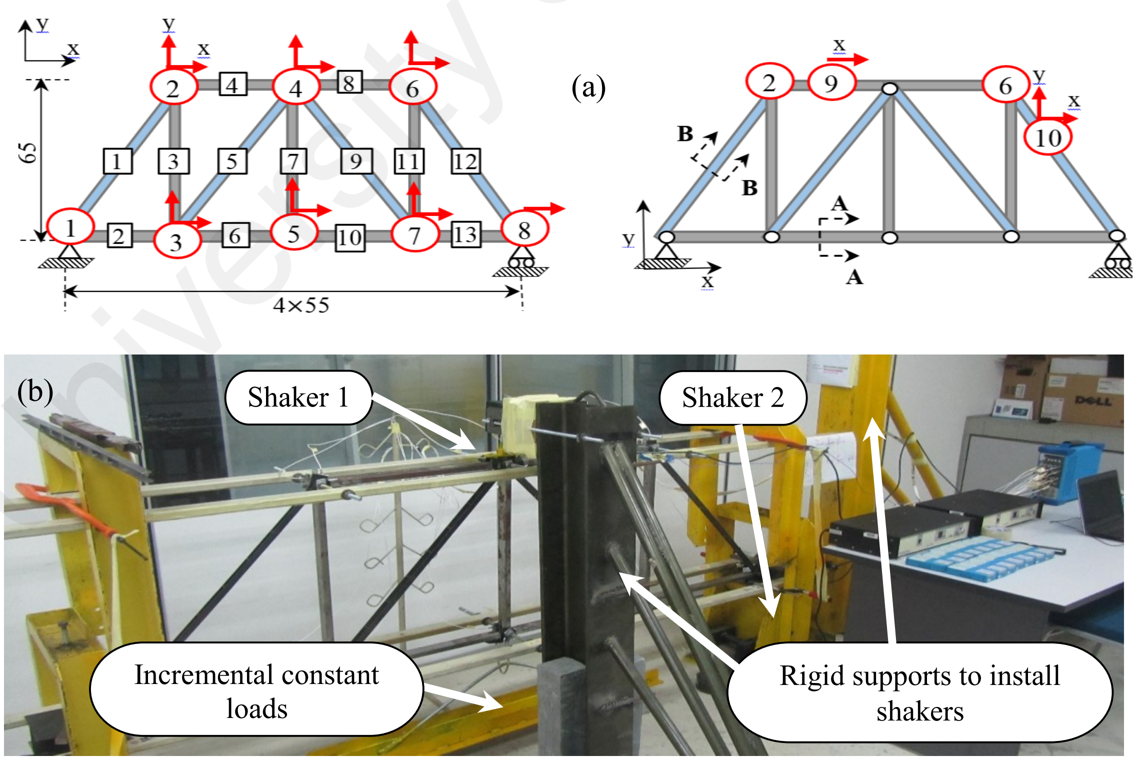

Figure 5.18: The schematic view of the test setup used for 2D truss, (a) the main layout of the test, elements and nodes numbering, (b) loading scenarios.

University of Malaya

In order to highlight the robustness of the proposed WMGA strategy compared with MGA, the fitness value histories of the first individual of each population (refers to the best individual and thus the best results) during 360 generations are comparatively depicted in Figure 5.19. For the purpose of a comprehensive comparison, the CPU time taken to proceed each SSRM step is also presented.

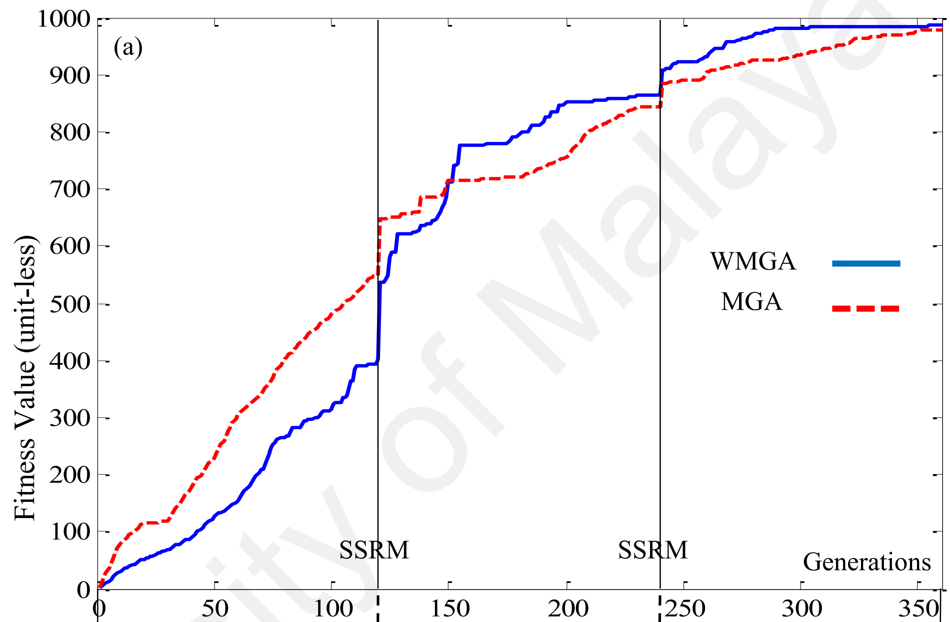

(b)	CPU Time (min)			Total:
WMGA:	7.42	8.53	16.49	**32.44**
MGA:	17.05	18.42	16.60	**52.07**

Figure 5.19: Fitness value history of the best individual for 2D truss identification (known mass), (a) the history of the best fitness value using WMGA and MGA, (b) computational time (min) recorded at each SSRM step (full measurement).

Figure 5.19 illustrates the superior performance of WMGA strategy in both exploration and exploitation phases of the genetic algorithms. It is shown that before employing the first SSRM the accuracy of results obtained from the MGA is more than that of using Haar wavelet. However, the time taken to process the exploration phase using Haar wavelet is

University of Malaya

considerably less than using MGA. It should be emphasized that, the sampling rate of 500 (sample point per second) was used for Haar wavelet (2M=2) compared with 2000 for MGA. It is observed that there is a sharp increase in accuracy of results for WMGA after the first SSRM step where 3D Legendre wavelets (2M=4) are used compared with MGA. In contrast, the accuracy of simulated response obtained by MGA is gradually increased at this stage. Subsequently, the precision of results in exploitation phase which basically involves the search on global optima is excellent using the second kind of Chebyshev wavelet (2M=8) at a sampling rate of 200. It can be concluded that, even by using larger sampling rates for WMGA strategy, the entire frequency content of externally applied forces as well as wide-band of natural frequencies of the structure are optimally captured, resulting in a very cost-effective and reliable approach. For instance, the total CPU time of 32.44 min was recorded on an I-5 CPU, 3.2GHz PC for used of WMGA whereas this value surged to about 52.07 min for MGA.

Table 5.11: Damage scenarios imposed to 2D truss shown in Figure 5.17.

	Damage scenarios (DS)			
Element No.	DS1	DS2	DS3	DS4
4	Large	_	Large	Large
12	_	Small	Small	Small
1,5,9	_	_	_	Small

Accordingly, the same scenarios of input force are applied to the current experiment for structural identification and damage detection. Structural identification of undamaged system is carried out assuming the known masses as those of measured one. In addition, the theoretical stiffness values (axial rigidities) are taken as the initial and the reference values.

University of Malaya

At this stage, only two cross-sectional areas of double strips were considered to estimate the axial rigidity of diagonals. Therefore, identification program achieved larger stiffness values for diagonals than the estimated. In referring to the presence of internal stiffeners, obtained results were logical, however, there were no way to precisely estimate the actual stiffness of diagonals. For this reason, in planning of identification and damage detection it was decided to run the program of damage detection 2 or 3 times, progressively. In fact, the strategy acts in calibrating the unknown stiffness values during the damage detection several times by fixing the identified stiffness values as known parameters for subsequent steps. It is anticipated that reliable detections will be achieved at the second or the third steps of strategy. Accordingly, damage scenarios (DS) are used step-by-step and results of detections of both damage locations and damage magnitudes are depicted in Figure 5.20 corresponding to 8 repeats of damage detection program.

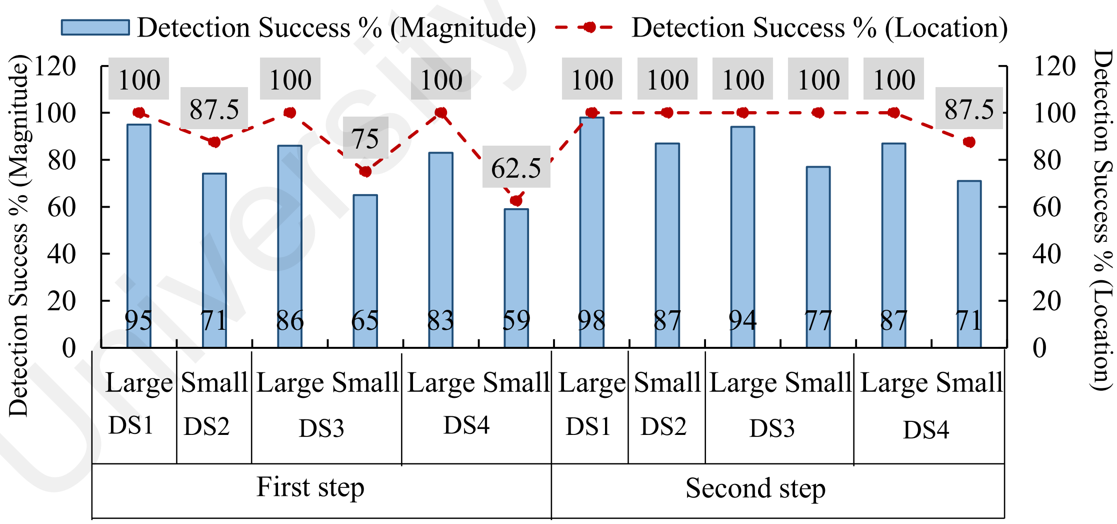

Figure 5.20: Damage detection success % (location and magnitude) after 8 repeats for different damage scenarios (DS) through two steps (full measurement).

Figure 5.20 demonstrates the excellent results for cases when a single magnitude of damage is to be detected. However, for multiple damages the identified magnitudes and

University of Malaya

locations of large damages are sufficiently accurate. It can be seen from the figure that for the cases of detection of a single small damage and a single large damage being considered, success in location and magnitude is considerably less than cases when the same magnitude of damages are to be detected. In other words, it can be concluded that the damage detection is less satisfactory for multiple damages of different damage magnitudes. From several tests conducted, it can be deduced that, the large damages often causes false detections on other levels of damage. Consequently, detection of small damages will be somehow impossible and the damage detection strategy has to be run again. In contrast, for the cases of a single or multiple damages of similar magnitude being considered, the detection results are exceptional. Finally, it should be emphasized here that one of the main source of error detections is assumption of lumped mass for this 2D structure which in fact is not accurate assumption for the real structural model. This diversely affects the response simulated compared with response measured, resulting in the quality of the fitness evaluation.

5.5 Chapter summary

This chapter presented the experimental verification of the proposed WMGA strategy for structural identification and damage detection of three real structures. For this purpose, some of the promising results obtained from the experimental works were highlighted. Additional results are given in Appendix E, accordingly. Basically, experimental evaluations are necessary in presenting a realistic assessment of numerical aspects of structural health monitoring approaches involving structural identification and damage detection strategies. However, there is a lack of investigations on use of various structural models due to the much greater difficulties for experimental evaluations rather than numerical studies. Aforementioned experimental models were considered for structural identification of output-

University of Malaya

only data as well as structural identification and damage detection of input/output measured data. Force identification was carried out on a MDOF shear building subjected to base excitation. It was shown that, even though the measurement of input forces was not available, the accuracy of identified stiffness values was sufficiently acceptable. Subsequently, the proposed strategy was performed for identification and damage detection of a MDOF shear building and a 2D pin-jointed truss structure. The approach utilizes measurement and identified values of undamaged structure in order to calibrate the structural model prior to damage detection. This arises by fixing the identified mass of intact system for detection of damaged structure. This provided considerably simpler and fast computations for damage detection where it was considered as a known mass problem. In addition, the identified values from identification of intact structure helped to initiate the search limits of damage detection strategy to be the nearest values to the real ones.

It was shown that the modelling errors are reduced due to the calibration steps and it is very important to use the same forces for both identification and damage detection strategies. The damage detection results were impressive, especially when a single damage magnitude is to be detected. For detection of damage scenarios involving large and small damages, the modelling errors causes more false detections. It was observed that for these cases the large damages are more easily detected rather than the small ones. It was demonstrated that by using adaptive wavelet functions through an improved search limit reduction strategy, the genetic algorithm phases are optimally proceeded, resulting in very cost-effective and reasonably accurate results.

University of Malaya

CHAPTER 6: CONCLUSIONS AND RECOMMENDATIONS

6.1 Introduction

The main findings of this research are presented in this chapter. These are categorized into two main aspects. The first aspect involves the proposed wavelet-based method for structural dynamics (forward analysis). Accordingly, the second aspect involves structural health monitoring (inverse analysis) using the proposed wavelet-based method.

6.2 Structural simulation (forward analysis)

Numerical approaches are the only options for structural simulation because in most cases, the applied excitations are not explicit functions. In addition, the technique for a solution of general dynamic equilibrium can become very expensive for cases where a complex loading is applied on large-scaled structures. It was presented that, orthogonal polynomials can be widely implemented as a practical analysis of time dealing problems, particularly in the form of wavelet analysis. It was emphasized that the obvious effectiveness from the property of orthogonality is that the repeated components with similar characteristics are neglected in the analytical process. Consequently, computational calculations are considerably reduced and computation time involved is therefore decreased, hence the accuracy of responses will be more desirable. One of the popular classifications of wavelet operators is originated from orthogonal polynomials. It was recognized that, several attractive mathematical characteristics of these wavelets such as efficient multi-scale decompositions, localization properties in physical and wave-number spaces and fast wavelet transforms, have obtained

University of Malaya

the practice of this efficient tool especially for the numerical solution of ordinary differential equations (ODEs).

It is inferred that, the accuracy of responses is directly related to the basis function of mother wavelet to be implemented, depending on the kind of problems. Moreover, in structural dynamics, the compatibility of a wavelet basis function is related on not only the degrees of freedom but also the similarity of basic functions to the lateral loading, emphasizing on frequency contents. Remarkably, the cost-effective computations in advanced dynamic analysis are obtained for the use of adaptive wavelet functions. This has constituted the distinction of the proposed wavelet-based approach over other numerical methods.

In addition, it was shown that wavelet functions are theoretically characterized into the two main categories. The first being the two-dimensional (2D) wavelets whereby a definite basis function of wavelet is being shifted for all scaled functions. The other category is three-dimensional (3D) wavelets involving used of an improved wavelet basis function being shifted on each new scale of the mother wavelet. Subsequently, a signal with wide-band frequency components is evaluated accurately by 3D wavelets rather than 2D ones, where scale, transition and time are expressed as dimensions, respectively. In this research, free scales of 2D Haar wavelet, 3D Chebyshev wavelets of the first (FCW) and second kind (SCW) and 3D Legendre wavelets (LW) were employed in order to construct the formulations of the proposed scheme for solving structural dynamics problems.

It was recognized that, for the purpose of structural simulations, the simple basis function of Haar wavelet can be indirectly applied on its own free-scaled functions. It is concluded that, because of the inherent simple shape function of Haar wavelet, the accuracy of responses is undesirable even employing large-scaled functions. Furthermore, in order to improve

University of Malaya

inadequacy of Haar wavelet identified as the simplest and 2D wavelet basis function, it is indispensable to utilize 3D and adaptive wavelet basis functions.

It was expressed that, adaptive wavelets are those that grow in three dimensions, referring to time, scale and frequency. For instance, Chebyshev and Legender wavelets are presented as the cases of adaptive wavelets. In addition, the continuous basis functions of wavelet stemmed from Chebyshev and Legendre polynomials have been introduced in contrast to the discreet Haar wavelets. It was discussed that, the most popular characteristics of Chebyshev wavelets is various weight functions of Chebyshev polynomials that has direct influence on the stability and accuracy of responses. However, it is perceived that, the stability of results computed by the family of Chebyshev and Legendre wavelets are independent from initial accelerations. It can be concluded that, compatibility can be satisfied through the capturing the broad frequency of complex excitations by oscillated shape functions of free-scaled Chebyshev and Legendre wavelets. However, from the computational time point of view (computational efficiency) it is inferred that, the construction of different scales of Legendre wavelet is more optimum than that of Chebyshev and will lead to a computationally efficient structural simulation strategy.

Accordingly, it is concluded that the accuracy of results obtained from the first operator of integration is perfect for the use of Chebyshev and Legendre wavelets. The accuracy of results was assessed with respect to the second operation of integration in terms of different error measurements. It can be inferred that, because of the variable weight functions of Chebyshev wavelets, and therefore less end point errors of integration, the most accurate results are achieved by using the second kind of Chebyshev wavelets and then the first kind. However, from the accuracy point of view, the Legendre wavelets are ranked at third place after SCW and FCW. Furthermore, the stability analysis demonstrates that the proposed method lies on an unconditionally stable procedure. This allows the use of longer time

University of Malaya

intervals in order to perform the proposed method. It is concluded that, even by using longer time steps the entire frequency components are integrated on adaptive collocation points and resulting in a very cost-effective procedure for structural dynamic problems, particularly structural simulation of large-scaled mechanical systems.

Besides that, it was shown that the global time interval can be divided into many local collocation points, and a set of collocations will collectively and intricately cover the signal of externally applied force. Thus, the employed operation on the compatible collocation points can be adaptive with the features of the signal, i.e., frequency content of the signal. Based on this underlying finding, the application of different wavelet basis functions at different collocations is beneficial for structural dynamic problems. Overall, it can be concluded that, the principle on the use of the proposed indirect, explicit and unconditionally stable method is time domain analysis, however, the numerical approach is not blind on the frequency components of both lateral excitations and natural characteristics of the structure.

6.3 Structural health monitoring (inverse analysis)

The proposed method has been extended in order to develop an optimum operator of derivative with respect to time, initially. It is demonstrated that, aforementioned operators (constructed using different wavelets) are capable of calculating the first and the second derivatives with reasonably desirable accuracies. The proposed operators of derivative can be utilized in variety of science and engineering disciplines such as non-linear analysis of highly non-linear problems, numerical interpolation, numerical approximation and so forth. Later, the proposed operator of derivative is utilized to optimally measure the sensitivity of acceleration data (namely, jerk measurement). It is concluded that, the proposed operation of derivative is very sensitive to small changes of accelerations even selecting considerably

University of Malaya

small sampling rates (long time intervals). Thus, for the cases where online identification is considered the fitness evaluation is significantly enhanced towards identifying the unknown parameters. It is confirmed that, because of the property of unconditional stability, from computational efficiency point of view the fitness evaluation is notably improved by using longer time intervals. The emphasis is on precisely capturing broad frequency contents with adaptive collocation points of wavelets.

The proposed wavelet-based strategy for structural simulation has been implemented in conjunction with modified genetic algorithms for solving inverse problems. As GA works on the basis of natural selection and using only forward analysis, it can readily be employed to a broad range of problems without the necessity of developing the equations or auxiliary information such as gradients required by some classical methods. It is concluded that, the fitness evaluation of GA-based individuals within populations is benefitted by using an optimum structural simulation method at longer time steps as proposed before. This allows the use of different species with various GA-based operators and resulting in considerable enhancement of GAs strategy. It was recognized that the main advantage of performing multi-species is that various GA-based operators can be employed to complement one another. The multi-species populations are improved for the accurate exploration and exploitation of search spaces. An improved search space reduction method (SSRM) is proposed using adaptive wavelet functions. It is shown that, by optimally reducing the search limits of parameters that converged quickly, the accuracy of not only those identified unknowns but also identification of other unknown parameters is significantly increased.

The analysis of convergence and computational efficiency was introduced as the necessary and sufficient criteria to evaluate evolutionary procedures. It is inferred that, the GA-based exploration and exploitation phases are optimally satisfied by conducting improved SSRM, and resulting in a greater convergence rate. In addition, lesser effect of input-output noise to the signal were recorded for the proposed wavelet-based modified GA strategy (WMGA). Finally, it can be concluded that, especially for large-scaled structures the identification of numerous unknowns is optimally achieved by the remarkably less computation time involved and resulting in very cost-effective strategy compared with existing algorithms. The application of wavelet transforms for such problems not only provides pattern recognition, but also significantly reduces input signal-to-noise ratio.

An efficient output-only identification strategy is developed by using the wavelet-based modified GAs (WMGA) in time domain. It is concluded that, the procedure lies on a predictor/corrector approach. For the use of the proposed method, mass values are supposed to be known values and the measurements of all adjacent DOFs to the force should be available. The strategy works by the simultaneous prediction/correction of the input forces as the structural parameters (stiffness and damping) are being identified. It is demonstrated that, planning in force identification is very important as the underlying presumption is that the structure is initially at rest. It is also shown that, the proposed scheme is conducted in time domain. However, all frequency contents are captured at longer time steps using adaptive collocation points. As a consequence the effect of noise is significantly reduced.

The proposed evolutionary process has been extended to the structural damage detection through a progressive calibrating algorithm. The strategy utilizes measurements and identified values of undamaged structure in order to calibrate the structural model prior to damage detection. By fixing the identified mass of the intact system for damage detection of damaged structure the identification can be readily performed. This provides considerably simple and fast computations for damage detection so that it can be considered as a known mass problem. In addition, the identified values from identification of the intact structure helps to initiate the search limits of damage detection strategy to be nearest values to the real ones.

University of Malaya

Numerical results of damage detection demonstrates the superiority of the proposed method especially for online scenarios. It is also shown that, the proposed method gave the minimum false detection for online imposed damages, where the jerk evaluation gained much better indication of damage rather than acceleration itself. Consequently, the proposed algorithm can be considered as a sufficiently reliable strategy especially for long time identification and online assessment of large-scaled structures. From the experimental works it is concluded that, the modelling errors are reduced due to the calibration steps and it is very important to use the same forces for both identification and damage detection strategies. The damage detection showed perfect results, especially when a single damage magnitude is to be detected. For detection of damage scenarios involving large and small damages, the modelling errors causes more false detections. It is observed that, for these cases the large damages are more easily detected rather than those of small ones. To overcome this issue, the program for damage detection may be run several times in site (suitable for practical cases) to guarantee the accuracy of damage detection program. Finally, it can be concluded that by using adaptive wavelet functions through an improved search limit reduction strategy, the genetic algorithm phases are optimally proceeded and resulting in very cost-effective and reasonably accurate results.

6.4 Recommendations

This research has accomplished its proposed objectives as mentioned in the contribution of each objective. Accordingly, this section is devoted to suggest some of the useful recommendations based on the findings of this research for future research works.

University of Malaya

6.4.1 Future work direction

It could be beneficial for future research works to proceed in the direction outlined below:

- Investigate the performance of more wavelet basis functions through the proposed method for structural simulation and inverse problems.
- Evaluate the proposed method for structural health monitoring of shell, plate and composite structures.
- Compare the computational efficiency of the proposed method through another heuristic optimization strategies such as particle swarm, ant colony, and water cycle optimization techniques.
- Perform an experimental work involving online monitoring in order to detect online damages using the proposed fitness function.
- Implement the proposed strategy for structural identification and damage detection of infrastructures.
- Adopt the proposed strategy of sensitivity evaluation for dynamic identification of nanomaterial.
- Improve impact detection and placement strategies in order to optimally detect the location and magnitude of impacts.

University of Malaya

APPENDICES

Appendix A: Static and dynamic condensation procedures

Generally, in many practical structural identification and damage detection problems the measurement of entire degrees-of-freedom (DOFs) of a structure is not possible i.e., torsional DOFs or due to insufficient number of accelerometers (sensors). Two procedures may be preferred in order to ensure that the measured DOFs (coordinates) and modes are the same as the calculated ones. The first one involves expanding the experimental data to the same number of DOFs as the calculated ones, while the second is reducing the computed results to the same number of DOFs as the measured ones. Accordingly, in this research the second strategy is applied for the cases of incomplete measurements. Several methods can be implemented in order to reduce the size of characteristic's matrices due to the measured DOFs. For instance, Guyan static condensation method and Guyan dynamic condensation method are two of the popular and mostly utilized ones. In this study, Guyan dynamic condensation approach is utilized as it concerns with the effect of inertia, and hence for identification problems seems much more reliable than static condensation method.

A.1 Guyan static condensation method (GSC)

Basically, this method involves the reduction of mass and stiffness matrices from the existing DOFs to the measured DOFs. Assumption of $\{u\}$, $\{\ddot{u}\}$ and $\{f\}$ as the vectors of displacements, accelerations and externally applied loads, the mass [M] and stiffness [K] matrices are divided into two partitions for measured (master, subscript *m*) and unmeasured (omitted, subscript *o*) DOFs as follows (Friswell and Mottershead, 1995):

$$\begin{bmatrix} [M_{mm}] & [M_{mo}] \\ [M_{om}] & [M_{oo}] \end{bmatrix} \begin{Bmatrix} \ddot{u}_m \\ \ddot{u}_o \end{Bmatrix} + \begin{bmatrix} [K_{mm}] & [K_{mo}] \\ [K_{om}] & [K_{oo}] \end{bmatrix} \begin{Bmatrix} u_m \\ u_o \end{Bmatrix} = \begin{Bmatrix} f_m \\ 0 \end{Bmatrix} \tag{A.1}$$

Here, the inertia terms are neglected to derive the main equation of GSC as follows:

$$[K_{om}]\{u_m\} + [K_{oo}]\{u_o\} = [T_o]\{u_m\} \tag{A.2}$$

In Equation (A.2), T_o represents the static transformation from full vectors and master DOFs. Equation (A.2) is then employed to eliminate the omitted DOFs as follows:

$$\begin{Bmatrix} u_m \\ u_o \end{Bmatrix} = \begin{bmatrix} [I] \\ -[K_{oo}]^{-1}[K_{om}] \end{bmatrix} \{u_m\} = [T_o]\{u_m\} \tag{A.3}$$

In Equation (A.3), $[I]$ is the identity matrix. Accordingly, the reduced mass $[M_R]$ and the reduced stiffness $[K_R]$ obtained from GSC method are derived as follows:

$$\begin{gathered} [M_R] = [T_o]^T[M][T_o] \\ [K_R] = [T_o]^T[K][T_o] \end{gathered} \tag{A.4}$$

A.2 Guyan dynamic condensation method (GDC)

Described GSC technique ignores the effects of inertia. In contrast, GDC method concerns with the inertia effects by considering a sets of frequencies. Basically, the method lies on an iterative method using predicted frequencies to correct the actual reduced model. Similarly, the mass and stiffness matrices are divided into two parts due to the master and omitted DOFs. The modified transformation matrices corresponding to the master and omitted eigenvectors $\emptyset$ are obtained as follows (Salvini and Vivio, 2007):

$$\begin{Bmatrix} \emptyset_m \\ \emptyset_o \end{Bmatrix} = \begin{bmatrix} [I] \\ -([K_{oo}] - \omega^2[M_{oo}])^{-1}([K_{om}] - \omega^2[M_{om}]) \end{bmatrix} \{\emptyset_m\} = [T_D]\{\emptyset_m\} \tag{A.5}$$

Subsequently, the reduced mass $[M_R]$ and the reduced stiffness $[K_R]$ obtained from GDC procedure are derived using the dynamic transformation matrix $[T_D]$ as follows:

$$
\begin{aligned}
[M_R] &= [T_D]^T[M][T_D] \\
[K_R] &= [T_D]^T[K][T_D]
\end{aligned}
\tag{A.6}
$$

Accordingly, the GDC method is utilized in this research for the cases of incomplete measurements to reduce the size of matrices due to different sensor placements.

University of Malaya

Appendix B: Optimum sensor placement

The brief description on the utilized strategy for optimum sensor placement is presented in this Appendix. Basically, a GA-based decimal two-dimensional array coding is proposed for this purpose as tabulated in Table B.1.

Table B.1: Operation process of decimal two-dimensional array strategy for the optimum sensor placement.

Variables (DOFs)		1	2	3	..	Number of available sensors
Individual gene pair before crossover and forced migration	Parent 1:	6	19	31	..	69
	Parent 2:	2	69	7	..	19

Accordingly, for the optimal sensor placement the fitted genetic individual returns to the lesser differences of response simulated for all DOFs compared with those of simulated for reduced DOFs. For this aim, the response of structure is first simulated based on externally applied forces and complete measurement. The identified values are supposed as the basis values for further comparison. With reference to Table B.1, assuming that the total number of DOFs available for measurements is 69 DOFs. Accordingly, the total number of strings is the total number of available sensors. In addition, the operators of GA strategy i.e., crossover and mutation are utilized to process optimization procedure. The new operator of forced migration avoid generating same values for parents and correspondingly for offspring individuals.

University of Malaya

Appendix C: Optimum node numbering of large-scaled structures

This Appendix presents a brief description on the utilized strategy for optimum node numbering. Similar to the previous Appendix, a GA-based decimal two-dimensional array coding is proposed for this purpose as tabulated in Table C.1.

Table C.1: Operation process of decimal two-dimensional array strategy for the optimum node numbering.

Variables (sequence of nodal numbering)		Coordinate 1	Coordinate 2	Coordinate 3	…	Total number of coordinates including supports
Individual gene pair before crossover and forced migration	Parent 1:	6	19	31	…	69
	Parent 2:	2	69	7	…	19

Accordingly, Figure C.1 illustrates a square Nodes× DOFs-dimensional stiffness matrix.

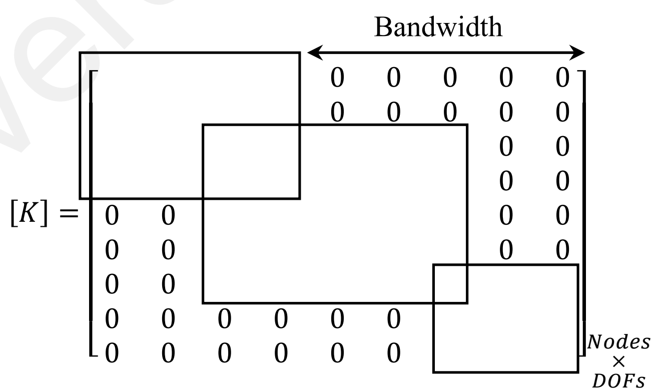

Figure C.1: The construction of stiffness matrix.

The nodal coordinates are fixed here and each node can be placed randomly at a coordinate for different genetic individuals. The corresponding stiffness matrix is then modelled for each

University of Malaya

individual based on new nodal coordinates, the characteristics and geometry of the structure. The highest fitness of each individual for optimal node numbering returns to the shortest bandwidth of stiffness matrix shown in Figure C.1 for structural elements considered. Consequently, one may obtain the fitness value =1 / (Bandwidth [K]).

University of Malaya

Appendix D: Structural simulation results

This appendix is devoted to the applicability analysis of the proposed wavelet-based method for structural simulation of finite element (FE) models. Two examples are: a four nodes quadrilateral element subjected to a wide-frequency content excitation and a 2D plane-stress system discretized into 400 constant-strain-triangular (CST) elements. It should be pointed out that for a clear comparison, vibration analysis (the effect of low frequencies) is constrained to the considered applications. For this purpose, unrealistic properties have been employed to get smooth responses. For considered problems, a sub-function has been codified in MATLAB, to simulate stiffness, mass and damping matrix of FE models.

D.1 A four nodes quadrilateral element

Figure D.1 shows an 8 degrees of freedom element known as a quadrilateral element, that is fully restrained on nodes 1 and 2 by two simple supports in the x and y directions. Furthermore, a concentrated dynamic load is applied on node 3 in x direction. The characteristics of the considered system as well as time dependent loading and nodal coordinates are shown in the figure. In addition, damping ratio is assumed proportional to 0.01 percent of stiffness. To calculate time-history responses, including horizontal displacements, minimum period for the last degree of freedom T_min=1.369 sec thus, Δt≤0.55T_min= 0.75 sec shall be utilized as time increment so as to satisfy the numerical procedures e.g., central difference method. In addition, nodal shape functions have been determined from normal shape function of quadrilateral element (1, s, r, sr). Accordingly, to construct element stiffness matrix and the effect of external load, 4 Gauss points have been implemented for its isoparametric element.

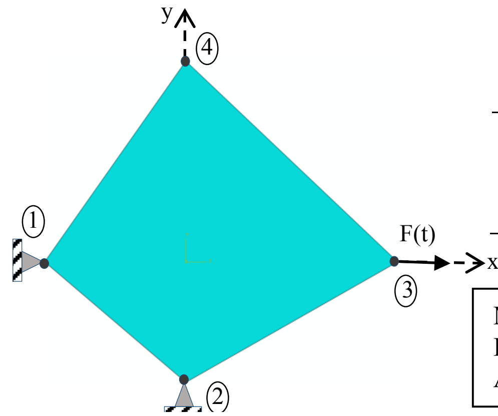

Node	Coordinates	
	x(m)	y(m)
1	-0.04	0
2	0	-0.03
3	0.06	0
4	0	0.05

Mass density (ρ)=78e8 kN/m^3
E=2.1e8 kN/m^2
Area=0.004 m^2, t=0.02 m, ν =0.3

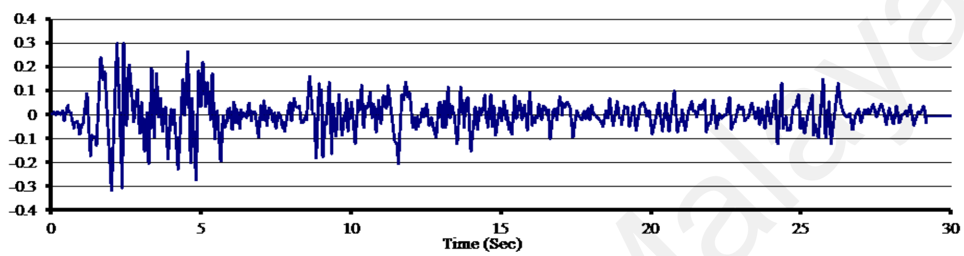

El Centro-USA (Imperial valley-1940) as the function of F(t).

Figure D.1: A four nodes quadrilateral element under a broad-frequency content loading.

This example is analyzed by six numerical methods, including linear acceleration, average acceleration, central difference, Wilson (θ=1.4), the proposed method using 16th scale of Haar and 2nd, 4th scale of the first kind of Chebyshev wavelet (FCW and designated by 2M16, 2M2 and 2M4, respectively) and piecewise modal Duhamel integration. The responses being analyzed analytically by Mode Superposition method by using all modes are implied as Duhamel or modal exact solution. In addition, for an accurate analysis of wide-frequency content loading Δt=0.02sec and Δt=0.1sec has been utilized for common numerical procedures and the proposed approach, respectively. Eventually, results including time-history displacement of 5th degree of freedom (horizontal degree of node 3) and relative measurement of errors have been plotted on figures below, respectively.

Figure D.2 shows the first 10 sec horizontal time-history displacements of node 3, which are calculated also by the first 16 scale of Haar and 2nd and 4th scale of Chebyshev wavelet (FCW). It can be seen from the figure that the result of the proposed method (using FCW) is

University of Malaya

very close to the exact result than central difference, average acceleration or Wilson-θ method.

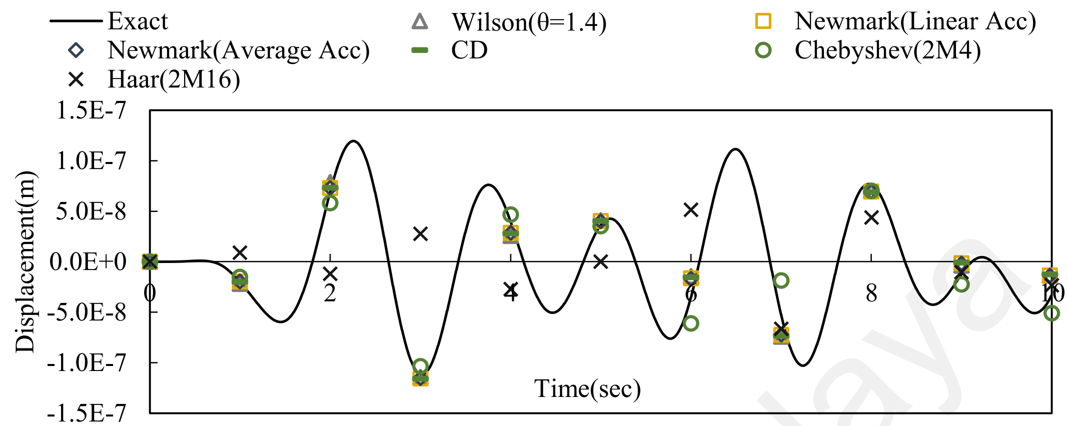

Figure D.2: The first 10 sec horizontal displacement time-history for node 3, shown in Figure D.1.

Finally, total average error and computational time have been plotted in Figure D.3. This figure illustrates comparatively, relative errors and time consumption of numerical integration schemes. However as mentioned earlier, those results calculated by Haar wavelet had the maximum error of 75.5% while, computational time recorded the minimum value of 10.83sec compared with 28.47sec for accurate scale of FCW or 32.62sec for linear acceleration from family of Newmark-β method.

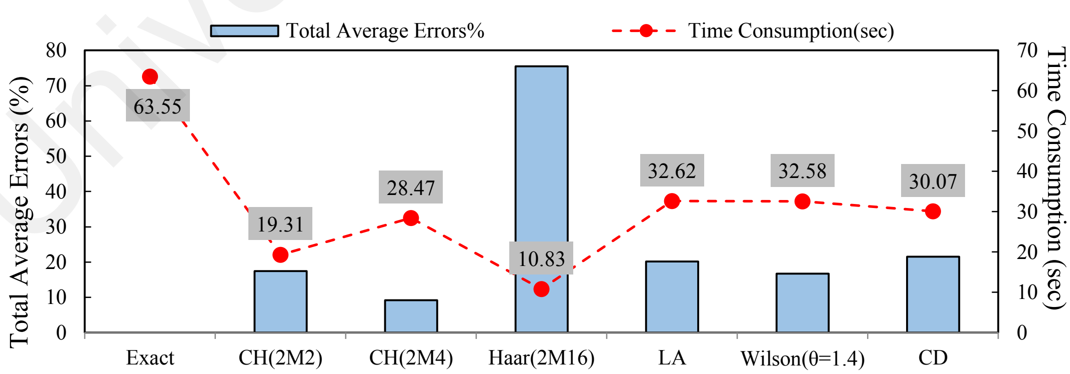

Figure D.3: Total average errors in horizontal displacement of node 3, shown in Figure D.1 and relative computational time (CH(2Mμ)= μ scale of the first kind of Chebyshev wavelet, CD= central difference, LA=linear acceleration).

University of Malaya

D.2 A plane stress system discretized into CST elements

Figure D.4 describes a 456 degrees of freedom (DOF) and plane-stress problem. The case considered contains 400 CST elements under a nodal and harmonic dynamic load. In addition, damping ratio is assumed proportional to 0.01 percentage of stiffness. The least period of this system is T_min=0.106sec thus, making Δt≤0.55T_min= 0.06sec as time increment. It is be noted that, the first 3 polynomials from Pascal triangle (1, x, y) have been selected to map the shape functions and nodal forces.

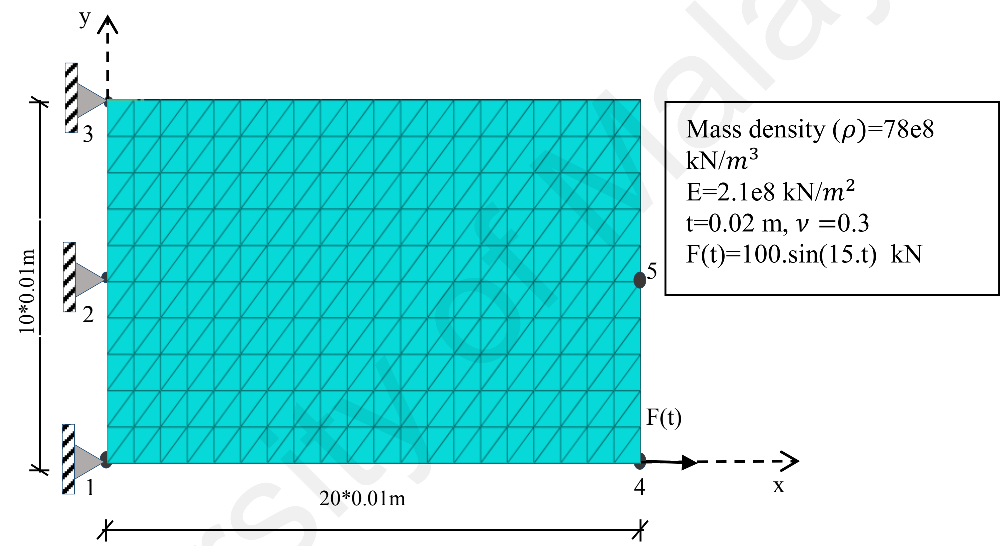

Figure D.4: A plane-stress problem discretized by 400 CST elements under harmonic loading.

The first 10 sec horizontal time-history displacements assigned to node 5, was calculated with the proposed method, including 2nd scale of Haar wavelet and 4th scale of the first kind of Chebyshev wavelet (designated by 2M4). In addition, common integration procedures, including average acceleration family of Newmark-β, Wilson-θ and central difference method were computed and plotted in Figure D.5. The time interval of Δt=0.1 sec and Δt=0.2 sec has been utilized to compute results for common numerical procedures and the proposed approach, respectively.

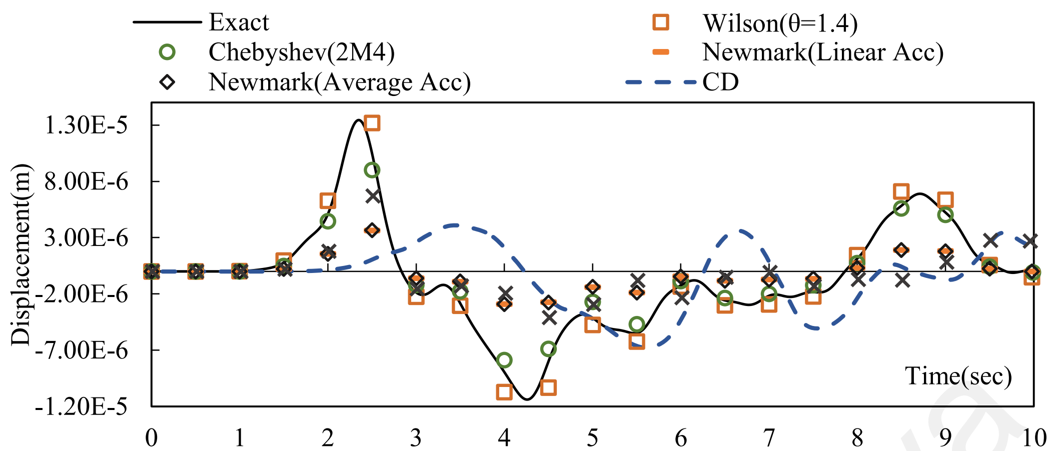

Figure D.5: Horizontal displacement of node 5, shown in Figure D.4.

As observed from Figure D.5, the results calculated using the proposed method for most of the considered time are closer to the exact results (which was calculated by mode supervision method). It is assumed that the 4th scale of FCW is an insufficiently accurate scale, even though the results are precise enough. Thus, the proposed method is notable over other numerical procedures, particularly in the real and practical cases of dynamic analysis. It is obvious from this figure that the results calculated by central difference method is unacceptable since conditional stability is not satisfied when Δt=0.1sec.

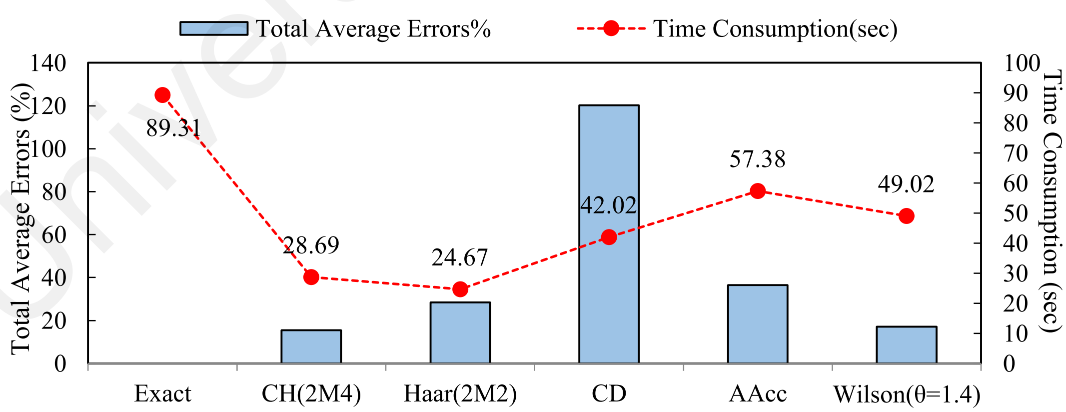

Figure D.6: Total average errors in horizontal displacement of node 5, shown in Figure D.4., and relative computational time. (CH(2Mμ)= μ scale of the first Chebyshev wavelet, CD=central difference, AAcc=average acceleration).

Finally, total average error and computational time corresponding to the horizontal time history displacement of node 5 is plotted in Figure D.6. It can be seen from the figure that responses were calculated in 28.69sec by 4^{th} scale of Chebyshev wavelet, whereas, the time taken was 49.02sec for Wilson-θ method; although, the accuracy of results are almost the same i.e., 16% error. Figure D.6 also highlights the efficiency of the proposed method, particularly when the first kind of Chebyshev wavelet (known as 3D wavelet function) was utilized.

University of Malaya

Appendix E: Structural identification and damage detection results

This appendix presents some of the additional results (following by results presented in Chapters 4 and 5 of this study) on structural identification and damage detection of different structural systems. For this purpose, a numerical investigation is first carried out for structural health monitoring of a simple SDOF system, numerically. Second, the proposed wavelet-based scheme for optimum measurement of structural responses is validated for measuring the dynamic responses of a SDOF experiment as well as a simulated 2D truss structure. Later, some of the complementary results have been presented regarding to the incomplete measurement of the third experiment presented in Chapter 5 (2D truss structure).

E.1 A simulated SDOF system

Figure E.1 shows an idol SDOF system with the only DOF on X direction (a shear SDOF). The system's characteristics are shown in the figure. This structure is subjected to two different impact loads at the first 0-2sec of vibration analysis. The first, impact of 2 (ton) strikes the only DOF at t=0.01sec (is shown in Figure E.1(a)) and the structure is freely vibrated until the second impact of 4 (ton) at t=1sec (Figure E.1(b)). In addition, β is defined as the percentage of reduction (the coefficient of damage) executed on the stiffness of the column 2i at t=1sec. Accordingly, the time-history of acceleration known as the measured accelerometer data (designated by Original-Acceleration) and displacement (designated by Original-Displacement) which were calculated using Newmark method are illustrated in Figure E.2.

University of Malaya

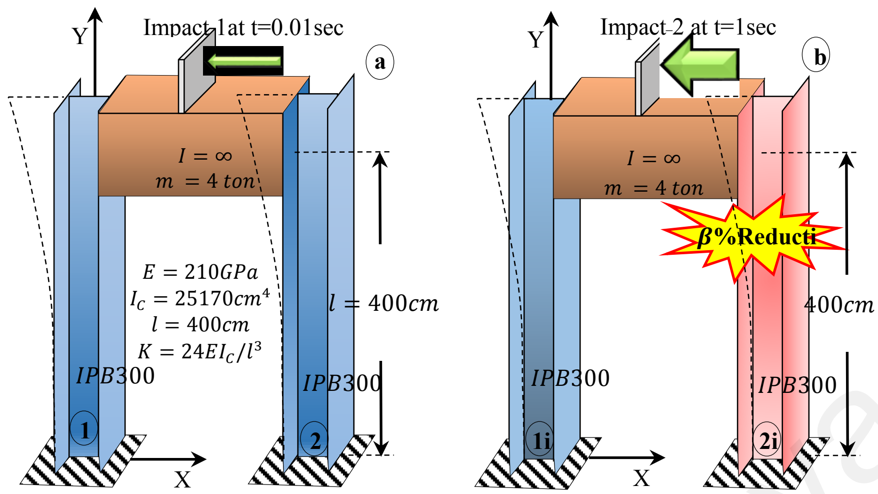

Figure E.1: A SDOF system under impact loads at two stages of (a) 2 (ton) on undamaged system at t=0.01sec (b) 4 (ton) on damaged system at t=1sec.

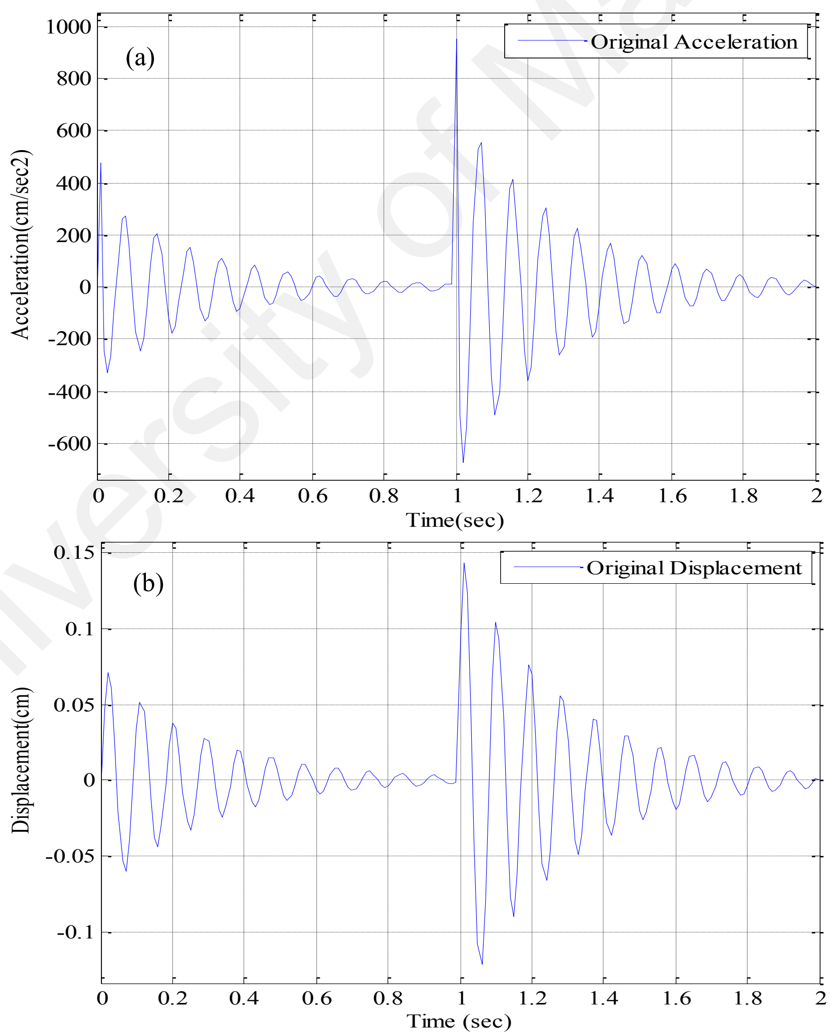

Figure E.2: The first two seconds time-history of (a) acceleration (b) displacement of the SDOF system shown in Figure E.1.

University of Malaya

In addition, the approximation of the measured acceleration is performed using different scales of wavelet. To highlight the effect of various scales of the first kind of Chebyshev wavelet (FCW), coefficients of this wavelet (designated by ChebyW-Coefficients), the approximation of accelerations (designated by App-Acc-Cheby) and original accelerometer data (designated by Orig-Acc) are depicted and compared in Figure E.3, emphasizing on the 4th and 32nd scales of FCW (designated by 2M4 and 2M32) for t=0.98-1.1sec.

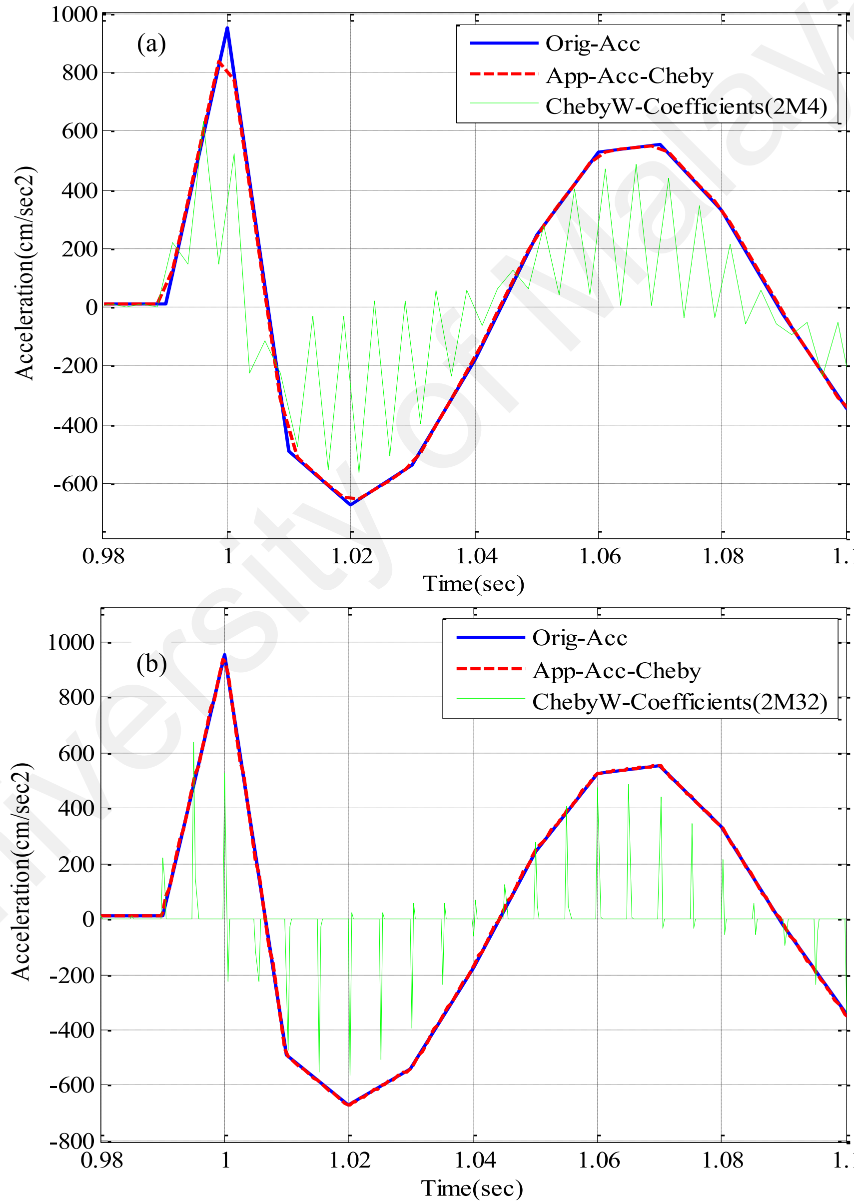

Figure E.3: Coefficients of Chebyshev wavelet (FCW) for, (a) the 4th scale (b) the 32nd scale (ChebyW=Chebyshev wavelet, Acc=acceleration, App=approximation, Orig=Original).

University of Malaya

It is obviously shown in Figure E.3 that, for the purpose of an accurate decomposition in achieving a sufficiently precise measurement, larger scales of corresponding wavelet (e.g., FCW, SCW or LW) shall be utilized, particularly, for the approximation of wide-frequency content accelerometer data. Moreover, measured displacements of the SDOF system are plotted in Figure E.4 (t=0.98-1.3sec) using d_t=0.05sec for the 2nd and 8th scales of FCW (designated by Disp-Cheby 2M2 and 2M8) and compared with original displacements (d_t=0.01sec) known as recorded data (due to the reduction of β=50%).

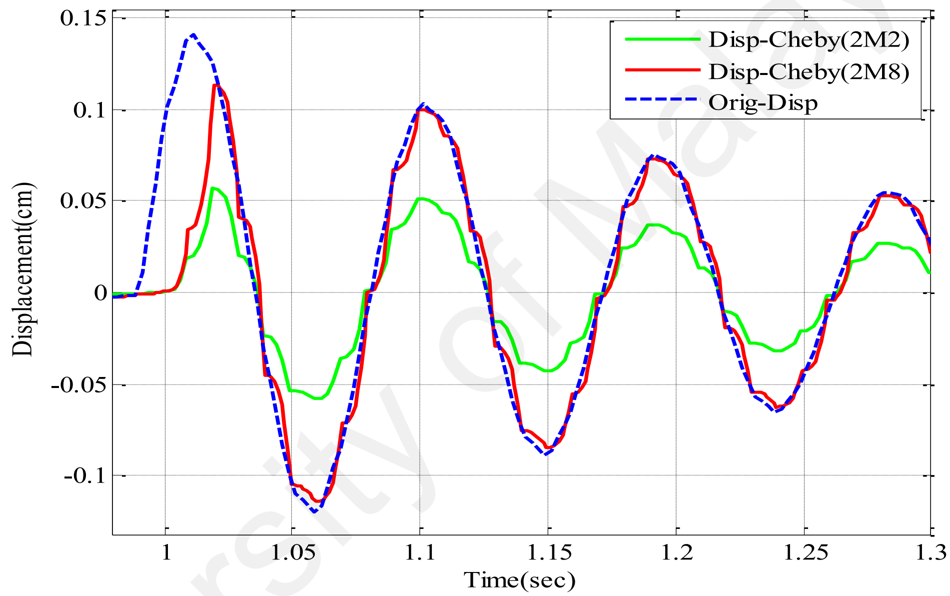

Figure E.4: The measured time-history of displacement of the SDOF system shown in Figure E.1 at t=0.98-1.3sec (Disp-Cheby=measured displacements using Chebyshev wavelet (FCW), Orig-Disp=original recorded displacement).

As it was anticipated, the measured displacements using the 8th scale of Chebyshev wavelet (FCW) is closer to the originally recorded displacements rather than the 2nd scale. Even though, in order to compare the efficiency of diverse scales of FCW in detail, the percentile average and relative error and computation time involved of the measured displacements at t=0-2sec, corresponding to different scales are shown in Figure E.5.

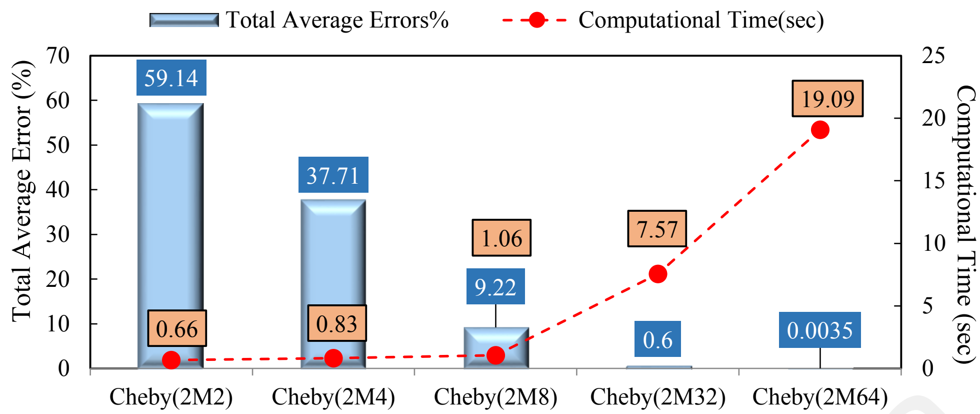

Figure E.5: Total average error and computational time for the measurement of displacements using different scales of the first kind of Chebyshev wavelet (Cheby=Chebyshev wavelet).

Figure E.5 demonstrates that, the complex and accurate scales of FCW (2M32 or 2M64) achieved the considerably minimum measurement of errors, e.g., 0.0035% for the 64th scale, however, the computation time involved surged the maximum values, e.g., 19.09sec. As a noticeable feedback, the practice of such scales yields non-optimum computation, thus, is incapable of online measurement. It should be noted that, because of the simple application of SDOF and uncomplicated lateral loading, those quantities were slightly changed between the first two scales. In other words, for the complex structures subjected to the wide-frequency component excitation, larger scales shall be implemented.

Practically, one of the main contributions of the structural measurement is to track the time-varying characteristics of mechanical systems, i.e., stiffness or damping of structures. For this purpose, the time-history of stiffness for damaged and undamaged phases of considered SDOF are plotted in Figures E.6 and E.7, respectively. For the computation of the time-history stiffness (K), a controller coefficient was given to track displacement data bigger than a known value (K is satisfied for u > u Controller), otherwise, the quantity of flexibility (f=1/K) may be considered.

University of Malaya

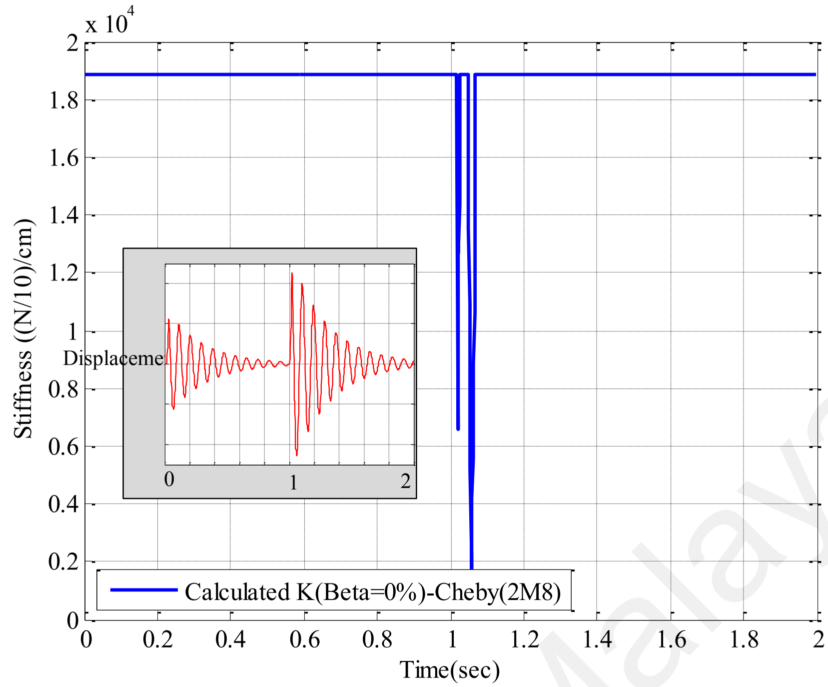

Figure E.6: Stiffness (K) evaluation of the SDOF system shown in Figure E.1 (β=0%), using the measured data (shown displacements) by the 8th scale of Chebyshev wavelet (FCW Cheby2M8).

Accordingly, in order to impose the damage scenario on the column 2i shown in Figure E.1, β=75% is applied to reduce relevant stiffness at t=1sec. It should be noted that d_t=0.05sec has been utilized as the time increment of the proposed measurement approach which is appropriate for the online measurement in contrast to d_t=0.01sec for the sampling rate of data collection. It can be seen from Figure E.7 that, the reduced stiffness and its location on time axis is accurately monitored even by employing a large time increment.

Furthermore, the time-history of the maximum stress which is placed at the base of the SDOF system is illustrated in Figure E.8, in order to obtain the border of elastic behavior, and resulting in an optimum integrity and safety analysis of the considered structure.

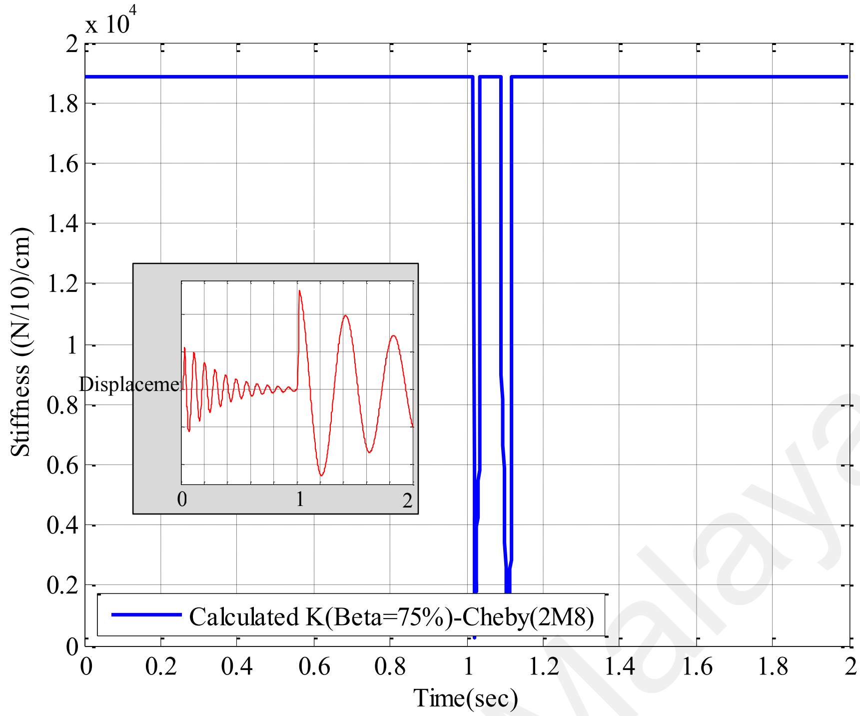

Figure E.7: Stiffness (K) evaluation of the SDOF system shown in Figure E.1 (β=75%), using the measured data (shown displacements) by the 8th scale of Chebyshev wavelet (FCW Cheby2M8).

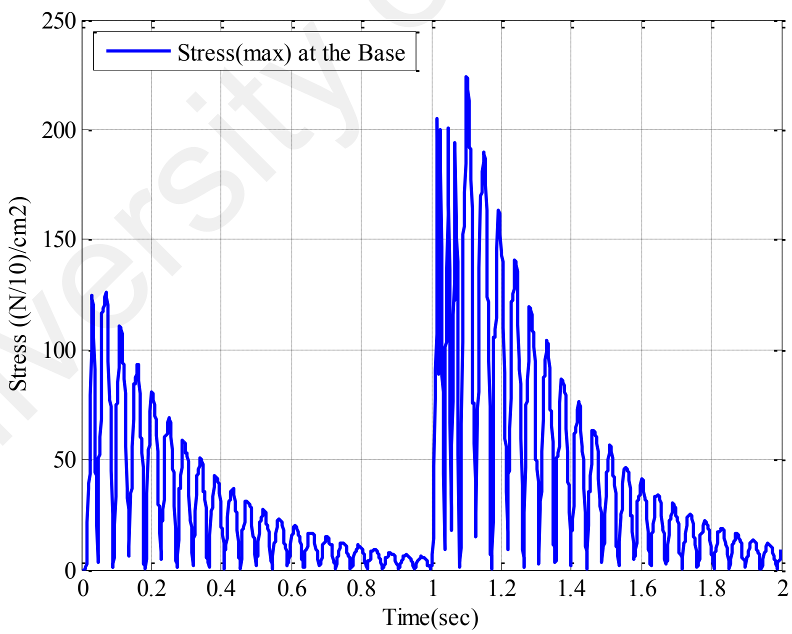

Figure E.8: Time history of maximum stress at the base of the SDOF system shown in Figure E.1 using the measured data for (β=75%) by the 8th scale of Chebyshev wavelet (FCW Cheby2M8).

University of Malaya

Consequently, this figure shows the effectiveness of the low scales of Chebyshev wavelet (2M8) together with using a long time interval of numerical approximation, which is satisfactory optimum for the online measurement of structural responses.

E.2 Optimum measurement of structural responses of a SDOF model

A simple SDOF test setup is evaluated under a regular hammer test, experimentally. Accordingly, g= 9.81 m/sec2 is presumed as the ground acceleration. As shown in Figure E.9, the considered system provided by two narrow aluminum columns and a rigid Plexiglas, which are only vibrating in the x direction. In order to invoke only one DOF, the thickness of the columns was chosen to be much narrower than its width (≅1/37). The geometry and details of the experiment setup are shown in the figure. As illustrated in the figure, a non-contact laser device was installed on the base in order to identify the accurate time-history of displacements (at sampling rate 102.4).

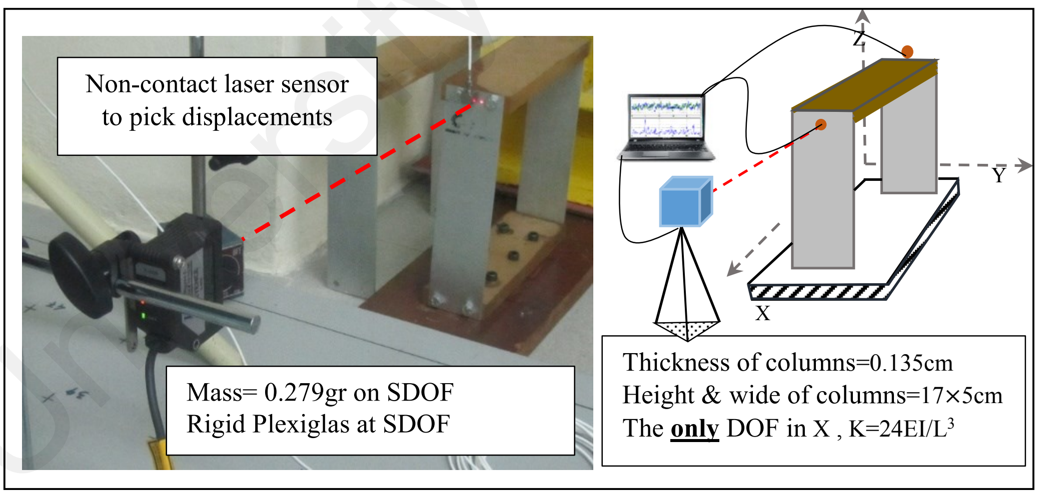

Figure E.9: The ideal SDOF experiment setup and the schematic view, measuring displacements by laser sensor.

Moreover, two piezoelectric sensors (accelerometers) were attached on the DOF of the system. To evaluate the proposed method of measurement, a hammer strikes the structure from 1sec after its initial condition. Accordingly, the time-history of the velocity corresponding to the SDOF has been computed for the 4th scale of Haar and FCW (designated by Cal-Vel-Cheby and Haar) for the time interval of d_t=0.05 sec as depicted in Figure E.10. The results were compared against those picked by the non-contact laser sensor for d_t=0.009766 sec (designated by Orig-Vel).

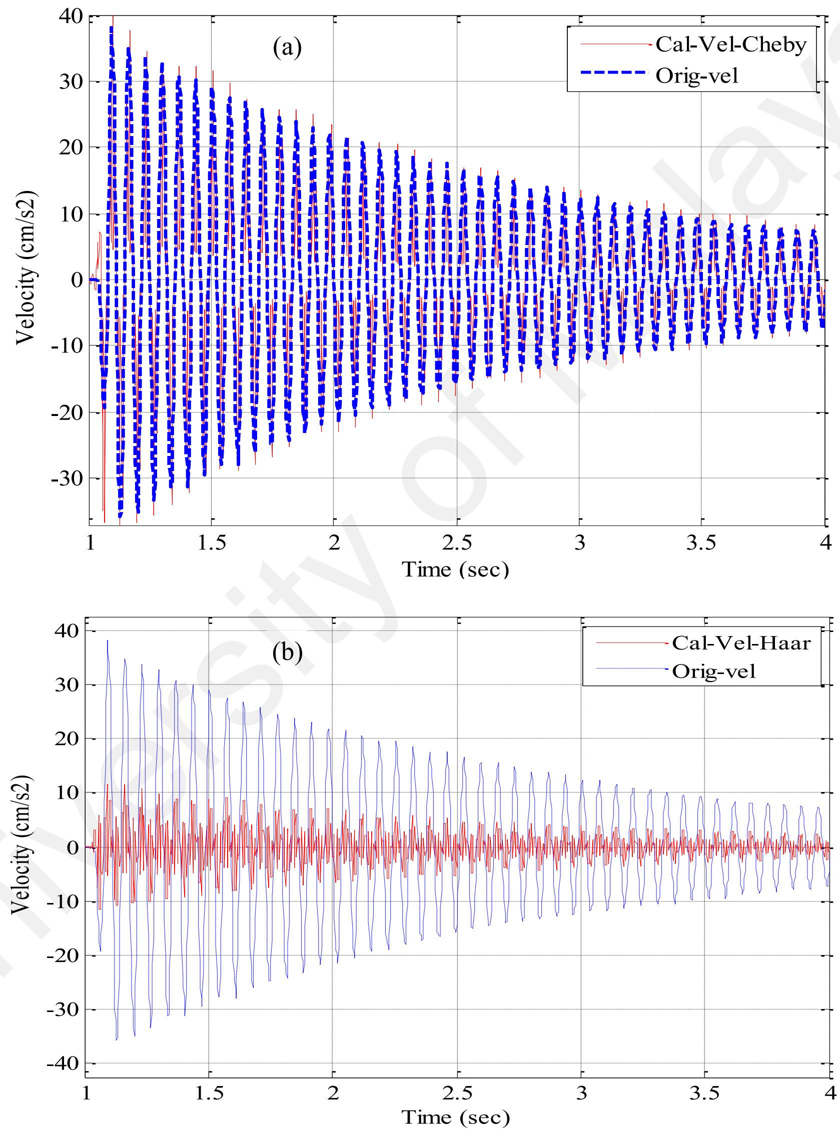

Figure E.10: Time history of velocity for SDOF system shown in Figure E.9., (a) calculated velocity using the 4th scale of Chebyshev wavelet of the first kind (Cal-Vel-Cheby), (b) calculated velocity using the 4th scale of Haar wavelet (Cal-Vel-Haar).

University of Malaya

To clarify the discrepancy between the computed results through the proposed method, approximation of the original acceleration (accelerometer data) is plotted in Figure E.11 corresponding to the 4th scale of Haar and Chebyshev wavelet (FCW) by illustrating the wavelet coefficients for 1 to 1.2 sec.

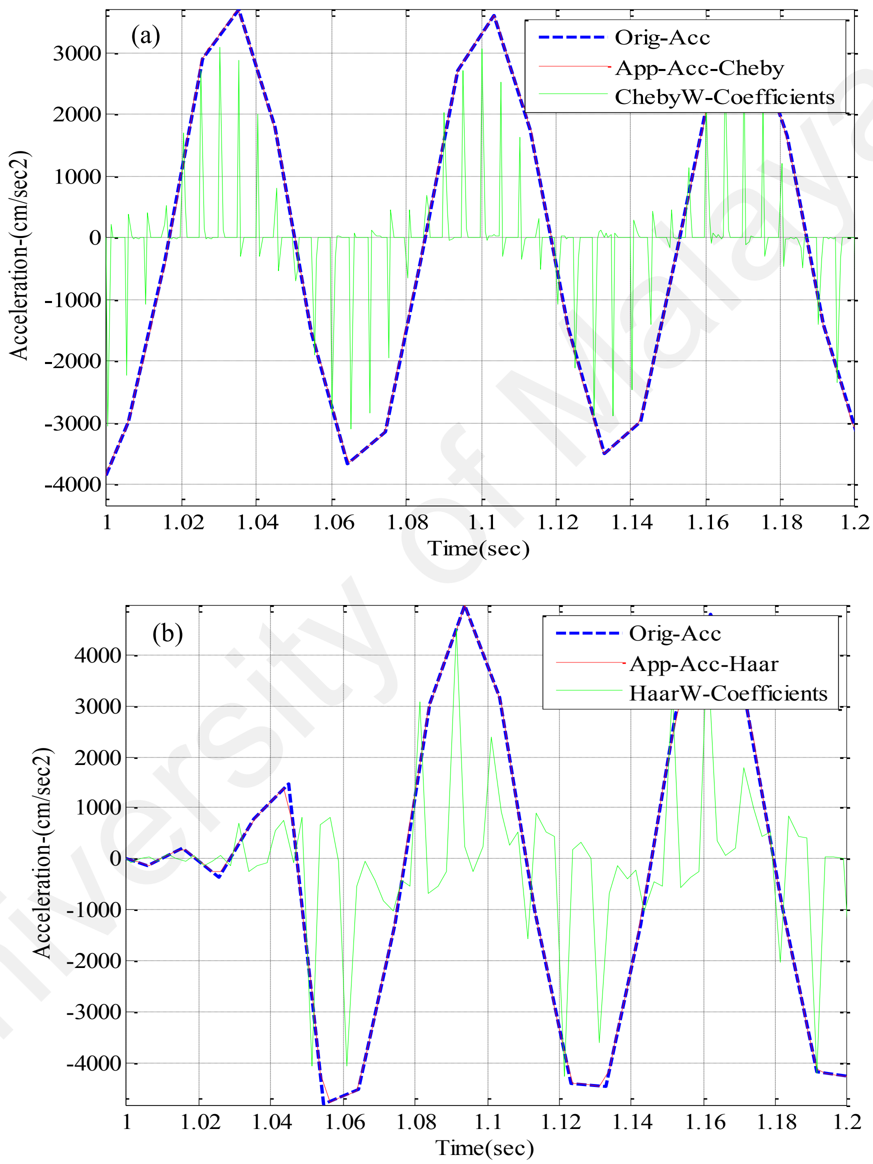

Figure E.11: Coefficients of wavelet for the 4th scale of (a) ChebyW-Coefficients=Chebyshev wavelet (FCW), (b) HaarW-Coefficients=Haar wavelet (App-Acc= approximation of original acceleration).

Figures E.10 and E.11 clearly demonstrate the source of significant errors of Haar wavelet (2M=4) for d_t=0.05 sec, while it is shown that details of the acceleration are accurately captured by the coefficients of FCW for the same conditions. Therefore, a sufficiently precise approximation is satisfied at the first step of the proposed scheme. Furthermore, to evaluate the practice of various scale of Haar wavelet in detail, computed responses for the same d_t=0.05 sec and 8^{th}, 32^{nd} and 64^{th} scales of simple Haar wavelet (designated by HA(2M)) were compared with the 4^{th} scale of complex Chebyshev wavelet (FCW). The results depicted in Figure E.12 are from the computational time involved and percentile total average error (PTAE) point of view.

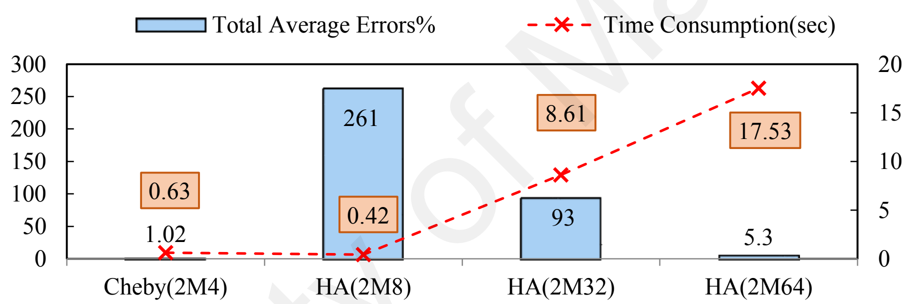

Figure E.12: Computational time and PTAE for various scale of Haar (HA) and the 4th scale of the first kind of Chebyshev wavelet (Cheby).

It is apparent from Figure E.12 that for the accurate scales of 2D and simple Haar wavelet (2M64), the cost of analysis is dramatically increased. However, the optimum results can be computed even using a low scale of 3D and complex Chebyshev wavelet (FCW). Consequently, it is shown that the practice of Haar wavelet is not applicable for the online measurement of dynamic responses, however, for an initial evaluation it may be considered where the fastest computation is satisfied by implementation of this basis function. Eventually, the time-history of displacement of the only DOF is optimally calculated through the proposed measurement scheme, particularly, using a long time interval of d_t=0.05 sec by the 4^{th} scale of FCW (designated by Cal-Disp-Cheby) and is compared with those measured by the laser sensor (Orig-Disp) at the sampling rate of 102.4 S/s (shown in Figure E.13).

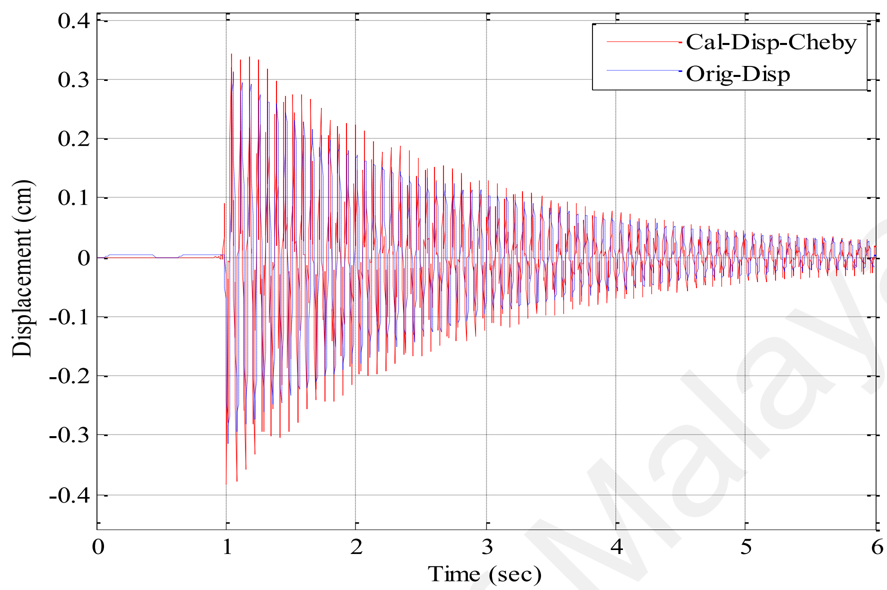

Figure E.13: The first 6 sec time-history displacement of SDOF system shown in Figure E.9 (Cal-Disp-Cheby = Calculated displacement using Chebyshev wavelet FCW, Orig-Disp=Original displacement).

The capability of the proposed algorithm for measurement is clearly illustrated in Figure E.13, using low scales of Chebyshev wavelet. It should be pointed out again that details of the broad-frequency component acceleration are completely captured by the diverse scale of this comprehensive wavelet function in contrast to the simple Haar wavelet. Finally, the third derivative of displacement with respect to time namely, Jerk ($\ddot{u}$(t)) is considered using the 8th scale of FCW (designated by computed jerk), as depicted in Figure E.14 and compared with a normal incremental calculation (d(Acc)/dt) for the long interval of d_t=0.5 sec. Moreover, it was shown before that the measurement of this value is very helpful to make an engineering judgment on the behavior of a dynamic system.

Figure E.14 shows that the proposed method optimally and exactly detects the time of the strike at the first second in contrast with the normal incremental calculation. Overall, it is demonstrated that the quantity of jerk as one of the reliable criteria of dynamic behavior is optimally measured through the proposed method which is capable of optimal and online measurement of dynamic responses.

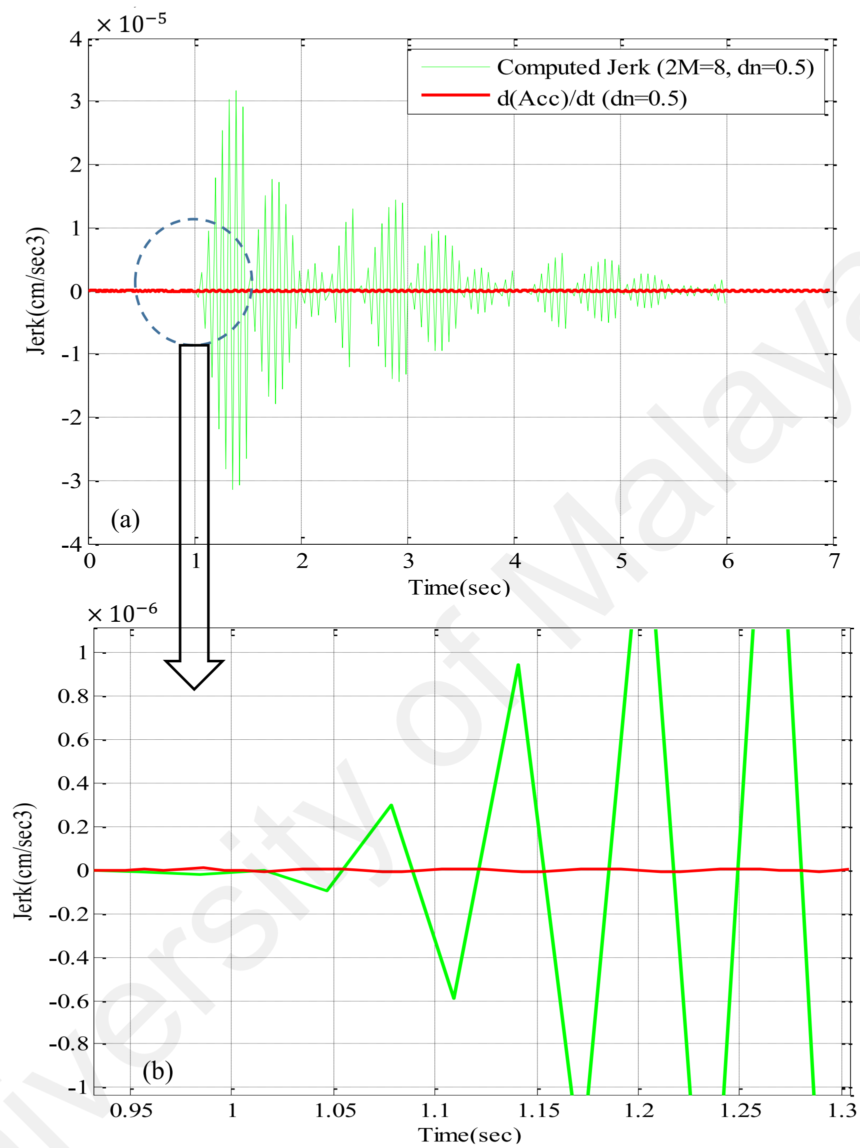

Figure E.14: The first 7 sec analysis of the third derivative of displacement (jerk). (a) 0-7 sec computed jerk using the 8th scale of Chenyshev wavelet (FCW) vs. normal calculation of the derivative with respect to time (d(Acc)/dt). (b) Zooming plane on 0.9-1.3 sec.

E.3 A 2D truss constructed with bar elements coupled with damage

Figure E.15 describes a pin-jointed and 2D truss composed of nine DOFs and 10 members. This structure is excited for 6sec by a harmonic loading (F(t)=20.Sin(15t)_N) which is applied on node 3, shown in Figure E.15. Additionally, the characteristics of all members are constant and addressed in the figure, as well as mass per length, modulus of elasticity, the cross-sectional area and the geometric information. To evaluate a damaged scenario (in overall linear behavior), it is assumed that at the 3rd second of excitation, because of a local exclusive motivation such as a strong explosion, only two internal members of 1 and 2 (shown in Figure E.15(a)) are completely collapsed. The current configuration is shown in Figure E.15(b), corresponding to t=3-6sec of loading. Equivalently, accelerometer data associated on each DOF is recorded using Newmark scheme at the sampling rate of 100 or d_t=0.01sec (a schematic view is illustrated in the figure on node 2).

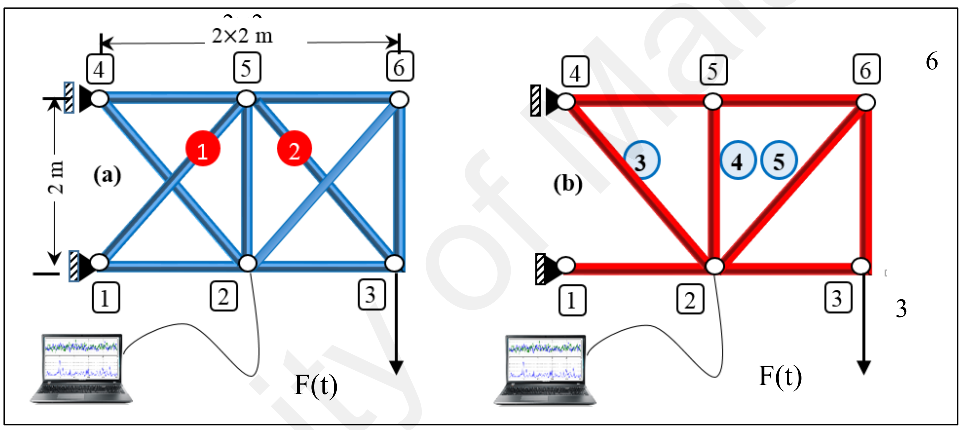

E=70 GPa, $\bar{m}$ = 50 kg/m, A= 1e-4 m^2, $F(t)$=20. $Sin(15t)$ N

Numbering of DOFs :

Node number	1	2	3	4	5	6
Horizontal DOF	-	1	3	-	6	8
Vertical DOF	-	2	4	5	7	9

Figure E.15: A 2D and pin-jointed truss under a harmonic loading at 6 sec (a) reference configuration; intact system, (b) updated configuration; elements 1 and 2 are removed at t=3 sec.

In addition, the first 6sec time-history of acceleration known as measured accelerometer data corresponding to the vertical and horizontal DOF of node 3 (shown in Figure E.15) is plotted in Figure E.16. Therefore, for the further operations on node 3, such as the

University of Malaya

measurement of either integration or derivatives of responses in time domain, aforementioned data is used.

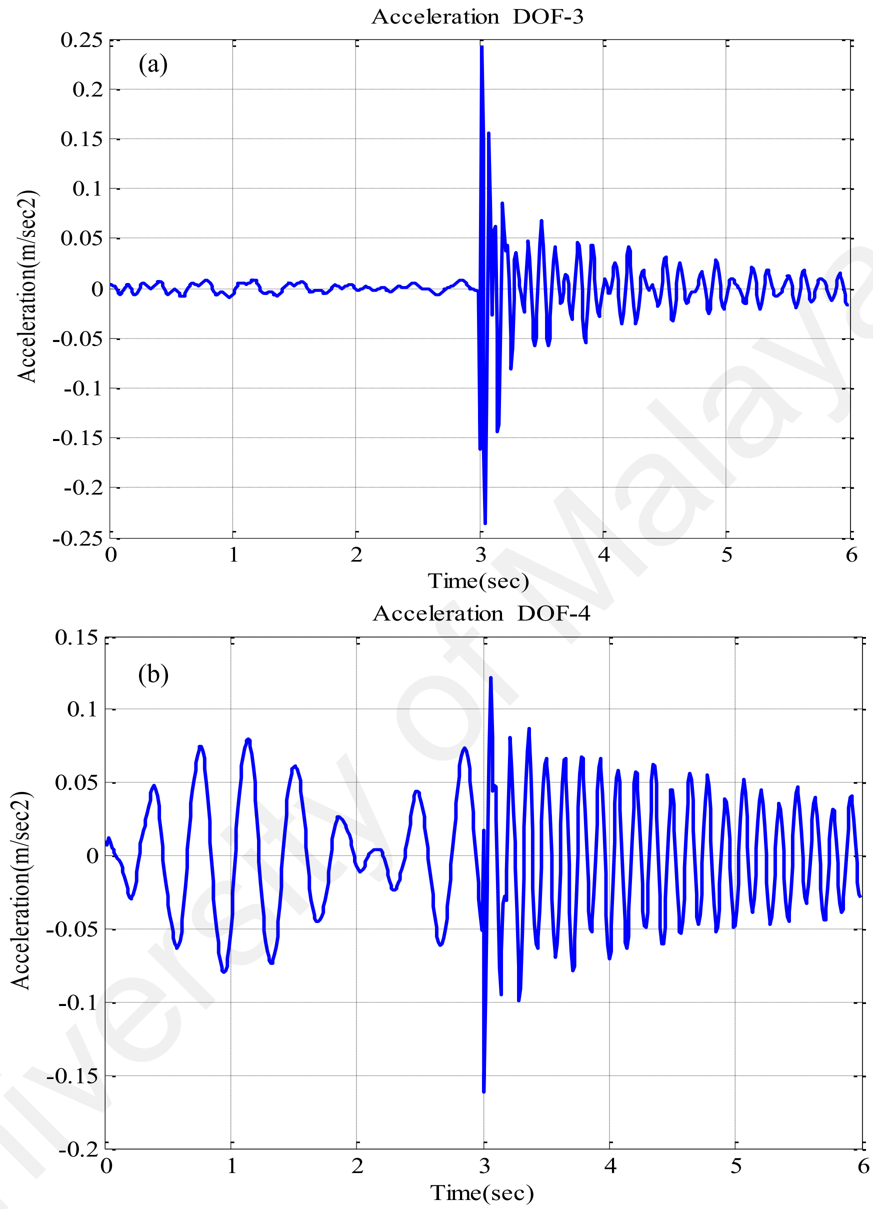

Figure E.16: The first 6 sec time-history of the acquired accelerometer data for (a) DOF=3, (b) DOF=4.

The displacement measurement is accomplished for any DOF, once the corresponding accelerometer data is considered. For example, the time-history of displacement for the horizontal DOF of node 2 (DOF=1) was measured from t=2.9-6sec using the 4^{th} and the 8^{th} scales of Chebyshev wavelet (FCW) and depicted in Figure E.17. It is observed that, considerably large computational time increment of d_t=0.1sec (designated by Δ_t^w) was utilized while, it was d_t=0.01sec (designated by Δ_t^sor sampling rate of 100 S/s) for recording original data.

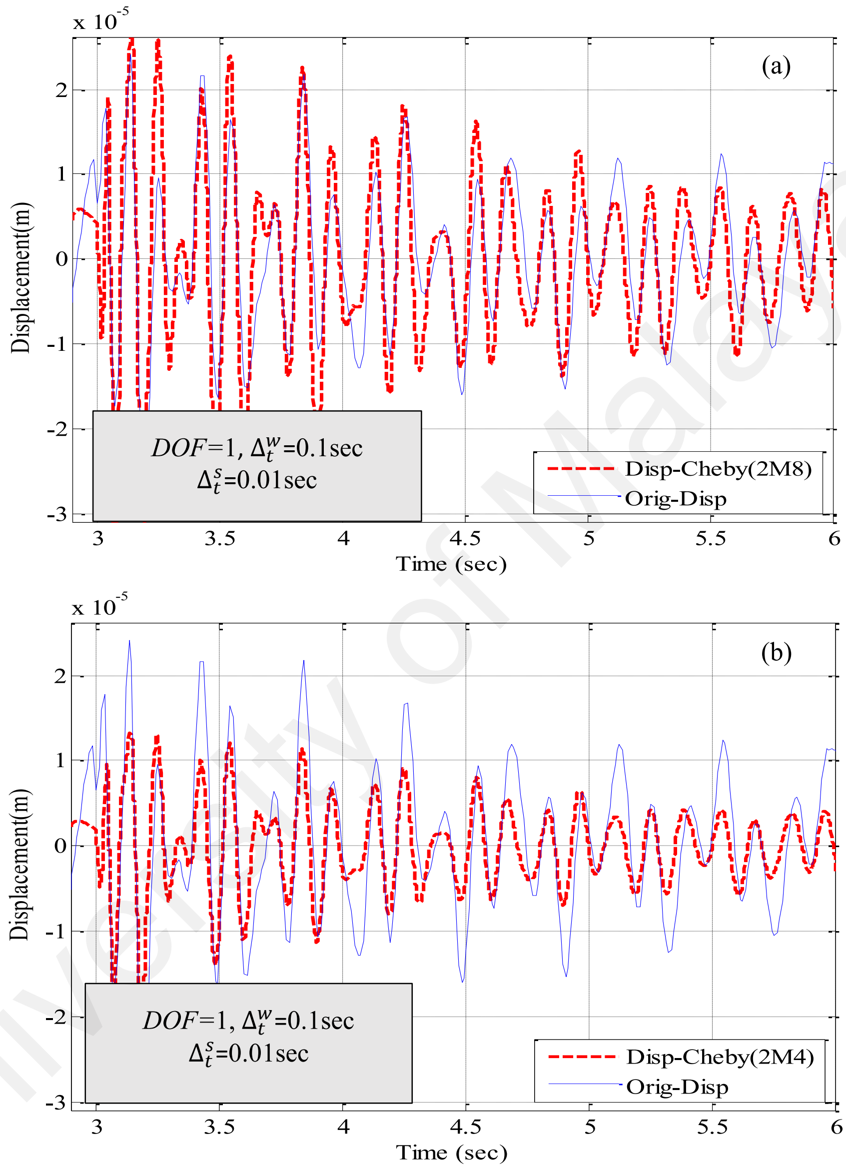

Figure E. 17: The measured displacements (Disp) of DOF=1 for t=2.9-6 sec using (a) the 8th scale of Chebyshev wavelet, FCW (Cheby2M8), (b) the 4th scale of Chebyshev wavelet, FCW (Cheby2M4), (Δ_t^w= d_t wavelet and Δ_t^s= d_t original sampling rate).

It can be induced from Figure E.17 that, despite the implementation of a very large time increment, the accuracy of the measured displacement is sufficient, particularly, at the start of the damage scenario (at t=3sec). The reason for this lies on the capability of the wavelet

University of Malaya

in which that, highly transient structural responses are precisely captured in the vicinity of sudden changes of the inherent characteristics. As was mentioned earlier, to achieve a more accurate measurement, larger scales of wavelet shall be utilized. However, from the optimization point of view it may be unnecessary for simple structures under harmonic loadings. Subsequently, the time-history of jerk for the horizontal DOF of node 5 (DOF=6) was measured from t=2.9-3.5sec using the 8th scale of FCW and compared to the normal incremental calculation of jerk for time instance of d_t=0.01sec shown in Figure E.18. This figure shows that, because of the considered short computational time interval, the normal incremental results are still reliable.

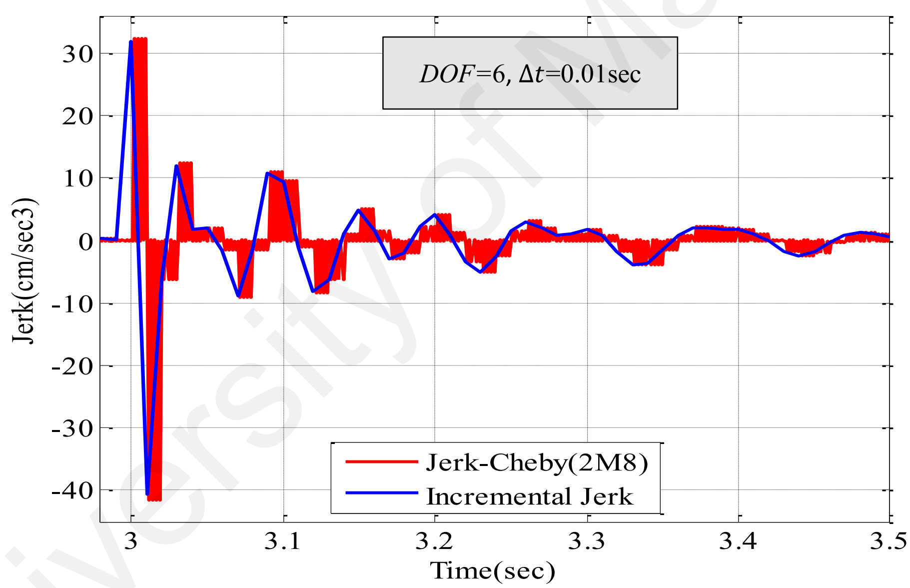

Figure E.18: The measured time-history of jerk for DOF=6 and t=2.9-3.5sec, using the 8th scale of Chebyshev wavelet, FCW (Cheby2M8) and normal incremental derivative for Δt=0.01sec.

For the aim of damage localization, the jerk measurement is reasonably valuable, while, this quantity shows one of the very sensitive dynamic response to the changes of the physical parameters or geometry of structures. Finally, the efficiency of the proposed method for the purpose of an online measurement is demonstrated in Figure E.19. The time-history of jerk is illustrated for t=0-6sec using a very large time interval of d_t=0.5sec (DOF 7 represents

University of Malaya

the vertical DOF of node 5). It is clearly distinguishable from the figure that the normal incremental computation of jerk is disable to measure this quantity at d_t=0.5sec. In contrast, the exact location of damage on time domain is optimally detected by measuring the value of jerk using the proposed method. It is clearly observed in Figure E.19(b), there is a significant fluctuation on the measured quantity of jerk at undamaged stage. This is most likely due to the same direction of the externally applied force with corresponding DOF.

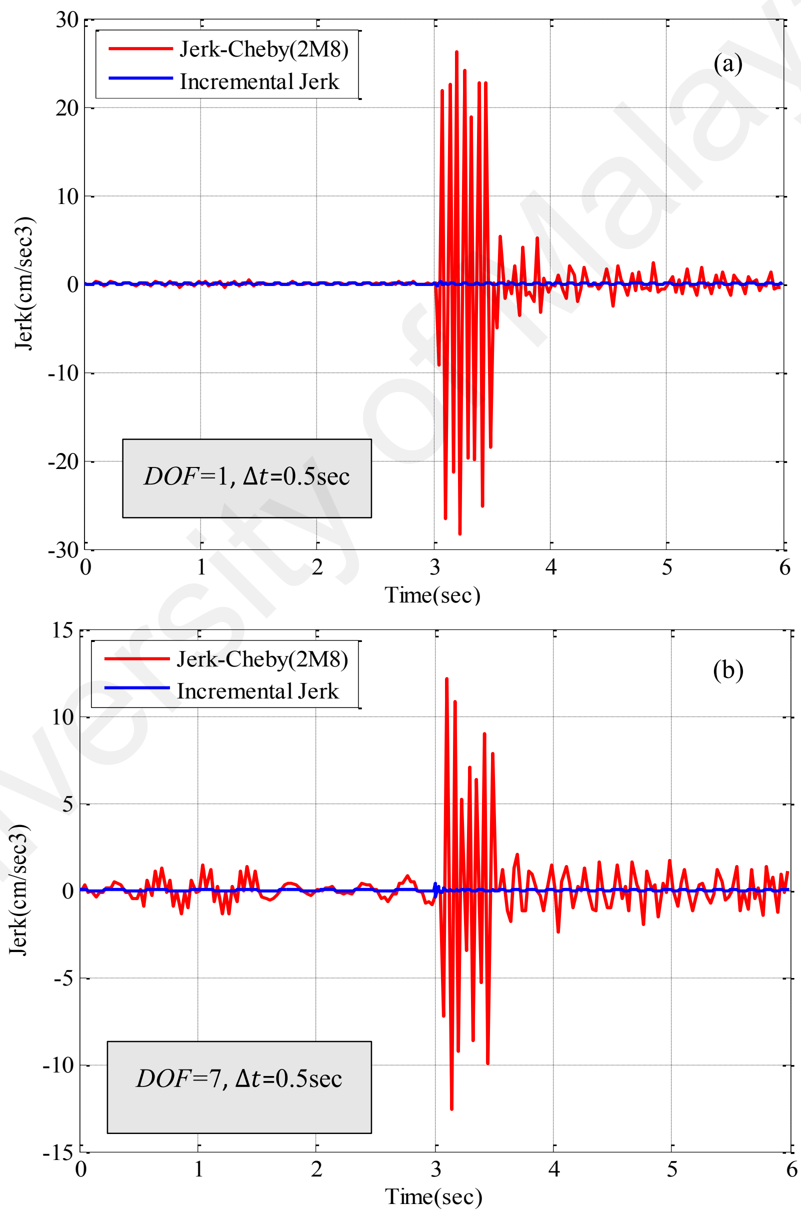

Figure E.19: The measured time-history of jerk for t=0-6 sec, using the 8th scale of Chebyshev wavelet, FCW (Cheby2M8) and normal incremental derivative for Δt=0.5 sec (a) DOF=1, (b) DOF=7.

University of Malaya

Consequently, it is shown that the comparison of the optimum measurement of structural responses as well as jerk and displacement elaborates the detailed structural durability and integrity and resulting in significant enhancement of the proposed strategy for solving the governing inverse problem (i.e., using genetic algorithm strategy). The aforementioned measurement technique is computationally suitable for transitional and rotational DOFs located at near surface or deep elements.

E.4 Stiffness identification results for Case (c), Ex. 4.6.1, Chapter 4

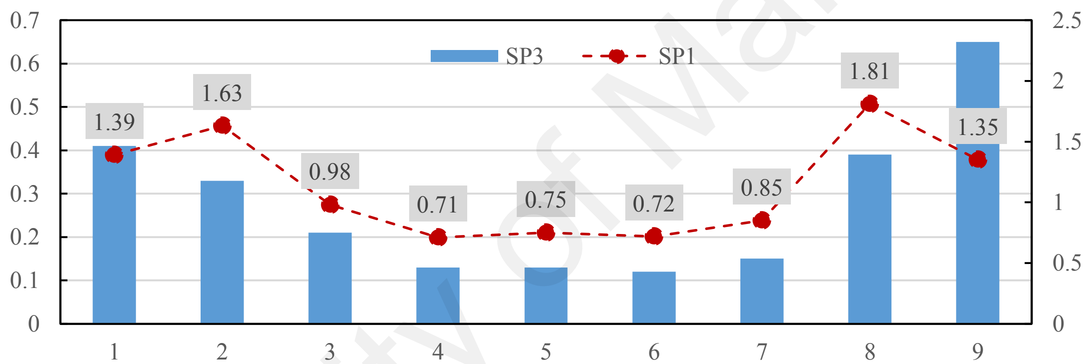

Figure E.20: Relative errors (%) in identified stiffness value of story 1-9 corresponding to SP1 and SP3 shown in Table 4.3.

E.5 Truss structure considered in Chapter 5

In this subsection, the effectiveness of the proposed WMGA strategy for structural identification of the 2D truss structure considered in Chapter 5 is investigated corresponding to different sensor placement scenarios (incomplete measurement). Figure E.20 represents the geometry of the considered structure as well as nodal numbering.

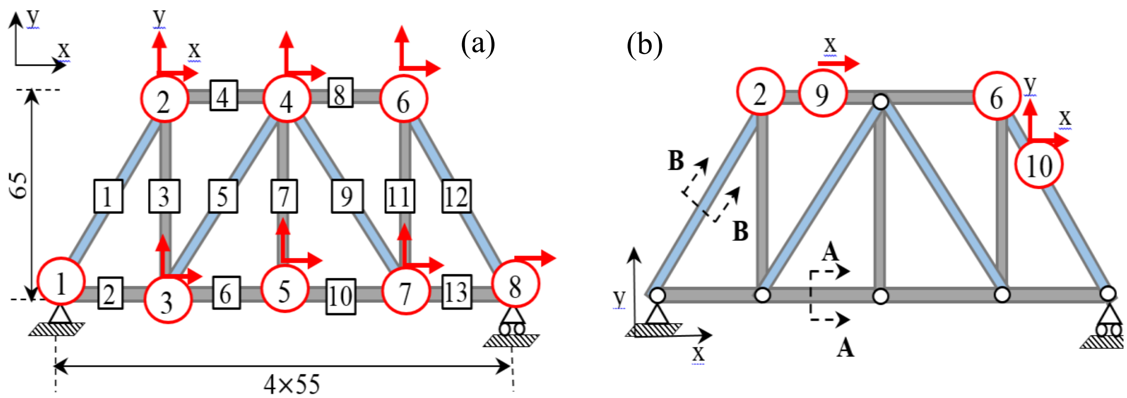

Figure E.21: The schematic view of the test setup used for 2D truss; the main layout of the test, elements and nodes numbering, (a) intact structure, (b) damage is imposed on elements 4 and 12.

In referring to Chapter 5, there are three loadings are governed on this structure at 8-x, 5-y and 4-y. The identification of intact structure shown in Figure E.21(a) is considered due to the incomplete measurement of responses. For this purpose, the program for optimum sensor placement is run for the total number of sensors available and representing the sensor placement scenarios (SP) and results are shown in Table E.1.

Table E.1: Optimum sensor placements.

Total number of available sensors (SP)	Preferred measured DOFs
3	3-y, 4-y, 7-x
6	3-x, 4-x, 4-y, 5-x, 5-y, 7-x
9	3-x, 3-y, 4-x, 4-y, 5-x, 5-y, 7-x, 7-y, 8-x
12	2-y, 3-x, 3-y, 4-x, 4-y, 5-x, 5-y, 7-x, 7-y, 8-x, 6-x, 6-y

Accordingly, the structural identification of intact structure is conducted using WMGA strategy corresponding to different sensor placements displayed in Table E.1 and the maximum error (%) obtained for identified stiffness of each structural element is depicted in Figure E.22.

University of Malaya

It was anticipated that, the accurate identification is achieved by the most complete measurement as SP12 shown in Figure E.22. This figure obviously shows that, for elements between two measured DOFs the most reliable identifications are obtained. In contrast, for elements that the adjacent DOFs are not measured the maximum error reached to the highest value. It should be noted here that, the algorithm of optimum sensor placement compares the closeness of results obtained for reduced system and simulated response of the whole structure. For this reason, the highest influence of element's stiffness is seen on its coupled DOFs, and therefore for elements that at least one adjacent DOFs is measured the identified stiffness is much more accurate.

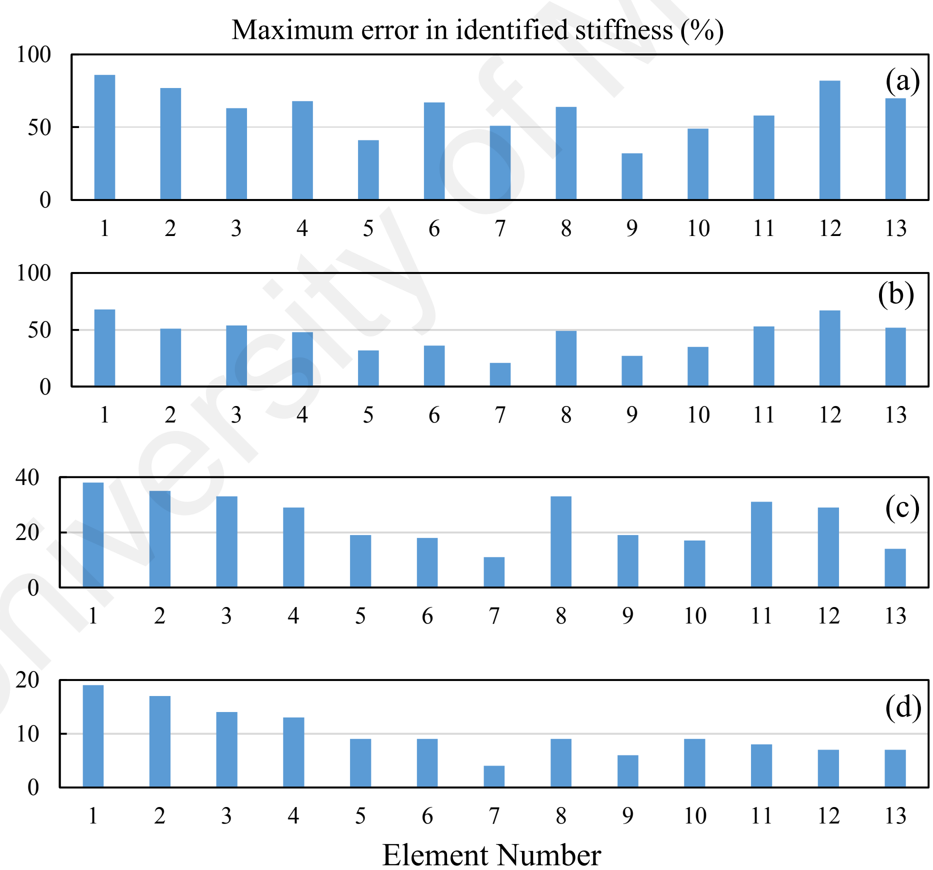

Figure E.22: The maximum error (%) obtained for identified stiffness of each structural element shown in Figure E.20, (a) SP3, (b) SP6, (c) SP9, (d) SP12.

University of Malaya

REFERENCES

Aktan, A.E., Lee, K.L., Chuntavan, C., and Aksel, T. (1994). *Modal testing for structural identification and condition assessment of constructed facilities.* Paper presented at the Proceedings-Spie the International Society for Optical Engineering.

Akula, V.R., and Ganguli, R. (2003). Finite element model updating for helicopter rotor blade using genetic algorithm. *AIAA Journal, 41*(3): 554-556.

Babolian, E., and Fattahzadeh, F. (2007). Numerical solution of differential equations by using Chebyshev wavelet operational matrix of integration. *Applied Mathematics and Computation, 188*(1): 417-426.

Balamurugan, R., Ramakrishnan, C.V., and Singh, N. (2008). Performance evaluation of a two stage adaptive genetic algorithm (TSAGA) in structural topology optimization. *Applied Soft Computing, 8*(4): 1607-1624.

Bathe, K.J. (2006). *Finite element procedures*: Klaus-Jurgen Bathe.

Bathe, K.J., and Ramaswamy, S. (1980). An accelerated subspace iteration method. *Computer Methods in Applied Mechanics and Engineering, 23*(3): 313-331.

Bathe, K.J., and Wilson, E.L. (1972a). Large eigenvalue problems in dynamic analysis. *Journal of the Engineering Mechanics Division, 98*(6): 1471-1485.

Bathe, K.J., and Wilson, E.L. (1972b). Stability and accuracy analysis of direct integration methods. *Earthquake Engineering & Structural Dynamics, 1*(3): 283-291.

Bathe, K.J., and Wilson, E.L. (1973). Stability and accuracy analysis of direct integration methods. *Earthquake Engineering and Structural Dynamics, 1*(3): 283-291.

Beck, J.L., and Katafygiotis, L.S. (1998). Updating models and their uncertainties. I: Bayesian statistical framework. *Journal of Engineering Mechanics, 124*(4): 455-461.

Bicanic, N., and Chen, H.P. (1998). Damage identification in framed structures using natural frequencies. *International Journal for Numerical Methods in Engineering*(40): 4451-4468.

Bracewell, R. (1965). The Fourier transform and its applications. *New York*.

Brigham, E.O. (1988). *The fast Fourier transform and its applications* (Vol. 1): Prentice Hall Englewood Cliffs, NJ.

University of Malaya

Buades, A., Coll, B., and Morel, J.M. (2005). A review of image denoising algorithms, with a new one. *Multiscale Modeling & Simulation, 4*(2): 490-530.

Caravani, P., Watson, M.L., and Thomson, W.T. (1977). Recursive least-squares time domain identification of structural parameters. *Journal of Applied Mechanics, 44*(1): 135-140.

Cattani, C. (2004). Haar wavelet-based technique for sharp jumps classification. *Mathematical and Computer Modelling, 39*(2): 255-278.

Cawley, P., and Adams, R.D. (1979). The location of defects in structures from measurements of natural frequencies. *The Journal of Strain Analysis for Engineering Design, 14*(2): 49-57.

Chang, S.Y. (2002). Explicit pseudodynamic algorithm with unconditional stability. *Journal of Engineering Mechanics, 128*(9): 935-947.

Chang, S.Y. (2010). A new family of explicit methods for linear structural dynamics. *Computers & Structures, 88*(11): 755-772.

Chen, C.F., and Hsiao, C.H. (1997). *Haar wavelet method for solving lumped and distributed-parameter systems.* Paper presented at the Control Theory and Applications, IEE Proceedings.

Chui, C.K. (1992). Wavelet analysis and its applications, vol. 1, An introduction to wavelets: Academic Press.

Chui, C.K. (1995). Wavelet analysis and its applications. Texas A&M University College Station Department of Mathematics: DTIC Document.

Chui, C.K. (2014). *An introduction to wavelets* (Vol. 1): Academic press.

Chung, J., and Lee, J.M. (1994). A new family of explicit time integration methods for linear and non-linear structural dynamics. *International Journal for Numerical Methods in Engineering, 37*(23): 3961-3976.

Cohen, A., Dahmen, W., and DeVore, R. (2003). Adaptive wavelet schemes for nonlinear variational problems. *SIAM Journal on Numerical Analysis, 41*(5): 1785-1823.

Cohen, L. (1989). Time-frequency distributions-a review. *Proceedings of the IEEE, 77*(7): 941-981.

Cooley, J.W., and Tukey, J.W. (1965). An algorithm for the machine calculation of complex Fourier series. *Mathematics of Computation, 19*(90): 297-301.

University of Malaya

Creed, S. (1987). Assessment of large engineering structures using data collected during in-service loading. *Procedings of Structural Assessment Based on Full and Large Scale Testing*.

Dahmen, W., Kurdila, A., and Oswald, P. (1997). *Multiscale wavelet methods for partial differential equations* (Vol. 6): Academic Press.

Daubechies, I. (1988). Orthonormal bases of compactly supported wavelets. *Communications on Pure and Applied Mathematics, 41*(7): 909-996.

Daubechies, I. (1992). *Ten lectures on wavelets* (Vol. 61): SIAM.

Deb, K., and Agrawal, R.B. (1994). Simulated binary crossover for continuous search space. *Complex Systems, 9*(3): 1-15.

Deb, K., and Gulati, S. (2001). Design of truss-structures for minimum weight using genetic algorithms. *Finite Elements in Analysis and Design, 37*(5): 447-465.

Debnath, L., and Bhatta, D. (2014). *Integral transforms and their applications*: CRC press.

Devore, R.A., Jawerth, B., and Lucier, B.J. (1992). Image compression through wavelet transform coding. *Information Theory, IEEE Transactions on, 38*(2): 719-746.

Dipasquale, E., and Cakmak, A.S. (1990). Seismic damage assessment using linear models. *Soil Dynamics and Earthquake Engineering, 9*(4): 194-215.

Dokainish, M.A., and Subbaraj, K. (1989). A survey of direct time-integration methods in computational structural dynamics—I. Explicit methods. *Computers & Structures, 32*(6): 1371-1386.

Ewins. (2000). *Modal testing: theory, practice and application* (Vol. 2): Research studies press Baldock.

Fan, W., and Qiao, P. (2009). A 2-D continuous wavelet transform of mode shape data for damage detection of plate structures. *International Journal of Solids and Structures, 46*(25): 4379-4395.

Fang, S.E., and Perera, R. (2009). Power mode shapes for early damage detection in linear structures. *Journal of Sound and Vibration, 324*(1): 40-56.

Farge, M. (1992). Wavelet transforms and their applications to turbulence. *Annual Review of Fluid Mechanics, 24*(1): 395-458.

Farrar, C.R., Baker, W.E., Bell, T.M., Cone, K.M., Darling, T.W., Duffey, T.A., . . . Migliori, A. (1994). Dynamic characterization and damage detection in the I-40 bridge over the Rio Grande. *Los Alamos National Lab., NM (United States)*.

Faverjon, B., and Sinou, J.J. (2009). Identification of an open crack in a beam using an a posteriori error estimator of the frequency response functions with noisy measurements. *European Journal of Mechanics and Solids, 28*(1): 75-85.

Franulović, M., Basan, R., and Prebil, I. (2009). Genetic algorithm in material model parameters' identification for low-cycle fatigue. *Computational Materials Science, 45*(2): 505-510.

Friswell, M., and Mottershead, J.E. (1995). *Finite element model updating in structural dynamics* (Vol. 38): Springer Science & Business Media.

Furuta, H., Kameda, T., Nakahara, K., Takahashi, Y., and Frangopol, D.M. (2006). Optimal bridge maintenance planning using improved multi-objective genetic algorithm. *Structure and Infrastructure Engineering, 2*(1): 33-41.

Gabor, D. (1946). Theory of communication. Part 1: The analysis of information. *Journal of the Institution of Electrical Engineers-Part III: Radio and Communication Engineering, 93*(26): 429-441.

Galli, A.W., Heydt, G.T., and Ribeiro, P.F. (1996). Exploring the power of wavelet analysis. *Computer Applications in Power, IEEE, 9*(4): 37-41.

Ghanem, R., and Shinozuka, M. (1995). Structural-system identification. I: Theory. *Journal of Engineering Mechanics, 121*(2): 255-264.

Goedecker, S., and Ivanov, O. (1998). The solution of multi-scale partial differential equations using wavelets. *ARXiv Preprint Physics/9803011*. doi: 10.1063/1.168739

Goldberg, D.E., and Holland, J.H. (1988). Genetic algorithms and machine learning. *Machine Learning, 3*(2): 95-99.

Grossman, A., Morlet, J., and Paul, T. (1986). *Transforms associated to square integrable group representations. ii: Examples.* Paper presented at the Annales de l'IHP Physique Théorique.

Grossmann, A., and Morlet, J. (1984). Decomposition of Hardy functions into square integrable wavelets of constant shape. *SIAM Journal on Mathematical Analysis, 15*(4): 723-736.

University of Malaya

Grossmann, A., Morlet, J., and Paul, T. (1985). Transforms associated to square integrable group representations. I. General results. *Journal of Mathematical Physics, 26*(10): 2473-2479.

Gurley, K., and Kareem, A. (1999). Applications of wavelet transforms in earthquake, wind and ocean engineering. *Engineering Structures, 21*(2): 149-167.

Haar, A. (1910). Zur theorie der orthogonalen funktionensysteme. *Mathematische Annalen, 69*(3): 331-371.

Haberman, R. (2013). Applied partial differential equations with Fourier series and boundary value problems. *Applied Mathematics and Computation, 10*: 12.

Heil, C.E., and Walnut, D.F. (1989). Continuous and discrete wavelet transforms. *SIAM Review, 31*(4): 628-666.

Hemez, F.M., and Doebling, S.W. (1999). *A validation of Bayesian finite element model updating for linear dynamics.* Paper presented at the 17th SEM International Modal Analysis Conference.

Hubbard, B.B. (1998). *The world according to wavelets the story of a mathematical technique in the making*: Universities Press.

Hughes, T.J.R. (2012). *The finite element method: linear static and dynamic finite element analysis*: Courier Corporation.

Imregun, M., Visser, W.J., and Ewins, D.J. (1995). Finite element model updating using frequency response function data: I. Theory and initial investigation. *Mechanical Systems and Signal Processing, 9*(2): 187-202.

Jaffard, S., Meyer, Y., and Ryan, R.D. (2001). *Wavelets: tools for science and technology*: SIAM.

Jeffrey, A. (2001). *Advanced engineering mathematics*: Academic Press.

Jinwen, T.D.Q.W.W. (2009). The finite element model updating of structure based on wavelet packet analysis and support vector machines. *Journal of Huazhong University of Science and Technology (Nature Science Edition), 6*: 027.

Jung, D.S., and Kim, C.Y. (2009). FE model updating based on hybrid genetic algorithm and its verification on numerical bridge model. *Structural Engineering and Mechanics, 32*(5): 667-683.

University of Malaya

Kalman, R.E. (1960). A new approach to linear filtering and prediction problems. *Journal of Fluids Engineering, 82*(1): 35-45.

Kim, H.M., and Bartkowicz, T.J. (1993). Damage detection and health monitoring of large space structures. *Sound and Vibration, 27*: 12-12.

Kitagawa, G. (1996). Monte Carlo filter and smoother for non-Gaussian nonlinear state space models. *Journal of Computational and Graphical Statistics, 5*(1): 1-25.

Ko, J.M., and Ni, Y.Q. (2005). Technology developments in structural health monitoring of large-scale bridges. *Engineering Structures, 27*(12): 1715-1725.

Ko, J.M., Ni, Y.Q., and Chan, H.T. (1999). *Dynamic monitoring of structural health in cable-supported bridges.* Paper presented at the 1999 Symposium on Smart Structures and Materials.

Koh, C.G., Hong, B., and Liaw, C.Y. (2003). Substructural and progressive structural identification methods. *Engineering Structures, 25*(12): 1551-1563.

Körner, Thomas William. (1989). *Fourier analysis*: Cambridge university press.

Kougioumtzoglou, I.A., and Spanos, P.D. (2013). An identification approach for linear and nonlinear time-variant structural systems via harmonic wavelets. *Mechanical Systems and Signal Processing, 37*(1): 338-352.

Kwak, H.G., and Kim, J. (2009). An integrated genetic algorithm complemented with direct search for optimum design of RC frames. *Computer-Aided Design, 41*(7): 490-500.

Lepik, U. (2005). Numerical solution of differential equations using Haar wavelets. *Mathematics and Computers in Simulation, 68*(2): 127-143.

Lepik, U. (2008a). Haar wavelet method for solving higher order differential equations. *International Journal of Mathematics & Computation, 1*(N08): 84-94.

Lepik, U. (2008b). Haar wavelet method for solving higher order differential equations. *International Journal of Mathematics & Computation™, 1*(N08): 84-94.

Lepik, U. (2008c). Solving integral and differential equations by the aid of non-uniform Haar wavelets. *Applied Mathematics and Computation, 198*(1): 326-332.

Lepik, U. (2009a). Haar wavelet method for solving stiff differential equations. *Mathematical Modelling and Analysis, 14*(4): 467-481.

University of Malaya

Lepik, U. (2009b). Solving fractional integral equations by the Haar wavelet method. *Applied Mathematics and Computation, 214*(2): 468-478.

Lévy, P. (1954). Le mouvement brownien. *Mémorial des Sciences Mathématiques, 126*: 1-84.

Lindholm, B.E., and West, R.L. (1996). *A Bayesian statistics approach to updating finite element models with frequency response data (part i: theory).* Paper presented at the Proceedings of the 14th International Modal Analysis Conference.

Ling, S.H., and Leung, F.H.F. (2007). An improved genetic algorithm with average-bound crossover and wavelet mutation operations. *Soft Computing, 11*(1): 7-31.

Ling, X., and Haldar, A. (2004). Element level system identification with unknown input with Rayleigh damping. *Journal of Engineering Mechanics, 130*(8): 877-885.

Littlewood, J.E., and Paley, R.E.A. (1931). Theorems on Fourier series and power series. *Journal of the London Mathematical Society, 1*(3): 230-233.

Liu, G.R., and Chen, S.C. (2002). A novel technique for inverse identification of distributed stiffness factor in structures. *Journal of Sound and Vibration, 254*(5): 823-835.

Liu, M., Frangopol, D.M., and Kim, S. (2009). Bridge system performance assessment from structural health monitoring: a case study. *Journal of Structural Engineering, 135*(6): 733-742.

Liu, X., Lieven, N.A.J., and Escamilla, A.P.J. (2009). Frequency response function shape-based methods for structural damage localisation. *Mechanical Systems and Signal Processing, 23*(4): 1243-1259.

Ljung, L., and Glover, K. (1981). Frequency domain versus time domain methods in system identification. *Automatica, 17*(1): 71-86.

Mackenzie, D. (2001). Wavelets: seeing the forest and the trees. *Beyond Discovery (National Academy of Sciences, Washington, 2001)*.

Mahdavi, S.H., and Razak, H.A. (2013). A wavelet-based approach for vibration analysis of framed structures. *Applied Mathematics and Computation, 220*: 414-428.

Mahdavi, S.H., and Razak, H.A. (2015a). A comparative study on optimal structural dynamics using wavelet functions. *Mathematical Problems in Engineering*.

University of Malaya

Mahdavi, S.H., and Razak, H.A. (2015b). An efficient iterative scheme for solution of non-linear problems using family of Chebyshev operations. *Mathematical Problems in Engineering*.

Mahdavi, S.H., and Razak, H.A. (2015c). Indirect time integration scheme for dynamic analysis of space structures using wavelet functions. *Journal of Engineering Mechanics (ASCE)*.

Mahdavi, S.H., and Shojaee, S. (2013). Optimum time history analysis of SDOF structures using free scale of Haar wavelet. *Structural Engineering and Mechanics, 45*(1): 95-110.

Maia, N.M.M., and Esilva, J.M.M. (1997). *Theoretical and experimental modal analysis*: Research Studies Press Taunton.

Maleknejad, K., Sohrabi, S., and Rostami, Y. (2007). Numerical solution of nonlinear Volterra integral equations of the second kind by using Chebyshev polynomials. *Applied Mathematics and Computation, 188*(1): 123-128.

Mallat, S. (1999). A wavelet tour of signal processing, (wavelet analysis & its applications).

Mallat, S.G. (1989a). Multiresolution approximations and wavelet orthonormal bases. *Transactions of the American Mathematical Society, 315*(1): 69-87.

Mallat, S.G. (1989b). A theory for multiresolution signal decomposition: the wavelet representation. *Pattern Analysis and Machine Intelligence, IEEE Transactions, 11*(7): 674-693.

Mallat, S.G. (1999). *A wavelet tour of signal processing*: Academic Press.

Marano, G.C., Quaranta, G., and Monti, G. (2011). Modified genetic algorithm for the dynamic identification of structural systems using incomplete measurements. *Computer‐Aided Civil and Infrastructure Engineering, 26*(2): 92-110.

Mares, C., Mottershead, J.E., and Friswell, M.I. (2006). Stochastic model updating: part 1—theory and simulated example. *Mechanical Systems and Signal Processing, 20*(7): 1674-1695.

Marwala, T. (2002). Finite element model updating using wavelet data and genetic algorithm. *Journal of Aircraft, 39*(4): 709-711.

Marwala, T., and Sibisi, S. (2005). Finite element model updating using Bayesian framework and modal properties. *Journal of Aircraft, 42*(1): 275-278.

University of Malaya

Mason, J.C., and Handscomb, D.C. (2002). *Chebyshev polynomials*: CRC Press.

Maybeck, P.S. (1982). *Stochastic models, estimation, and control* (Vol. 3): Academic Press.

Messina, A., Williams, E.J., and Contursi, T. (1998). Structural damage detection by a sensitivity and statistical-based method. *Journal of Sound and Vibration, 216*(5): 791-808.

Meyer, Y. (1989). Orthonormal wavelets *Wavelets* (pp. 21-37): Springer.

Meyer, Y. (1993). Wavelets-algorithms and applications. *Society for Industrial and Applied Mathematics Translation, 1*: 1-142.

Michalewicz, Z. (1996). *Genetic algorithms+ data structures= evolution programs*: Springer Science & Business Media.

Michalewicz, Z. (2013). *Genetic algorithms+ data structures= evolution programs*: Springer Science & Business Media.

Migliori, A. (1991). Resonant ultrasound spectroscopy: Google Patents.

Newland, D.E. (1993). Harmonic wavelet analysis. *Proceedings of the Royal Society of London. Series A: Mathematical and Physical Sciences, 443*(1917): 203-225.

Ni, Y.Q., Zhou, X.T., and Ko, J.M. (2006). Experimental investigation of seismic damage identification using PCA-compressed frequency response functions and neural networks. *Journal of Sound and Vibration, 290*(1): 242-263.

Nooshin, H., and Disney, P. (1991). Elements of formian. *Computers & Structures, 41*(6): 1183-1215.

Okasha, N.M., and Frangopol, D.M. (2009). Lifetime-oriented multi-objective optimization of structural maintenance considering system reliability, redundancy and life-cycle cost using GA. *Structural Safety, 31*(6): 460-474.

Oppenheim, A.V., Schafer, R.W., and Buck, J.R. (1989). *Discrete-time signal processing* (Vol. 2): Prentice-Hall Englewood Cliffs.

Perera, R., and Ruiz, A. (2008). A multistage FE updating procedure for damage identification in large-scale structures based on multiobjective evolutionary optimization. *Mechanical Systems and Signal Processing, 22*(4): 970-991.

University of Malaya

Perry, M.J. (2007). *Modified genetic algorithm approach to system identification with structural and offshore application.* National University of Singapore.

Perry, M.J., Koh, C.G., and Choo, Y.S. (2006). Modified genetic algorithm strategy for structural identification. *Computers & Structures, 84*(8): 529-540.

Qiao, P., and Cao, M. (2008). Waveform fractal dimension for mode shape-based damage identification of beam-type structures. *International Journal of Solids and Structures, 45*(22): 5946-5961.

Qiao, P., Lu, K., Lestari, W., and Wang, J. (2007). Curvature mode shape-based damage detection in composite laminated plates. *Composite Structures, 80*(3): 409-428.

Quek, S.T., Wang, Q., Zhang, L., and Ang, K.K. (2001). Sensitivity analysis of crack detection in beams by wavelet technique. *International Journal of Mechanical Sciences, 43*(12): 2899-2910.

Rader, C.M. (1968). Discrete Fourier transforms when the number of data samples is prime. *Proceedings of the IEEE, 56*(6): 1107-1108.

Razzaghi, M., and Yousefi, S. (2000). Legendre wavelets direct method for variational problems. *Mathematics and Computers in Simulation, 53*(3): 185-192.

Razzaghi, M., and Yousefi, S. (2001). Legendre wavelets method for the solution of nonlinear problems in the calculus of variations. *Mathematical and Computer Modelling, 34*(1): 45-54.

Ren, W.X., and Sun, Z.S. (2008). Structural damage identification by using wavelet entropy. *Engineering Structures, 30*(10): 2840-2849.

Ricker, N. (1953). The form and laws of propagation of seismic wavelets. *Geophysics, 18*(1): 10-40.

Rio, G., Soive, A., and Grolleau, V. (2005). Comparative study of numerical explicit time integration algorithms. *Advances in Engineering Software, 36*(4): 252-265.

Rioul, O., and Vetterli, M. (1991). Wavelets and signal processing. *IEEE Signal Processing Magazine, 8*(5): 14-38.

Salajegheh, E., and Heidari, A. (2005). Time history dynamic analysis of structures using filter banks and wavelet transforms. *Computers & Structures, 83*(1): 53-68.

Salawu, O.S. (1995). Non-destructive assessment of structures using the integrity index method applied to a concrete highway bridge. *Insight, 37*(11): 875-878.

University of Malaya

Salawu, O.S. (1997). Detection of structural damage through changes in frequency: a review. *Engineering Structures, 19*(9): 718-723.

Salvini, P., and Vivio, F. (2007). Dynamic reduction strategies to extend modal analysis approach at higher frequencies. *Finite Elements in Analysis and Design, 43*(11): 931-940.

Sato, T., and Chung, M. (2005). Structural identification using adaptive Monte Carlo filter. *Journal of Structural Engineering, JSCE, 51*: 471-477.

Sazonov, E., and Klinkhachorn, P. (2005). Optimal spatial sampling interval for damage detection by curvature or strain energy mode shapes. *Journal of Sound and Vibration, 285*(4): 783-801.

Schulz, M.J., Pai, P.F., and Abdelnaser, A.S. (1996). *Frequency response function assignment technique for structural damage identification.* Paper presented at the Proceedings of the International Society for Optical Engineering.

Sestieri, A., and Damb, W. (1988). *Why be modal, i. e., how to avoid the use of modes in the modification of vibrating systems.* Paper presented at the International Modal Analysis Conference, 6 th, Kissimmee, FL.

Shinozuka, M., and Ghanem, R. (1995). Structural system identification. II: Experimental verification. *Journal of Engineering Mechanics, 121*(2): 265-273.

Shone, S.P., Mace, B.R., and Waters, T.P. (2009). Locating damage in waveguides from the phase of point frequency response measurements. *Mechanical Systems and Signal Processing, 23*(2): 405-414.

Sirca, G.F., and Adeli, H. (2012). System identification in structural engineering. *Scientia Iranica, 19*(6): 1355-1364.

Söderström, T., and Stoica, P. (2002). Instrumental variable methods for system identification. *Circuits, Systems and Signal Processing, 21*(1): 1-9.

Steenackers, G., and Guillaume, P. (2006). Finite element model updating taking into account the uncertainty on the modal parameters estimates. *Journal of Sound and Vibration, 296*(4): 919-934.

Strang, G. (1993). Wavelet transforms versus Fourier transforms. *Bulletin of the American Mathematical Society, 28*(2): 288-305.

University of Malaya

Strömberg, J.O. (2006). A modified Franklin system and higher order spline systems on R n as unconditional bases for Hardy spaces. *Fundamental Paper in Wavelet Theory*: 197-215.

Tan, D., Qu, W., and Wang, J. (2009). The finite element model updating of structure based on wavelet packet analysis and support vector machines. *J Huazhong Univ Sci Technol (Nat Sci Ed), 37*: 104-107.

Todorovska, M.I., and Trifunac, M.D. (2008). Earthquake damage detection in the Imperial County Services Building III: analysis of wave travel times via impulse response functions. *Soil Dynamics and Earthquake Engineering, 28*(5): 387-404.

Tu, Z., and Lu, Y. (2008). FE model updating using artificial boundary conditions with genetic algorithms. *Computers & Structures, 86*(7): 714-727.

Vanik, M.W., Beck, J.L., and Au, S.K. (2000). Bayesian probabilistic approach to structural health monitoring. *Journal of Engineering Mechanics, 126*(7): 738-745.

Vasilyev, O.V., and Paolucci, S. (1997). A fast adaptive wavelet collocation algorithm for multidimensional PDEs. *Journal of Computational Physics, 138*(1): 16-56.

Wang, R.J., Shang, D.G., Li, L.S., and Li, C.S. (2008). Fatigue damage model based on the natural frequency changes for spot-welded joints. *International Journal of Fatigue, 30*(6): 1047-1055.

Wang, Y., and Fan, Q. (2012). The second kind Chebyshev wavelet method for solving fractional differential equations. *Applied Mathematics and Computation, 218*(17): 8592-8601.

Welch, G., and Bishop, G. (2001). An introduction to the kalman filter. *Proceedings of the Siggraph Course, Los Angeles*.

West, W.M. (1982). Single point random modal test technology application to failure detection. *Shock and Vibration Information; Center the Shock and Vibration Bull 52*.

White, C., Li, H.C.H., Whittingham, B., Herszberg, I., and Mouritz, A.P. (2009). Damage detection in repairs using frequency response techniques. *Composite Structures, 87*(2): 175-181.

Williams, E.J., Messina, A., and Payne, B.S. (1997). *A frequency-change correlation approach to damage detection.* Paper presented at the Proceedings-Spie the International Society for Optical Engineering.

University of Malaya

Wilson, E.L., Farhoomand, I., and Bathe, K.J. (1972). Nonlinear dynamic analysis of complex structures. *Earthquake Engineering & Structural Dynamics, 1*(3): 241-252.

Yousefi, S., and Razzaghi, M. (2005). Legendre wavelets method for the nonlinear Volterra–Fredholm integral equations. *Mathematics and Computers in Simulation, 70*(1): 1-8.

Zabel, V. (2003). *Applications of wavelet analysis in system identification.* Inst. für Strukturmechanik.

Zapico, J.L., González, B.A., Gonzalez, M.P., and Alonso, R. (2008). Finite element model updating of a small steel frame using neural networks. *Smart Materials and Structures, 17*(4): 045016.

Zheng, Y.M., Sun, H.H., Zhao, X., Chen, W., Zhang, R.H., and Shen, X.D. (2009). Finite element model updating of a long-span steel skybridge. *Journal of Vibration Engineering, 1*: 019.

Zhong, S., and Oyadiji, S.O. (2008). Analytical predictions of natural frequencies of cracked simply supported beams with a stationary roving mass. *Journal of Sound and Vibration, 311*(1): 328-352.

Zhong, S., and Oyadiji, S.O. (2011). Detection of cracks in simply-supported beams by continuous wavelet transform of reconstructed modal data. *Computers & Structures, 89*(1): 127-148.

Zhong, S., Oyadiji, S.O., and Ding, K. (2008). Response-only method for damage detection of beam-like structures using high accuracy frequencies with auxiliary mass spatial probing. *Journal of Sound and Vibration, 311*(3): 1075-1099.

University of Malaya

LIST OF PUBLICATIONS AND PAPERS PRESENTED

International ISI ranked journals:

- Mahdavi, S.H., and Razak, H.A. (2013). A wavelet-based approach for vibration analysis of framed structures. *Applied Mathematics and Computation*, 220: 414-428.
- Mahdavi, S.H., and Razak, H.A. (2015). Indirect time integration scheme for dynamic analysis of space structures using wavelet functions. *Journal of Engineering Mechanics (ASCE)*, DOI: 10.1061/(ASCE) 13 EM.1943-7889.0000914.
- Mahdavi, S.H., Razak, H.A., Shojaee, S., and Mahdavi, M.S. (2015). A comparative study on application of Chebyshev and spline methods for geometrically non-linear analysis of truss structures. *International Journal of Mechanical Sciences,* 101: 241-251, DOI: 10.1016/j.ijmecsci.2015.08.001.
- Mahdavi, S.H., and Razak, H.A. (2014). Optimum dynamic analysis of 2D frames using free-scaled wavelet functions. *Latin American Journal of Solids and Structures*, 11: 1036-1048.
- Mahdavi, S.H., and Razak, H.A. (2015). A comparative study on optimal structural dynamics using wavelet functions. *Mathematical Problems in Engineering*, Vol. 2015, Article ID 956793, 10 pages, 2015. DOI: 10.1155/2015/956793.
- Mahdavi, S.H., and Razak, H.A. (2015). An efficient iterative scheme using family of Chebyshev's operations. *Mathematical Problems in Engineering*, Vol 2015 (2015), Article ID 205295, 10 pages, 2015. DOI: 10.1155/2015/205295.
- Mahdavi, S.H., and Razak, H.A. (2015) An efficient approach for dynamic analysis of space trusses using free-scaled Legendre wavelets. *Arabian Journal for Science and Engineering*, 1-10.

International journals:

- Mahdavi, S.H., and Razak, H.A. (2014). Optimal time history analysis of 2D trusses using free-scaled wavelet functions. *Aust. J. Basic & Appl. Sci.,* 8(19): 127-130.
- Mahdavi, S.H., and Razak, H.A. (2015). A wavelet-based scheme for optimum measurement/monitoring of structural responses. *Journal of Physics: Conference Series* 628, 012024, doi:10.1088 / 1742-6596/628 /1/ 012024.

University of Malaya

Papers presented in international conferences:

- Mahdavi, S.H., and Razak, H.A. (2013). Optimal dynamic analysis of 2D trusses using free scale of wavelet functions. *The International Conference on Engineering and Built Environment (ICEBE), Kuala Lumpur, Malaysia, 2013.*

- Mahdavi, S.H., and Razak, H.A. (2015). A wavelet-based scheme for optimum measurement /monitoring of dynamic responses of structures", *11th International Conference on Damage Assessment of Structures (DAMAS 2015), Ghent University, Belgium.* http://dx.doi.org/10.1088/1742-6596/628/1/012024.

Papers submitted to international ISI ranked journals (under review):

- Mahdavi, S.H., and Razak, H.A. An efficient approach for measurement of structural responses coupled with damage using free-scaled wavelet functions. *Measurement*, submitted.

- Mahdavi, S.H., and Razak, H.A. A numerical assessment of structural dynamic problems using Chebyshev and Legendre wavelets. *Meccanica*, submitted.

- Razak, H.A., and Mahdavi, S.H. A wavelet-based strategy for structural identification and damage detection using modified genetic algorithms. *Computers and Structures,* submitted.

- S.H. Mahdavi, H.A. Razak, "Optimal sensor placement for time domain identification using a wavelet-based genetic algorithm", *Smart Materials and Structures*, submitted.

- S.H. Mahdavi, H.A. Razak, "A wavelet-based genetic algorithm strategy for optimal sensor\exciter placement capable of time-domain identification of large-scale structures", *Expert Systems with Applications*, submitted.

University of Malaya